TGFβ signaling in cancer progression
Liu, S.

Cover Page

Universiteit Leiden

The handle http://hdl.handle.net/1887/92349 holds various files of this Leiden University dissertation.

Author: Liu, S.
Title: TGFβ signaling in cancer progression
Issue Date: 2020-05-28

TGFβ signaling
in cancer progression

Sijia Liu

Stellingen

behorende bij het proefschrift

TGFβ signaling in cancer progression

1. Deubiquitinase (DUB) activity profiling is an elegant approach to draw a landscape of global DUB activities in breast cancer subtypes. (This thesis)

2. UCHL1 promotes TGFβ-induced breast cancer metastasis and is highly enriched in the exosome fraction of TNBC cell conditioned media and TNBC patient sera. (This thesis)

3. Cell permeable activity-based probes for DUBs are useful tools for studying their activity *in vitro* and *in vivo*. (This thesis)

4. Targeting TGFβ type I receptor can combat the development of vemurafenib drug-resistance in advanced melanoma. (This thesis)

5. TGFβ family members regulate the fate of cell during development, tissue homeostasis and regeneration, and are major players in tumorigenesis, fibrotic disorders, immune malfunctions and congenital diseases. (David et al, 2018, Nat Rev Mol Cell Biol)

6. DUBs are key determinants of cellular processes that are highly relevant to pathologies such as oncology, autoimmune disorders, chronic inflammation and neurodegeneration. (Harrigan et al, 2018, Nat Rev Drug Discov)

7. The contents of exosome secreted by cancer cells reflect the biological changes that are associated with cancer progression, potentially offering a comprehensive assessment of cancer diagnosis, prognosis, and progression. (LeBleu et al, 2020, Trends Cancer)

8. Breast cancer high-resolution proteomic profiling identified TGFβ type II receptor and UCHL1 as specific proteins that are highly enriched in aggressive TNBC basal B subclass cell lines. (Kosok et al, 2020, iScience)

9. Hope for the best, prepare for the worst, never lose curiosity in between. (Inspired by Maya Angelou and Albert Einstein)

10. Yesterday is history, tomorrow is a mystery, today is a gift, that's why we call it the present. (Inspired by Alice Morse Earle)

TGFβ signaling
in cancer progression

Sijia Liu

TGFβ signaling
in cancer progression

Proefschrift

ter verkrijging van

de graad van Doctor aan de Universiteit Leiden,

op gezag van Rector Magnificus prof.mr. C.J.J.M. Stolker,

volgens besluit van het College voor Promoties

te verdedigen op donderdag 28 mei 2020

klokke 16:15 uur

door

Sijia Liu

geboren te Chengde, China

in 1988

Promotor: Prof. Dr. P. ten Dijke
Co-promotor: Dr. P.P. Geurink

Leden promotiecommissie:
Prof. Dr. T.K. Sixma (Netherlands Cancer Institute)
Prof. Dr. A. Moustakas (Uppsala University)
Prof. Dr. A.C.O. Vertegaal

Contents

Chapter 1

General introduction

Chapter 1

Cancer is a large diverse group of genetic diseases that can be triggered virtually everywhere in our body. Cancer cells differ from normal cells in that they are frequently shaped abnormally, grow uncontrollably, pass through their usual boundaries to invade, survive in blood circulation and metastasize to other organs or tissues (1). Among all cancers, breast cancer is the most prevalent cancer in females worldwide, impacting approximately 2 million women each year and leading to a huge number of cancer-related deaths (1). Distant metastasis is the cause of almost 90% of breast cancer-related deaths (2). Once metastases have been triggered, current therapies frequently fail to provide durable treatments (3). Cancer patients may present themselves in the clinic when their cancer has already spread to other tissues or organs. Therefore, a better understanding of the underlying mechanisms of the key initial steps in the metastasis process is needed to find new biomarkers for early diagnosis, make existing standard chemo/radiotherapy more effective and less toxic, develop (new and combinatorial) targeted therapies that provide long-lasting effects and increase the number of cancer patients who respond to immune therapies.

The cytokine transforming growth factor-β (TGFβ) is frequently produced at high levels by breast tumors and correlates with poor prognosis (4). TGFβ is a strong driver of epithelial-mesenchymal transition (EMT), which plays an important role in mediating cancer cell migration, invasion and metastasis (Figure 1) (5). Cancer cells with a mesenchymal phenotype are also more prone to become chemotherapy resistant than cancer cells with an epithelial phenotype (6). Combinatorial targeting or subsequent interference with TGFβ signaling after radiotherapy/chemotherapy has been shown to make cancers more responsive or regain responsiveness to therapy (7). TGFβ not only acts directly on cancer cells in the late stages of tumorigenesis but also manipulates the microenvironment to create a favorable niche for rapid tumor growth and metastasis by stimulating angiogenesis, activating cancer-associated fibroblasts and suppressing the immune system (8).
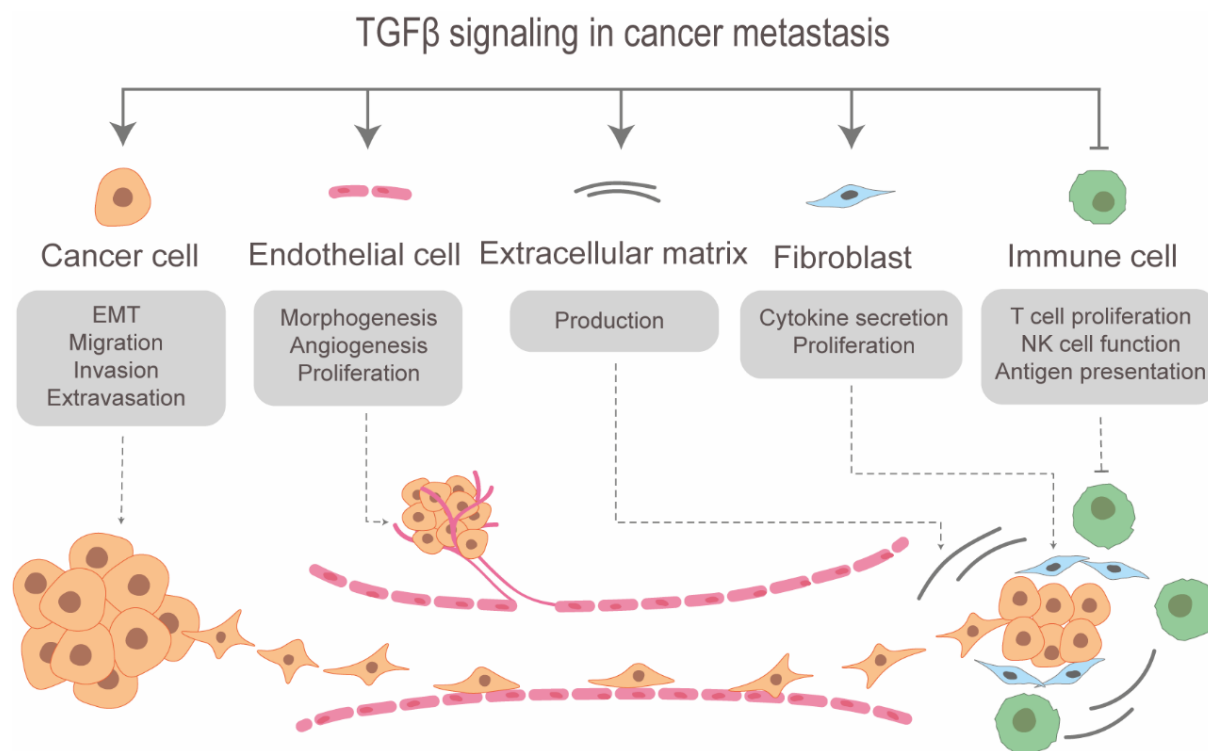
Figure 1. The role of TGFβ signaling in cancer metastatic progression. TGFβ promotes epithelial-mesenchymal transition (EMT), migration, invasion and metastasis of late-stage cancer cells. The TGFβ signaling networks between cancer cells and the microenvironment (fibroblasts, immune and endothelial cells) contribute to cancer metastasis by blocking the immune system, stimulating angiogenesis and promoting cytokine secretion and extracellular matrix production.

Breast cancer is a highly heterogeneous disease that can be classified into different subtypes based on histological and molecular characteristics (Figure 2). Based on the cellular origin from which the tumor evolved, cancer can be classified as (i) carcinoma, when derived from epithelial cells, or (ii) sarcoma, when derived from stromal parts. Based on gene expression profiling, breast cancer can be classified into five major molecular subtypes: luminal A and luminal B (expressing the estrogen receptor (ER)), human epidermal growth factor receptor 2 (HER2) and basal-like (9). Different subtypes show different clinical features; for example, basal-like breast cancers are more aggressive than luminal-like breast cancers (10), and ER-negative breast cancers are more aggressive than ER-positive breast cancers (11). However, among all breast cancer cases, triple-negative breast cancer (TNBC) is the most aggressive subtype, accounting for 12-17% of total breast cancers. TNBC lacks amplifications of ER, progesterone receptor (PR), and HER2 (12). As TNBC does not respond to anti-hormonal therapies and has a low response to chemotherapy/radiotherapy, TNBC remains the most challenging subtype to treat (13). Therefore, there is an unmet need for clinically meaningful molecular targets and effective pharmacological inhibitors to improve the therapy of TNBC patients.
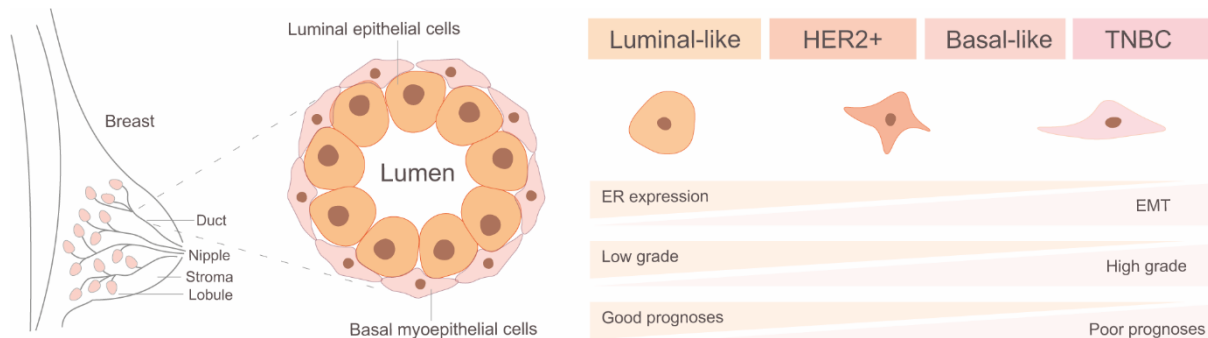
Figure 2. Histological and molecular characteristics of breast cancer. The histological subtype described in the left panel is ductal carcinoma, the most frequent subtype of breast cancer. The molecular characteristics of different breast cancer subtypes described on the right are important indicators for clinical prediction and therapy.

Ubiquitination is emerging as an important posttranslational modification for regulating protein stability, localization and functions in cancer cells (14). Ubiquitination is regulated by E1, E2 and E3 enzymes and reversed by deubiquitinases (DUBs). In humans, there are around 100 DUB family members, and some of them have been discovered to play pivotal roles during cancer progression (15). A catalytic cysteine in the catalytic domain is present in most DUBs, which renders them attractive targets for small-molecule drug development (16). The first clinical drug to target the ubiquitin system for cancer therapy was *bortezomib* (*Velcade*), which is a proteasome inhibitor that has been successfully applied in the treatment of multiple myeloma and mantel cell lymphoma (17). Currently, first-generation DUB inhibitors are undergoing clinical trials (16). The discovery of DUB activity-based probes

(ABPs) provides important tools to obtain fundamental new insights into DUB function and for drug discovery and development (16,18).

Melanoma is the most aggressive skin cancer in the world, with more than 60 thousand deaths in 2018 (19). Somatic mutation of BRAF (V600E) is often found in metastatic melanoma with poor prognosis (20). The clinical application of BRAF inhibitors such as *vemurafenib* (*Zelboraf*) and *dabrafenib* (*Tafinlar*) has significantly increased the median survival of metastatic melanoma patients by approximately 6 months (21-22). However, clinical trial data have demonstrated that 40% of patients develop drug resistance, for which the underlying mechanism remains unclear (21-22). Recent studies found elevated TGFβ signaling in drug-resistant melanoma with BRAF mutations, but the potential for targeting TGFβ signaling in the treatment of drug-resistant melanoma was not investigated.

In this thesis, I start with a general introduction in **Chapter 1** to introduce the general role of TGFβ signaling during cancer progression. In **Chapter 2**, I provide a mechanistic overview of all the DUBs that have been shown to impact the TGFβ signaling pathway in cancer and discuss the therapeutic value of DUB inhibitors for cancer treatment. In **Chapter 3**, we provide detailed working protocols for studying the metastasis of breast cancer cells in zebrafish xenograft models. In **Chapter 4**, I provide details on DUB activity profiling experiments, in which we found UCHL1 as a potential tumor-promoting protein that facilitates TGFβ-induced TNBC metastasis. In particular, we focus on UCHL1 as a new therapeutic target and demonstrate its promise in the stratification of breast cancer subtypes. In **Chapter 5**, we describe our development of an activity-based probe for monitoring UCHL1 activity in live cells and zebrafish embryos. In **Chapter 6**, we investigate the feasibility of targeting TGFβ signaling in BRAF inhibitor-resistant melanoma. In **Chapter 7**, I summarize all the studies in the thesis and provide some future projects related to our results.

References

1. Ferlay J, Colombet M, Bray F. Global Cancer Observatory. International Agency for Research on Cancer. 2018.
2. Fouad TM, Kogawa T, Liu DD, Shen Y, Masuda H, El-Zein R, et al. Overall survival differences between patients with inflammatory and noninflammatory breast cancer presenting with distant metastasis at diagnosis. Breast Cancer Res Treat 2015;152(2):407-16.
3. Massagué J, Obenauf AC. Metastatic colonization by circulating tumor cells. Nature 2016;529:298.
4. Barcellos-Hoff MH, Akhurst RJ. Transforming growth factor-β in breast cancer: too much, too late. Breast Cancer Res 2009;11(1):202.
5. Hao Y, Baker D, Ten Dijke P. TGF-β-Mediated Epithelial-Mesenchymal Transition and Cancer Metastasis. Int J Mol Sci 2019;20(11).
6. van Staalduinen J, Baker D, Ten Dijke P, van Dam H. Epithelial-mesenchymal-transition-inducing transcription factors: new targets for tackling chemoresistance in cancer? Oncogene 2018;37(48):6195-211.
7. Colak S, Ten Dijke P. Targeting TGF-β Signaling in Cancer. Trends in cancer 2017;3(1):56-71.
8. Batlle E, Massague J. Transforming Growth Factor-β Signaling in Immunity and Cancer. Immunity 2019;50(4):924-40.
9. Sorlie T, Perou CM, Tibshirani R, Aas T, Geisler S, Johnsen H, et al. Gene expression patterns of breast carcinomas distinguish tumor subclasses with clinical implications. Proc Natl Acad Sci U S A 2001;98(19):10869-74.
10. Leidy J, Khan A, Kandil D. Basal-like breast cancer: update on clinicopathologic, immunohistochemical, and molecular features. Arch Pathol Lab Med 2014;138(1):37-43.
11. Rochefort H, Glondu M, Sahla ME, Platet N, Garcia M. How to target estrogen receptor-negative breast cancer? Endocr Relat Cancer 2003;10(2):261-6.
12. Foulkes WD, Smith IE, Reis-Filho JS. Triple-Negative Breast Cancer. N Engl J Med 2010;363(20):1938-48.
13. Garrido-Castro AC, Lin NU, Polyak K. Insights into Molecular Classifications of Triple-Negative Breast Cancer: Improving Patient Selection for Treatment. Cancer Discov 2019;9(2):176-98.
14. Ciechanover A. The unravelling of the ubiquitin system. Nat Rev Mol Cell Biol 2015;16(5):322-4.
15. Liu S, de Boeck M, van Dam H, Ten Dijke P. Regulation of the TGF-β pathway by deubiquitinases in cancer. Int J Biochem Cell Biol 2016;76:135-45.
16. Harrigan JA, Jacq X, Martin NM, Jackson SP. Deubiquitylating enzymes and drug discovery: emerging opportunities. Nat Rev Drug Discov 2017;17:57-78.
17. Adams J. Development of the proteasome inhibitor PS-341. Oncologist 2002;7(1):9-16.
18. de Jong A, Merkx R, Berlin I, Rodenko B, Wijdeven RH, El Atmioui D, et al. Ubiquitin-based probes prepared by total synthesis to profile the activity of deubiquitinating enzymes. Chembiochem 2012;13(15):2251-8.
19. Davies H, Bignell GR, Cox C, Stephens P, Edkins S, Clegg S, et al. Mutations of the BRAF gene in human cancer. Nature 2002;417(6892):949-54.
22. Sosman JA, Kim KB, Schuchter L, Gonzalez R, Pavlick AC, Weber JS, et al. Survival in BRAF V600-mutant advanced melanoma treated with vemurafenib. N Engl J Med 2012;366(8):707-14.
21. Chapman PB, Hauschild A, Robert C, Haanen JB, Ascierto P, Larkin J, et al. Improved survival with vemurafenib in melanoma with BRAF V600E mutation. N Engl J Med 2011;364(26):2507-16.
22. Flaherty KT, Puzanov I, Kim KB, Ribas A, McArthur GA, Sosman JA, et al. Inhibition of mutated, activated BRAF in metastatic melanoma. N Engl J Med 2010;363(9):809-19.

Chapter 2

Regulation of the TGFβ pathway by deubiquitinases in cancer

Sijia Liu[1] , Miriam de Boeck[1] , Hans van Dam[1] , Peter ten Dijke[1, 2]

[1]Department of Cell and Chemical Biology, Leiden University Medical Center, The Netherlands.

[2]Ludwig Institute for Cancer Research, Science for Life Laboratory, Uppsala University, Sweden.

Chapter 2

Abstract

The transforming growth factor β (TGFβ) pathway regulates diverse cellular processes. It signals via serine/threonine kinase receptors and intracellular Smad and non-Smad effector proteins. In cancer cells, aberrant TGFβ signaling can lead to loss of growth inhibition and an increase in invasion, epithelial-to-mesenchymal transition (EMT) and metastasis. Therapeutic targeting of the pro-oncogenic TGFβ responses is currently being explored as a potential therapy against certain invasive and metastatic cancer types. The ubiquitin post-translational regulation system is emerging as a key regulatory mechanism for the control of TGFβ pathway components. In this review, we focus on the role of deubiquitinases (DUBs), which counteract the activity of E3 ubiquitin ligases. We will discuss the mechanisms by which specific DUBs control Smad and non-Smad TGFβ signaling routes, and how perturbation of the expression and function of DUBs contributes to misregulation of TGFβ signaling in cancer.

Key words: TGFβ, Smad, Ubiquitin, Deubiquitinase, Cancer.

1. Introduction

TGFβ family members, which include TGFβs, activins and bone morphogenetic proteins (BMPs) (1), play prominent roles in regulating cell cycle progression, differentiation, migration/invasion, and survival/apoptosis of a large variety of cell types (2). Their pleiotropic functions are highly dependent on context; in diverse cellular microenvironments they can have different, and even opposing functions (3,4). TGFβ family members play pivotal roles in maintaining tissue homeostasis during development. Aberrant TGFβ family signaling has been associated with multiple human diseases, including fibrosis, immune disorders and cancer (5). TGFβ family members signal via cell surface type I and type II serine/threonine kinase receptors, which mediate intracellular responses via Smad transcriptional regulators (6) and non-Smad pathways (7). Each step of the TGFβ family signaling cascades is intricately controlled by positive and negative regulation. An important mechanism of regulation is via covalent and reversible post-translational modification of TGFβ pathway components, including receptors and Smads, by ubiquitin (8,9).

The ubiquitin system was first described in the late 1970s by Hershko and Ciehanover (10,11). Over the past few decades, this system was identified as one of the most critical and versatile post-translational modifications, which can control a vast range of cellular processes, including cell-cycle control, DNA damage repair and membrane trafficking. While first recognized as a signal for protein degradation (12), ubiquitination has now been found to have much broader roles including regulation of the binding and/or enzymatic activities of proteins involved in cell signaling, trafficking, endocytosis, autophagy, transcription, immunity, and DNA damage response (13,14). Ubiquitination requires ubiquitin-activating enzymes (E1), ubiquitin conjugating enzymes (E2), and ubiquitin ligase enzymes (E3) (15).

Deubiquitinases (DUBs) are isopeptidases that can reverse the ubiquitination process, by removing ubiquitin from their substrate proteins (16). Misregulation of ubiquitin enzymes as well as DUBs has been shown to be closely linked to cancer (e.g. a higher risk of cancer metastasis) as shown by clinical database analysis and animal models (17). DUBs have emerged as critical regulatory mediators of several signaling pathways that are involved in

human cancers, such as tumor protein p53 (p53) signaling (18) and c-Jun NH2-terminal kinase (JNK) signaling (19). In this review we will focus on the role of DUBs in the regulation of TGFβ family signaling and how perturbation of this system may be involved in cancer. We will also discuss the therapeutic value of DUB inhibitors for the treatment of cancer patients.

2. The TGFβ pathway

The human TGFβ family of cytokines (TGFβs, activins and BMPs) comprises 33 members (20,21). They are structurally and functionally related, secreted dimeric proteins. They share a characteristic cysteine knot structure and exert pleiotropic effects. There are three human TGFβ isoforms, TGFβ1, TGFβ2, and TGFβ3. TGFβ is a potent growth inhibitor in normal tissues (22,23) and also pre-malignant cells and acts as a tumor suppressor. However, tumor cells can become selectively refractory to the cytostatic effects of TGFβ through the activation of proto-oncogenes or inactivation of tumor suppressor genes. In late phases of tumorigenesis, tumor cells may remain responsive to TGFβ; it can induce the so-called epithelial to mesenchymal transition (EMT) and endow tumor cells with high migratory and invasive potential (24) (25).

Moreover, during tumor progression tumor cells frequently start expressing high levels of TGFβ (26). This may also indirectly contribute to tumor growth by creating a favorable microenvironment through its stimulatory effects on immune suppression and angiogenesis. Consequently, TGFβ can also act as a potent stimulator of metastasis. TGFβ can switch from tumor suppressor in the early phase of tumorigenesis to a tumor promoter at late phases (23).

BMP family members were first discovered as secreted proteins, which induce the formation of bone and cartilage (27-29). Subsequently, BMPs were found to play a role in non-skeleton related processes, including angiogenesis, energy metabolism, neurogenesis and ventral mesoderm specification (30,31).

Activins were initially discovered as regulators of follicle stimulating hormone secretion by pituitary cells. Additionally, activins were shown to exhibit multifunctional activities such as erythroid differentiation in bone, muscle formation, and regulation of endocrine function (32). Like TGFβs, BMPs and activins, as well as other family members such as nodal, anti-mullerian hormone (AMH) and growth and differentiation factors (GDFs), are emerging as important regulators of tumor progression (33-37).

TGFβ family members trigger biological processes by binding to type I and type II single transmembrane spanning serine/threonine kinase receptors (6,38,39). The basic structure of type I receptors is similar to that of type II receptors; both of them have small cysteine-rich extracellular regions and intracellular portions containing kinase domains. One difference is the GS domain, a region rich in glycine and serine residues, which is only found in the juxtamembrane region in the intracellular domain of type I receptors. TGFβ ligands initiate signaling by stimulating the formation of heteromeric complexes of type I and type II receptors. Upon complex formation, the constitutively active type II kinase triggers the phosphorylation of serine and threonine residues in the GS domains of type I receptors (40). This leads to the activation of type I receptor kinases, which phosphorylate specific intracellular Smad effector proteins (6,38,39).

Chapter 2

The TGFβ canonical Smad pathways can be divided into two branches (Fig. 1) One is used (predominantly) by TGFβ and activins, which signal through intracellular receptor-regulated (R-) Smad2 and Smad3 effectors (6). The other branch is mainly employed by BMPs, which signal via R-Smad1, Smad5 and Smad8 (41).
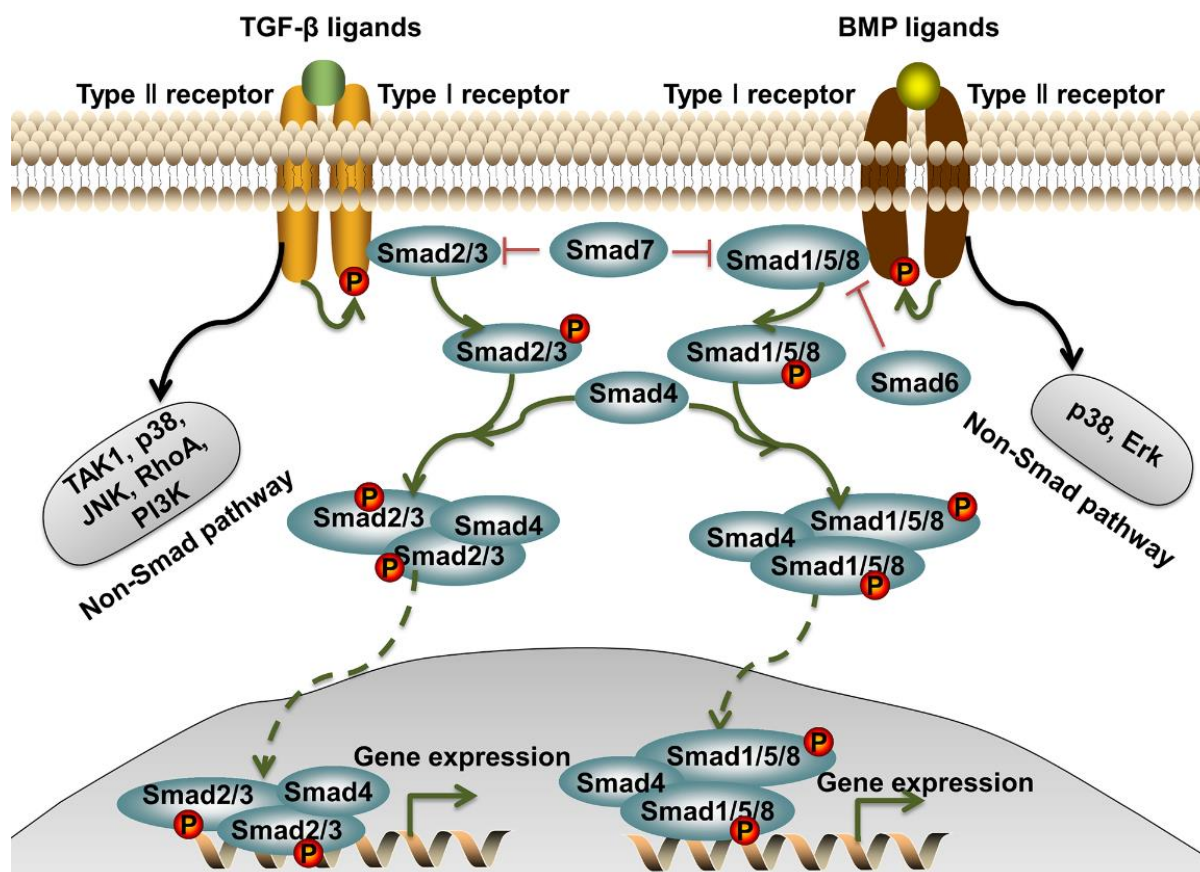

Figure 1. A schematic representation of the Smad and non-Smad TGFβ/BMP pathways. Ligand binding to TGFβ/BMP receptors on the cell surface induces phosphorylation of TGFβ/BMP type I receptors, which induces phosphorylation of Smad2/3 and Smad1/5/8. Phosphorylated Smad2/3 and Smad1/5/8 associate with Smad4, translocate to the nucleus, and bind to DNA to trigger TGFβ/BMP-mediated gene expression. TGFβ receptors also can initiate activation of TGFβ associated kinase 1 (TAK1), p38 and Jun N-terminal kinase (JNK) mitogen-activated protein kinases (MAPKs) pathways, small Rho-like GTPase pathway, and phosphoinositide 3 kinase (PI3K)/Akt-mTOR pathway. BMP receptors also activate the non-Smad p38 and Ras-Erk-MAPK pathways.

R-Smads are phosphorylated by activated type I receptors and form heteromeric complexes with common mediator (Co-) Smad4 (42-44). Subsequently R-Smad-Smad4 complexes translocate to the nucleus, where they regulate gene transcriptional responses, in collaboration with co-activators and co-repressors and DNA-binding transcription factors (45) R-Smads and Smad4 have a conserved N- terminal MH1 and C-terminal MH2 domain. The MH1 domain of Smads can bind to DNA whereas the MH2 domain mediates Smad oligomerization and Smad-receptor interactions. Both MH1 and MH2 domains have been shown to interact with many protein partners.

The two inhibitory (I)-Smads, Smad6 and Smad7, can inhibit canonical Smad signaling by competing with R-Smads for binding to activated receptors (46), thereby suppressing R-Smad

phosphorylation. I-Smads can also interact with Smad4 preventing the interaction between Smad4 and phosphorylated (R)-Smads (47).

Moreover, I-Smads can recruit E3-ubiquitin ligases i.e. Smurf1 and Smurf2, to ubiquitinate type I receptors for subsequent proteasomal degradation (48,49) thereby terminating signaling (50). I-Smads only have an MH2 domain, which mediates the interaction with type I receptors.

In addition to the canonical Smad pathway, TGFβ family members can also activate so-called non-Smad pathways to instigate a multitude of intracellular changes (7). There are various branches including the p38 and Jun N-terminal kinase (JNK) mitogen-activated protein kinases (MAPKs) pathways, ubiquitin ligase tumor necrosis factor (TNF)-receptor associated factor (TRAF6) and TGFβ activated kinase 1 (TAK1). Other branches contain the phosphoinositide 3 kinase (PI3K)/Akt-mTOR pathway, the NF-κB pathway, the Ras-Erk-MAPK pathway, and the small Rho-like GTPase pathway (Fig. 1). There is extensive crosstalk between Smad and non-Smad pathways, e.g. MAP kinases can directly phosphorylate the Smads in their linker regions (51).

3. The ubiquitin system

3.1. Ubiquitination and deubiquitination

Ubiquitin is an 8.5 kDa, ubiquitously expressed regulatory protein, which contains seven lysine residues (i.e. Lys6, Lys11, Lys27, Lys29, Lys33, Lys48 and Lys63) in its 76 amino acid sequence (52). Ubiquitination (covalent attachment of one or more ubiquitin residues) is an important post-translational modification that modulates protein function, localization, degradation and turnover, thereby serving as a regulator for many aspects of cell physiology in eukaryotes (53).

There are three types of enzymes that play an important role in the conjugation of ubiquitin to its substrates: E1 ubiquitin-activating enzyme, binds to the C-terminal glycine residue of ubiquitin in an ATP-dependent fashion. E2 conjugating enzymes transfer the ubiquitin protein from the E1 to their own cysteine residue, and E3 ligase enzymes catalyse ubiquitin conjugation to the target protein (Fig. 2) (54,55). A group of E3 ligases utilizes their *homologous to the E6AP carboxyl terminus* (HECT) domain to transfer the ubiquitin from E2 to E3, and subsequently to the protein substrate. Another group of E3 ligases can use a *really interesting new gene* (RING) finger domain to directly transfer ubiquitin from E2 to a substrate protein (Fig. 2) (56). Target proteins can be monoubiquitinated or polyubiquitinated (57). Polyubiquitination is the process by which ubiquitin molecules form a polyubiquitin chain through linkage to their internal lysine residues or to the amino terminal methionine residue of the previous ubiquitin (58).

Deubiquitinating enzymes (DUBs) are isopeptidases that can reverse the ubiquitination process by removing ubiquitin from the target protein (16). DUBs have three main functional activities: 1) generation of free ubiquitin from the ubiquitin precursor, 2) reverse the 'ubiquitin signal' by removing the ubiquitin from the substrate protein—this ubiquitin is recycled to the free ubiquitin pool to maintain homeostasis, 3) some DUBs edit ubiquitin chains to alter the ubiquitin signal (Fig. 2).
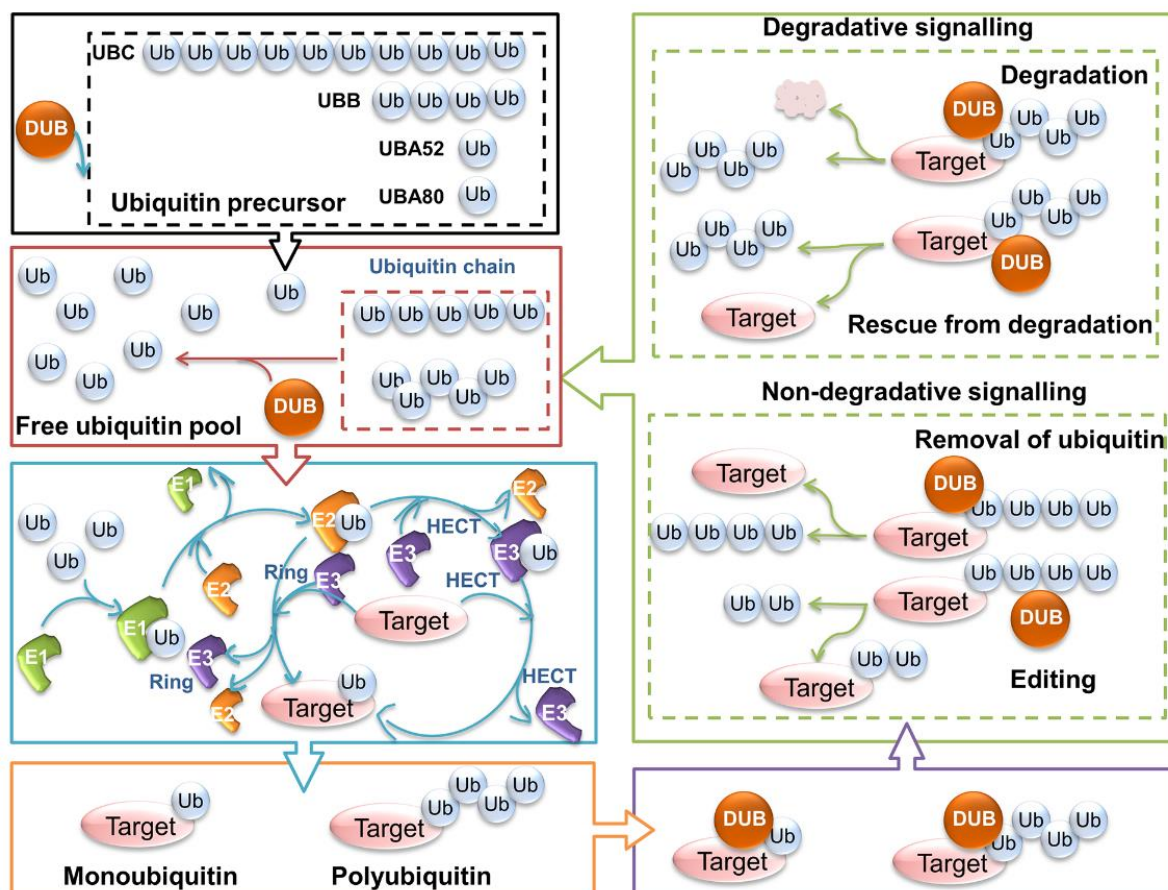
Figure 2. An overview of ubiquitination and deubiquitination processes and the general roles of deubiquitination. Different processes are marked with different colour frames. The black frame represents the generation of ubiquitin (Ub) by its four encoding genes (UBC, UBB, UBA52 and UBA80); deubiquitinases (DUBs) stimulate the generation of free ubiquitin from ubiquitin precursors. The red frame represents the free ubiquitin pool. The blue frame illustrates the conjugation process of ubiquitin to target proteins by the E1 ubiquitin-activating enzyme, E2 ubiquitin-conjugating enzyme, and HECT/Ring E3 ubiquitin ligase enzyme. The orange frame shows the monoubiqutinated and polyubiquitinated target protein. The purple frame shows that DUBs can target proteins with different ubiquitin chains. The green frame explains the function of DUBs in degradative signaling and non-degradative signaling; the removed ubiquitin chains are recycled to the free ubiquitin pool for future use (59,60).

3.2.   Human deubiquitinating enzymes

There are nearly 100 DUBs encoded by the human genome until 2016. Of these, 79 DUBs them have been shown to have functional activity (16,61,62). They can be divided into five families based on the architecture of their catalytic domains: ubiquitin COOH-terminal hydrolases (UCHs), ubiquitin-specific proteases (USPs), ovarian tumor proteases (OTUs), Machado-Joseph disease proteases (MJDs) and *JAB1/ MPN/MOV34* proteases (JAMMs) (16). The human DUB families are summarized in Figure 3. Members of the UCH, USP, OTU and MJDs are cysteine proteases, which utilize a catalytic triad of conserved amino acids characterized by the classical cysteine protease, papain (63). The JAMM/MPN+ family members are zinc metalloproteases, in which invariant His, Asp, and Ser residues coordinate the catalytic zinc (59).
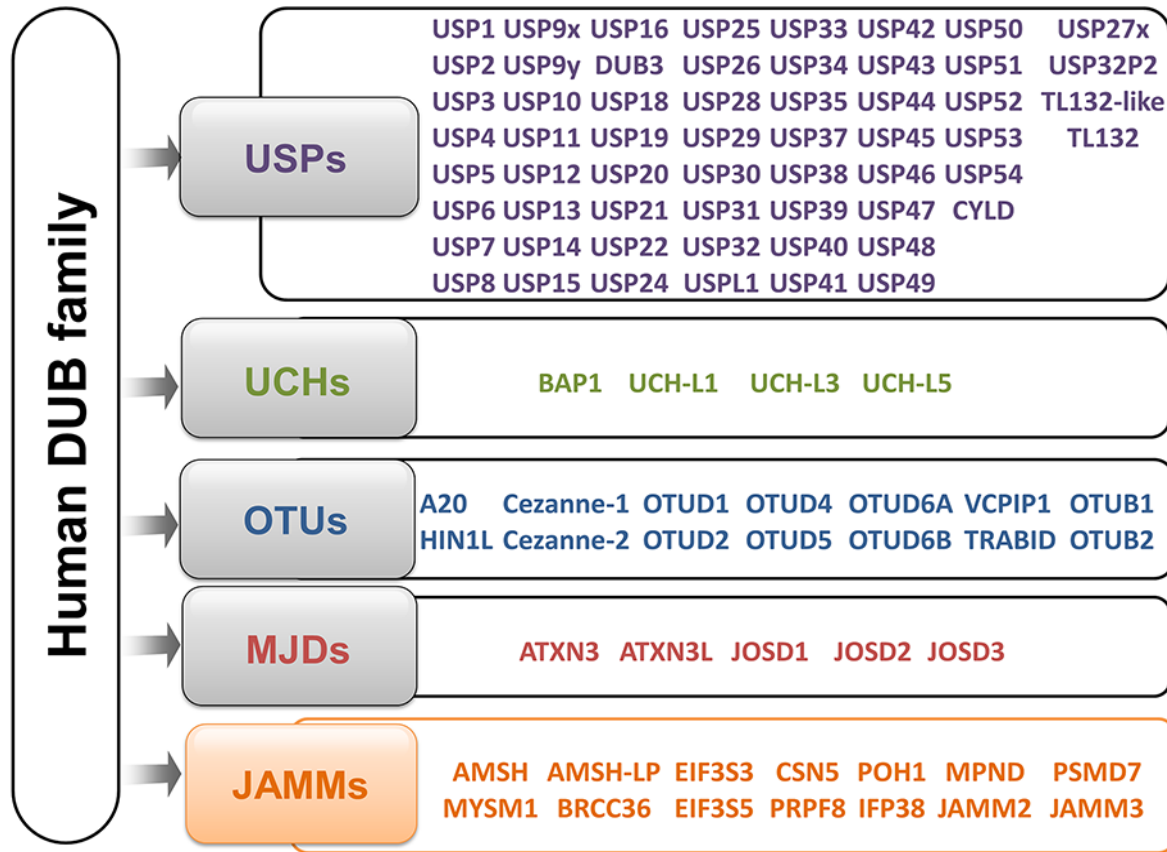
Figure 3. An overview of human DUBs. The 95 putative DUBs can be divided into five families: 58 USPs, 4 UCHs, 14 OTUs, 5 MJDs, and 14 JAMMs. DUBs in the grey frame are cysteine proteases. DUBs in the orange frame are metalloproteases.

The **USP** family is the largest family with around 60 proteases, and the sizes of these proteases range from 50 kDa to 300 kDa. USPs are characterized by a conserved active site composed of a catalytic triad including Cys, His, and Asp (or Asn) residues. Most USPs contain several distinct subdomains within their catalytic domain, such as the zinc finger ubiquitin-specific protease domain (ZnF-UBP), the ubiquitin-associated domain (UBA) and the ubiquitin-interacting motif (UIM) (64). The non-catalytic domains differ at the amino acid sequence level. It has been reported that these non-catalytic domains are important for the localization of individual USPs (65). Most USPs carry a ZnF-UBP binding domain (66), which can specifically recognize the free COOH terminal Gly-Gly motif of free ubiquitin (67,68).

UCH family members were the first structurally characterized DUBs. There are four members in humans: UCHL1, UCHL3, UCHL5/UCH37, and BRCA1-associated protein 1 (BAP) (69). The proteasome associated UCHL5 and the tumor suppressor BAP1 cleave the ubiquitin chains using their more extended cross-over loops (70).

OTU family members can be classified in 3 subgroups: OTUBs, OTUDs, and A20-like OTUs (71). A20 (TNFAIP3) has been reported extensively due to its critical function in the NF-κB pathway (72,73).

The **Josephin** family consists of four members: ataxin-3 (ATXN3), ataxin 3-like (ATXN3L), *Josephin domain containing 1* (JOSD1), and *Josephin domain containing 2* (JOSD2).

ATXN3 is mutated in spinocerebellar ataxia type 3 or Machado-Joseph disease (74). It serves as a polyubiquitin chain-editing enzyme and controls the folding and stability of proteins (75). The ubiquitin hydrolase activity of ATXN3 is essential for a normal lifespan. Reportedly, it regulates longevity by controlling insulin like growth factor 1 (IGF-I) signaling (76). ATXN3L, JOSD1 and JOSD2 all have a catalytic triad, consisting of one cysteine and two histidine residues which exhibits deubiquitinating activity.

JAMM family members contain a signature 'H-x-H-P-x[6]-S-x[2]-D' motif within the Mpr1-Pad1-N-terminal (MPN) domain. The JAMMs are the only family of DUBs that have zinc-metalloprotease activity (77). *Associated molecule with SH3 domain proteases* (AMSH) can cleave Lys63-linked polyubiquitin chains specifically, and thereby facilitate vesicle trafficking and receptor recycling. *Associated molecule with SH3 domain-like proteases* (AMSH-LP) contains one JAMM core and two conserved insertions. The other members of the JAMM family are *BRCA1/BRCA2-containing complex subunit 36* (BRCC36) (78), *26S proteasome-associated PAD1 homolog1* (POH1/PSMD14), *Myb-like with SWIRM and MPN domains 1* (MYSM1), *MPN domain-containing protein* (MPND), and *COP9 signalosome subunit 5* (CSN5/JAB1) (77,79).

3.3.   Regulation of the TGFβ pathway by ubiquitin system

Ubiquitination of the receptors and Smads tightly regulate TGFβ signaling. Smad ubiquitin regulatory factors (Smurfs) 1 and 2 are critical E3 ubiquitin-protein ligases negatively regulating the TGFβ pathway by promoting TGFβ type I receptor and R-Smad polyubiquitination and degradation. Smurf1 contains a HECT domain, interacts with the TGFβ type I receptor through Smad7 and triggers receptor degradation (80). Smurf1 can target non-activated Smad1 and Smad5 for proteasomal degradation as well, thereby inhibiting BMP signaling (81). Smurf2 can also be recruited by Smad7 to target the TGFβ type I receptor for degradation (82). Smad1 and Smad2 can be ubiquitinated by Smurf2 under steady-state conditions (83,84).

In addition, the tumor necrosis factor receptor-associated factor (TRAF) family ubiquitin enzymes play a critical role in TGFβ signaling. TRAF4 can associate with the TGFβ receptor complex in a Smad7-independent manner, which can rescue receptors from degradation. TRAF4 can also activate non-Smad signaling by ubiquitinating TAK1. Both of these functions promote metastasis of breast cancer cells in zebrafish and mice (85).

In line with the above mentioned ubiquitin-related functions, DUBs have been reported to play three main roles in TGFβ signaling: 1) protect the receptors, R-Smads and Co-Smads from degradation, leading to enhanced TGFβ signaling; 2) deubiquitinate I-Smads thereby inhibiting TGFβ signaling; 3) regulate non-Smad pathways.

4. DUBs in TGFβ pathways and related cancers

Here, we provide a comprehensive review of the DUBs that regulate TGFβ /Smad signaling (schematically depicted in Fig. 4) and discuss DUBs regulation of non-Smad signaling. We will also provide a summary on the action of these DUBs in TGF-β pathways and the gene expression level of them in related cancers in Table 1.

Table 1. Summary of DUBs implicated in TGFβ/BMP signaling and their expression level in cancers.

DUB	Mode of action in TGFβ pathway	Expression level in cancers (compared with normal tissue) (17,114)	
		Overexpression	Underexpression
USP4	Deubiquitinates TGFβ type I receptor (87) and TAK1 (111)	Myeloma, liver, melanoma, brain, bladder, adrenocortical carcinoma (115) (116).	Testicular, lung, head and neck squamous cell carcinoma (HNSCC), renal, brain.
USP11	Deubiquitinates TGFβ type I receptor (88)	Lung, myeloma, HNSCC, skin, colorectal cancer and melanoma (89).	Brain, renal, testis, pancreas, HNSCC.
USP15	Deubiquitinates BMP type I receptor, TGFβ type I receptor (90), and (92) R-Smads (98)	Vulva, brain, breast cancer, lymphoma, ovarian cancer and glioblastoma (90).	Brain, bladder, testicular, liver, melanoma.
UCH37	Deubiquitinates TGFβ type I receptor (94)	Lung, breast, ovarian, vulva, parathyroid.	Brain, pancreas, breast.
OTUB1	Deubiquitinates pSmad2/3 (99), thereby protecting them from degradation (100)	Bladder, lung, prostate, HNSCC, breast cancer.	Brain, HNSCC, testis, cervical, renal, sarcoma.
USP9x	Deubiquitinates Smad4 (117) and Smurf (106)	Brain, gastric, cervical, colon, leukaemia, lymphoma, kidney cancer, prostate cancer, sarcoma (118).	Brain, bladder, testicular, leukaemia, lymphoma.
CYLD	Deubiquitinates SMAD7 (119) deubiquitinates AKT thus reducing stability of Smad3 (112)	Leukaemia, renal, testis, myeloma, breast cancer (120,121), melanoma (122), colon cancer (123), and lung cancer (124).	Brain, ovarian, lung, HNSCC, bladder.
AMSH	Inhibits Smad6 (107),	Lung, liver, bladder, leukaemia, colon.	Leukaemia.
AMSH2	Inhibits Smad7 (108)	Kidney, liver, brain, HNSCC.	Brain, testicular, leukaemia.
A20	Deubiquitinates TAK1, inhibits non-Smad TGFβ pathway MAPK/JNK pathway (113)	HNSCC, leukaemia, lung, brain, cervical.	Bladder, ovary, lung, lymphoma, sarcoma.

4.1. DUBs targeting TGFβ/BMP receptors

USP4 was found to interact with and deubiquitinate the TGFβ type I receptor, thereby opposing the action of Smad7/Smurf2-mediated ubiquitination. USP4 is a very stable protein, which can deubiquitinate itself to control its own stability (86). USP4 can promote TGFβ-induced invasion and metastasis of breast cancer cells in a zebrafish xenograft model. Moreover, this report showed that USP4 was phosphorylated by AKT, leading to increased USP4 membrane-localization and promoting USP4 self-association, leading to enhanced TGFβ signaling. AKT-induced breast cancer cell migration could be inhibited by depletion of USP4 (87).

USP11 has been shown to interact with Smad7 and override the negative effects of Smad7 on the TGFβ pathway. It deubiquitinates the TGFβ type I receptor and thereby potentiates TGFβ signaling (Fig. 4). Depletion of USP11 could inhibit TGFβ induced Smad2/3 phosphorylation, TGFββ mediated transcriptional responses and epithelial to mesenchymal transition (EMT) in NMuMG breast cancer cells (88). USP11 downregulation suppressed tumor growth in a HCT116 colon cancer cell xenograft model and in a UACC-62 melanoma cell xenograft model (89). However, the mechanism by which USP11 regulates the TGFβ pathway in colon cancer and melanoma needs further study.

USP15 has been reported as a key regulator of the TGFβ pathway based on a functional RNAi screen by Seoane's group. USP15 binds to the Smad7-Smurf2 complex and, like USP4 and USP11, deubiquitinates the TGFβ type I receptor, thereby maintaining the stability of this receptor and enhancing TGFβ signaling. A xenograft glioblastoma model showed that the oncogenic capacity of patient-derived glioma-initiating cells could decrease due to the

depletion of USP15. USP15 appears to be a key factor in glioblastoma pathogenesis by regulating the TGFβ pathway (90). Eichhorn et al. found that USP15 not only targets the TGFβ type I receptor complex but also deubiquitinates Smurf2. These authors performed proteomic analysis and found that USP15 deubiquitinates Smurf2 on Lys734, a residue required for Smurf2 catalytic activity, leading to enhanced TGFβ signaling (91). Similar results were reported by Zhang et al, which showed that TRAF4 can promote the recruitment of USP15 to the TGFβ type I receptor, which antagonizes receptor degradation by Smurf2 (85). In addition, USP15 plays a critical role in BMP signaling by interacting with BMP type I receptor and Smad6. Herhaus and co-workers showed that USP15 can interact with and deubiquitinate BMP type I receptors, thereby promoting phosphorylation of Smad1 (92) (Fig. 4). They also showed that depletion of USP15 in Hela cells increased polyubiquitination of BMP type I receptor, and inhibited BMP-mediated Smad1 phosphorylation and BMP target gene transcription. Loss of USP15 in mouse myoblast cells suppressed BMP-induced osteoblast differentiation. Furthermore, they found that USP15 modulates the BMP pathway during *Xenopus* embryogenesis (92).

USP4, USP11 and USP15 are structurally highly similar and contain significant protein sequence similarity (59). All three DUBs play particularly prominent roles in modulating the ubiquitination of TGFβ type I receptor while USP15 and USP11 can also regulate downstream effectors. USP4 can form stable homodimers and can also interact with USP11 and USP15 (Fig. 4). USP4 has been shown to bind directly to TGFβ type I receptor, and is able to recruit USP15 and USP11 to the TGFβ type I receptor (93).

UCH37 binds strongly to Smad7 and weakly to Smad2 and Smad3. It subsequently interacts with Smurf ubiquitin ligases to deubiquitinate the TGFβ type I receptor and modify TGFβ-induced transcription (Fig. 4) (94). UCH37 knockdown inhibits transcription of TGFβ target genes and slows lateral cell migration (96). The interplay between Smurf-mediated ubiquitination and UCH37-mediated deubiquitination can influence cancers that are regulated by the TGFβ pathway (94). Interestingly, it has been shown that UCH37 plays a critical role in TGFβ-induced cell migration but not TGFβ-regulated cell proliferation and EMT (95). In human ovarian cancer, higher expression of UCH37 is associated with tumor recurrence after curative resection (96). Also, UCH37 is associated with poor prognosis of esophageal squamous cell carcinoma patients after curative resection (97).

4.2. DUBs targeting R-Smads

In addition to its effects on the TGFβ and BMP receptors described above, **USP15** can target the DNA-binding domains of R-Smads and antagonise R-Smad monoubiquitination, leading to enhanced activity of TGFβ and BMP pathways (Fig. 4) (98). As mentioned above, USP15 is required for TGFβ and BMP responses in mammalian cells and *Xenopus* embryos. It has been shown that knockdown of USP15 in immortalized HaCaT keratinocytes can impair TGFβ/SMAD-dependent growth arrest. In MDA-MB-231 metastatic breast cancer cells, USP15 is required for TGFβ-induced cell motility.

OTUB1 has been shown to interact with E2 enzymes and antagonize efficient ubiquitin transfer from E2 enzymes to E3 enzymes, thereby inhibiting the ubiquitination of Smad2/3 (Fig. 4) (99). It has been shown that OTUB1 interacts with phosphorylated SMAD2/3 at the C-terminus specifically after TGFβ stimulation. Further studies revealed that endogenous

OTUB1 can inhibit the ubiquitination of phosphorylated Smad2/3 and prevent its proteasomal degradation (Fig. 4). OTUB1 is thereby important for TGFβ-induced gene transcription and cell migration. (100).
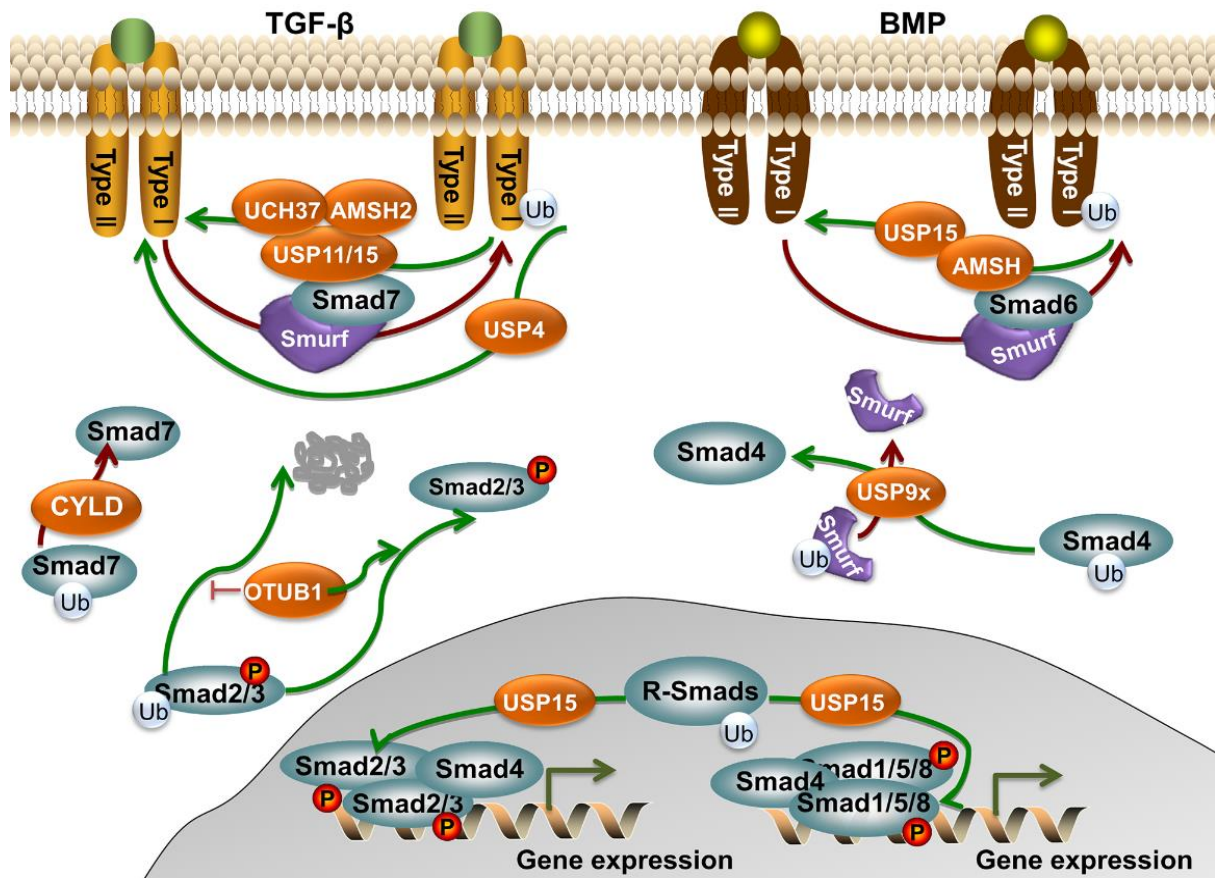

Figure 4. A schematic representation of DUBs regulating Smad signaling. USP4/11/15, UCH37 and AMSH2 deubiquitinate the TGFβ type I receptor which stimulates the activity of the TGFβ/Smad pathway. USP15/AMSH deubiquitinate the BMP type I receptor, which enhances the activity of the BMP pathway. USP15 can target the R-Smad DNA-binding domains and antagonise R-Smad mono-ubiquitination. USP9x deubiquitinates Smad4 and Smurf. CYLD deubiquitinates Smad7. OTUB1 deubiquitinates pSmad2/3 to protect it from proteasomal degradation.

4.3. DUBs targeting Co-Smad

USP9x is an essential DUB for TGFβ signaling by counteracting Smad4 mono-ubiquitination (101). Its counterpart, Ectodermin (Ecto), was reported as a mono-ubiquitinating factor that blocks Smad4 activity (102) (Fig. 4). It was also shown that Ecto binds to Smad2 and Smad3 and disturbs the association between Smad4 and Smad2/3, leading to inhibition of the TGFβ pathway (103). Lysine K519 was identified as the most principal residue for Smad4 mono-ubiquitination *in vivo*, which can inhibit Smad4 by preventing its association with active Smad2/3. USP9x reverses K519 ubiquitination, augmenting the activity of the TGFβ pathway. USP9x was found to be required for TGFβ-induced growth arrest in colon cancer cells and cell migration in breast cancer cells (101). *Drosophila* and mouse knockout models also revealed important functions of USP9x in TGFβ responses. Loss of the USP9x homologue Fat facets in *Drosophila* inhibits the activity of the Smad4 homologue Medea through ubiquitination of Medea on K738 (equivalent to K519 in human Smad4) (104). In mice,

TGFβ-dependent exogenesis was inhibited when USP9x is knocked out in neural progenitors (105). Interestingly, USP9x also has the potential to negatively regulate the TGFβ pathway by deubiquitinating and stabilizing the Smurf1 E3 ligase, depletion of USP9X destabilizes Smurf1 and blocks Smurf1-dependent cell migration in MDA-MB-231 cells. (Fig. 4) (106).

4.4.   DUBs targeting I-Smads

AMSH has been reported to antagonize Smad6 function, and promote BMP signaling (Fig. 4). AMSH was found to be a direct binding partner of Smad6, and not of R-Smads and Co-Smads. Ectopic expression of AMSH enhanced BMP-mediated Smad1 phosphorylation, and increased BMP-induced reporter activity, growth arrest and apoptosis (107). Besides, **AMSH2** can negatively regulate the function of Smad7. It suppresses Smad7 binding to TGFβ type I receptor, thereby preventing TGFβ type I receptor ubiquitination and degradation by the E3 ubiquitin ligase, Smurf1/2 (Fig. 4) (108).

CYLD has been shown to hydrolyse Lys63-linked polyubiquitin chains selectively (109). CYLD also can deubiquitinate Lys63-polyubiquitinated Smad7 (Fig. 4), and thereby inhibit TGFβ signaling and influence the TGFβ-dependent development of regulatory T cells (Tregs). As a result of this, the level of Tregs is increased in CYLD knockout mice (110).

4.5.   Examples of DUB-mediated non-Smad signaling

As mentioned above, **USP4** binds to and deubiquitinates the TGFβ type I receptor and associates with AKT, leading to enhanced TGFβ signaling and AKT-induced breast cancer cell migration (87). USP4 has multiple functions in non-Smad signaling. It can deubiquitinate transforming growth factorβ-activated kinase 1 (TAK1) *in vitro* and *in vivo*. Tumor necrosis factor-α (TNFα) promotes the interaction between USP4 and TAK1 and the deubiquitination of TAK1, leading to the attenuation of TAK1-mediated NF-κB activation. Furthermore, it was found that overexpression of USP4 can inhibit interleukin-1 β (IL-1β), lipopolysaccharide (LPS), and TGFβ-induced NF-κB-dependent luciferase reporter activity and IκB kinase (IKK) phosphorylation. Knockdown of USP4 promoted IL-1β, LPS, and TGFβ-induced NF-κB activation (111).

Lim and co-workers showed that **CYLD** suppresses TGFβ signaling and prevents lung fibrosis by (indirectly) reducing the stability of Smad3, in an AKT, GSK3β and *E3 ligase carboxy terminus of Hsc70-interacting protein* (CHIP)-dependent manner. They also demonstrated that CYLD can deubiquitinate polyubiquitinated AKT, leading to the inhibition of AKT, resulting in activation of GSK3β, which enhances CHIP-induced Smad3 degradation and suppression of the TGFβ pathway (112) .

A20 has been reported to be a negative regulator of non-Smad TGFβ signaling. It was shown that Smad6 recruits A20 to deubiquitinate K63-linked polyubiquitination of TRAF6, leading to inhibition of TGFβ1-induced activation of the TRAF6-TAK1-p38/JNK MAPK pathway in AML-12 mouse liver cells and primary hepatocytes. Knockdown of Smad6 or A20 in cell and animal models maintained TAK1 and p38 MAPK/JNK phosphorylation, leading to increased apoptosis (113).

5. DUB inhibitors

The first drug to target the ubiquitin system as a cancer therapy was the proteasome inhibitor (PI), *Bortezomib* (125). It was approved as a clinical treatment for multiple myeloma achieving US$1.4 billion in worldwide sales in 2009. However, the toxicity and drug resistance limit its efficacy in the clinic (126). Recently, researchers have begun to develop specific inhibitors of DUBs with therapeutic potential (127). Based on the available preclinical data and reported studies, the DUB inhibitors with potential therapeutic relevance to human cancers are shown in Table 2 (128-130).

Table 2. DUBs inhibitors with possible application in human cancers.

DUB inhibitor	Target	Mechanism	Effects related to cancer
b-AP15 (proteasome-inhibitory agent)	UCHL5, USP14	Inhibits the activity of regulatory particle (19S RP) associated UCHL5 and USP14, resulting in accumulation of polyubiquitin (131).	Inhibits tumor progression in human cancer cells and mouse *in vivo* models of solid tumors: breast, lung, colon, and head and neck carcinoma (131).
AC17 (4-arylidene curcumin analogue)	UCHL5, USP14	Irreversibly inhibits the DUB activity of 19S RP-associated UCHL5 and USP14 (132).	Inhibits tumor growth in a lung carcinoma xenograft model with no observable toxicity (132).
Azepan-4-ones (proteasome-inhibitory agent)	UCHL5, USP14	Inhibits the activity of two DUBs, UCHL5 and USP14, that are associated with 19S RP (133).	Effectively treats cancer refractory to conventional chemotherapy and particularly cancers refractory to bortezomib. Examples of cancer types are multiple myeloma and solid tumor malignancies (133).
WP1130 (degrasyn)	USP9x, USP5, USP14, UCHL5	Induces rapid accumulation of polyubiquitinated (K48/K63-linked) proteins into juxtanuclear aggresomes, without affecting 20S proteasome activity (134).	Induces growth arrest and apoptosis in melanoma. Inhibiton of tumor-activated DUBs results in downregulation of antiapoptotic proteins and upregulation of proapoptotic proteins (134).
Tricyclic heterocyclics	USP14	Inhibits the USP14 26S proteasome activity (135)	Inhibits tumorigenesis in cancer by suppressing proteasome activity (136).
P5091	USP7	None reported.	Induces apoptosis in multiple myeloma tumors including bortezomib-relapsed myeloma (137).
USP8i	USP8	Inhibits USP8.	Inhibits USP8 in non-small cell lung carcinoma cells (138).
BA (Betulinic acid)	Multiple	Inhibits multiple DUBs, resulting in accumulation of polyubiquitin, decreased oncoproteins, increased apoptotic cell death (139).	Inhibits tumor growth and promotes apoptosis in a transgenic model of prostate cancer (139).
Isatin O-acyl oximes	UCH-L1	Selectively inhibits UCH-L1	Selective inhibition of UCH-L1 increases proliferation of the H1299 lung tumor cell line (140).

6. Conclusions

In advanced cancers in which TGFβ acts as a tumor promoter, DUBs that activate the TGFβ pathway are regarded as promising therapeutic targets for the development of specific inhibitors. There is increasing interest in this area of drug discovery to complement ongoing efforts to design drugs specifically targeting the ubiquitin system (141). As we have discussed above, USP4 can target the TGFβ type I receptor and promote invasion and metastasis of breast cancer and high USP15 expression correlated with enhanced pSmad2 expression in tissue samples of glioblastoma patients. Moreover, inhibition of USP15 decreased TβRI and pSmad2 concentrations in these cells, thus corroborating the notion that USP15 stabilizes TβRI and promotes TGFβ/Smad2 signaling (142).

In light of these findings, it could be interesting to investigate and develop drugs that specifically target USP4 and USP15. Inhibition of USP4 would be expected to inhibit the invasion and metastasis of breast cancer and drugs that target USP15 could reduce the oncogenic potential of glioblastomas. One of the main stumbling blocks to developing specific DUB inhibitors is that the active site of many DUBs are quite similar and structurally not optimal for small molecule binding, and it may thus be difficult to generate specific DUB inhibitors that target the protease activity directly.

Another challenge of targeting DUBs for therapeutic purposes is that many of DUBs have multiple substrates. Consequently, inhibiting DUB protease activity may be associated with unwanted side-effects. One approach to overcome these limitations would be to identify inhibitors that target a specific DUB-substrate interaction. Ongoing research in this area is already showing promise by modulating DUB activity through targeting of protein–protein interactions (141).

Other DUBs warrant further research with respect to their potential roles in the TGFβ pathway and cancer. For example, USP22 overexpression can promote EMT and TGFβ expression, whereas depletion of USP22 can reverse EMT and reduce metastasis of lung adenocarcinomas. In 76% of 146 lung adenocarcinoma patient specimens, USP22 expression was positive and correlated with TGFβ expression (143). Moreover, USP22 is an oncogene upregulated in multiple cancers. Knockdown of USP22 was found to suppress cell proliferation *in vitro* and tumor growth *in vivo* by inducing G1 phase cell cycle arrest through synergy with TGFβ1 (144).

Up to now, there have been no reports identifying DUBs that target the TGFβ and BMP type II receptors. This could be an interesting line of investigation. Further systematic functional analysis of DUBs could be performed using CRISPR/CAS9 knock out cell lines or conditional knock out mouse models. The development of selective chemical inhibitors for each DUB will also help to elucidate the functions and mechanisms of action of specific DUBs. Finally, further understanding of the functions and mechanisms of the DUBs targeting TGFβ pathway components in specific cancers may lead to a generation of new cancer therapeutics.

Acknowledgements

References

1. Heldin CH, Landstrom M, Moustakas A. Mechanism of TGF-β signaling to growth arrest, apoptosis, and epithelial-mesenchymal transition. Curr Opin Cell Biol 2009;21(2):166-76.
2. Massague J, Blain SW, Lo RS. TGFβ signaling in growth control, cancer, and heritable disorders. Cell 2000;103(2):295-309.
3. Ikushima H, Miyazono K. TGF-β signal transduction spreading to a wider field: a broad variety of mechanisms for context-dependent effects of TGF-β. Cell Tissue Res 347 (2012), pp. 37-49.
4. Akhurst RJ, Padgett RW. Matters of context guide future research in TGFβ superfamily signaling. Sci. Signal 8 (2015), pp. 1-10.
5. Massagué J. TGFβ in cancer. Cell 2008;134(2):215-30.
6. Heldin C-H, Miyazono K, Ten Dijke P. TGF-β signalling from cell membrane to nucleus through SMAD proteins. Nature 1997;390(6659):465-71.
7. Moustakas A, Heldin C-H. Non-Smad TGF-β signals. J Cell Sci 2005;118(16):3573-84.
8. De Boeck M, ten Dijke P. Key role for ubiquitin protein modification in TGFβ signal transduction. Ups J Med Sci 2012;117(2):153-65.
9. Xu P, Liu J, Derynck R. Post-translational regulation of TGF-β receptor and Smad signaling. FEBS Lett 2012;586(14):1871-84.
10. Ciehanover A, Hod Y, Hershko A. A heat-stable polypeptide component of an ATP-dependent proteolytic system from reticulocytes. Biochem Biophys Res Commun 2012;425(3):565-70.
11. Hershko A, Ciechanover A. Mechanisms of intracellular protein breakdown. Annu Rev Biochem 1982;51:335-64.
12. Welchman RL, Gordon C, Mayer RJ. Ubiquitin and ubiquitin-like proteins as multifunctional signals. Nat Rev Mol Cell Biol 2005;6(8):599-609.
13. Ye Y, Blaser G, Horrocks MH, Ruedas-Rama MJ, Ibrahim S, Zhukov AA, et al. Ubiquitin chain conformation regulates recognition and activity of interacting proteins. Nature 2012;492(7428):266-70.
14. Husnjak K, Dikic I. Ubiquitin-binding proteins: decoders of ubiquitin-mediated cellular functions. Annu Rev Biochem 2012;81:291-322.
15. Hershko A, Ciechanover A. The ubiquitin system. Annu Rev Biochem 1998;67:425-479.
16. Nijman SM, Luna-Vargas MP, Velds A, Brummelkamp TR, Dirac AM, Sixma TK, et al. A genomic and functional inventory of deubiquitinating enzymes. Cell 2005;123(5):773-86.
17. Sacco JJ, Coulson JM, Clague MJ, Urbé S. Emerging roles of deubiquitinases in cancer-associated pathways. IUBMB life 2010;62(2):140-57.
18. Yamaguchi T, Kimura J, Miki Y, Yoshida K. The deubiquitinating enzyme USP11 controls an IκB kinase α (IKKα)-p53 signaling pathway in response to tumor necrosis factor α (TNFα). J Biol Chem 2007;282(47):33943-8.
19. Reiley W, Zhang M, Sun S-C. Negative regulation of JNK signaling by the tumor suppressor CYLD. J Biol Chem 2004;279(53):55161-7.
20. Massague J. The transforming growth factor-β family. Annu Rev Cell Biol 1990;6:597-641.
21. Sakaki-Yumoto M, Katsuno Y, Derynck R. TGF-β family signaling in stem cells. Biochim Biophys Acta 2013;1830(2):2280-96.
22. Shipley GD, Pittelkow MR, Wille JJ, Jr., Scott RE, Moses HL. Reversible inhibition of normal human prokeratinocyte proliferation by type β transforming growth factor-growth inhibitor in serum-free medium. Cancer Res 1986;46(4 Pt 2):2068-71.
23. Roberts AB, Anzano MA, Wakefield LM, Roche NS, Stern DF, Sporn MB. Type β transforming growth factor: a bifunctional regulator of cellular growth. Proc Natl Acad Sci U S A 1985;82(1):119-23.
24. Miyazono K. Transforming growth factor-β signaling in epithelial-mesenchymal transition and progression of cancer. Proc Jpn Acad Ser B Phys Biol Sci 2009;85(8):314-23.
25. Derynck R, Muthusamy BP, Saeturn KY. Signaling pathway cooperation in TGF-β-induced epithelial-mesenchymal transition. Curr Opin Cell Biol 2014;31:56-66.

2

26. Derynck R, Goeddel DV, Ullrich A, Gutterman JU, Williams RD, Bringman TS, et al. Synthesis of messenger RNAs for transforming growth factors α and β and the epidermal growth factor receptor by human tumors. Cancer Res 1987;47(3):707-12.

27. Urist MR, Mikulski A, Lietze A. Solubilized and insolubilized bone morphogenetic protein. Proc Natl Acad Sci U S A 1979;76(4):1828-32.

28. Reddi AH. Bone and cartilage differentiation. Curr Opin Genet Dev 1994;4(5):737-44.

29. Salazar VS, Gamer LW, Rosen V. BMP signalling in skeletal development, disease and repair. Nat Rev Endocrinol 2016;12(4):203-21.

30. Rider C, Mulloy B. Bone morphogenetic protein and growth differentiation factor cytokine families and their protein antagonists. Biochem J 2010;429:1-12.

31. Miyazono K, Kamiya Y, Morikawa M. Bone morphogenetic protein receptors and signal transduction. J Biochem 2010;147(1):35-51.

32. Xia Y, Schneyer AL. The biology of activin: recent advances in structure, regulation and function. J Endocrinol 2009;202(1):1-12.

33. Antsiferova M, Werner S. The bright and the dark sides of activin in wound healing and cancer. J Cell Sci 2012;125(Pt 17):3929-37.

34. Wakefield LM, Hill CS. Beyond TGFβ: roles of other TGFβ superfamily members in cancer. Nat Rev Cancer 2013;13(5):328-41.

35. Kim JH, MacLaughlin DT, Donahoe PK. Mullerian inhibiting substance/anti-Mullerian hormone: A novel treatment for gynecologic tumors. Obstet Gynecol Sci 2014;57(5):343-57.

36. Kirsammer G, Strizzi L, Margaryan NV, Gilgur A, Hyser M, Atkinson J, et al. Nodal signaling promotes a tumorigenic phenotype in human breast cancer. Semin Cancer Biol 2014;29:40-50.

37. Davis H, Raja E, Miyazono K, Tsubakihara Y, Moustakas A. Mechanisms of action of bone morphogenetic proteins in cancer. Cytokine Growth Factor Rev 2016;27:81-92.

38. Wrana JL, Attisano L, Wieser R, Ventura F, Massague J. Mechanism of activation of the TGFβ receptor. Nature 1994;370(6488):341-6.

39. Derynck R, Zhang YE. Smad-dependent and Smad-independent pathways in TGF-β family signalling. Nature 2003;425(6958):577-84.

40. Wrana JL, Attisano L, Wieser R, Ventura F, Massague J. Mechanism of activation of the TGF-β receptor. Nature 1994;370(6488):341-7.

41. Moustakas A, Souchelnytskyi S, Heldin C-H. Smad regulation in TGF-β signal transduction. J Cell Sci 2001;114(24):4359-69.

42. Lagna G, Hata A, Hemmati-Brivanlou A, Massague J. Partnership between DPC4 and SMAD proteins in TGF-β signalling pathways. Nature 1996;383(6603):832-6.

43. Nakao A, Imamura T, Souchelnytskyi S, Kawabata M, Ishisaki A, Oeda E, et al. TGF-β receptor-mediated signalling through Smad2, Smad3 and Smad4. EMBO J 1997;16(17):5353-62.

44. Zhang Y, Feng XH, Derynck R. Smad3 and Smad4 cooperate with c-Jun/c-Fos to mediate TGF-β-induced transcription. Nature 1998;394(6696):909-13.

45. Massagué J. TGF-β signal transduction. Annu Rev Biochem 1998;67(1):753-91.

46. Hayashi H, Abdollah S, Qiu Y, Cai J, Xu YY, Grinnell BW, et al. The MAD-related protein Smad7 associates with the TGFβ receptor and functions as an antagonist of TGFβ signaling. Cell 1997;89(7):1165-73.

47. Hata A, Lagna G, Massague J, Hemmati-Brivanlou A. Smad6 inhibits BMP/Smad1 signaling by specifically competing with the Smad4 tumor suppressor. Genes Dev 1998;12(2):186-97.

48. Kavsak P, Rasmussen RK, Causing CG, Bonni S, Zhu H, Thomsen GH, et al. Smad7 binds to Smurf2 to form an E3 ubiquitin ligase that targets the TGF β receptor for degradation. Mol Cell 2000;6(6):1365-75.

49. Ebisawa T, Fukuchi M, Murakami G, Chiba T, Tanaka K, Imamura T, et al. Smurf1 interacts with transforming growth factor-β type I receptor through Smad7 and induces receptor degradation. J Biol Chem 2001;276(16):12477-80.

50. Itoh S, ten Dijke P. Negative regulation of TGF-β receptor/Smad signal transduction. Curr Opin Cell Biol 2007;19(2):176-84.

51. Moustakas A, Heldin CH. Non-Smad TGF-β signals. J Cell Sci 2005;118(Pt 16):3573-84.

52. Pickart CM, Eddins MJ. Ubiquitin: structures, functions, mechanisms. Biochim Biophys Acta 2004;1695(1):55-72.

53. Weissman AM. Themes and variations on ubiquitylation. Nat Rev Mol Cell Biol 2001;2(3):169-78.

54. Hershko A, Heller H, Elias S, Ciechanover A. Components of ubiquitin-protein ligase system. Resolution, affinity purification, and role in protein breakdown. J Biol Chem 1983;258(13):8206-14.

55. Hochstrasser M. Origin and function of ubiquitin-like proteins. Nature 2009;458(7237):422-9.

56. Pickart CM. Mechanisms underlying ubiquitination. Annual review of biochemistry 2001;70(1):503-33.

57. Komander D, Rape M. The ubiquitin code. Annu Rev Biochem 2012;81:203-29.

58. Ikeda F, Dikic I. Atypical ubiquitin chains: new molecular signals. EMBO Rep 2008;9(6):536-42.

59. Komander D, Clague MJ, Urbé S. Breaking the chains: structure and function of the deubiquitinases. Nat Rev Mol Cell Biol 2009;10(8):550-63.

60. Chernorudskiy AL, Gainullin MR. Ubiquitin system: direct effects join the signaling. Sci Signal 2013;6(280):pe22.

61. Scheel H. Comparative analysis of the ubiquitin-proteasome system in Homo sapiens and Saccharomyces cerevisiae: Universität zu Köln; 2005.

62. Burrows JF, McGrattan MJ, Rascle A, Humbert M, Baek K-H, Johnston JA. DUB-3, a cytokine-inducible deubiquitinating enzyme that blocks proliferation. J Biol Chem 2004;279(14):13993-4000.

63. Storer AC, Ménard R. Catalytic mechanism in papain family of cysteine peptidases. Methods Enzymol 1994;244:486.

64. Ye Y, Scheel H, Hofmann K, Komander D. Dissection of USP catalytic domains reveals five common insertion points. Mol Biosyst 2009;5(12):1797-808.

65. Thorne C, Eccles RL, Coulson JM, Urbé S, Clague MJ. Isoform-Specific Localization of the Deubiquitinase USP33 to the Golgi Apparatus. Traffic 2011;12(11):1563-74.

66. Bonnet J, Romier C, Tora L, Devys D. Zinc-finger UBPs: regulators of deubiquitylation. Trends Biochem Sci 2008;33(8):369-75.

67. Pai M-T, Tzeng S-R, Kovacs JJ, Keaton MA, Li SS-C, Yao T-P, et al. Solution structure of the Ubp-M BUZ domain, a highly specific protein module that recognizes the C-terminal tail of free ubiquitin. J Mol Biol 2007;370(2):290-302.

68. Reyes-Turcu FE, Horton JR, Mullally JE, Heroux A, Cheng X, Wilkinson KD. The ubiquitin binding domain ZnF UBP recognizes the C-terminal diglycine motif of unanchored ubiquitin. Cell 2006;124(6):1197-208.

69. Johnston SC, Riddle SM, Cohen RE, Hill CP. Structural basis for the specificity of ubiquitin C-terminal hydrolases. EMBO J 1999;18(14):3877-87.

70. Zi-Ren Z, Yu-Hang Z, Shuai L, Ai-Xin S, Hong-Yu H. Length of the active-site crossover loop defines the substrate specificity of ubiquitin C-terminal hydrolases for ubiquitin chains. Biochem J 2012;441(1):143-9.

71. Quesada V, Ordóñez GR, Sanchez LM, Puente XS, López-Otín C. The Degradome database: mammalian proteases and diseases of proteolysis. Nucleic Acids Res 2009;37(suppl 1):D239-43.

72. Harhaj EW, Dixit VM. Regulation of NF-κB by deubiquitinases. Immunol Rev 2012;246(1):107-24.

73. Shembade N, Harhaj EW. Regulation of NF-&kgr; B signaling by the A20 deubiquitinase. Cell Mol Immunol 2012;9(2):123-30.

74. Nicastro G, Menon RP, Masino L, Knowles PP, McDonald NQ, Pastore A. The solution structure of the Josephin domain of ataxin-3: structural determinants for molecular recognition. Proc Natl Acad Sci U S A 2005;102(30):10493-8.

75. Mao Y, Senic-Matuglia F, Di Fiore PP, Polo S, Hodsdon ME, De Camilli P. Deubiquitinating function of ataxin-3: insights from the solution structure of the Josephin domain. Proc Natl Acad Sci U S A 2005;102(36):12700-5.

76. Kuhlbrodt K, Janiesch PC, Kevei É, Segref A, Barikbin R, Hoppe T. The Machado-Joseph disease deubiquitylase ATX-3 couples longevity and proteostasis. Nat Cell Biol 2011;13(3):273-81.

77. Sato Y, Yoshikawa A, Yamagata A, Mimura H, Yamashita M, Ookata K, et al. Structural basis for specific cleavage of Lys 63-linked polyubiquitin chains. Nature 2008;455(7211):358-62.

78. Dong Y, Hakimi M-A, Chen X, Kumaraswamy E, Cooch NS, Godwin AK, et al. Regulation of BRCC, a holoenzyme complex containing BRCA1 and BRCA2, by a signalosome-like subunit and its role in DNA repair. Mol Cell 2003;12(5):1087-99.

79. Cope GA, Suh GS, Aravind L, Schwarz SE, Zipursky SL, Koonin EV, et al. Role of predicted metalloprotease motif of Jab1/Csn5 in cleavage of Nedd8 from Cul1. Science 2002;298(5593):608-11.

80. Ebisawa T, Fukuchi M, Murakami G, Chiba T, Tanaka K, Imamura T, et al. Smurf1 interacts with transforming growth factor-β type I receptor through Smad7 and induces receptor degradation. J Biol Chem 2001;276(16):12477-80.

81. Zhu H, Kavsak P, Abdollah S, Wrana JL, Thomsen GH. A SMAD ubiquitin ligase targets the BMP pathway and affects embryonic pattern formation. Nature 1999;400(6745):687-93.

82. Kavsak P, Rasmussen RK, Causing CG, Bonni S, Zhu H, Thomsen GH, et al. Smad7 binds to Smurf2 to form an E3 ubiquitin ligase that targets the TGFβ receptor for degradation. Mol Cell 2000;6(6):1365-75.

83. Lin X, Liang M, Feng X-H. Smurf2 is a ubiquitin E3 ligase mediating proteasome-dependent degradation of Smad2 in transforming growth factor-β signaling. J Biol Chem 2000;275(47):36818-22.

84. Zhang Y, Chang C, Gehling DJ, Hemmati-Brivanlou A, Derynck R. Regulation of Smad degradation and activity by Smurf2, an E3 ubiquitin ligase. Proc Natl Acad Sci U S A 2001;98(3):974-9.

85. Zhang L, Zhou F, de Vinuesa AG, de Kruijf EM, Mesker WE, Hui L, et al. TRAF4 promotes TGF-β receptor signaling and drives breast cancer metastasis. Mol Cell 2013;51(5):559-72.

86. Wada K, Kamitani T. UnpEL/Usp4 is ubiquitinated by Ro52 and deubiquitinated by itself. Biochem Biophys Res Commun 2006;342(1):253-8.

87. Zhang L, Zhou F, Drabsch Y, Gao R, Snaar-Jagalska BE, Mickanin C, et al. USP4 is regulated by AKT phosphorylation and directly deubiquitylates TGF-β type I receptor. Nat Cell Biol 2012;14(7):717-26.

88. Al-Salihi MA, Herhaus L, Macartney T, Sapkota GP. USP11 augments TGFβ signalling by deubiquitylating ALK5. Open Biol 2012;2(6):120063.

89. Lee E, Seong D, Seo J, Jeong M, Lee H, Song J. USP11-dependent selective cIAP2 deubiquitylation and stabilization determine sensitivity to Smac mimetics. Cell Death Differ 2015.

90. Eichhorn PJ, Rodón L, Gonzàlez-Juncà A, Dirac A, Gili M, Martínez-Sáez E, et al. USP15 stabilizes TGF-β receptor I and promotes oncogenesis through the activation of TGF-β signaling in glioblastoma. Nat Med 2012;18(3):429-35.

91. Iyengar PV, Jaynes P, Rodon L, Lama D, Law KP, Lim YP, et al. USP15 regulates SMURF2 kinetics through C-lobe mediated deubiquitination. Sci Rep 2015;5:14733.

92. Herhaus L, Al-Salihi MA, Dingwell KS, Cummins TD, Wasmus L, Vogt J, et al. USP15 targets ALK3/BMPR1A for deubiquitylation to enhance bone morphogenetic protein signalling. Open Biol 2014;4(5):140065.

93. Zhang L, Zhou F, de Vinuesa AG, de Kruijf EM, Mesker WE, Hui L, et al. TRAF4 promotes TGF-β receptor signaling and drives breast cancer metastasis. Mol Cell 51 (2013), pp. 559-572.

94. Wicks SJ, Haros K, Maillard M, Song L, Cohen RE, ten Dijke P, et al. The deubiquitinating enzyme UCH37 interacts with Smads and regulates TGF-β signalling. Oncogene 2005;24(54):8080-4.

95. Cutts AJ, Soond SM, Powell S, Chantry A. Early phase TGFβ receptor signalling dynamics stabilised by the deubiquitinase UCH37 promotes cell migratory responses. Int J Biochem Cell Biol 2011;43(4):604-12.

96. Wang L, Chen Y-J, Xu K, Wang Y-Y, Shen X-Z, Tu R-Q. High expression of UCH37 is significantly associated with poor prognosis in human epithelial ovarian cancer. Tumour Biol 2014;35(11):11427-33.

97. Chen Y, Fu D, Xi J, Ji Z, Liu T, Ma Y, et al. Expression and clinical significance of UCH37 in human esophageal squamous cell carcinoma. Dig Dis Sci 2012;57(9):2310-7.

98. Inui M, Manfrin A, Mamidi A, Martello G, Morsut L, Soligo S, et al. USP15 is a deubiquitylating enzyme for receptor-activated SMADs. Nat Cell Biol 2011;13(11):1368-75.

99. Wiener R, Zhang X, Wang T, Wolberger C. The mechanism of OTUB1-mediated inhibition of ubiquitination. Nature 2012;483(7391):618-22.

100. Herhaus L, Al-Salihi M, Macartney T, Weidlich S, Sapkota GP. OTUB1 enhances TGFβ signalling by inhibiting the ubiquitylation and degradation of active SMAD2/3. Nat Commun 2013;4.

101. Dupont S, Mamidi A, Cordenonsi M, Montagner M, Zacchigna L, Adorno M, et al. FAM/USP9x, a deubiquitinating enzyme essential for TGFβ signaling, controls Smad4 monoubiquitination. Cell 2009;136(1):123-35.

102. Dupont S, Zacchigna L, Cordenonsi M, Soligo S, Adorno M, Rugge M, et al. Germ-layer specification and control of cell growth by Ectodermin, a Smad4 ubiquitin ligase. Cell 2005;121(1):87-99.

103. Heldin C-H, Moustakas A. A new twist in Smad signaling. Dev Cell 2006;10(6):685-6.

104. Stinchfield MJ, Takaesu NT, Quijano JC, Castillo AM, Tiusanen N, Shimmi O, et al. Fat facets deubiquitylation of Medea/Smad4 modulates interpretation of a Dpp morphogen gradient. Development 2012;139(15):2721-9.

105. Stegeman S, Jolly LA, Premarathne S, Gecz J, Richards LJ, Mackay-Sim A, et al. Loss of Usp9x disrupts cortical architecture, hippocampal development and TGFβ-mediated axonogenesis. PLoS One 2013;8(7):e68287.

106. Xie Y, Avello M, Schirle M, McWhinnie E, Feng Y, Bric-Furlong E, et al. Deubiquitinase FAM/USP9X interacts with the E3 ubiquitin ligase SMURF1 protein and protects it from ligase activity-dependent self-degradation. J Biol Chem 2013;288(5):2976-85.

107. Itoh F, Asao H, Sugamura K, Heldin CH, ten Dijke P, Itoh S. Promoting bone morphogenetic protein signaling through negative regulation of inhibitory Smads. EMBO J 2001;20(15):4132-42.

108. Ibarrola N, Kratchmarova I, Nakajima D, Schiemann WP, Moustakas A, Pandey A, et al. Cloning of a novel signaling molecule, AMSH-2, that potentiates transforming growth factor β signaling. BMC Cell Biol 2004;5(1):2.

109. Komander D, Lord CJ, Scheel H, Swift S, Hofmann K, Ashworth A, et al. The structure of the CYLD USP domain explains its specificity for Lys63-linked polyubiquitin and reveals a B box module. Mol Cell 2008;29(4):451-64.

110. Zhao Y, Thornton AM, Kinney MC, Ma CA, Spinner JJ, Fuss IJ, et al. The deubiquitinase CYLD targets Smad7 protein to regulate transforming growth factor β (TGF-β) signaling and the development of regulatory T cells. J Biol Chem 2011;286(47):40520-30.

110. Fan Y, Yu Y, Mao R, Tan X, Xu G, Zhang H, et al. USP4 targets TAK1 to downregulate TNFα-induced NF-κB activation. Cell Death Differ 2011;18(10):1547-60.

112. Lim JH, Jono H, Komatsu K, Woo C-H, Lee J, Miyata M, et al. CYLD negatively regulates transforming growth factor-β-signalling via deubiquitinating Akt. Nat Commun 2012;3:771.

113. Jung SM, Lee J-H, Park J, Oh YS, Lee SK, Park JS, et al. Smad6 inhibits non-canonical TGF-β1 signalling by recruiting the deubiquitinase A20 to TRAF6. Nature Commun 2013;4.

114. Rhodes DR, Kalyana-Sundaram S, Mahavisno V, Varambally R, Yu J, Briggs BB, et al. Oncomine 3.0: genes, pathways, and networks in a collection of 18,000 cancer gene expression profiles. Neoplasia 2007;9(2):166-80.

115. Velázquez-Fernández D, Laurell C, Geli J, Höög A, Odeberg J, Kjellman M, et al. Expression profiling of adrenocortical neoplasms suggests a molecular signature of malignancy. Surgery 2005;138(6):1087-94.

116. Laurell C, Velázquez-Fernández D, Lindsten K, Juhlin C, Enberg U, Geli J, et al. Transcriptional profiling enables molecular classification of adrenocortical tumours. Eur J Endocrinol 2009;161(1):141-52.

117. Dupont S, Mamidi A, Cordenonsi M, Montagner M, Zacchigna L, Adorno M, et al. FAM/USP9x, a deubiquitinating enzyme essential for TGFβ signaling, controls Smad4 monoubiquitination. Cell 2009;136(1):123-35.

118. Luise C, Capra M, Donzelli M, Mazzarol G, Jodice MG, Nuciforo P, et al. An atlas of altered expression of deubiquitinating enzymes in human cancer. PloS One 2011;6(1):e15891.

119. Zhao Y, Thornton AM, Kinney MC, Ma CA, Spinner JJ, Fuss IJ, et al. The deubiquitinase CYLD targets Smad7 protein to regulate transforming growth factor β (TGF-β) signaling and the development of regulatory T cells. J Biol Chem 2011;286(47):40520-30.

120. Weigelt B, Peterse JL, Van't Veer LJ. Breast cancer metastasis: markers and models. Nat Rev Cancer 2005;5(8):591-602.

121. Hutti JE, Shen RR, Abbott DW, Zhou AY, Sprott KM, Asara JM, et al. Phosphorylation of the tumor suppressor CYLD by the breast cancer oncogene IKKε promotes cell transformation. Mol Cell 2009;34(4):461-72.

122. Massoumi R, Kuphal S, Hellerbrand C, Haas B, Wild P, Spruss T, et al. Down-regulation of CYLD expression by Snail promotes tumor progression in malignant melanoma. J Exp Med 2009;206(1):221-32.

123. Zhang J, Stirling B, Temmerman ST, Ma CA, Fuss IJ, Derry JM, et al. Impaired regulation of NF-κB and increased susceptibility to colitis-associated tumorigenesis in CYLD-deficient mice. J Clin Invest 2006;116(11):3042.

124. Lim JH, Stirling B, Derry J, Koga T, Jono H, Woo C-H, et al. Tumor suppressor CYLD regulates acute lung injury in lethal Streptococcus pneumoniae infections. Immunity 2007;27(2):349-60.

125. Adams J. Development of the proteasome inhibitor PS-341. Oncologist 2002;7(1):9-16.

126. Chauhan D, Catley L, Li G, Podar K, Hideshima T, Velankar M, et al. A novel orally active proteasome inhibitor induces apoptosis in multiple myeloma cells with mechanisms distinct from Bortezomib. Cancer cell 2005;8(5):407-19.

127. Buac D, Shen M, Schmitt S, Kona FR, Deshmukh R, Zhang Z, et al. From bortezomib to other inhibitors of the proteasome and beyond. Curr Pharm Des 2013;19(22):4025.

128. D'Arcy P, Linder S. Molecular pathways: translational potential of deubiquitinases as drug targets. Clin Cancer Res 2014;20(15):3908-14.

129. Farshi P, Deshmukh RR, Nwankwo JO, Arkwright RT, Cvek B, Liu J, et al. Deubiquitinases (DUBs) and DUB inhibitors: a patent review. Expert Opin Ther Pat 2015:1-18.

130. Love KR, Catic A, Schlieker C, Ploegh HL. Mechanisms, biology and inhibitors of deubiquitinating enzymes. Nat Chem Biol 2007;3(11):697-705.

131. D'Arcy P, Brnjic S, Olofsson MH, Fryknäs M, Lindsten K, De Cesare M, et al. Inhibition of proteasome deubiquitinating activity as a new cancer therapy. Nat Med 2011;17(12):1636-40.

132. Zhou B, Zuo Y, Li B, Wang H, Liu H, Wang X, et al. Deubiquitinase inhibition of 19S regulatory particles by 4-arylidene curcumin analog AC17 causes NF-κB inhibition and p53 reactivation in human lung cancer cells. Mol Cancer Ther 2013;12(8):1381-92.

133. Lesinski GB, Raig ET, Guenterberg K, Brown L, Go MR, Shah NN, et al. IFN-α and bortezomib overcome Bcl-2 and Mcl-1 overexpression in melanoma cells by stimulating the extrinsic pathway of apoptosis. Cancer Res 2008;68(20):8351-60.

134. Kapuria V, Peterson LF, Fang D, Bornmann WG, Talpaz M, Donato NJ. Deubiquitinase inhibition by small-molecule WP1130 triggers aggresome formation and tumor cell apoptosis. Cancer Res 2010;70(22):9265-76.

135. Finley D. Recognition and processing of ubiquitin-protein conjugates by the proteasome. Annu Review Biochem 2009;78:477.

136. Finley DJ, King RW, Lee B-H, Lee MJ, Gahman TC. Compositions and Methods for Enhancing Proteasome Activity. Google Patents; 2011;WO2011094545A3.

137. Chauhan D, Tian Z, Nicholson B, Kumar KS, Zhou B, Carrasco R, et al. A small molecule inhibitor of ubiquitin-specific protease-7 induces apoptosis in multiple myeloma cells and overcomes bortezomib resistance. Cancer Cell 2012;22(3):345-58.

138. Byun S, Lee S-Y, Lee J, Jeong C-H, Farrand L, Lim S, et al. USP8 is a novel target for overcoming gefitinib resistance in lung cancer. Clin Cancer Res 2013;19(14):3894-904.

139.   Reiner T, Parrondo R, de Las Pozas A, Palenzuela D, Perez-Stable C. Betulinic acid selectively increases protein degradation and enhances prostate cancer-specific apoptosis: possible role for inhibition of deubiquitinase activity. PLoS One 2013;8(2):e56234.

140.   Liu Y, Lashuel HA, Choi S, Xing X, Case A, Ni J, et al. Discovery of inhibitors that elucidate the role of UCH-L1 activity in the H1299 lung cancer cell line. Chem Biol 2003;10(9):837-46.

141.   Cohen P, Tcherpakov M. Will the ubiquitin system furnish as many drug targets as protein kinases? Cell 2010;143(5):686-93.

142.   Eichhorn PJ, Rodon L, Gonzalez-Junca A, Dirac A, Gili M, Martinez-Saez E, et al. USP15 stabilizes TGF-β receptor I and promotes oncogenesis through the activation of TGF-β signaling in glioblastoma. Nat Med 2012;18(3):429-35.

143.   Hu J, Yang D, Zhang H, Liu W, Zhao Y, Lu H, et al. USP22 promotes tumor progression and induces epithelial–mesenchymal transition in lung adenocarcinoma. Lung Cancer 2015;88(3):239-45.

144.   Ji M, Shi H, Xie Y, Zhao Z, Li S, Chang C, et al. Ubiquitin specific protease 22 promotes cell proliferation and tumor growth of epithelial ovarian cancer through synergy with transforming growth factor β1. Oncol Rep 2015;33(1):133-40.

2

Chapter 3

Invasive Behavior of Human Breast Cancer Cells in Embryonic Zebrafish

Jiang Ren[1, *], Sijia Liu[1, *], Chao Cui[1,] and Peter ten Dijke[1]

[1]Department of Molecular Cell Biology, Leiden University Medical Center, The Netherlands

Chapter 3

Abstract:

In many cases cancer patients do not die of a primary tumor but rather because of metastasis. Although numerous rodent models are available for studying cancer metastasis *in vivo*, other efficient, reliable, low-cost models are needed to quickly access the potential effect of (epi)genetic changes or pharmacological compounds. As such, we illustrate and explain the feasibility of xenograft models using human breast cancer cells injected into zebrafish embryos that support this goal. Under the microscope, fluorescent protein or chemically labeled human breast cancer cells are transplanted into transgenic zebrafish embryos Tg (*fli:GFP*) at the site of the perivitelline space or duct of Cuvier (Doc) 48 h after fertilization. Shortly afterwards, the temporal-spatial process of cancer cell invasion, dissemination, and metastasis in the living fish body is visualized under a fluorescent microscope. The models using different injection sites, i.e. perivetelline space or Doc, are complementary to one another, reflecting the early stage (intravastion step) and late stage (extravasation step) in the multistep metastatic cascade of events. Moreover, peritumoral and intratumoral angiogenesis can be observed with injection into the perivitelline space. The entire experimental period is no more than 8 days. These two models combine cell labeling, micro-transplantation, and fluorescence imaging techniques, enabling rapid evaluation of cancer metastasis in response to genetic and pharmacological manipulations.

Introduction:

Overt cancer metastasis in the clinic comprises a series of complex and multi-step events known as the 'metastatic cascade'. The cascade has been extensively reviewed and can be dissected into successive steps: local invasion, intravasation, dissemination, arrest, extravasation, and colonization (1,2). Better understanding of the pathogenesis of cancer metastasis and the development of potential treatment strategies *in vivo* require robust host models of cancer cell spread. Rodent models are well established and widely used to evaluate metastasis (3), but these approach have low efficiency, ethical limitations, and are costly as a forefront model to determine whether a particular manipulation could affect the metastatic phenotype. Other efficient, reliable, low-cost models are needed to quickly access the potential effect of (epi)genetic changes or pharmacological compounds. Due to the high genetic homology to humans and transparency of the embryos, the zebrafish (*Dano rerio*) has emerged as an important vertebrate model and is being applied increasingly in studying developmental processes, microbe-host interactions, human disease, drug screening, and other areas (4). The cancer metastasis models established in zebrafish may provide ideal solutions to the shortcomings of rodent models (5,6).

Although spontaneous neoplasia is scarcely discovered in wild zebrafish (7), there are several longstanding techniques to induce desired cancer in zebrafish. Carcinogen-induced gene mutations or signaling pathways-activation can model carcinogenesis histologically and molecularly resembling human disease in zebrafish (7-9). By taking advantage of diverse forward and reverse genetic manipulations of oncogenes or tumor suppressors, (transgenic) zebrafish also have enabled potential studies of cancer formation and maintenance (6,10). The induced cancer models in zebrafish cover a broad spectrum of cancer types in digestive, reproductive, blood, nervous systems, as well as the epithelium(6).

Invasive behavior of human breast cancer cells in embryonic zebrafish

The utilization of zebrafish in cancer research has expanded recently by the establishment of human tumor cell xenograft models in this organism. This was first reported with human metastatic melanoma cells that were successfully engrafted in zebrafish embryos at blastula stage in 2005 (11). Several independent laboratories have validated the feasibility of this pioneering work by introduction of a diverse range of mammalian cancer cells lines into zebrafish at various sites and developmental stages (5). For example, injection near the blastodisk and blastocyst of blastula stage, injection into the yolk sac, perivitelline space, duct of Cuvier (Doc), and posterior cardinal vein of 6 h to 5 day old embryo, and injection into peritoneal cavity of 30 days old immunosuppressed larvae (5,12). Additionally, allogeneic tumor transplantations were also reported in zebrafish (12,13). One of the great advantages of using xenografts is that the engrafted cancer cells can be easily fluorescently labeled and distinguished from normal cells. Hence, investigation into dynamic behaviors of microtumor formation (14), cell invasion and metastasis (15-17), tumor-induced angiogenesis (15,18), and interaction between cancer cells and host factors (17) can be clearly visualized in the live fish body, especially when transgenic zebrafish lines are applied (5).

Inspired by the high potential of zebrafish xenograft models in evaluating metastasis, we demonstrated transvascular extravasation properties of different breast cancer cell lines into tail fin area of Tg (*fli:GFP*) zebrafish embryos by Doc injection (16). The role of transforming growth factor-β (TGF-β) (16) and bone morphogenetic protein (BMP) (19) signaling pathway in pro-/anti-breast cancer cell invasion and metastasis were also investigated in this model. Moreover, we also recapitulated the intravasation ablity of various breast cancer cell lines into circulation using xenograft zebrafish model by perivitelline space injection.

This article presents detailed protocols for zebrafish xenograft models based upon injection of human breast cancer cells into perivitelline space or Doc injection. Using high-resolution fluorescence imaging, we show the representative process of intravastion into blood vessel and invasive behavior of different human breast cancer cells from blood vessel into avascular tailfin area.

Protocol:

All research using zebrafish, including housing and experiments, was carried out according to the international guidelines and approved by the local Institutional Committee for Animal Welfare (Dier Ethische Commissie (DEC) of the Leiden University Medical Center. Note: As summarized in Figure 1, the protocol is roughly dissected into four steps, embryo collection (Figure 1A), microinjection (Figure 1B), screening (Figure 1C), and analysis (Figure 1D).

1. Prepare the injection needles

Prepare injection needles with borosilicate glass microcapillary. Put the microcapillary in a micropipette puller device with the following settings: air pressure 500; heat 650; pull 100; velocity 200; time 40. Keep the injection needles in a needle holder plate until used for injection.

---

2. Prepare of the fluorescent genetically labeled breast cancer cells for injection

1. Culture human breast cancer MDA-MB-231 cells at 37 °C in DMEM-high glucose media containing L-glutamine, 10% fetal bovine serum and 1:100 Penicillin-Streptomycin-Glutamine.

2. Culture breast epithelial cell line MCF10A (M1), MCF10Aras (M2) at 37 °C in DMEM/F12 media containing L-glutamine, with 5% horse serum, 20 ng/mL epidermal growth factor, 10 mg/mL insulin, 100 ng/mL cholera enterotoxin, 0.5 mg/mL hydrocortisone, and 1:100 Pen-Strep.

3. Produce mCherry lentivirus by co-transfecting PLKO-mCherry, pCMV-VSVG, pMDLg-RRE (gag/pol), and pRSV-REV plasmid into HEK293T cells. Harvest cell supernatants 48 h after transfection and store at -80 °C.

4. Infect MDA-MB-231 and M2 cells at 30% confluence for 24 h with lentiviral supernatants diluted 1:1 with normal culture medium in the presence of 5 ng/mL polybrene.

5. Select single cell clones by diluting cells in a 96-well plate, which allows the outgrowth of isolated cell clones, until obtaining the stable mCherry-expressing cell lines.

6. Culture one T75 flask of cells for injection. Harvest the cells at 80% confluence by 0.5% trypsin-EDTA treatment. Wash the cells with 1× PBS 2-3 times.

7. Re-suspend the cells in about 200 µL PBS. Store at 4 °C for less than 5 h before injection.
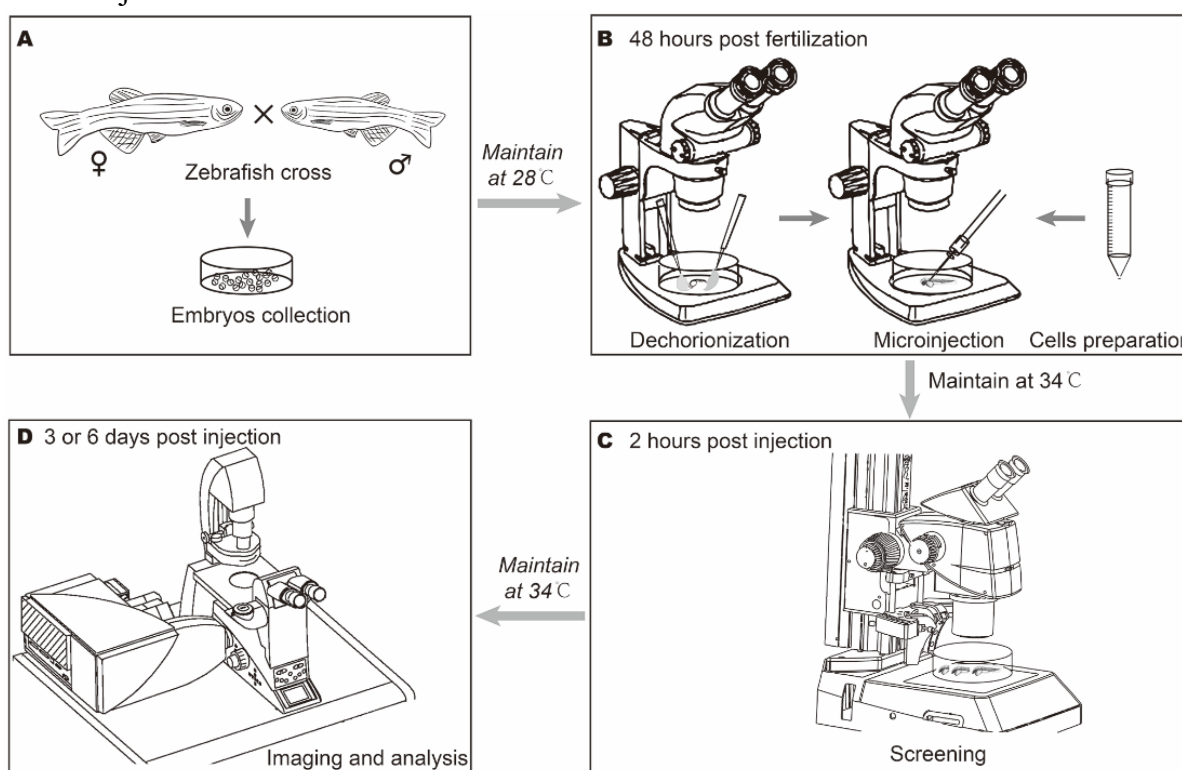
Figure 1. Main steps for investigating the invasive behavior of breast cancer cells in embryonic zebrafish. (A) After crossing parental zebrafish overnight, Tg (*fli1:GFP*) zebrafish embryos were collected the following morning and maintained at 28 °C. (B) The embryos were dechorionated with fine tweezers under a stereo microscope 48 h post fertilization (hpf). The labeled breast cancer cells were collected and re-suspended in a small amount of PBS. After well-preparation, suspended cells were loaded into one needle. Approximately 400

cells were injected into the duct of Cuvier (Doc) of the perivitelline space under a stereo microscope. The injected embryos were maintained at 34 °C. (C) 2 hours post-njection (hpi), the embryos were subjected to careful screening under a fluorescence stereo microscope. The embryos were maintained at 34 °C for 3 or 6 d. During the interval, embryos could be subjected to designed treatment. (D) Cancer cell dissemination by perivitelline space injection or invasion by Doc injection was detected, counted, and imaged by confocal microscopy 3 or 6 days post-njection (dpi).

3. Prepare Zebrafish Embryos for Injection

1. Set up zebrafish breeding pairs and collect embryos as shown in a previous Jove article by Rosen et al (20).

2. Select the embryos that are at 0-4 hpf by removing the unfertilized and abnormal embryos. Keep the embryos in a petri-dish filled with egg water (60 µg/mL sea salts; ~60 embryos/dish) and incubate at 28 °C.

3. Dechorionate the embryos with fine tweezers at 48 hpf.

4. Anesthetize the embryos with 200 µg/mL 3-aminobenzoic acid buffer approximately 10 min prior to injection, but no longer than 2 h prior to injection.
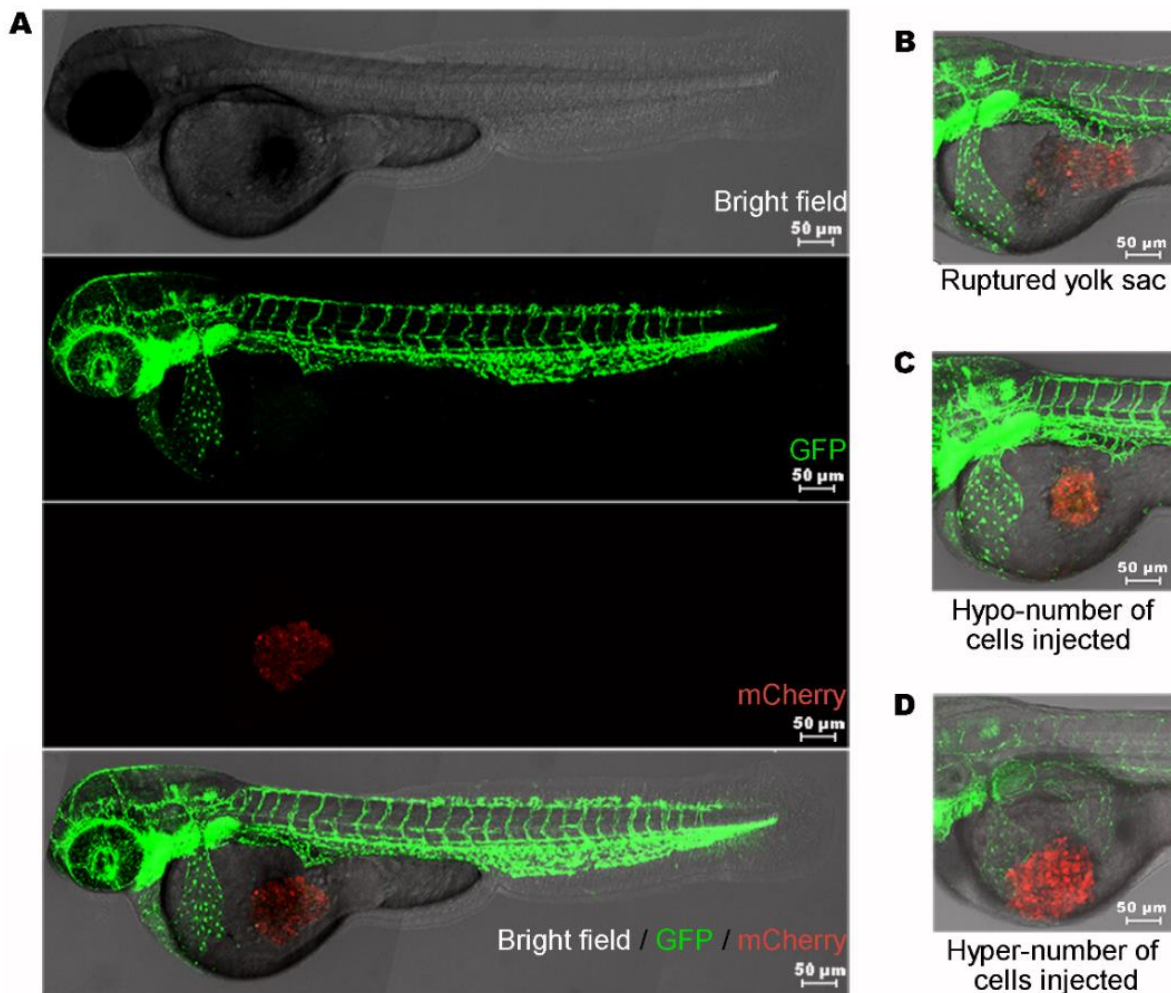
Figure 2. Perivitelline space injection site and common errors. (A) Approximately 400 mCherry-labeled cells (MDA-MB-231) were injected into the perivitelline space. The Brightfield (upper most), green vasculature (middle upper), and red cell mass (middle lower) of injected zebrafish embryos were captured by confocal microscope. The merged image (lower most) of three channels shows the stereo location of the cell mass in the embryo. (B) The cells did not target the perivitelline space appropriately. The yolk sac was ruptured. (C) A hypo-number of injected cells (much less than 400). (D) Hyper-number of injected cells (much more than 400). The cell mass was too close to the duct of Cuvier, which has a broad blood stream. Scale bar = 50 µm.

4. Perivitelline space injection of human breast cancer cells

1. Load 15 µL of the cell suspension into an injection needle. Mount the needle onto the micromanipulator and break off the needle tip with fine tweezers to obtain a tip opening diameter of 5-10 µm.

2. Use a pneumatic picopump and a manipulator to perform microinjection. Adjust the picopump to inject 400 cells each time. Prior to injection, count the cell numbers manually by injecting the cells on the top of a dish containing 1% agarose.

3. Line up anesthetized embryos (2-3 days post fertilization (dpf)) on a flat 1% agarose injecting plate.

4. Orient the injection plate by hand during injections to place the embryos in the preferred position for inserting the needle (*i.e.*, diagonally).

5. Point the needle tip to the injection site and gently insert the needle tip into the perivitelline space between the yolk sac and the periderm of the zebrafish embryo (Figure 2A).

6. Inject approximately 400 mCherry-labeled tumor cells. Make sure that the yolk sac is not ruptured to avoid implantation into the yolk sac.

5. Doc injection of human breast cancer cells

1. Prepare injection needle and zebrafish embryos as described previously.

2. Use a 45° needle angle so that the Doc can be approached from the dorsal side of the embryo.

3. Insert the needle into the starting point of the Doc (Figure 3A) just dorsal to where the duct starts broadening over the yolk sac and inject ~400 cells. The injection is correct if the volume within the duct expands directly after the pulse and the yolk sac.
   Note: Several consecutive injections can be performed without extracting the needle.

4. Transfer the injected zebrafish embryos to egg water.
   Note: As considerable variation exists among individual zebrafish embryos; relatively large number of zebrafish embryos should be injected with cancer cells.

5. Maintain the zebrafish embryos at 34 °C to accommodate the optimal temperature requirements for fish and mammalian cells.

6. Screen the injected embryos.

1. Screen each fish under a fluorescence stereo microscope at 2 h post-injection (hpi) for perivitelline space injection (Figure 2) or at 2-24 hpi for Doc injection (Figure 2), to ensure all the embryos are injected with similar number of tumor cells. Remove the embryos with injection errors, such as rupture (Figure 2B) or injection (Figure 3B) of yolk sac, and pick out embryos with a hypo- (Figure 2C and Figure 3B) or hyper- (Figure 2D and Figure 3B) number of injected cells. Keep only the embryos with approximately 400 cells in culture.

2. Rule out the possibility that cells are introduced directly into the circulation during the injection process by removing the embryos with cells already in the circulation from further analysis. Also remove any embryo with a cell mass close to the Doc (Figure 2D).
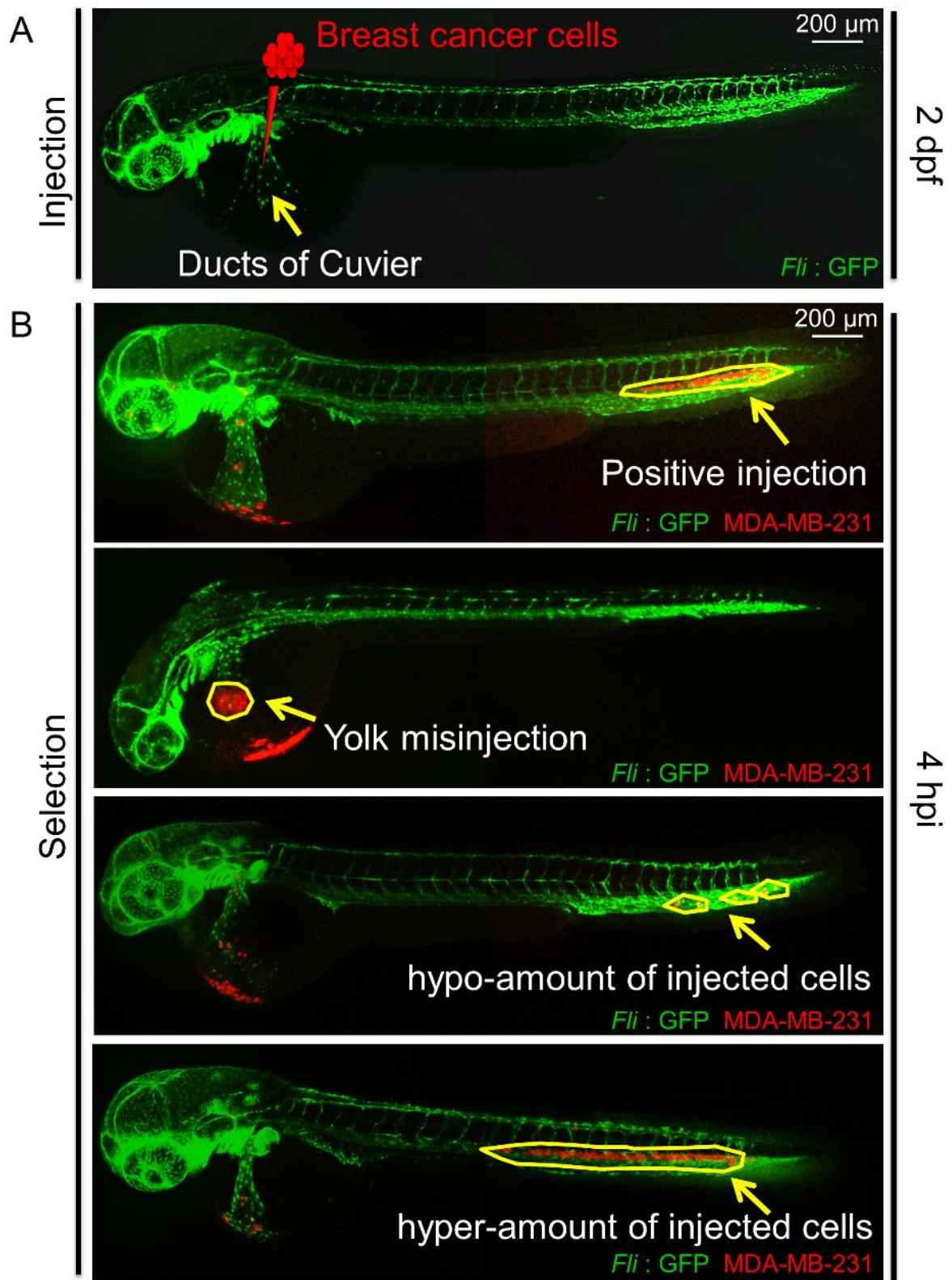
Figure 3. Overview of duct of Cuvier (Doc) injection. (A) Schematic of Doc injection at 2 days post-fertilization (dpf) with breast cancer cells in zebrafish embryos. Arrow indicates Doc. (B) Examples of positive injection with ~400 breast cancer cells, negative injections including the yolk mis-injection and incorrect number of cells injection at 4 hpi. Arrows and circles indicate injected cells.

7. Image and analyze the metastatic process.

1. Collect several anesthetized embryos with a wide-tip Pasteur pipette, and transfer them onto the glass bottom of a polystyrene dish.
2. Remove excess water and keep a limited amount of egg water. Manipulate the embryo into position with a hair loop tool, and place a cover on top of the glass.
3. Use an inverted confocal microscope in combination with water-immersion or long-distance dry objectives. The embryo should be positioned so that the region of interest is as close to the objective as possible.
4. Perform imaging immediately after anesthesia to reduce the risk of embryo death due to liquid evaporation.
   1. Capture signals from GFP-labeled vasculature and mCherry labeled tumor cells at the same position of the embryos to co-register injected cells with blood vessels by merging the two imaging channels.
   2. For each zebrafish embryo, collect two different sets of images from the head region and tail region.
5. Quantify the number of disseminated cells.
   1. For perivitelline space injection, count the cells that disseminated from the cell mass toward the embryonic fish body within the head and tail regions. The regions are beyond the boundaries of the heart cavity frontally, on top of the swim bladder dorsally, and beyond the urogenital opening caudally.
   2. For Doc injection, count the number of individual cells that invade the collagen fibers of the tail fin from circulation (MDA-MB-231) or the number of clusters formed by cells collectively (M2).
6. To study invasion and metastasis in more detail, confocal microscopy is highly recommended.
   1. Use low magnification (× 4 objective) to image the whole body and obtain an overview of the tumor cell dissemination pattern.
   Note: Higher magnification (× 20 and × 40 objectives) is suitable for studying intra- and peri-tumoral angiogenesis and precise localization of disseminated cells in the embryo body.
   2. Use a 488-nm laser to scan the zebrafish embryo vasculature, and a 543-nm laser to scan implanted tumor cells labeled with red fluorescence. Obtain a high-quality image, by scanning each embryo in eight to ten steps. Scan and average each step six times.
7. Carefully place the embryo back into the egg water if it is required for further experiments.

8. Perform statistical analysis using one-way analysis of variance (ANOVA) followed by post hoc analysis.

Representative Results:

In the embryonic xenograft zebrafish model with perivitelline space injection, the hematogenous dissemination of labeled cancer cells in the fish body is considered as active migration. This process can be detected and quantified under a fluorescent microscope as described in the methods above. To illustrate this xenograft model we followed the dissemination process of different breast cancer cell lines with known (or lack of) invasion/metastasis potential according to *in vitro* and *in vivo* mouse studies, including the benign normal breast epithelial M1 cells, HRAS-transformed premalignant M2 cells, and highly metastatic MDA-MB-231 cells 1 day post-njection (dpi) onward.

A high-resolution confocal microscopy image showed that MDA-MB-231 cells (red) exhibit an aggressive phenotype with irregular borders in the perivitelline space. Pseudopodial-like protrusions and invasive fronts were also frequently present (Figure 4A, left). A few cells disseminated into the blood circulation as early as 1 dpi (Figure 4A, right). At 2 dpi, clear dissemination was observed in the distal parts of the fish (Figure 4A, right). The number of disseminated cells increased further at 3 dpi (Figure 4A and B). In contrast, when M2 cells were challenged in zebrafish, they exhibited modest spread in the fish body after 2 dpi (Figure 4C). They also showed increased dissemination with time lapse (Figure 4D).

As shown in Figure 4E and F, M1 cells infrequently disseminated into the zebrafish circulation, and even active local migration within the perivitelline space was infrequent during the period of observation. The M1 cell mass was virtually detained at the original injection site. If defining positive dissemination or metastasis as >5 cells in the fish body (4), MDA-MB-231 and M2 cell metastasis was observed in 92% and 57% of fish, respectively, at 3 dpi (Figure 4G).

In contrast, no positive dissemination was observed with M1 cells. Therefore, this zebrafish model of human cancer cell progression accurately reflects the relative level of metastatic potential of the different cells in mice. Neovascularization (green) that sprouted from the subintestinal plexus of the embryonic zebrafish and penetrated into the MDA-MB-231 or M2 cell mass, was also present vividly through perivitelline space injection (Figure 4A and C, left). Consistent with the disability in dissemination, only slight neovascularization was detected upon M1 cell implantation (Figure 4E).

In the embryonic xenograft zebrafish model with mCherry-labeled MDA-MB-231 cells Doc injection, the labeled cancer cells in the tail fin of zebrafish is considered as active extravasation. The mCherry-labeled MDA-MB-231 cells were injected at 2 dpf. At 3 dpi, the cells started to migrate out of the vessels to the tail fin, which is enriched with collagen. Single MDA-MB-231 cells migrated one by one independently from the vessels to the distant tail fin (Figure 5A). At 6 dpi, invasion can be quantified by counting the number of cells that have migrated into the tail fin tissue. n mCherry-labeled M2 cells Doc injection model, injection was also performed at 2 dpf. However, a clustered phenotype is observed during the active extravasation process. At 1 dpi, M2 cells started to migrate out from the vessels into the caudal hematopoietic tissue (CHT) of the zebrafish. At 2 dpi the migrated M2 cells started to form a cluster between the vessels in the CHT (Figure 5B). Quantification of the M2 invasive cell clusters number in CHT region can be conducted at 6 dpi.
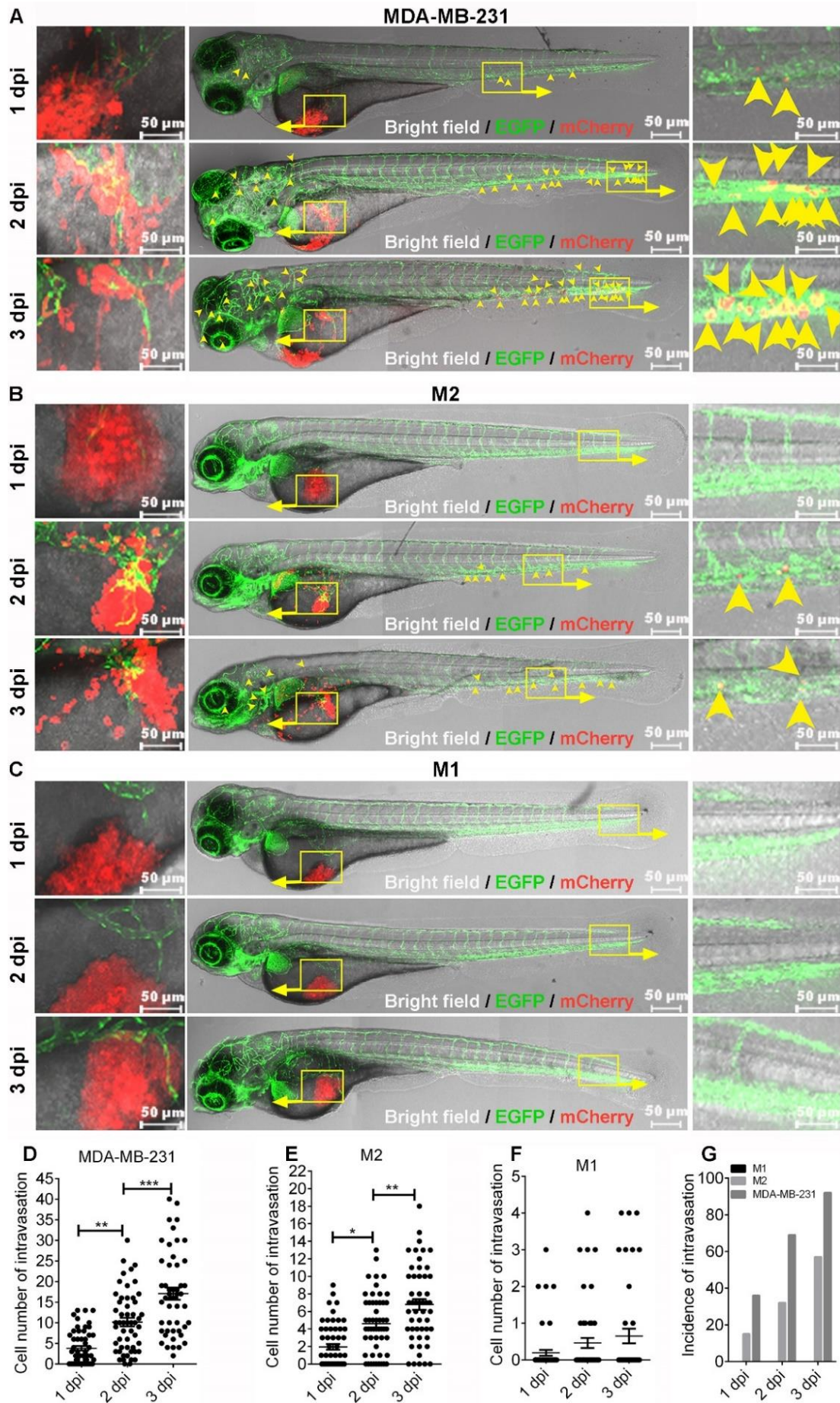
Figure 4. Comparison of dissemination ability among various breast cell lines. Approximately 400 mCherry-labeled MDA-MB-231, MCF10Aras (M2), or MCF10A (M1) cells were injected into the perivitelline space of zebrafish embryos 48 hpf. The injected embryos were followed for 3 days. (A, C, and E) High-resolution micrographs showing the representative migration and dissemination process of MDA-MB-231 (A), M2 (C), and M1 (E) cells in individual embryonic bodies 1, 2, and 3 days post-injection (dpi). Left, cell migration in the perivitelline space (red) and the peritumoral and intratumoral vasculature (green). Yellow signals indicate the overlap of microvessels and cells. Right, yellow arrowheads indicate single disseminated cells. Scale bar = 50 µm (B, D, and G) Quantification of the number of disseminated cells in each embryonic body at 1, 2, 3 dpi. Results are expressed as the Mean ± SEM. Results from one-way analysis of variance (ANOVA) followed by the post hoc analysis are shown. P <0.05 was accepted as statistically significant (*0.01 < P <0.05; **0.001 < P <0.01; *** P <0.001. (F) Comparison of the incidence of metastasis for MDA-MB-231, M2, and M1 cells in embryonic bodies at 1, 2, 3 dpi.
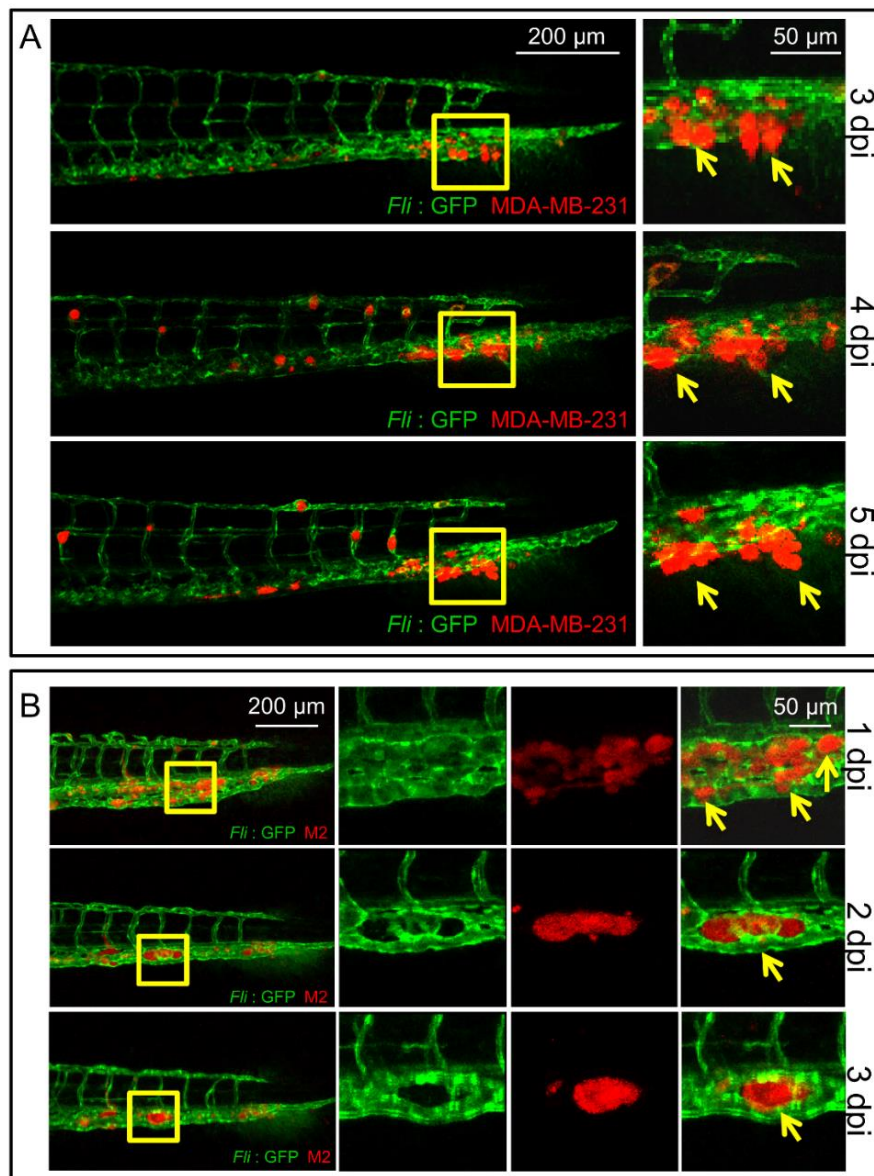
Figure 5. Different behavior of MDA-MB-231 and M2 cell metastasis in zebrafish with duct of Cuvier injection. (A) Representative confocal images of the zebrafish followed at 3, 4, 5 dpi to show the single cell migration behavior of the MDA-MB-231 cells in zebrafish. Arrows indicate invasive MDA-MB-231 cells that migrated out of the vessels to the tail fins. Scale bar = 200 µm in the left column, 50 µm in the right column. (B) Representative confocal images of the zebrafish followed at 1, 2, 3 dpi to show the cell cluster migration behavior of M2 cells in zebrafish. Arrows indicate invasive M2 cells that migrated out of the vessels to the caudal hematopoietic tissue (CHT) and formed a cluster between the vessels.

Chapter 3

Discussion:

Here, we described two methods for investigating the invasive behavior of breast cancer cells in Tg (*fli1:GFP*) zebrafish embryos based on perivitelline space and Doc injection. By injecting cancer cells labeled with chemical dye or fluorescent protein into transgenic zebrafish embryos, the dynamic and spatial characteristics of invasion and metastasis can be clearly tracked in real-time at the single cell or cluster level under a fluorescence microscope. In most cases, the rapid progression of metastasis in zebrafish ensures that the assay can be performed within 1 week after transplantation. Moreover, powerful statistics can be obtained with large cohorts of fish.

Early and late events of the metastatic cascade could be simulated and recapitulated by injecting cancer cells into the perivitelline space or Doc, respectively. The perivitelline space is the confined space between the periderm of the fish and the yolk sac, which allows one to monitor dissemination of single tumor cells from primary sites in the living body. After implantation, the cancer cells undergo local migration and invasion within the perivitelline space (considered the primary site), then intravasate into blood vessels and disseminate along with the circulation. At the head and tail fin (considered distant target sites), cancer cells accumulate in narrow capillary beds and extravasate. Therefore, the number of cells that are found at the distant sites in the fish body is a measurement of metastatic capability. In addition, more extravasated cells could be observed at later time points, which is also shown in the Doc injection assay.

The Doc is an enlarged common cardinal vein with an extensive blood stream (21). Directly targeting the Doc as an injection site introduces cancer cells into the circulatory system. In practice, breast cancer cells diffuse throughout the embryonic body via the blood stream instantly after Doc injection. The cells then arrest at the caudal vein and dorsal aorta. Extravasation, invasion, and micrometastasis formation can be observed successively within 6 days. As reported previously(16), metastatic MDA-MB-231 cells and premalignant mammary M2 cells exhibit different invasive phenotypes. MDA-MB-231 cells undergo single cell invasion of the collagen matrix-rich tail fin. Thus, the invasion potential of MDA-MB-231 cells can be measured by counting the number of cells that have extravasated and invaded the tail fin tissue. In contrast, M2 cells form clusters of different sizes and undergo collective invasion of the CHT. Quantitating the invasion potential of M2 cells by counting the number of clusters in this protocol is difficult, and is preferably performed by making a 3D image using confocal microscopy and determining the volume of clustered tumor cells.

The technical challenge in cancer cell microinjection is successfully targeting the perivitelline space or Doc. The microinjection of large numbers of embryos is a tedious procedure requiring a highly skillful and patient operator. Factors that contribute to variations in the results in individual fish include the developmental stage of the embryo when injecting, differences in the number of cells injected, and the leakage of cells into the yolk sac. Though rare, the manipulation could unintentionally but inevitably penetrate the vasculature and introduce cells into the circulatory system directly, especially in perivitelline space injection. To further reduce variation and ensure the reliability of analyses, microscopic examination is necessary to exclude unqualified fish at a given time point throughout the process. In addition, blinded analysis by a professional without knowledge of the setting is strongly suggested to achieve unbiased quantification.

Invasive behavior of human breast cancer cells in embryonic zebrafish

In summary, the two models we introduced here shed light on visualizing the processes of cell invasion and metastasis *in vivo* without invasive procedures. Although we only studied breast cancer cells in the two models regarding metastatic potential, they could be extrapolated to other types of cancer. Moreover, the models could have broader applications in excavating the mechanisms and new molecular targets controlling cancer cell metastasis using (epi)genetic manipulation. Due to the higher penetrability of zebrafish embryos by small-molecule compounds as compared to the feeding or injection of rodents (22), the two presented models also have advantages in high-throughput screening of potential new anti-invasion/metastasis drugs.

Acknowledgements:

Materials

Name	Company	cat #	Comments
Agarose	MP Biomedicals	AGAF0500	
Borosilicate glass capillary	Harvard Apparatus	300038	
Cholera enterotoxin	Calbiochem	227035	
Confocal microscope	Leica	SP5 STED	
DMEM-high glucose media containing L-glutamine	ThermoFisher Scientific	11965092	
DMEM/F-12 media containing L-glutamine	ThermoFisher Scientific	21041025	
Dumont #5 forceps	Fine Science Tools Inc	11252-20	
Epidermal growth factor	Merck Millipore	01-107	
Fetal bovine serum	ThermoFisher Scientific	16140071	
Fluorescent stereo microscope	Leica	M165 FC	
HEK293T cell line	American Type Culture Collection	CRL-1573	
Hydrocortisone	SigmaAldrich	227035	
Horse serum	ThermoFisher Scientific	26050088	
Insulin	SigmaAldrich	I-6634	
MCF10A (M1) cell line			Kindly provided by Dr. Fred Miller (Barbara Ann Karmanos Cancer Institute, Detroit, MI, USA)
MCF10Aras (M2) cell line			
MDA-MB-231 cell line	American Type Culture Collection	CRM-HTB-26	
Manual micromanipulator	World Precision Instruments	M3301R	
Micropipette puller	Sutter Instruments	P-97	
Wide-tip Pasteur pipette (0,5-20 ul)	Eppendorf	F276456I	
pCMV-VSVG plasmid			Kindly provided by Prof. Dr. Rob Hoeben (Leiden University Medical Center, Leiden, The Netherlands)
pMDLg-RRE (gag/pol) plasmid			
pRSV-REV plasmid			
Penicillin-Streptomycin (10,000	ThermoFisher Scientific	15140122	

U/mL)			
PLV-mCherry plasmid	Addgene	36084	
Pneumatic picoPump	World Precision Instruments	SYS-PV820	
Polybrene	SigmaAldrich	107689	
Prism 4 software	GraphPad Software		
Stereo microscope	Leica	MZ16FA	
Tg (*fli:EGFP*) zebrafish strain			Kindly provided by Dr. Ewa Snaar-Jagalska (Institute of Biology, Leiden University, Leiden, The Netherlands)
Tris-base	SigmaAldrich	11814273001	
Tricaine (3-aminobenzoic acid)	SigmaAldrich	A-5040	
Trypsin-EDTA (0.5%)	ThermoFisher Scientific	15400054	
Petri dishes, polystyrene (60 × 15 mm)	SigmaAldrich	P5481-500EA	
Polystyrene dish with glass bottom	WillCo	GWST-5040	

The video of this article can be found at https: https://www.jove.com/video/55459/

References:

1. Wan L, Pantel K, Kang Y. Tumor metastasis: moving new biological insights into the clinic. Nat Med 2013;19(11):1450-64.
2. Obenauf AC, Massagué J. Surviving at a distance: Organ-specific metastasis. Trends Cancer 2015;1(1):76-91.
3. Saxena M, Christofori G. Rebuilding cancer metastasis in the mouse. Mol Oncol 2013;7(2):283-96.
4. Teng Y, Xie X, Walker S, White DT, Mumm JS, Cowell JK. Evaluating human cancer cell metastasis in zebrafish. BMC cancer 2013;13(1):1.
5. Konantz M, Balci TB, Hartwig UF, Dellaire G, André MC, Berman JN, *et al.* Zebrafish xenografts as a tool for in vivo studies on human cancer. Ann N Y Acad Sci 2012;1266(1):124-37.
6. Zhao S, Huang J, Ye J. A fresh look at zebrafish from the perspective of cancer research. J Exp Clin Cancer Res 2015;34(1):1.
7. Stanton MF. Diethylnitrosamine-induced hepatic degeneration and neoplasia in the aquarium fish, Brachydanio rerio. J Natl Cancer Inst 1965;34(1):117-30.
8. Lam SH, Wu YL, Vega VB, Miller LD, Spitsbergen J, Tong Y, *et al.* Conservation of gene expression signatures between zebrafish and human liver tumors and tumor progression. Nat Biotechnol 2006;24(1):73-5.
9. Spitsbergen JM, Kent ML. The state of the art of the zebrafish model for toxicology and toxicologic pathology research—advantages and current limitations. Toxicol Pathol 2003;31(1 suppl):62-87.
10. Stoletov K, Klemke R. Catch of the day: zebrafish as a human cancer model. Oncogene 2008;27(33):4509-20.
11. Lee LM, Seftor EA, Bonde G, Cornell RA, Hendrix MJ. The fate of human malignant melanoma cells transplanted into zebrafish embryos: assessment of migration and cell division in the absence of tumor formation. Dev Dyn 2005;233(4):1560-70.
12. Mizgirev I, Revskoy S. Generation of clonal zebrafish lines and transplantable hepatic tumors. Nat Protoc 2010;5(3):383-94.

13.	Mizgireuv IV, Revskoy SY. Transplantable tumor lines generated in clonal zebrafish. Cancer Res 2006;66(6):3120-5.

14.	Stoletov K, Montel V, Lester RD, Gonias SL, Klemke R. High-resolution imaging of the dynamic tumor cell–vascular interface in transparent zebrafish. Proc Natl Acad Sci U S A 2007;104(44):17406-11.

15.	Rouhi P, Jensen LD, Cao Z, Hosaka K, Länne T, Wahlberg E, *et al.* Hypoxia-induced metastasis model in embryonic zebrafish. Nat Protoc 2010;5(12):1911-8.

16.	Drabsch Y, He S, Zhang L, Snaar-Jagalska BE, ten Dijke P. Transforming growth factor-β signalling controls human breast cancer metastasis in a zebrafish xenograft model. Breast Cancer Res 2013;15(6):R106.

17.	He S, Lamers GE, Beenakker JWM, Cui C, Ghotra VP, Danen EH, *et al.* Neutrophil-mediated experimental metastasis is enhanced by VEGFR inhibition in a zebrafish xenograft model. J Pathol 2012;227(4):431-45.

18.	Nicoli S, Presta M. The zebrafish/tumor xenograft angiogenesis assay. Nat Protoc 2007;2(11):2918-23.

19.	de Boeck M, Cui C, Mulder AA, Jost CR, Ikeno S, ten Dijke P. Smad6 determines BMP-regulated invasive behaviour of breast cancer cells in a zebrafish xenograft model. Sci Rep 2016;6.

20.	Rosen JN, Sweeney MF, Mably JD. Microinjection of zebrafish embryos to analyze gene function. J Vis Exp 2009(25):e1115.

21.	Lawson ND, Weinstein BM. Arteries and veins: making a difference with zebrafish. Nat Rev Genet 2002;3(9):674-82.

22.	Zon LI, Peterson RT. In vivo drug discovery in the zebrafish. Nat Rev Drug Discov 2005;4(1):35-44.

3

Chapter 4

Deubiquitinase activity profiling identifies UCHL1 as a candidate oncoprotein that promotes TGFβ-induced breast cancer metastasis

Sijia Liu[1,7], Román González-Prieto[1], Mengdi Zhang[5], Paul P. Geurink[1,7], Raymond Kooij[1,7], Prasanna Vasudevan Iyengar[1,7], Maarten van Dinther[1,7], Erik Bos[1], Xiaobing Zhang[4], Sylvia Le Dévédec[4], Bob van de Water[4], Roman I. Koning[1], Hong-Jian Zhu[6], Wilma Mesker[3], Alfred Vertegaal[1], Huib Ovaa[1,7], Long Zhang[5], John W. M. Martens[2], Peter ten Dijke[1,7]

[1]Department of Cell and Chemical Biology, Leiden University Medical Center, Leiden, The Netherlands;
[2]Erasmus MC Cancer Institute, Rotterdam, The Netherlands;
[3]Department of Surgery, Leiden University Medical Center, Leiden, The Netherlands;
[4] Division of Drug Discovery and Safety, Leiden Academic Center for Drug Research, Leiden, The Netherlands;
[5]Life Sciences Institute and Innovation Center for Cell Signaling Network, Zhejiang University, China
[6]Department of Surgery, The University of Melbourne, Melbourne, Australia
[7]Oncode Institute, Leiden University Medical Center, Einthovenweg 20, 2333 ZC, Leiden, Netherlands

Chapter 4

Abstract

Purpose: Therapies directed to specific molecular targets are still unmet for triple-negative breast cancer (TNBC) patients. Deubiquitinases (DUBs) are emerging drug targets. The identification of a highly active DUBs in TNBC may lead to novel therapies.

Experimental Design: Using DUB activity probes, we profiled global DUB activities in 52 breast cancer cell lines and 52 patients' tumor tissues. To validate our findings *in vivo*, we employed both zebrafish and murine breast cancer xenograft models. Cellular and molecular mechanisms were elucidated using *in vivo* and *in vitro* biochemical methods. A specific inhibitor was synthesised and its biochemical and biological functions were assessed in a range of assays. Finally, we used patient sera samples to investigate clinical correlations.

Results: Two DUB activity profiling approaches identified UCHL1 as being highly active in TNBC cell lines and aggressive tumors. Functionally, UCHL1 promoted metastasis in zebrafish and murine breast cancer xenograft models. Mechanistically, UCHL1 facilitates TGFβ signaling-induced metastasis by protecting TGFβ type I receptor and SMAD2 from ubiquitination. We found that these responses are potently suppressed by the specific UCHL1 inhibitor, 6RK73. Furthermore, UCHL1 levels were significantly increased in TNBC patient sera, and highly enriched in sera exosomes as well as TNBC cell conditioned media. UCHL1 enriched exosomes stimulated breast cancer migration and extravasation, suggesting that UCHL1 may act in a paracrine manner to promote tumor progression.

Conclusion: Our DUB activity profiling identified UCHL1 as a candidate oncoprotein that promotes TGFβ-induced breast cancer metastasis and may provide a potential target for TNBC treatment.

Translational Relevance

Metastasis is the leading cause of breast cancer-associated death. Triple-negative breast cancer remains the most challenging subtype to treat. Deubiquitinases (DUBs) are emerging drug targets in cancer treatment. To discover new DUB targets, we profiled global DUB activities in 52 human breast cancer cell lines and 52 patients' tumor tissue samples. Two independent DUB activity profiling approaches identified UCHL1 as being highly active in TNBC cell lines and aggressive tumors. Mechanistically, UCHL1 facilitate TGFβ signaling-induced metastasis by restricting ubiquitination of TGFβ type I receptor and its downstream effector SMAD2. We further found UCHL1 covalent activity inhibitor 6RK73 can be used as a potential drug to specifically inhibit UCHL1 activity in breast cancer. Furthermore, we observed that TNBC patient sera contains high UCHL1 levels, which may represent a blood-based biomarker for early diagnosis of metastasis. In sum, our study has identified UCHL1 as a potential target for TNBC treatment.

Introduction

Breast cancer is the most frequently diagnosed cancer in women (1), approximately 90% of breast cancer-related deaths are due to metastasis (2). During the metastasis process, epithelial-mesenchymal transition (EMT) plays an important role, which can be induced by the secreted cytokine transforming growth factor-β (TGFβ) (3). In the late stage of tumorgenesis, TGFβ stimulates cell invasion and modifies the microenvironment to promote cancer cell intravasation into nearby vessels, and stimulate extravasation into distant tissues

and forming tumors-initiating seeds (4). Increasing evidence indicates that tumor cell-derived exosomes can profoundly influence the tumor local and systemic environment by transferring oncogenic cargo molecules (including protein, RNAs and lipids) to stromal or less aggressive tumor cells (5). Proteins that are enriched in circulating exosomes can be readily isolated from cancer patient blood and have been used as blood-based diagnostic and prognostic markers (6). Once metastasis has been triggered, current treatments frequently fail to provide durable responses (7). Therefore, an improved understanding of the underlying molecular and cellular mechanisms of metastasis is needed to better prevent and treat metastatic breast cancer.

As a highly heterogeneous disease, breast cancer can be classified into multiple subtypes with distinct metastatic potential based on genetic and clinical features (8). For instance, basal-like breast cancers are more aggressive than luminal and normal-like breast cancers (9), and estrogen receptor (ER) negative tumors are more aggressive than ER positive ones (10). The most aggressive subtype of breast cancer is triple-negative breast cancer (TNBC), which is defined as lacking expression of ER, progesterone receptor (PR), and human epidermal growth factor receptor 2 (HER2). TNBC subtype accounts for approximately 12% to 17% of breast cancers (11). TNBC remains the most challenging subtype of breast cancer to treat due to a low response rate to chemotherapy and lack of clinically meaningful molecular targets (12). Thus, there is an unmet need for newer molecular targets and effective drugs against these novel targets.

Post-translational modification of proteins by ubiquitination is emerging as a key regulatory mechanism in cell biology for regulating protein degradation and signaling activity (13). Ubiquitination is mediated by ubiquitin E3 ligase enzymes and reverted by deubiquitinases (DUBs). About 100 human DUBs have been identified and some of them play important roles in cancer progression (14). The majority of DUBs have a catalytic cysteine in the activity site of the protease, which render them attractive targets for small-molecule drug discovery screens (15). In recent studies, several independent groups have developed USP7 inhibitors (16-18), and, especially, the inhibitor FT671 showed significant inhibition of medulloblastoma, colorectal and lung tumors growth in mice (19). More than a decade after a Nobel prize was awarded for the discovery of the ubiquitin-proteasome system and clinical approval of proteasome and ubiquitin E3 ligase inhibitors, first-generation DUB inhibitors are now approaching to clinical trials (15). Besides, the development of DUB activity based probes (ABPs) provide very useful tools for monitoring target engagement and facilitate progress in drug discovery of DUBs (15,20).

Motivated to better understand the functional importance of differential DUB activities in breast cancer, we profiled DUB activity in different breast cancer subtypes with DUB ABPs. From these landscape profiles of DUB activities, we identified UCHL1 as being highly active in the more aggressive breast cancer subtype. Functionally, UCHL1 promoted TGFβ-induced breast cancer metastasis, and these responses were mitigated by genetic and pharmacological approaches. Furthermore, UCHL1 levels were significantly increased in exosome fractions of aggressive breast cancer patient sera. In this study, we also explored the function of UCHL1 enriched exosomes in promoting TNBC migration and extravasation.

Chapter 4

Materials and Methods

Ethics Statement and Preparation of Clinical Samples

ER positive and negative fresh frozen tumor tissues and sera were randomly selected from the historical tumor biobank at the Erasmus MC Cancer institute. Use of biospecimen for biomarker research has been approved by the Medical Ethics Committee of the Erasmus MC and was performed in accordance to the Code of Conduct of the Federation of Medical Scientific Societies in the Netherlands (http://www.federa.org/). TNBC and control sera samples were collected by the Leiden University Medical Center (LUMC) Surgical Oncology Biobank between October 2002 and March 2013 according to a standardized protocol. This study was approved by the Medical Ethics Committee of the LUMC and was performed in accordance to the Code of Conduct of the Federation of Medical Scientific Societies in the Netherlands (http://www.federa.org/). Sera samples from 10 TNBC patients were selected that had no prior treatment and sera from 25 volunteers were selected as controls. Sera samples from TNBC and controls were stored at -80° C.

Cell Lines and Cell Culture

HEK293T and A549 cells were originally obtained from American Type Culture Collection (ATCC) and cultured in Dulbecco's modified Eagles's medium (DMEM) supplemented with 10% fetal bovine serum (FBS) and 100U/ml penicillin-streptomycin (15140122; Gibco). The 52 breast cancer cell lines that were used in this study were cultured in Roswell Park Memorial Institute (RPMI) medium (11875093; Gibco) supplemented with 10% FBS, 100 IU/ml penicillin-streptomycin. All the 52 breast cancer cell lines were molecularly and biochemically characterized and are listed in Supplementary Table S1. All the cells were routinely tested for absence mycoplasma contamination and checked for authenticity by STR profiling.

Zebrafish Extravasation Assay of Human Breast Cancer Cells

Transgenic zebrafish lines Tg (fli1: EGFP) were raised according to standard procedures in compliance with the local Institutional Committee for Animal Welfare of the Leiden University. Zebrafish extravasation assay were prepared as previous described (21). Zebrafish were fixed with 4% paraformaldehyde (PFA) 6 days after injection. Imaging and quantification of the results were carried out on an inverted SP5 STED confocal microscope (Leica), At least 40 zebrafish were analyzed for each group and 3 representative images were taken. All the experiments were repeated at least three times, and representative results are shown.

Breast Cancer Metastasis Assay in Mice Xenograft Model

Mice were purchased from the animal husbandry center of the Shanghai Institute Cell Biology, Academia Sinica, Shanghai, China. For the intracardial injection, five-weeks-old female BALB/c nude mice were anesthetized with isoflurane and single-cell suspension of MDA-MB-231 BM Luc (100.000 /100ul PBS) cells or MDA-MB-436 Luc (300.000 /100ul PBS) cells were inoculated into the left heart ventricle according to the method described by Arguello et al (22). Ten mice were injected in each group. Bioluminescent imaging was used to verify successful injection and to monitor the outgrowth of metastasis weekly. Mice experiments were approved by the Zhejiang University Animal Welfare Committee.

6RK73 Synthesis

The 6RK73 compound was synthesized according to a reported procedure (23). NMR and analytical LC-MS analysis was performed to confirm the nature and purity of the compound.

Exosome Isolation from Cell and Sera

Exosome isolation were performed as previous described (24,25). Supernatants from cell and sera samples from patients were concentrated by 100 K NMWL centrifugal filtration (UFC910024; Millipore) at 4 °C 10 x 10^3g and washed twice with PBS. Exosomes were recovered from the concentrated supernatant by ultracentrifugation at 100 x 10^3g for 17 hours at 4 °C. Exosome pellets were resuspended in ice-cold PBS at 4 °C. The concentration of exosomal proteins was quantified using DC protein assay (Pierce).

Statistical Analysis

Statistical analysis was performed using Prism 8 software (GraphPad La Jolla, USA). Numerical data from triplicates are presented as the mean ± SD, except for analysis of Zebrafish experiments where a representative result is expressed as mean ± SEM. The significance of differences between two independent subjects was determined using the unpaired Student's t test. Two-way analysis of variance (ANOVA) has been used to analysis multiple subjects. The Kaplan-Meier method was used to evaluate metastasis free survival of mice between two groups. P value are indicated by asterisks in the figures: *, $P < 0.05$, **, $P < 0.01$, ***, $P < 0.001$ and ****, $P < 0.0001$. Differences at $P = 0.05$ and lower were considered significant.

See supplementary information for additional descriptions regarding methods that were used.

Results

DUB activity profiling identified UCHL1 as a highly active DUB in aggressive breast cancer

We first established a workflow to systematically determine the differential DUB activities in 52 human breast cancer cell lines and 52 breast cancer patient tumor tissues by using TAMRA-ubiquitin-VME, which is a ubiquitin-based activity probe for cysteine DUBs labeled on the N-terminus with a 5-carboxytetramethylrhodamine (TAMRA) dye and equipped with a reactive C-terminal vinyl methyl ester (VME) warhead (Fig. 1A). Among all the bands that were labelled with TAMRA ABP and visualized by fluorescence scanning, a band on the bottom of the gel displayed large variation in intensity levels between cell lines with representatives for Basal A, Basal B, Luminal, and Luminal HER2+ subtypes (Fig. 1B). To identify the DUB corresponding to this band, we used Biotin-ubiquitin-VME ABP to pull down the protein and identified it by liquid chromatography-tandem mass spectrometry (LC/MS-MS) (Fig. 1C). We performed the DUB identification in MDA-MB-436 cells, which showed strong intensity of the band of interest in the TAMRA and Biotin ABP result (Fig. 1D). The LC/MS-MS identified the DUB as UCHL1, and the Biotin-ubiquitin-VME ABPs were also identified and almost equally enriched with UCHL1 in the samples (Fig. 1E and Supplementary Fig. S1A).
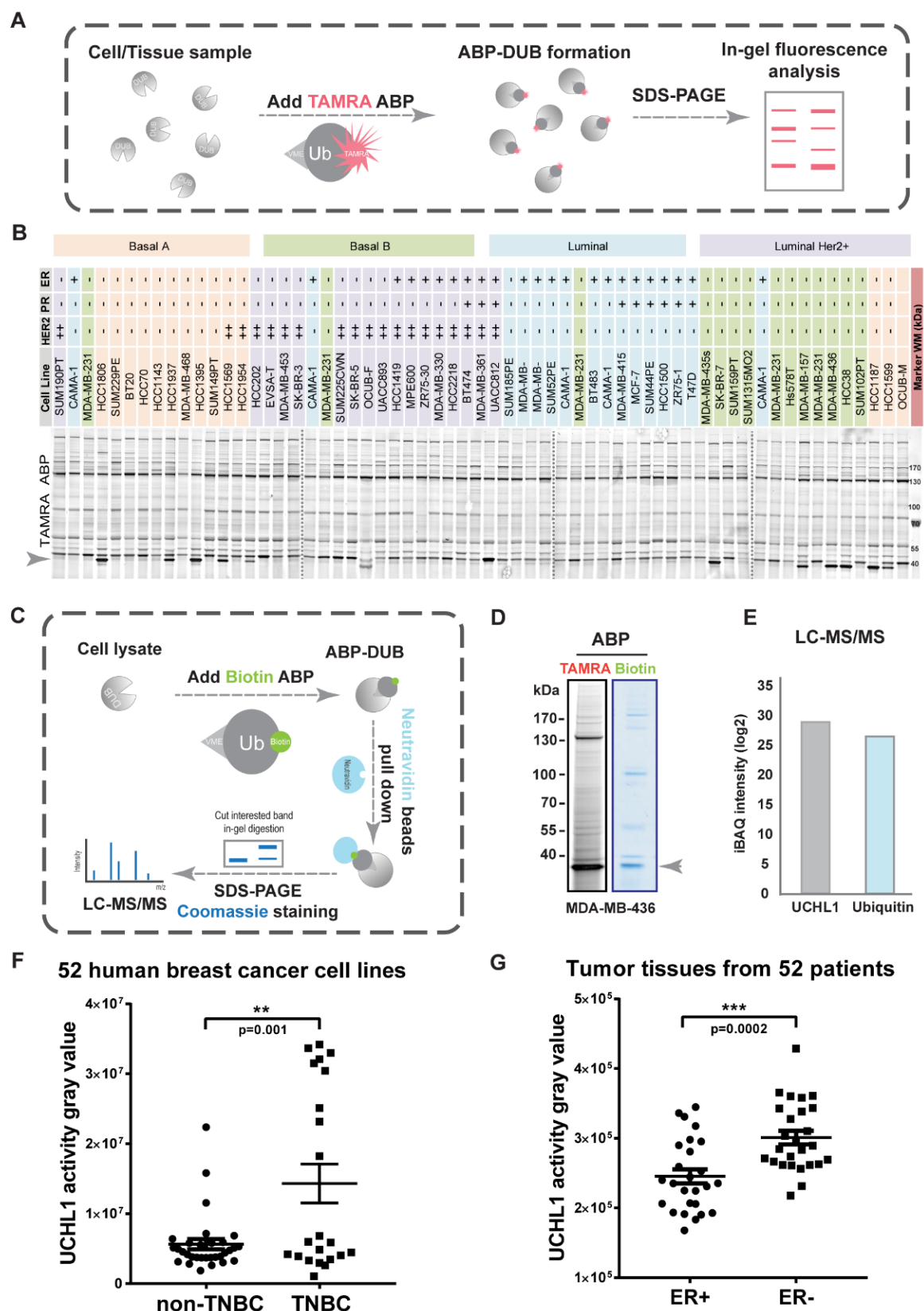
Figure 1. DUB activity profiling identified UCHL1 as being selectively highly activated in aggressive breast cancer tumor tissues and cell lines. **A,** Schematic overview of DUB activity profiling with TAMRA activity based probe (ABP). **B,** Atlas of DUB activity in 52 breast cancer cell lines. Four gels were merged together with dashed line in between two gels. **C,** DUB identification workflow with Biotin ABP. **D,** TAMRA ABP and Biotin ABP assay in MDA-MB-436 cells. **E,** LC-MS/MS

analysis of in-gel tryptic digestion of excised gel slice indicated in figure 1D. **F,** UCHL1 activity analysis of 52 breast cancer cell lines. **, $P < 0.01$, unpaired Student t test. **G,** UCHL1 activity gravy value analysis of 52 tissues from breast cancer patients. ***, $P < 0.001$, unpaired Student t test.

Next, we measured the intensities of the UCHL1-corresponding band in the TAMRA ABP profiling results by densitometry to compare UCHL1-corresponding activities between different breast cancer subtypes (Supplementary Table S1); UCHL1 activities were significantly increased in TNBC lines compared to non-TNBC cell lines (Fig. 1F). Next, DUB activity profiling with TAMRA ABP was performed in 26 ER+ and 26 ER- breast cancer patient tumor tissues (Supplementary Fig. S1B), and UCHL1-corresponding activities in ER- patient tumors were significantly higher than the activities in ER+ patient tumors (Fig. 1G and Supplementary Table S2).

The second parallel DUB activity profiling was performed with Biotin-ubiquitin-VME ABP combined with LC/MS-MS analysis in 20 randomly picked up Basal and Luminal human breast cancer cell lines (Fig. 2A; Supplementary Table S3). All the targets identified by LC/MS-MS were plotted by hierarchical clustering to compare biological replicates (Fig. 2B). Average label-free quantification (LFQ) $\log_2$ difference between Basal and Luminal, ER+ and ER-, and TNBC and non-TNBC subtype cell lines revealed that UCHL1 activity was highly enriched in Basal, ER negative and TNBC subgroups (Fig. 2C; Supplementary Table S4). To further validate the Biotin ABP profiling result of UCHL1, we compared UCHL1 activity detected by Biotin ABP and TAMRA ABP profiling, with the UCHL1 protein level measured by Western Blot (WB) in these 20 breast cancer cell lines (Fig. 2D). Both profiling results of UCHL1 activity showed similar results, and the UCHL1 protein level detected by WB was found to be a major determinant for UCHL1 activity level (Fig. 2D). Taken together, both DUB activity profiling methods identified UCHL1 as being highly activated in aggressive breast cancer.

UCHL1 promotes breast cancer metastasis in xenograft models

To explore the role of UCHL1 activity in breast cancer metastasis, we first analyzed the effect of its misexpression in breast cancer cells on extravasation in a zebrafish breast cancer xenograft model (Fig. 3A). First, we overexpressed UCHL1 in mCherry-expressing MDA-MB-231 cells, which has a low endogenous UCHL1 expression/activity level as determined by WB and TAMRA ABP assays (Fig. 3B and Supplementary Fig. S2A). Injection of the same number of cells into the circulation of zebrafish embryos revealed after 6 days significantly increased number of invasive cells in the UCHL1-Flag group compared to the vector control group (Fig. 3C and D). The proliferation of both cell lines when grown on plastic showed no significant difference (Supplementary Fig. S2B).

Next, we knocked down UCHL1 in mCherry-expressing MDA-MB-436 cells, which have high endogenous UCHL1 expression/activity level by using two independents short hairpin RNAs (shRNAs). The knockdown efficiency was validated by WB and TAMRA ABP assays (Fig. 3E and Supplementary Fig. S2C). The UCHL1 knockdown groups revealed not only less invasive cells but also a weaker metastatic phenotype (cells were unable to extravasate into zebrafish tail fin and formed clusters in between the blood vessels) compared with a non-targeting (NT) shRNA and empty vector (PLKO) control groups (Fig. 3F and G). The proliferation was not affected by UCHL1 depletion (Supplementary Fig. S2D).
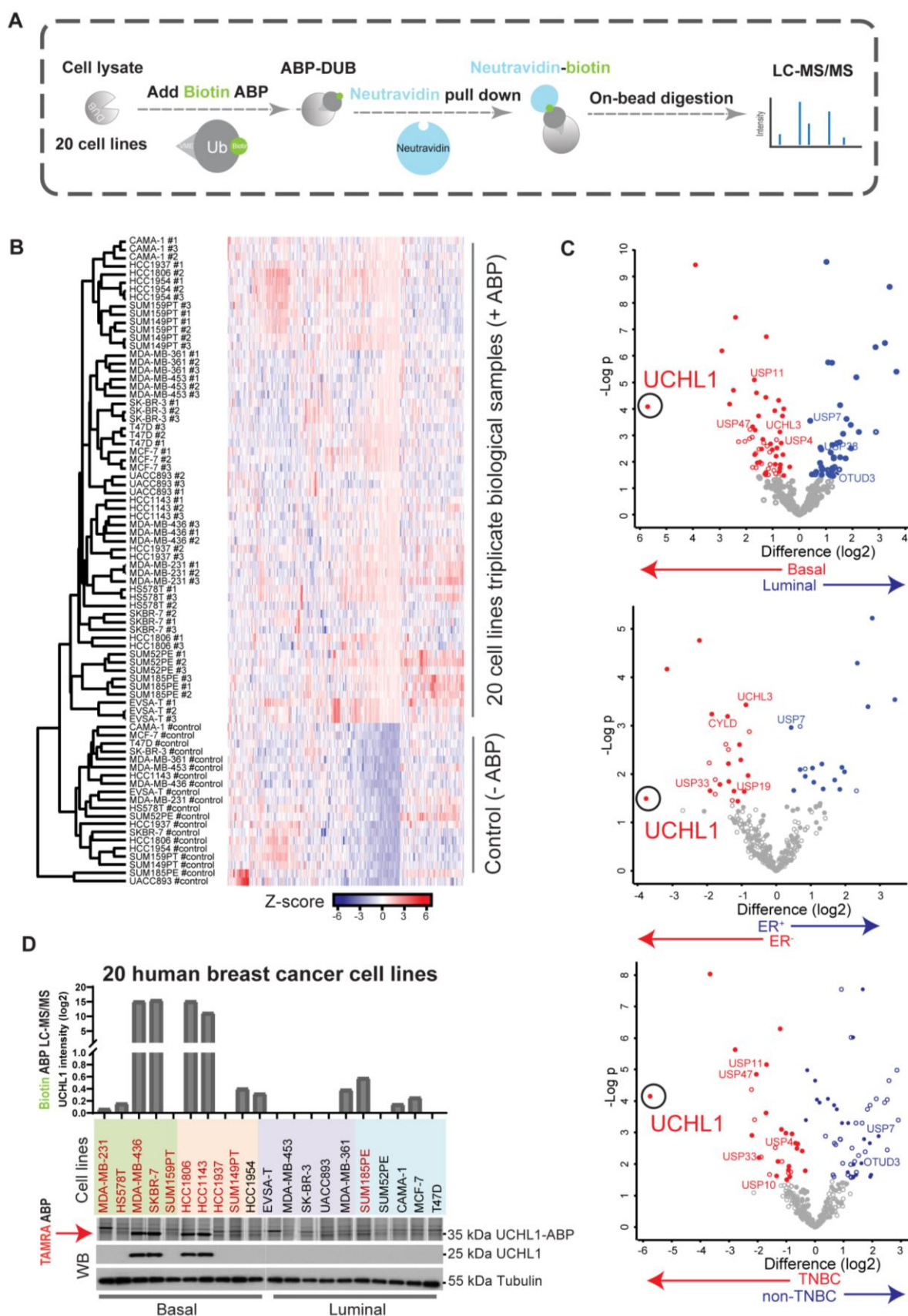
Figure 2. Quantitative DUB activity-based proteomic profiling identified UCHL1 as being selectively highly active in TNBC cell lines. **A,** Schematic overview of quantitative DUB activity profiling with Biotin ABP. **B,** Heatmap depicting sample clustering considering Z-score of proteins identified by LC-MS/MS after Biotin-ABP profiling. The tree indicates Euclidean distances between samples. **C,**

Scatterplots depicting statistical differences between cell lines grouped by tumor subtype. A filled dot indicates that a protein is statistically significantly different between any of the groups of study and the control sample set. An empty dot indicates that there is no statistically significant difference between any of the groups of study and the control sample group. Location of UCHL1 is marked with a circle. **D,** Biotin ABP, TAMRA ABP and WB analysis of UCHL1 in 20 breast cancer cell lines, TNBC cell lines were highlighted with red color. Two blots were merged together with a grey line in between two blots. Same blot was used for UCHL1 and Tubulin (loading control).

Next, to further confirm that UCHL1 promotes breast cancer metastasis, we used a mouse breast cancer xenograft model in which we intracardially injected breast cancer cells stably expressing firefly luciferase, into female BALB/c athymic nude mice. Bioluminescent images (BLI) were taken every week to monitor colonization in different organs after successful injection (Fig. 3H). UCHL1-overexpressing MDA-MB-231 cells exhibited significantly increased metastasis in different organs 35 days after injection (Fig. 3I and K) and shorter metastasis-free survival periods than the empty-vector control group (Fig. 3J).

Furthermore, nude mice were intracardially injected with luciferase-labelled PLKO control and sh1-UCHL1 knockdown MDA-MB-436 cells. The PLKO group showed metastasis in different organs at 49 days after injection (Fig. 3L and N), and shorter metastasis-free survival periods than sh1-UCHL1 group (Fig. 3M). Altogether, the mice and zebrafish results confirm that UCHL1 promotes breast cancer invasion and metastasis.

UCHL1 facilitates TGFβ signaling-induced TNBC migration and extravasation by protecting TβRI and SMAD2 from ubiquitination

Next, we investigated the underlying mechanism by which UCHL1 promoted breast cancer metastasis. Since EMT plays an important role during breast cancer metastasis (3), we firstly tested the effect of UCHL1 depletion in MDA-MB-436 cells on the levels of several mesenchymal markers. Knockdown of UCHL1 significantly decreased VIMENTIN, SNAIL and SLUG expression both at the RNA and protein level (Fig. 4A and B). In addition, qPCR results showed a modest decrease of *β-CATENIN*, *ZEB1* and *ZEB*2 expression upon UCHL1 depletion (Supplementary Fig. S3A). Since TGFβ is a key activator of EMT, we next examined whether UCHL1 can control TGFβ signaling. Indeed, ectopic expression of UCHL1 in MDA-MB-231 cells (low endogenous UCHL1 activity) promoted TGFβ-induced pSMAD2 levels, and this coincided with increased TGFβ type I receptor (TβRI) and SMAD2 levels (Fig. 4C). Knockdown of UCHL1 in MDA-MB-436 cells (high endogenous UCHL1 activity) suppressed pSMAD2, TβRI and SMAD2 levels (Fig. 4D). Besides, ectopic expression of UCHL1 in HEK293T cells upregulated the TGFβ-induced SMAD3/4 driven transcriptional CAGA$_{12}$-luc response, whereas knockdown of UCHL1 decreased this effect significantly (Supplementary Fig. S3C). To investigate whether UCHL1 interacts with TβRI, we performed immunoprecipitation (IP) of UCHL1 followed by WB for TβRI using HEK293T cell lysates. We observed that Flag-tagged UCHL1 interacted with both overexpressed and endogenous TβRI upon TGFβ treatment (Fig. 4E and supplementary Fig. S3D). Besides, we found that recombinant UCHL1 preferentially binds to ubiquitinated TβRI. This post-translational modification of TβRI is triggered by TGFβ treatment (Supplementary Fig. S3E). We also found in IP-WB experiments that UCHL1 interacts with SMAD2 in HEK293T cells. This endogenous interaction was not TGFβ dependent (Fig. 4E).
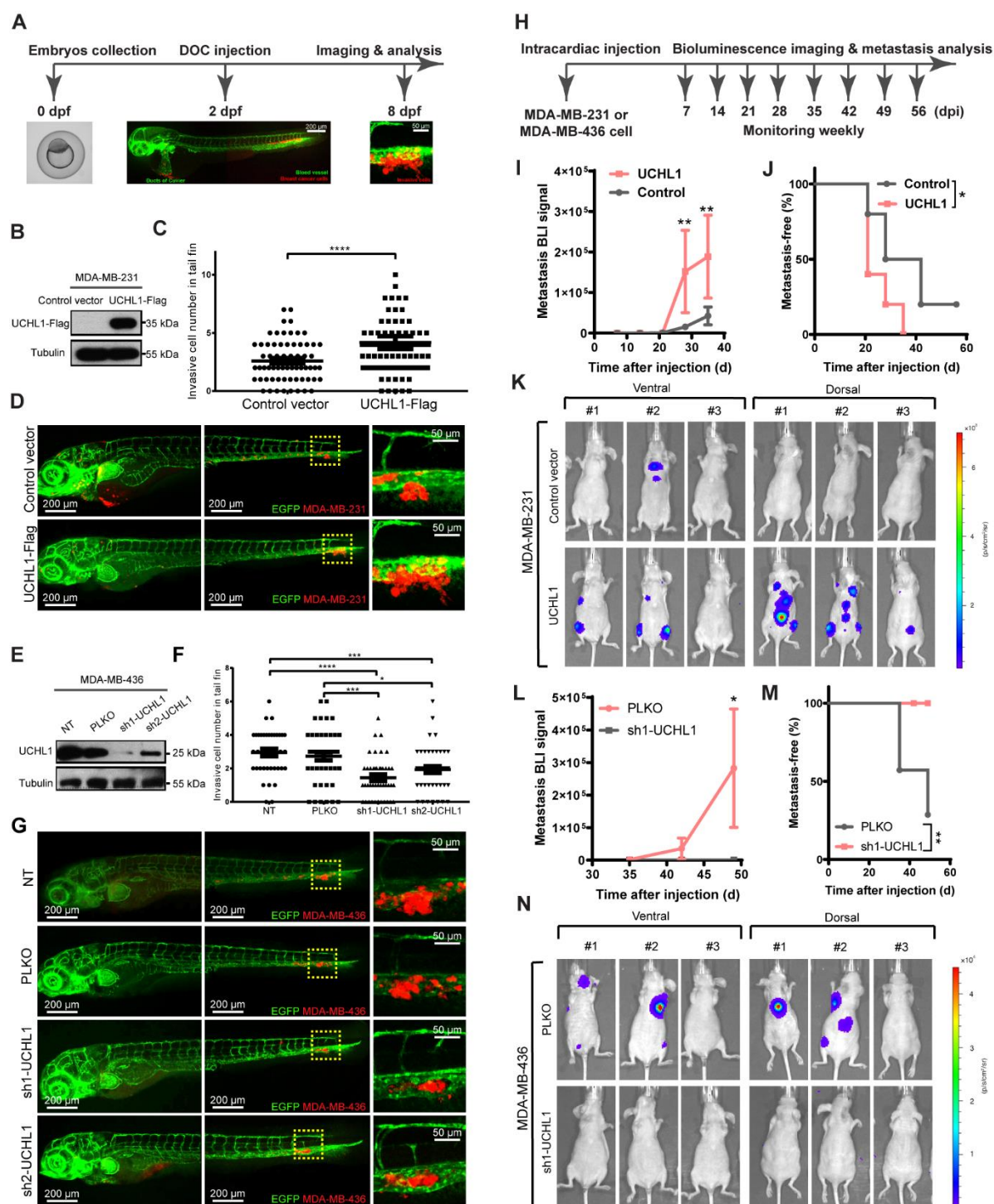
Figure 3. UCHL1 promotes breast cancer metastasis in zebrafish and mice xenograft models. **A,** Workflow of breast cancer extravasation experiment in a zebrafish model. The blood vessels and cancer cells are fluorescently labelled in green and red, respectively. **B,** UCHL1 overexpressing and control vector expressing MDA-MB-231 cell lines were established and validated by WB. Same blot was used for UCHL1 and Tubulin (loading control). **C,** Analysis of invasive cell numbers of control and UCHL1 groups in zebrafish metastasis experiment. ****, $P < 0.0001$, unpaired Student t test. **D,** Representative images of zebrafish from the control and the UCHL1 group with zoom-in of invasive cells on the right panel. **E,** Two UCHL1 shRNA knock down MDA-MB-436 cell lines and two control cell lines PLKO (empty vector) and NT (non-target) were established and validated by WB. Same blot was used for UCHL1 and Tubulin (loading control). **F,** Analysis of invasive cell numbers of each group in zebrafish metastasis assay. *, $P < 0.05$, ***, $P < 0.001$ and ****, $P < 0.0001$, two-

way analysis of variance (ANOVA). The location of nuclear and plasma membrane are indicated with a dashed line. **G**, Representative images from 4 groups with zoom-in on the right panel. **H,** Workflow of breast cancer metastasis experiment in mouse model. **I,** Bioluminescence imaging (BLI) signal of metastasis of control and UCHL1 overexpression in MDA-MB-231 cells were measured at indicated times. **, $P < 0.01$, two-way ANOVA. **J,** Percentage of metastasis-free mice in each group followed in time. *, $P < 0.05$, Log-rank test. **K,** BLI signal of metastasis of 3 representative mouse images with both ventral and dorsal side from each group at day 35 after injection. **L,** BLI signal of metastasis of PLKO and sh1-UCHL1 MDA-MB-436 cells were measured at indicated times. *, $P < 0.05$, two-way ANOVA. **M,** Percentage of metastasis-free mice in each group followed in time. **, $P < 0.01$, Log-rank test. **N,** BLI signal of metastasis of 3 representative mouse images with both ventral and dorsal side from each group at day 49 after injection.

As UCHL1 is a small protein in which either deletion of N- or C-terminal sequences will result in loss of solubility and misfolding (26), it is not possible to make truncated versions to study the responsible domain of UCHL1 for the interaction with TβRI and SMAD2. We therefore resorted to investigate the effect of specific amino acid mutations in UCHL1 on the interaction of UCHL1 with TβRI or SMAD2. These mutations were previously shown to interfere with UCHL1 DUB function (26,27). Our results showed that the catalytic triad mutants (C90S, C90A, D176N, H161D and H161Y), ubiquitin binding mutant (D30K), and double mutant (D30K & D176N) which are defective in DUB activity as measured by TAMRA-ABP assay, still interact with TβRI or SMAD2. However, the S18Y mutant of UCHL1 retained DUB activity in TAMRA-ABP assay but demonstrated a decreased interaction with TβRI or SMAD2 (Supplementary Fig. S4A and B). These results suggest the N-terminal region in vicinity of Serine[18] in UCHL1 plays an important role in the interaction with TβRI or SMAD2. To further validate and investigate the endogenous interactions and subcellular localization of TβRI-UCHL1 and SMAD2-UCHL1, we performed proximity ligation assays (PLA) in A549 cells. A549 cells were chosen as they contain a large cytoplasm unlike MDA MB 436 and HEK293T cells; the large cytoplasm facilitates studies on subcellular distribution. Results showed that the interaction between UCHL1 and TβRI occurs in a ligand dependent manner (Fig. 4F and Supplementary Fig. S3G-H). The interaction between UCHL1 and SMAD2 is not ligand dependent, but we found that the subcellular location of the interaction shifted from cytoplasm to nucleus after TGFβ treatment (Fig. 4F and supplementary Fig. S3F-H). Importantly, we found that the interaction between UCHL1 and TβRI occurs in the early endosome. The PLA signals for UCHL1-TβRI co-localized to a large extent with the early endosome marker FYVE-EGFP (Fig. 4G and supplementary video).

Next, we investigated whether UCHL1 can stabilize TβRI and SMAD2 protein levels. We examined the stability of TβRI or SMAD2 in the presence of cycloheximide upon misexpression of UCHL1 in HEK293T cells. Results demonstrated that UCHL1 overexpressing cells showed longer protein half-lives of TβRI and SMAD2 than control cells, while UCHL1 knockdown cells showed shorter protein half-lives of TβRI and SMAD2 than the PLKO cells (Fig. 4H and I). The mRNA level of TβRI and SMAD2 were not significantly different between UCHL1 overexpressing and knock down cells, compared to their control cells (Supplementary Fig. S4C and D). Thereafter, we investigated whether UCHL1 protects TβRI and SMAD2 from ubiquitination. We tested the ubiquitination of constitutively active TβRI (caTβRI) and SMAD2 with overexpression of wild type (WT) and catalytic inactive

mutant (C90A) UCHL1. Results showed that only WT UCHL1, but not C90A UCHL1 mitigates caTβRI and SMAD2 ubiquitination (Fig. 4J and K).
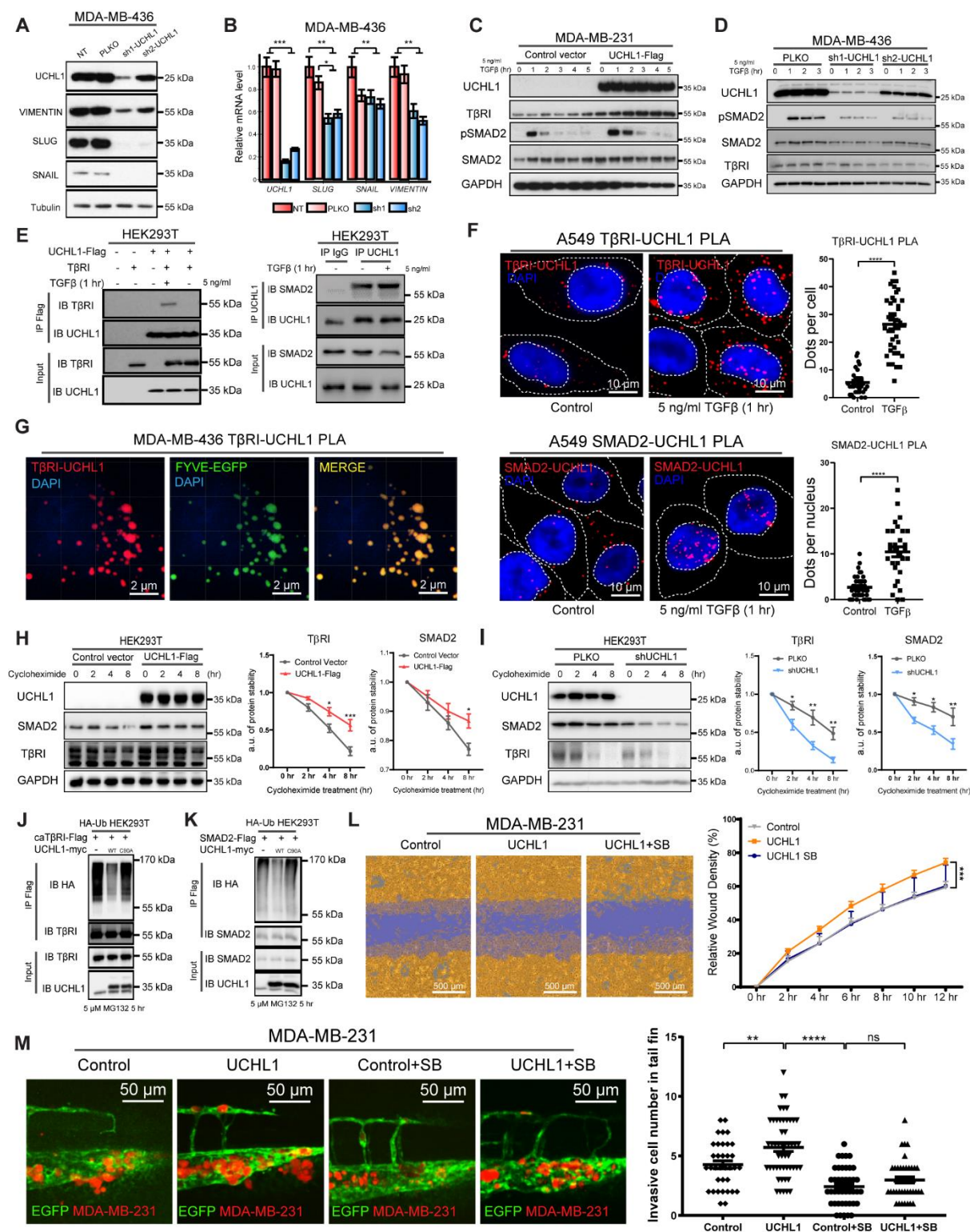
Figure 4. UCHL1 regulates mesenchymal phenotype of breast cancer cells and promotes TGFβ/SMAD signaling induced breast cancer extravasation. **A,** WB analysis of mesenchymal markers in UCHL1 shRNA knock down MDA-MB-436 cells. Same blot was used for UCHL1, SLUG and Tubulin (loading control). VIMENTIN and SNAIL blotting results were obtained from another blot using the same corresponding cell lysates. **B,** qPCR analysis of mesenchymal markers in UCHL1 shRNA knock down MDA-MB-436 cells. **,** P < 0.01, ***, P < 0.001, two-way ANOVA **C,** WB

analysis of TβRI, SMAD2 and TGFβ-induced pSMAD2 in control and UCHL1 overexpressed MDA-MB-231 cells. Same blot was used for TβRI and GAPDH (loading control). UCHL1 and pSMAD2 blotting results were obtained from another blot using the same corresponding cell lysates. SMAD2 result were obtained from another blot using the same corresponding cell lysates. **D,** WB analysis of TβRI, SMAD2 and pSMAD2 in PLKO and UCHL1 shRNA knockdown MDA-MB-436 cells. Same blot was used for UCHL1, pSMAD2 and GAPDH (loading control). TβRI and SMAD2 results were derived from another two blots using the same corresponding cell lysates. **E,** The Interaction of UCHL1 with TβRI was detected by immunoprecipitation (IP) of Flag-tagged UCHL1 and immunoblotting (IB) for TβRI in HEK293T cells (left). The endogenous interaction of UCHL1 with SMAD2 was detected by IP of endogenous UCHL1 and IB for SMAD2 in HEK293T cells (right). IP results were obtained from same blot. Input results were from another blot using the same corresponding cell lysates as used for IP. **F,** PLA of TβRI-UCHL1 and SMAD2-UCHL1 in A549 cells treated with or without 5 ng/ml TGFβ for 1 hour. Representative images are shown in the left panel and signal analysis are shown in the right panel. ****, P < 0.0001, unpaired Student t test. **G,** PLA of TβRI-UCHL1 in MDA-MB-436 cells transfected with early endosome marker FYVE-EGFP and treated with 5 ng/ml TGFβ for 1 hour. **H,** Expression levels of TβRI and SMAD2 were analysed by IB in UCHL1 overexpressed and control HEK293T cells treated with 10 µg/ml cycloheximide for the indicated times. WB results are shown in the left panel, and quantification of protein stability of TβRI and SMAD2 are shown in the two panels on the right. Same blot was used for TβRI and GAPDH (loading control). UCHL1 and SMAD2 blotting results were derived from another blot using the same corresponding cell lysates. **I,** Expression levels of TβRI and SMAD2 were analysed by IB in PLKO and shUCHL1 HEK293T cells treated with 10 µg/ml cycloheximide for the indicated times. WB results are shown in the left panel, protein stability analysis of TβRI and SMAD2 are shown in the right panel. Same blot was used for TβRI and GAPDH (loading control). UCHL1 and SMAD2 results were derived from another blot using the same corresponding cell lysates. **J,** Ubiquitination of TβRI was detected by IP of Flag-tagged constitutively active TβRI (caTβRI) from HA-Ub transfected HEK293T cells with WT-UCHL1-myc or C90A-UCHL1-myc overexpression. IP results were obtained from same blot. Input results were obtained from another blot using the same corresponding cell lysates. **K,** Ubiquitination of SMAD2 was detected by IP of Flag-tagged SMAD2 from HA-Ub transfected HEK293T cells with WT-UCHL1-myc or C90A-UCHL1-myc overexpression. IP results were obtained from same blot. Input results were obtained from another blot using the same corresponding cell lysates. **L,** Real-time scratch assay results of Control, UCHL1 and UCHL1+SB MDA-MB-231 cells. Representative scratch wounds are shown at the end time point of the experiment (left). The region of the original scratch is coloured in purple and the area of cell is coloured in yellow. Relative wound density (closure) were plotted at indicate times (right). **M,** *In vivo* zebrafish extravasation assay of UCHL1 overexpressed and control vector expressed MDA-MB-231 cells treated with or without TβRI kinase inhibitor SB-431542. SB groups zebrafish were treated with 5 µM inhibitor in the egg water for 6 days after injection, and refreshed every other day. **, *P* < 0.01, ****, *P* < 0.0001, two-way ANOVA. Representative images from 4 groups with zoom in of the tail fin area are shown in the left panel. Analysis of invasive cell number of Control, Control+SB, UCHL1 and UCHL1+SB groups in zebrafish extravasation assay are shown in the right panel.

In addition, we found that UCHL1 mainly regulates lysine 48-linked poly-ubiquitination of TβRI and SMAD2 (Supplementary Fig. S4E and F). Besides, we found that recombinant UCHL1 protein is able to deubiquitinate TβRI and SMAD2 *in vitro* directly, and *N*-ethylmaleimide (NEM) treatment blocked this process by inhibiting UCHL1 DUB activity (Supplementary Fig. S4H and I).

To investigate whether UCHL1-induced metastasis is dependent on its ability to potentiate TGFβ signaling, we employed the selective TβRI /SMAD signaling inhibitor SB431542 (SB) to block TGFβ receptor signaling in migration and extravasation assays. In a scratch assay, SB treatment blocked the ability of UCHL1 to promote MDA-MB-231 cell migration (Fig. 4L). Results of the extravasation assay showed that SB also blocked the stimulatory effect of

UCHL1 on MDA-MB-231 cell extravasation in an *in vivo* zebrafish xenograft model (Fig. 4 M). Besides, we performed functional rescue experiments. Ectopic expression of TβRI, SMAD2 or SMAD3 mimicked the promoting effect of UCHL1 on migration of MDA-MB-231 cells as measured by real-time imaging system (Supplementary Fig. S5A). In addition, we found that overexpression of TβRI, SMAD2 or SMAD3 partially compensated the inhibitory effect of UCHL1 knock down in MDA-MB-436 cells in a migration assay (Supplementary Fig. S5B). Altogether, these results demonstrate that UCHL1 facilitates TGFβ signaling-induced TNBC migration and extravasation by protecting TβRI and SMAD2 from ubiquitination. Besides, we found that DUB activity of UCHL1 is required for the metastasis-promoting activity of UCHL1. When we overexpressed C90A catalytically inactive mutant of UCHL1 in MDA-MB-231 cells, UCHL1 lost its promotion function and showed slightly dominant-negative regulation of migration and extravasation (Supplementary Fig. S5C and D).

UCHL1 activity inhibitor antagonizes TGFβ/SMAD signaling and inhibits breast cancer migration and extravasation

In order to study the effect of UCHL1 activity inhibition on the TGFβ pathway and breast cancer metastasis we turned to a recently reported panel of UCHL1 inhibitors and decided to synthesize and characterize one of the most potent ones (23). This compound, 6RK73 covalently binds to UCHL1 (Fig. 5A and Supplementary Fig. S6A), showed excellent inhibitory potency towards UCHL1 based on an *in vitro* half-maximum inhibitory concentration (IC_{50}) assay, and a high selectivity over other DUBs including its closest family members UCHL3 and UCHL5 (Fig. 5B). We examined its effect in living cells, and we took along the reversible competitive UCHL1 inhibitor LDN57444. 6RK73 showed more potent inhibition than LDN57444 on UCHL1 activity in MDA-MB-436 cells by TAMRA ABP assay; the inhibitory efficiency of 6RK73 was comparable to genetic knockdown of UCHL1 (Fig. 5C). Next, we used 6RK73 to test its specificity against UCHL1 activity on all the DUBs by performing a TAMRA ABP assay in patient tumor specimen, only UCHL1 band decreased among all the DUBs detected (Fig. 5D). We can conclude that 6RK73 displays a potent and specific inhibitory effect on UCHL1 both *in vitro* and *in vivo*.

To investigate whether 6RK73 can inhibit TGFβ signaling, we performed a $CAGA_{12}$-Luc transcriptional reporter assay in HEK293T cells. Treating cells with 6RK73 inhibited the TGFβ/SMAD-induced transcriptional response (Fig. 5E). Moreover, 6RK73 treatment of MDA-MB-436 cells displayed strong inhibition of the TGFβ-induced pSMAD2 and pSMAD3, and a decrease of TβRI and total SMAD protein levels; the inhibitory efficiency of 6RK73 was stronger than the effect observed after shRNA-mediated UCHL1 knockdown (Fig. 5F and Supplementary Fig. S6B). Furthermore, we tested the effect of 6RK73 on migration of MDA-MB-436 cells. 6RK73 treated MDA-MB-436 cells migrated significantly slower than the DMSO control group (Fig. 5G and H). To study 6RK73 function in extravasation, we used the MDA-MB-436 cells injected zebrafish xenograft treated with DMSO or 6RK73 that was added in the egg water surrounding the zebrafish embryos. Extravasation of the cells in 6RK73-treated zebrafish were potently inhibited (Fig. 5I and J). Taken together, 6RK73 showed specific inhibition of UCHL1 activity and TGFβ/SMAD2 and SMAD3 signaling, and potent inhibition of breast cancer migration and extravasation.
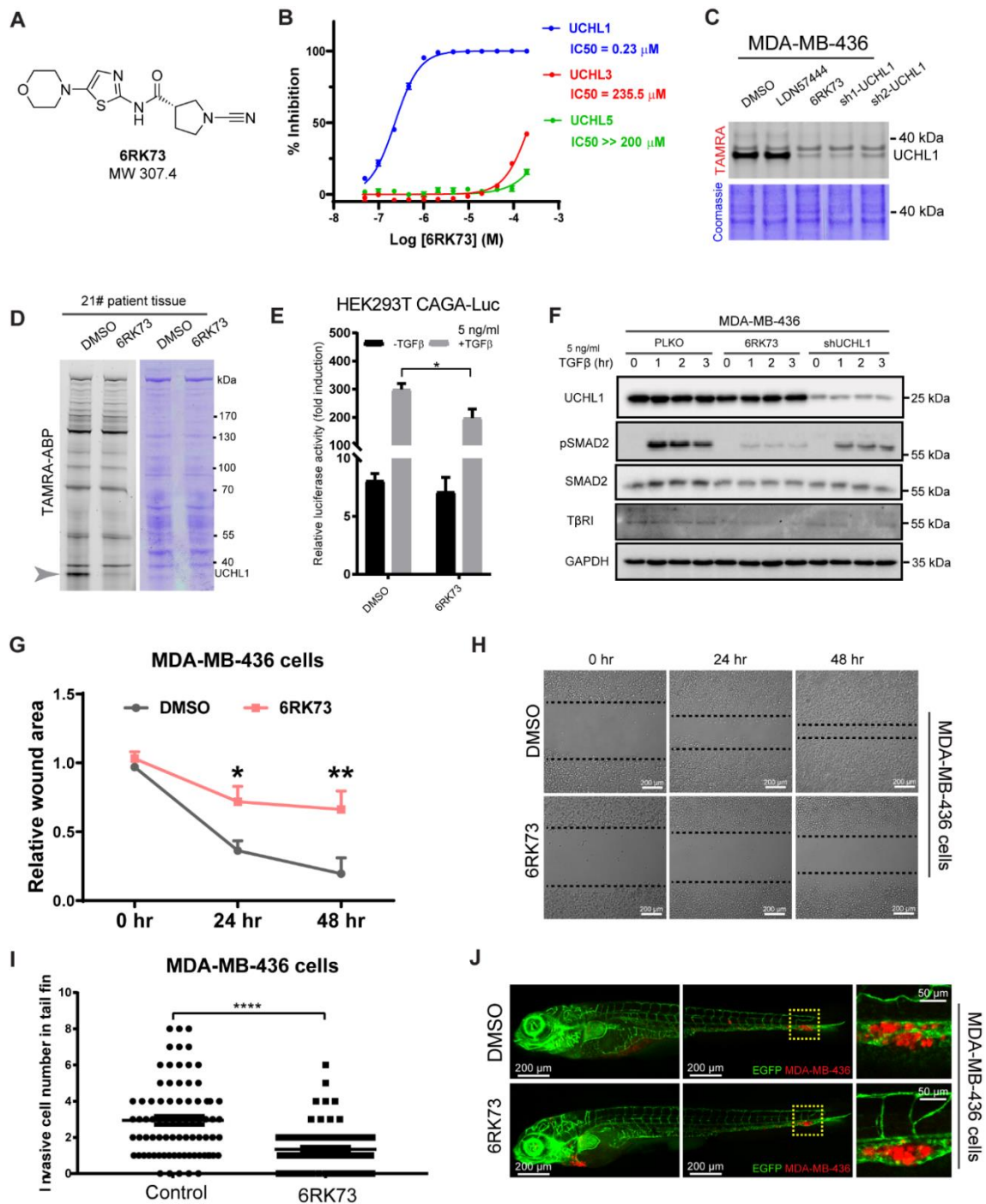
Figure 5. UCHL1 activity inhibitor antagonizes TGFβ signaling and inhibits breast cancer migration and extravasation. **A,** Chemical structure of the selective covalent UCHL1 activity inhibitor 6RK73. **B,** IC50 analysis of 6RK73. **C,** TAMRA ABP analysis of UCHL1 reversible activity inhibitor LDN67444 and covalent activity inhibitor 6RK73 in MDA-MB-436 cells, 5 µM LDN57444 or 6RK73 was added to the cells overnight. TAMRA and Coomassie results were obtained from the same gel. **D,** TAMRA ABP analysis of 6RK73 in 21# patient specimen, 5 µM 6RK73 was added in the lysate for 30 min. TAMRA and Coomassie results were obtained from the same gel. **E,** CAGA$_{12}$-Luc reporter analysis of 6RK73 in HEK293T cells, 5 µM 6RK73 was added to the cells overnight. *, $P < 0.05$, two-way ANOVA. **F,** WB analysis of TβRI, SMAD2 and pSMAD2 in MDA-MB-436 cells treated with or without 5 µM 6RK73 overnight. Same blot was used for UCHL1, pSMAD2 and GAPDH (loading control). TβRI and SMAD2 were obtained from another two blots using the same corresponding cell lysates. **G,** *In vitro* scratch wound healing assay of MDA-MB-436 cells treated

with and without 5 µM 6RK73 for 48 hr, time-lapse imaging was performed every hour. Relative wound area was analysed for each group at indicate times. *, $P < 0.05$, **, $P < 0.01$, two-way ANOVA. **H,** Representative images of cells from DMSO and 6RK73 groups. **I,** *In vivo* zebrafish extravasation assay of MDA-MB-436 cells, in which the injected zebrafish were treated with or without 6RK73 for 6 days. 5 µM 6RK73 was added in the egg water and refreshed every other day. Invasive cell number were analysed for DMSO and 6RK73 groups. ****, $P < 0.0001$, unpaired Student t test. **J,** Representative images of zebrafish from DMSO and 6RK73 groups with zoom in of invasive cells are shown in the right panel.

UCHL1[+] exosomes upregulate TGFβ signaling and serves as blood-based biomarker for aggressive breast cancer.

Clinically, UCHL1 has successfully been used as blood biomarker for traumatic brain injury and concussion (28). However, it is unknown whether UCHL1 has a role and/or is present in breast cancer patient sera. Therefore, we performed a UCHL1 enzyme-linked immunosorbent assay (ELISA) on sera samples collected from TNBC patients and healthy donors. Interestingly, UCHL1 protein levels in the TNBC group are significantly higher as compared to healthy controls (Fig. 6A). In addition, UCHL1 levels are also higher in ER negative patient sera than in sera from ER positive cases (Supplementary Fig. S6C). Nevertheless, UCHL1 is not a secreted protein, and this raised the question on how UCHL1 can be found in the blood circulation. A recent study demonstrated that cancer overexpressed proteins can be packaged in exosomes and enter circulation which is useful for minimally-invasive cancer detection (29). We hypothesized that UCHL1 overexpressed in aggressive breast cancer may be secreted via exosomes by cells and that circulated in the blood of patients via exosomes. To further verify this hypothesis, we isolated exosomes from breast cancer patient sera by differential ultracentrifugation (24), and found that the total amount of UCHL1 in sera is highly enriched in the isolated exosomes fraction (Fig. 6B). Next, we isolated exosomes from conditioned media of MDA-MB-436 (TNBC) and MCF-7 (non TNBC) cell cultures. ELISA results showed that the UCHL1 levels were higher in exosomes isolated from MDA-MB-436 cells than from MCF-7 cells. Moreover, UCHL1 level significantly decreased in exosomes isolated from MDA-MB-436 cells that were depleted for UCHL1 compared with PLKO cells (Fig. 6C). WB analysis of UCHL1, and that of a common exosomal marker protein Flotillin-1, showed lower UCHL1 levels in MCF7 exosomes than MDA-MB-436 exosomes, and a decreased UCHL1 level in shUCHL1 MDA-MB-436 exosomes (Fig. 6D). Exosomes are extracellular vesicles with a diameter of 50-200 nm (30). To further characterize the exosomes we isolated them from sera and cell conditioned media, we performed transmission electron microscopy (TEM) imaging to show the shape and size of these purified exosomes, and used nanoparticle tracking analysis (NTA) to determine their concentrations and size distributions. Results showed that both sera and cell samples displayed exosome-typical size and morphology by TEM analysis, and were enriched in the size from 100 nm to 200 nm vesicles by NTA analysis (Fig. 6E). Taken together, UCHL1 levels were significantly increased in TNBC patient sera, and highly enriched in exosomes of aggressive tumor bearing patient sera and TNBC cell conditioned media.

To further investigate whether UCHL1^{+} exosomes regulate TGFβ/SMAD signaling, we first tested the effect of the PLKO and shUCHL1 MDA-MB-436 exosomes on the CAGA$_{12}$-Luc transcriptional reporter activity in HEK293T cells. Treatment of UCHL1 containing

exosomes resulted in higher luciferase signal in HEK293T cells than exosomes in which UCHL1 was depleted (Fig. 6F).
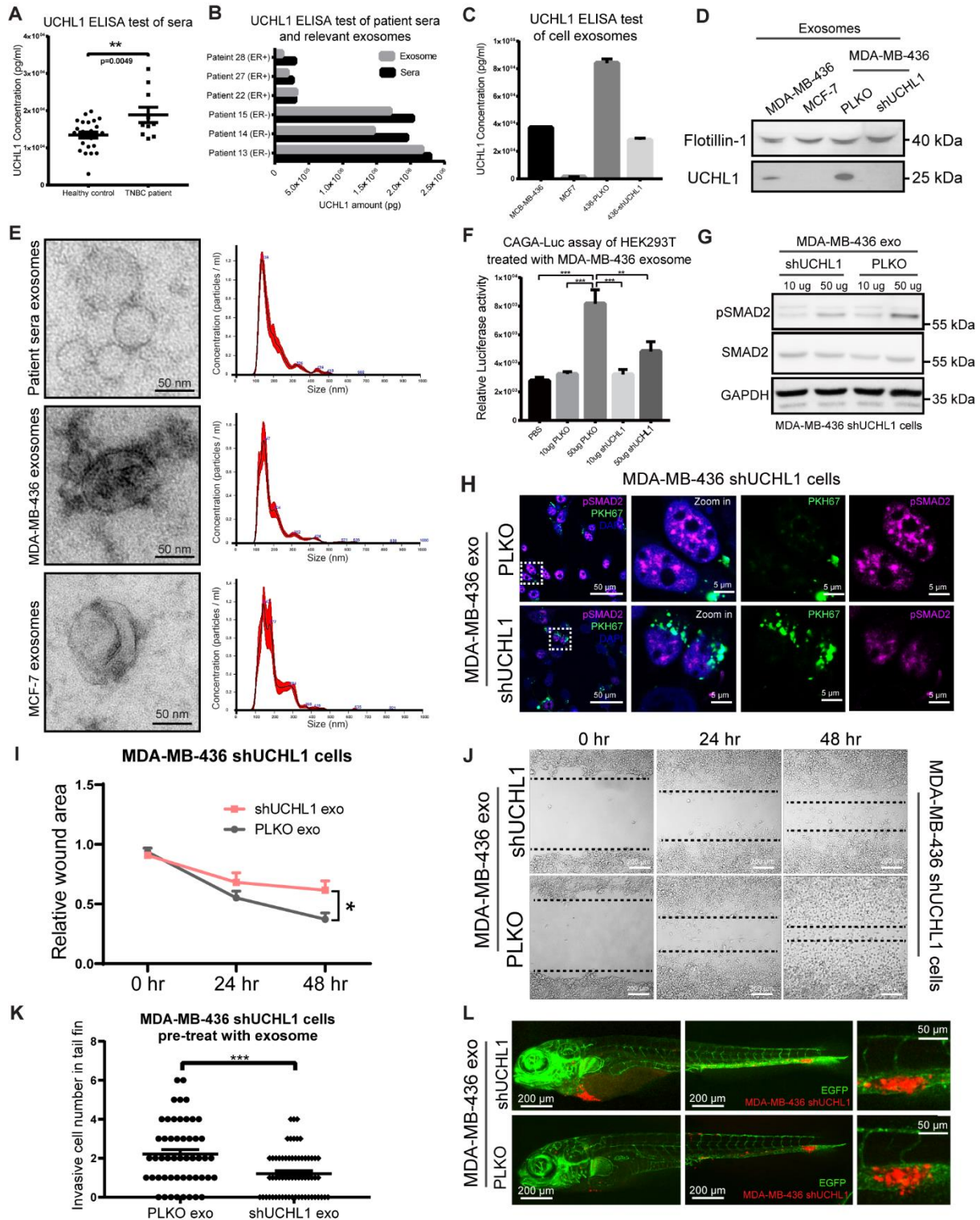
Figure 6. UCHL1$^+$ exosomes upregulate TGFβ signaling and serves as blood-based biomarker for aggressive breast cancer. **A,** ELISA analysis of UCHL1 levels in serum samples from healthy donors and TNBC patients. **, $P < 0.01$, unpaired Student t test. **B,** ELISA analysis of UCHL1 level in serum and relative exosomes from 6 breast cancer patients. **C,** ELISA analysis of UCHL1 level in exosomes from breast cancer cell lines. **D,** WB analysis of exosomes maker Flotillin-1 and UCHL1 in exosomes from four breast cancer cell lines. Same blot was used for UCHL1 and Flotillin-1 (loading

control). **E,** TEM imaging of exosomes from patient serum and breast cancer cell lines (left). Nanoparticle tracking analysis (NTA) of relative exosomes (right). X-axis represents exosomes size distribution. Y-axis shows the concentration of exosomes. **F,** CAGA$_{12}$-Luc transcriptional reporter analysis of HEK293T cells treated with UCHL1 high or low exosomes isolated from PLKO or shUCHL1 MDA-MB-436 cells. **, $P < 0.01$, ***, $P < 0.001$, two-way ANOVA. **G,** WB analysis of SMAD2 and pSMAD2 in MDA-MB-436 UCHL1 stable known down cells treated with exosomes isolated from PLKO or shUCHL1 MDA-MB-436 cells. Same blot was used for pSMAD2 and GAPDH (loading control). SMAD2 blotting results were obtained from another blot using the same corresponding cell lysates. **H,** Immunofluorescence staining of pSMAD2 in MDA-MB-436 UCHL1 stable known down cells treated with exosomes isolated from PLKO or shUCHL1 MDA-MB-436 cells labelled with green PKH67 exosomes dye. **I,** *In vitro* scratch wound healing assay of shUCHL1 MDA-MB-436 cells pre-treated with exosomes isolated from PLKO or shUCHL1 MDA-MB-436 cells for 24 hr, time-lapse imaging was carried out for 48 hours, images were taken every hour. Relative wound areas were analysed for each group at indicate times. *, $P < 0.05$, two-way ANOVA. **J,** Representative images of cells from PLKO and shUCHL1 groups. **K,** *In vivo* extravasation assay of zebrafish injected with shUCHL1 MDA-MB-436 cells pre-treated with exosomes isolated from PLKO or shUCHL1 MDA-MB-436 cells for 24 hr. Invasive cell number were analysed for PLKO and shUCHL1 groups. ***, $P < 0.001$, unpaired Student t test. **L,** Representative images of zebrafish from PLKO and shUCHL1 groups with zoom in of invasive cells on the right panel.

Consistent with this finding, pSMAD2 levels were also increased upon treatment with control exosomes from MDA-MB-436 cells but not by exosomes depleted of UCHL1 as analyzed by WB in MDA-MB-436 cells with UCHL1 knockdown (Fig. 6G). To further validate these results, we labelled the exosomes that were isolated from PLKO and shUCHL1 MDA-MB-436 cells with a fluorescent lipid dye (PKH67), and thereafter added them to MDA-MB-436 cells with UCHL1 knockdown. After the exosomes were taken up by the cells, we performed immunofluorescent (IF) staining of pSMAD2. Confocal microscopy imaging revealed that the pSMAD2 levels were higher in the cells which were treated with PLKO MDA-MB-436 cells exosomes than shUCHL1 MDA-MB-436 cells exosomes (Fig. 6H). To further evaluate the biological function of UCHL1$^+$ exosomes, we examined their effect on the migration of MDA-MB-436 cells with UCHL1 knockdown. Cells treated with PLKO MDA-MB-436 exosomes migrated more than exosomes depleted for UCHL1 (Fig. 6I and J). The potential function of UCHL1$^+$ exosomes was further validated in a zebrafish xenograft model by injecting MDA-MB-436 cells with UCHL1 knockdown. The cells pre-treated with PLKO MDA-MB-436 exosome showed more invasion and stronger extravasation phenotype than the cells pre-treated with shUCHL1 MDA-MB-436 exosome (Fig. 6K and L). Taken together, donor cells highly active for UCHL1 can via exosome transfer upregulate TGFβ/SMAD signaling in recipient cells and promote their migration and extravasation.

Discussion

Large-scale conventional genomic and proteomic profiling have been performed in breast cancer (31), and a growing numbers of DUBs have been uncovered to be aberrantly expressed in breast cancer (32). However, there is still very little knowledge on the overall activities of DUBs in breast cancer. Thus, we performed activity profiling studies using ABPs on DUBs in human breast cancer cell lines and patient tumor tissues to study its activity-related biological function in different subtypes of breast cancer. UCHL1 was identified as the most specific highly active DUB in the TNBC subtype, and targeting of its activity mitigated TNBC cell migration and metastasis.

In this work, two different ABP-based DUB activity profiling methods were performed. Each profiling method has its own advantages and drawbacks. The TAMRA ABP profiling method is a simple, fast and convenient method, which allow us to achieve a snapshot of the DUB activity landscape with a very small amount of protein, whereas the Biotin ABP profiling coupled to mass spectroscopy analysis method is a more laborious requiring a larger amount of protein, but enables for the identification of the DUBs in a quantitative manner. Both DUB activity profiling methods identified UCHL1 as the most specific highly active DUB in the TNBC subtype. In the Biotin ABP profiling, other DUBs such as USP4, were previously reported to promote breast cancer metastasis that were detected in the Biotin ABP profiling to be highly active in TNBC group (33). OTUD3 that displayed selective high activity in non-TNBC was found formerly to act as a suppressor in breast cancer tumorigenesis and metastasis (34) (Fig. 2C). There are some other interesting hits for which still little is known about their function in breast cancer that can be studied in the future (Supplementary Table S3 and S4). Although there are several reports that UCHL1 may possibly act as a tumor suppressor in breast cancer pathogenesis, most evidence supports its role as a positive regulator of tumorigenesis (35) (36). These differences may be attributed to differential action of UCHL1 in different breast cancer subtypes.

Functionally, we observed that UCHL1 promoted breast cancer migration, extravasation and metastasis both in zebrafish and mice xenograft models. Mechanistically, UCHL1 facilitates TGFβ/SMAD2 and SMAD3 signaling and TGFβ-induced TNBC migration and extravasation by protecting TβRI and SMAD2/3 from ubiquitination. Next, we found that UCHL1 mainly regulates lysine 48-linked ubiquitination of TβRI and SMAD2/3 (Supplementary Fig. S4E-G). The interaction of TβRI with UCHL1 was found to be ligand dependent. UCHL1 interacted more efficiently with ubiquitylated TβRI, and TGFβ triggers the ubiquitination of TβRI. The latter may thus contribute to the ligand-induced interaction between TβRI and UCHL1. The interaction between UCHL1 and TβRI occurs in early endosomes, where activated TGFβ receptor complexes promote SMAD dependent signaling responses (37). Although our results point to a pivotal role for UCHL1 in stimulating breast cancer extravasation by regulating TGFβ signaling, we do not preclude that UCHL1 may also promote invasion and metastasis by targeting other signaling proteins. Previous studies showed that UCHL1 can also regulate protein kinase B (AKT) and hypoxia-inducible factor 1 α (HIF1α) signaling (36) (38). However, upon shRNA-mediated knockdown in MDA-MB-436 cells we were unable to detect changes in AKT and HIF1α protein levels (Supplementary Fig. S3B), suggesting a context-dependent role for UCHL1 in breast cancer.

When comparing the UCHL1 inhibitor LDN57444 with 6RK73, LDN57444 is a reversible and competitive inhibitor of UCHL1 activity (IC_{50} = 0.88 µM) (39), whereas 6RK73 is a covalent irreversible inhibitor of UCHL1 activity (IC_{50} = 0.23 µM) (Fig. 5B and Supplementary Fig. S6A). LDN57444 also inhibit UCHL3 activity (IC_{50} = 25 µM) (39), whereas, 6RK73 showed almost no inhibition of UCHL3 (IC_{50} = 236 µM) (Fig. 5B). Besides, 6RK73 displayed a potent inhibition of breast cancer extravasation in zebrafish (Fig. 5I and J), and this result is reminiscent to the inhibitory effect observed upon genetic UCHL1 depletion (Fig. 3F and J). Clinically, high UCHL1 expression is also associated with many other types of cancers including lung, colorectal, and pancreatic (40). Thus, 6RK73 may provide a new

choice for the development of a clinical drug for targeting UCHL1 activity in the treatment of aggressive breast cancer and other UCHL1 overactive cancers.

In addition, UCHL1 was found to be highly enriched in TNBC patient sera compared with samples from healthy individuals. More importantly, we found that UCHL1 was specifically enriched in exosomes from aggressive breast cancer patient sera and TNBC cell conditioned medium. In this respect, our finding that UCHL1 and TβRI colocalize in early endosomes is of interest as early endosomes are precursor vesicles for exosomes (41). Another group, also recently detected UCHL1 in the exosomes of breast cancer patient sera, and high UCHL1 levels were found to be correlated with chemotherapy resistance phenotype (42). We found that UCHL1$^+$ exosomes upregulated TGFβ/SMAD signaling and promoted migration and extravasation of the recipient breast cancer cells. This suggests that UCHL1 may act in cancer cells in both cell autonomous and paracrine manners to stimulate tumorigenesis.

Altogether, our results demonstrate the important roles for UCHL1 in breast cancer migration and extravasation by upregulating TGFβ signaling and highlight a potential novel therapy for cancer treatment by targeting UCHL1. UCHL1-containing exosomes also have the potential to be a blood-based biomarker for early diagnosis of aggressive breast cancer. The selective, potent and covalent UCHL1 activity inhibitor 6RK73 may open new avenues for therapeutic intervention in breast cancer and beyond.
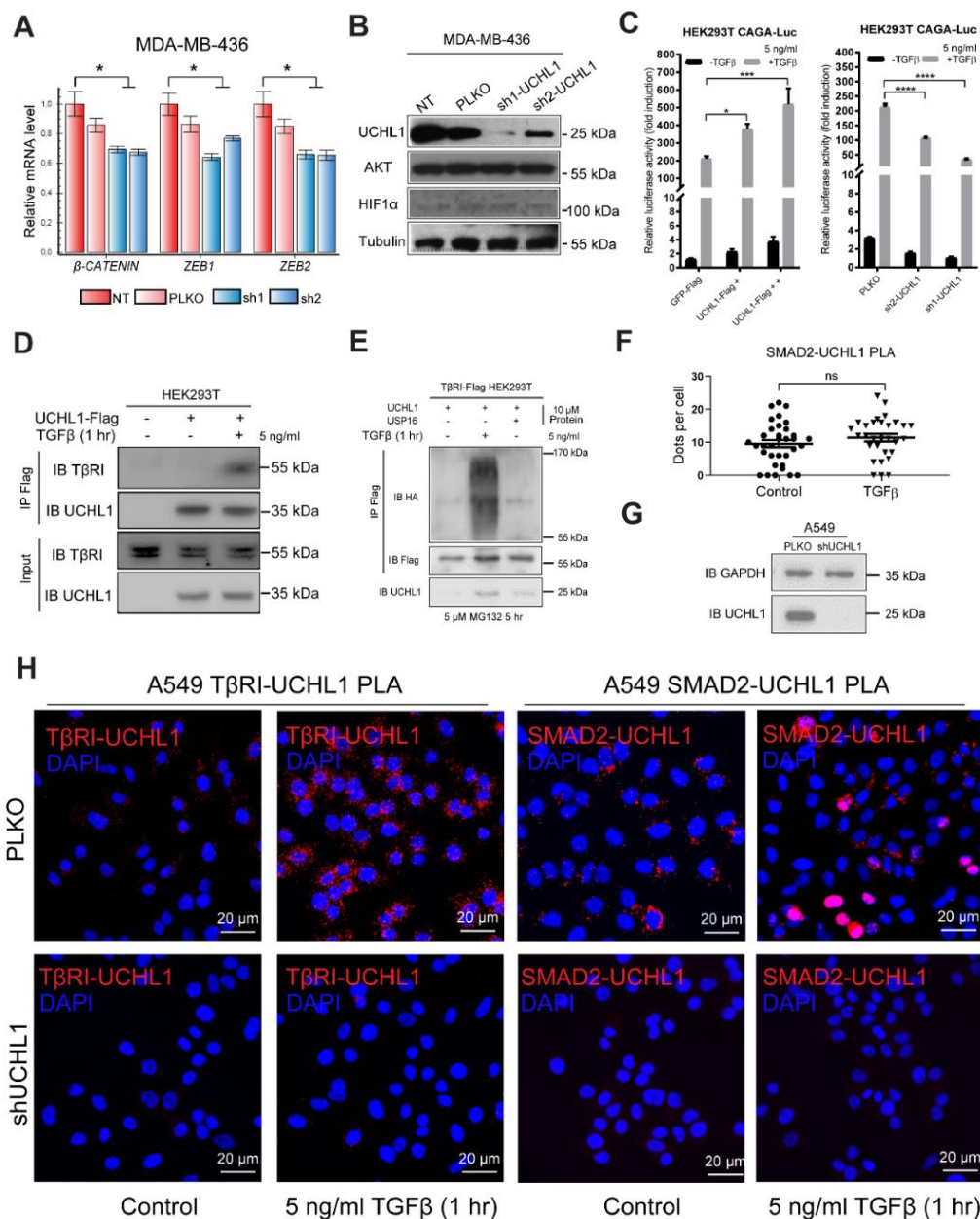
Supplementary Figures
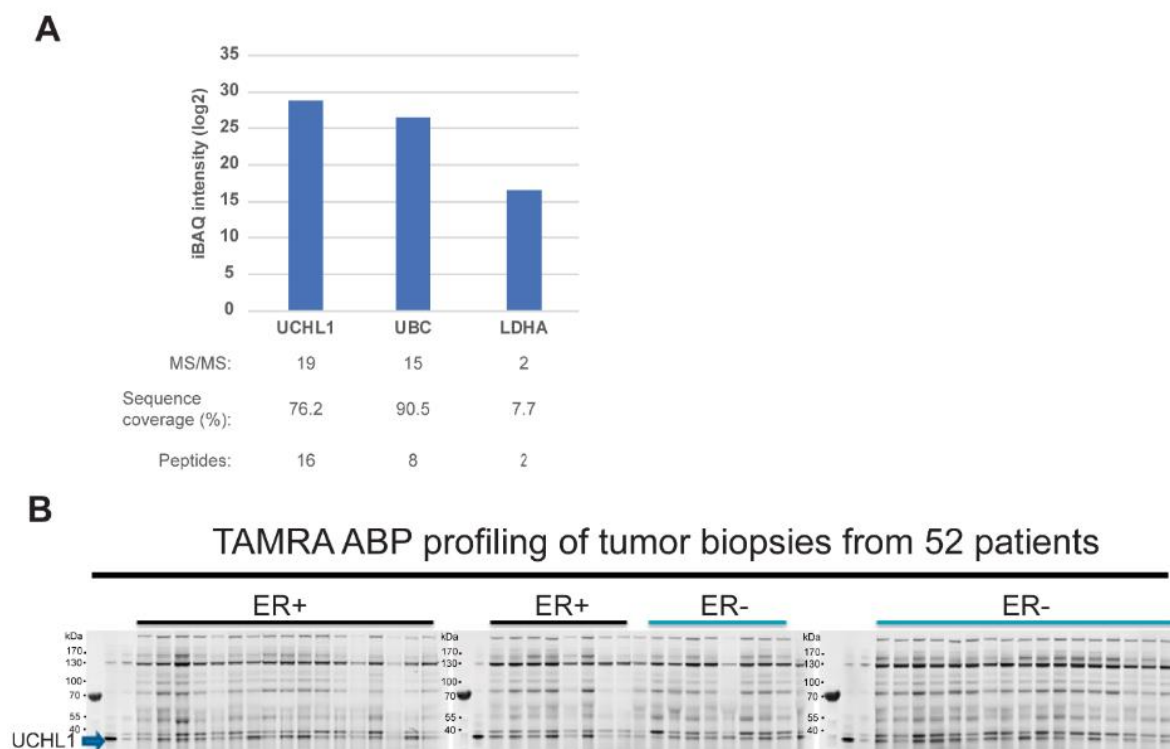
Supplementary Figure S1. Related to Figure 1. **A,** LC-MS/MS analysis of in-gel tryptic digestion of excised gel slice indicated in figure 1D. iBAQ values (log2), sequence coverage, spectral count and number of peptides identified, of proteins identified by more than 2 peptides are indicated. **B,** Global profiling of DUB activity in tumor tissues from 52 patients.
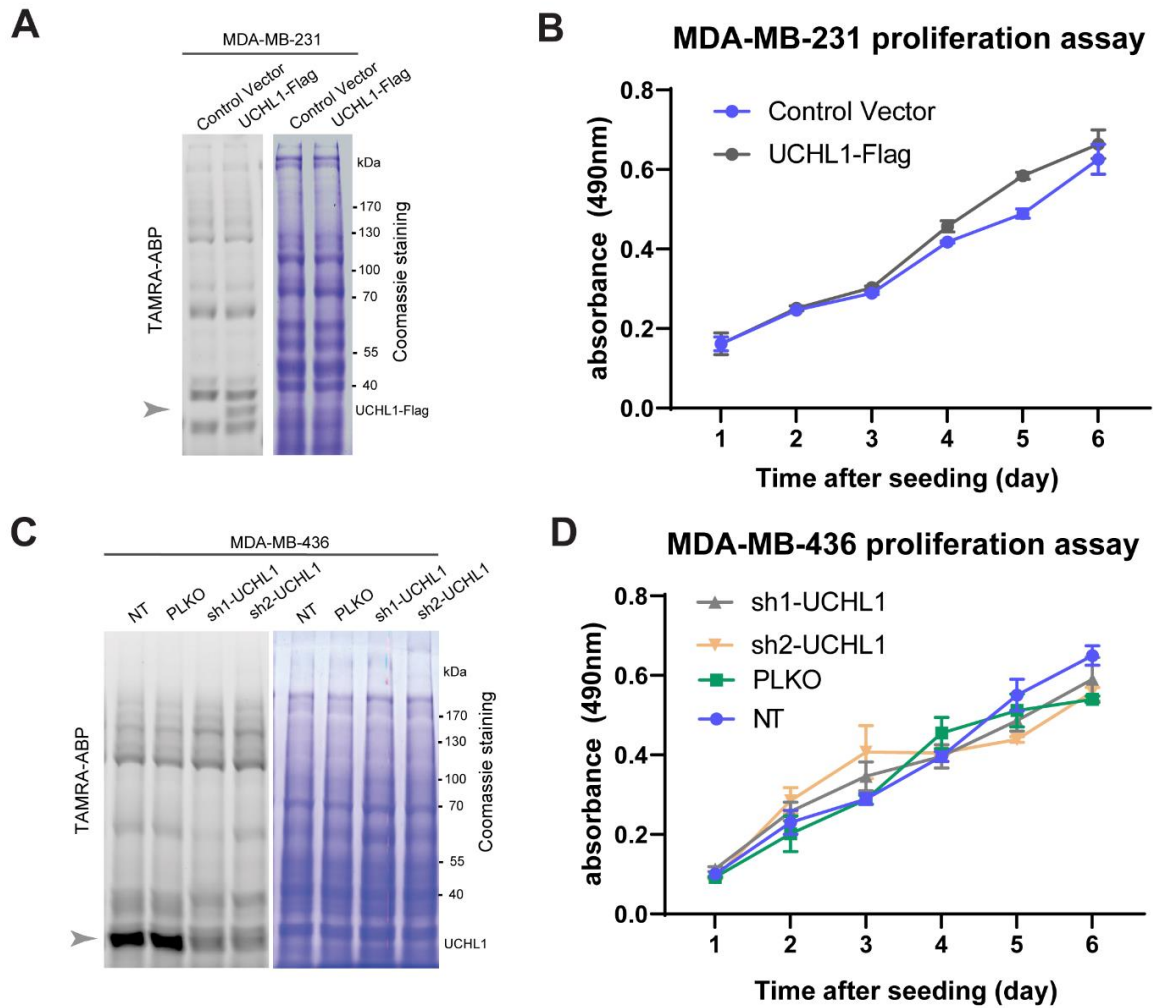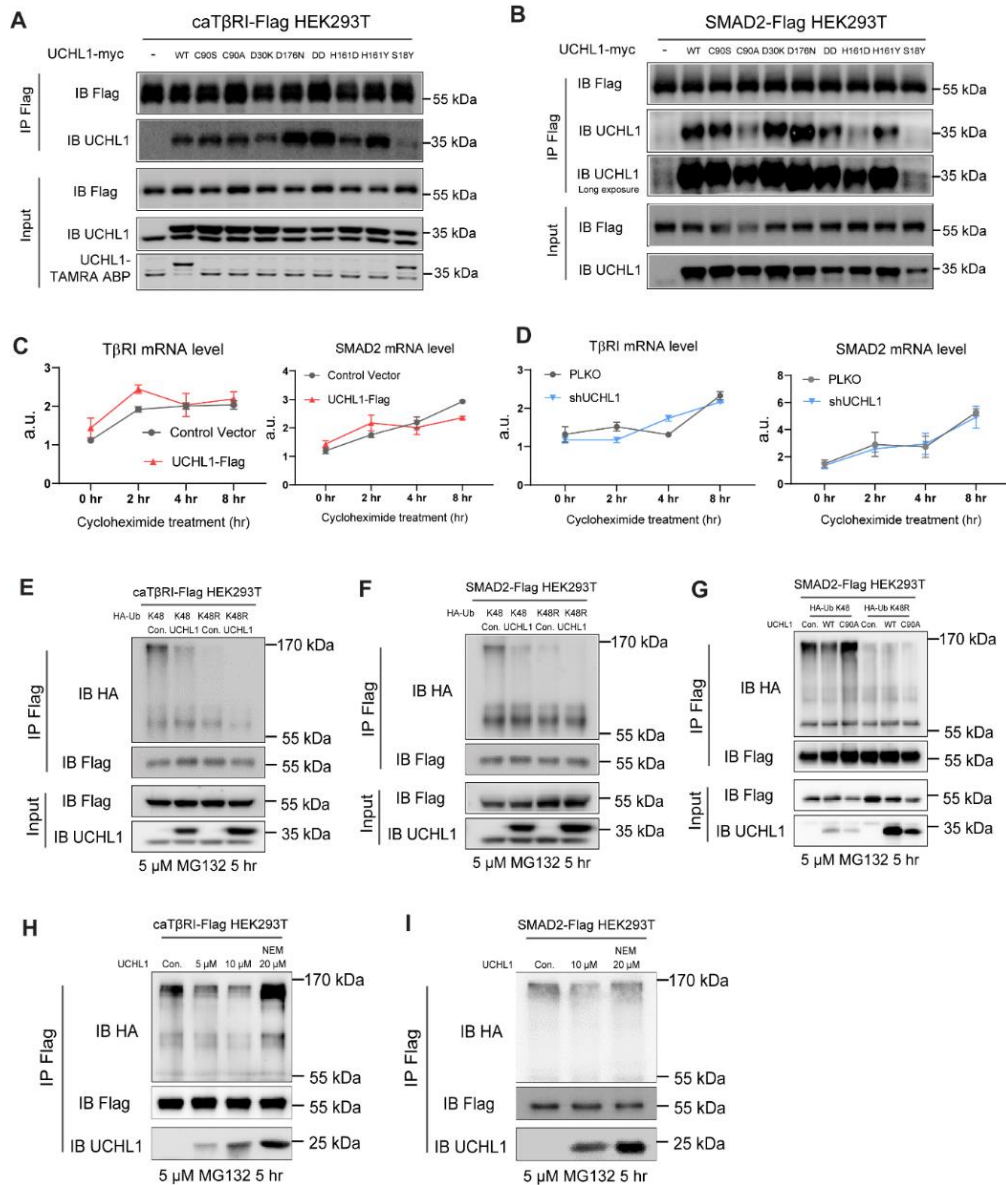
Supplementary Figure S2. Related to Figure 3. **A,** The UCHL1 activities of MDA-MB-231 cell lines stably transfected with control vector and UCHL1 expression vector were validated by TAMRA ABP assay. Coomassie staining of proteins in SDS-PAGE gel was used as loading controls. Arrowhead on left indicate UCHL1-Flag. TAMRA and Coomassie results were obtained from the same gel. **B,** Proliferation assay of MDA-MB-231 cell lines stably transfected with control vector and UCHL1 expression vector (as measured by MTS assay). **C,** Analysis of the UCHL1 activities in MDA-MB-436 cell lines infected with non-targeting (NT), empty vector (PLKO) and sh1-UCHL1 and sh2-UCHL1 lentivirus by TAMRA ABP assay. Coomassie of proteins in SDS-PAGE gel was used as loading control. Arrowhead on left indicates UCHL1. TAMRA and Coomassie results were obtained from the same gel. **D,** Proliferation assay of NT, PLKO, sh1-UCHL1 and sh2-UCHL1 MDA-MB-436 cell lines (as measured by MTS assay).
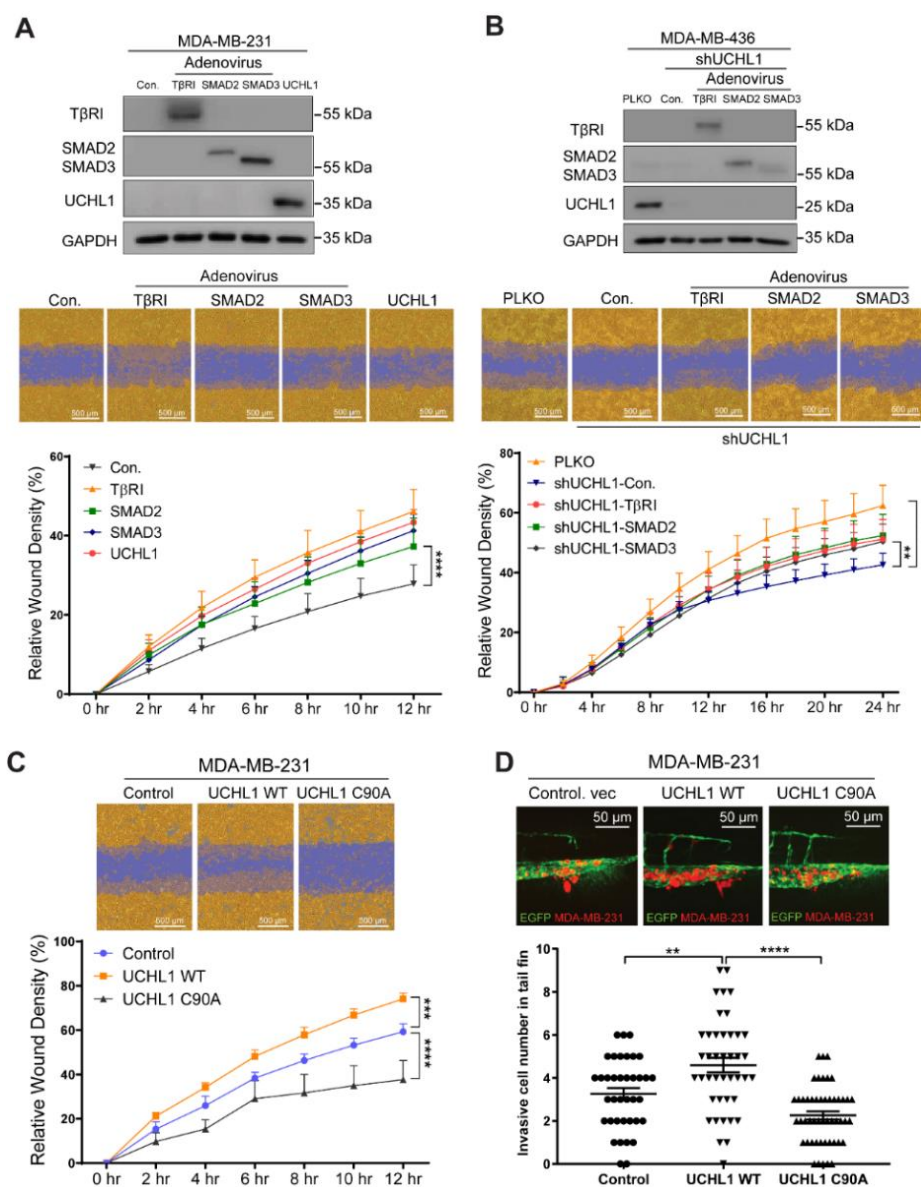
Supplementary Figure S3. Related to Figure 4. **A,** qPCR analysis of mesenchymal markers in UCHL1 shRNA knock down MDA-MB-436 cells versus NT and PLKO control infected cells. *, P < 0.05, two-way ANOVA. **B,** Western blot analysis of AKT and HIF1α expression levels in UCHL1 shRNA knock down MDA-MB-436 cells versus NT and PLKO control infected cells. Tubulin served as loading control and the same blot was probed for HIF1α levels. UCHL1 and AKT were from another blot using the same cell lysates. **C,** TGFβ-induced SMAD3/SMAD4-dependent CAGA$_{12}$-Luc transcriptional reporter analysis upon UCHL1 overexpression (left) and UCHL1 shRNA knock down (right) in HEK293T cell lines. *, P < 0.05, ***, P < 0.001 and ****, P < 0.0001, two-way ANOVA. **D,** Interaction of UCHL1 and TβRI as detected by immunoprecipitation (IP) of Flag-tagged UCHL1 and immunoblot (IB) for endogenous TβRI in HEK293T cells. IP results using TβRI and UCHL1 antibodies were obtained from the same blot. Input blotting results using TβRI and UCHL1 antibodies were obtained from the same blot using the same cell lysates as for IP. **E,** *In vitro* interaction of recombinant UCHL1 protein with TβRI that is ubiquitinated (isolated by IP from TβR1 transfected cells treated with TGF-β) and TβRI with low levels of ubiquitination (TβRI was treated with a general DUB USP16 to remove attached ubiquitin from TβRI). All results were obtained from one blot. **F,** Quantification of PLA analysis of endogenous interaction between UCHL1 and SMAD2 in A549 cells. Number of dots per cell in control and TGFβ (5 ng/ml) groups in SMAD2-UCHL1 PLA are shown. ns, not significant, unpaired Student *t* test. **G,** Western blot of UCHL1 in A549 PLKO and shUCHL1 cells. GAPDH served as loading control and the same blot was used to probe for UCHL1 levels. **H,** PLA of TβRI-UCHL1 and SMAD2-UCHL1 in PLKO and shUCHL1 A549 cells treated with or without 5 ng/ml TGFβ for 1 hr.
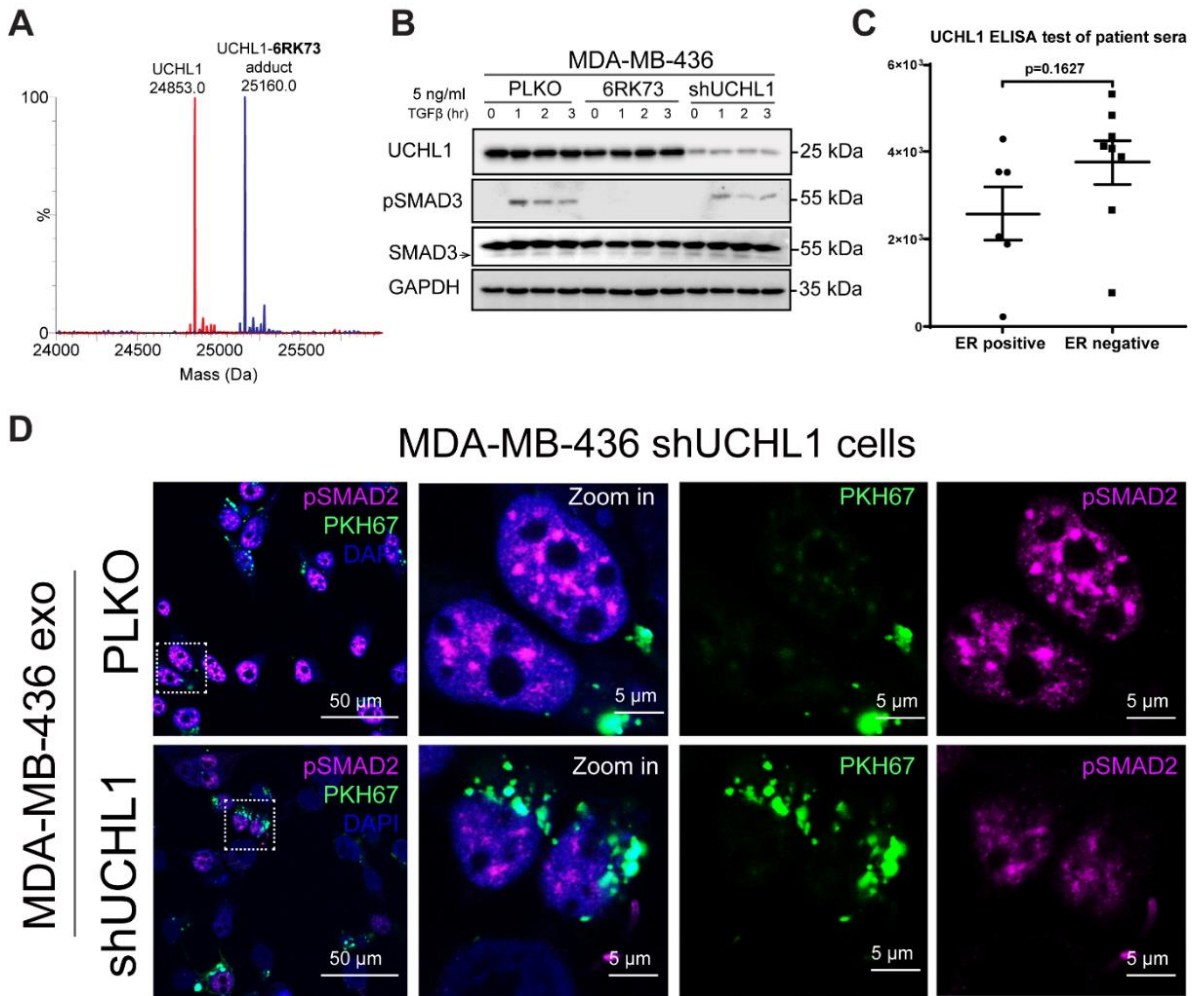
Supplementary Figure S4. Related to Figure 4. **A,** UCHL1-TβRI interaction and ubiquitination of TβRI in HEK293T cells that ectopically express UCHL1 with different specific amino acid mutations. IP results with Flag and UCHL1 antibodies were obtained from the same blot. Input results with Flag and UCHL1 were obtained from another blot using the same corresponding cell lysates as for IP. **B,** UCHL1-SMAD2 interaction and ubiquitination of SMAD2 in HEK293T cells that ectopically express UCHL1 with different specific amino acid mutations. IP results were from obtained same blot. Input results were obtained from another blot using the same corresponding cell lysates as for IP. **C,** qPCR analysis of TβRI and SMAD2 mRNA expression levels in the presence of cycloheximide in HEK293T cells upon control and UCHL1 overexpression HEK293T cells. **D,** qPCR analysis of TβRI and SMAD2 mRNA expression levels in the presence of cycloheximide in PLKO and shUCHL1 HEK293T cells. **E,** *In vivo* (de)ubiquitination assay of TβRI in K48 or K48R HA-Ub expressing HEK293T cells with WT-UCHL1-myc or control vector overexpression. IP results were obtained from same blot. Input results were from another blot using the same corresponding cell lysates as for IP. **F,** *In vivo* (de)ubiquitination assay of SMAD2 in K48 or K48R HA-Ub expressing HEK293T cells with WT-UCHL1-myc or control vector overexpression. IP results were obtained from same blot. Input results were obtained from another blot using the same corresponding cell lysates as for IP. **G,** *In vivo* ubiquitination assay of SMAD3 in K48 or K48R HA-Ub expressing HEK293T cells with WT-UCHL1-myc or C90A-UCHL1-myc overexpression. IP results were obtained from same blot. Input results were obtained from another blot using the corresponding cell lysates as for IP. **H,** *In vitro* (de)ubiquitination assay of TβRI incubated with recombinant UCHL1 or inactive UCHL1 protein without and with treatment with NEM. All results were obtained from one blot. **I,** *In vitro* (de)ubiquitination assay of SMAD2 incubated with recombinant UCHL1 or inactive UCHL1 without and with treatment of NEM. All results were obtained from one blot.

Supplementary Figure S5. Related to Figure 4. **A,** Real-time scratch assay of MDA-MB-231 cells that are engineered to overexpressed TβRI, SMAD2 or SMAD3 using the IncuCyte system. Western blot analysis of TβRI, SMAD2 or SMAD3 expression levels in MDA-MB-231 cells (above). Representative scratch wound results at the end time point of the experiment are shown (middle). The region of the original scratch is colored in purple and the area of cell migration into the scratch is colored in yellow. Relative wound density (closure) is plotted at indicate times (below). ****, $P < 0.0001$, two-way analysis of variance (ANOVA). GAPDH served as loading control and the same blot was used to probe for TβRI levels. UCHL1 and SMAD2/3 were from another blot using the same corresponding cell lysates. **B,** Real-time scratch assay of MDA-MB-436 shUCHL1 cells that are engineered to overexpressed TβRI, SMAD2 or SMAD3 using the IncuCyte system. Western blot of TβRI, SMAD2 or SMAD3 expression levels in MDA-MB-436 shUCHL1 cells (above). Representative scratch wound results at the end time point of the experiment are shown (middle). Relative wound density (closure) is plotted at indicate times (below). **, $P < 0.01$, ****, $P < 0.0001$, two-way analysis of variance (ANOVA). GAPDH served as loading control and this blot was used to probe for TβRI levels. UCHL1 and SMAD2/3 levels in corresponding cell lysates were determined using another blot. **C,** Real-time scratch assay of MDA-MB-231 cells that overexpress with UCHL1 WT or UCHL1 C90A using the IncuCyte system. Representative scratch wound results at the end time point of the experiment are shown (above). Relative wound density (closure) is plotted at indicate times (below). ***, $P < 0.001$, ****, $P < 0.0001$, two-way analysis of variance (ANOVA). **D,** *In vivo* zebrafish extravasation assay of MDA-MB-231 cells that overexpress UCHL1 WT or UCHL1 C90A. Representative images of zebrafish tail fin with zoom in of invasive cells (above). Analysis of invasive cell numbers of control, UCHL1 WT and UCHL1 C90A groups in zebrafish extravasation experiment (below). **, $P < 0.01$, ****, $P < 0.0001$, two-way analysis of variance (ANOVA).

Supplementary Figure S6. Related to Figure 5 and 6. **A,** Mass spectrometry analysis reveals covalent binding of 6RK73 to UCHL1. **B,** Western blot of SMAD3 and pSMAD3 in MDA-MB-436 cells treated with or without 6RK73 and shUCHL1 cells. GAPDH served as loading control and the same blot was used to detect UCHL1. pSMAD3 and SMAD3 were obtained from another two blots using the same corresponding cell lysates. **C,** ELISA analysis of UCHL1 levels in serum samples from ER positive and ER negative breast cancer patients. P=0.1627, unpaired Student t test. **D,** Immunofluorescence staining of pSMAD2 in MDA-MB-436 UCHL1 stable known down cells treated with exosomes isolated from PLKO or shUCHL1 MDA-MB-436 cells that were labelled with green PKH67 exosomes dye.

Supplementary information availability

Supplementary methods, Supplementary Tables S1-S6 and Supplementary Video are available upon request using the following link:
https://clincancerres.aacrjournals.org/content/early/2019/12/19/1078-0432.CCR-19-1373

Chapter 4

Authors' Contributions

Conception and design: P. ten Dijke, S. Liu

Development of methodology: S. Liu, M. van Dinther, R. González-Prieto, H. Zhu

Acquisition of data (provided animals, acquired and managed patients, provided facilities, etc.): S. Liu, R. González-Prieto, M. Zhang, P.P. Geurink, P.V. Iyengar, M. van Dinther, R. Kooij, E. Bos, X. Zhang, S. Le Dévédec, B. van de Water, R.I. Koning, W. Mesker, H. Ovaa, L. Zhang, A. Vertegaal, J.W.M. Martens, P. ten Dijke

Analysis and interpretation of data (e.g., statistical analysis, biostatistics, computational analysis): S. Liu, R. González-Prieto, M. Zhang, P.P. Geurink, P.V. Iyengar, M. van Dinther, R. Kooij, E. Bos, R.I. Koning, H. Zhu, W. Mesker, H. Ovaa, L. Zhang, A. Vertegaal, J.W.M. Martens, P. ten Dijke

Writing, review, and/or revision of the manuscript: S. Liu, R. González-Prieto, P.P. Geurink, J.W.M. Martens, P. ten Dijke

Study supervision: P. ten Dijke

Acknowledgments

References

1. Siegel RL, Miller KD, Jemal A. Cancer statistics, 2016. CA Cancer J Clin 2016;66:7-30.
2. Cummings MC, Simpson PT, Reid LE, Jayanthan J, Skerman J, Song S, *et al.* Metastatic progression of breast cancer: insights from 50 years of autopsies. J Pathol 2014;232:23-31.
3. Dongre A, Weinberg RA. New insights into the mechanisms of epithelial–mesenchymal transition and implications for cancer. Nat Rev Mol Cell Biol 2019;20:69-84.
4. Drabsch Y, ten Dijke P. TGF-β signaling in breast cancer cell invasion and bone metastasis. J Mammary Gland Biol Neoplasia 2011;16:97-108.
5. Becker A, Thakur BK, Weiss JM, Kim HS, Peinado H, Lyden D. Extracellular Vesicles in Cancer: Cell-to-Cell Mediators of Metastasis. Cancer Cell 2016;30:836-48.
6. Thery C. Cancer: Diagnosis by extracellular vesicles. Nature 2015;523:161-2.
7. Massagué J, Obenauf AC. Metastatic colonization by circulating tumor cells. Nature 2016;529:298-306.
8. Sorlie T, Perou CM, Tibshirani R, Aas T, Geisler S, Johnsen H, *et al.* Gene expression patterns of breast carcinomas distinguish tumor subclasses with clinical implications. Proc Natl Acad Sci U S A 2001;98:10869-74.

9. Leidy J, Khan A, Kandil D. Basal-like breast cancer: update on clinicopathologic, immunohistochemical, and molecular features. Arch Pathol Lab Med 2014;138:37-43.

10. Rochefort H, Glondu M, Sahla ME, Platet N, Garcia M. How to target estrogen receptor-negative breast cancer? Endocr Relat Cancer 2003;10:261-6.

11. Foulkes WD, Smith IE, Reis-Filho JS. Triple-Negative Breast Cancer. N Engl J Med 2010;363:1938-48.

12. Garrido-Castro AC, Lin NU, Polyak K. Insights into Molecular Classifications of Triple-Negative Breast Cancer: Improving Patient Selection for Treatment. Cancer Discov 2019;9:176-98.

13. Ciechanover A. The unravelling of the ubiquitin system. Nat Rev Mol Cell Biol 2015;16:322-4.

14. Liu S, de Boeck M, van Dam H, ten Dijke P. Regulation of the TGF-β pathway by deubiquitinases in cancer. Int J Biochem Cell Biol 2016;76:135-45.

15. Harrigan JA, Jacq X, Martin NM, Jackson SP. Deubiquitylating enzymes and drug discovery: emerging opportunities. Nat Rev Drug Discov 2017;17:57-78.

16. Kategaya L, Di Lello P, Rougé L, Pastor R, Clark KR, Drummond J, *et al.* USP7 small-molecule inhibitors interfere with ubiquitin binding. Nature 2017;550:534-38.

17. Lamberto I, Liu X, Seo HS, Schauer NJ, Iacob RE, Hu W, *et al.* Structure-Guided Development of a Potent and Selective Non-covalent Active-Site Inhibitor of USP7. Cell Chem Biol 2017;24:1490-500.

18. Pozhidaeva A, Valles G, Wang F, Wu J, Sterner DE, Nguyen P, *et al.* USP7-Specific Inhibitors Target and Modify the Enzyme's Active Site via Distinct Chemical Mechanisms. Cell Chem Biol 2017;24:1501-12.

19. Turnbull AP, Ioannidis S, Krajewski WW, Pinto-Fernandez A, Heride C, Martin ACL, *et al.* Molecular basis of USP7 inhibition by selective small-molecule inhibitors. Nature 2017;550:481-6.

20. de Jong A, Merkx R, Berlin I, Rodenko B, Wijdeven RH, El Atmioui D, *et al.* Ubiquitin-based probes prepared by total synthesis to profile the activity of deubiquitinating enzymes. Chembiochem 2012;13:2251-8.

21. Ren J, Liu S, Cui C, ten Dijke P. Invasive Behavior of Human Breast Cancer Cells in Embryonic Zebrafish. J Vis Exp 2017; 122:e55459.

22. Arguello F, Baggs RB, Frantz CN. A murine model of experimental metastasis to bone and bone marrow. Cancer Res 1988;48:6876-81.

23. Jones A, Kemp M, Stockley M, Gibson K, Whitlock G, Madin AJW. Novel Compounds. 2016 Patent WO 2016/046530 A1.

24. Gao L, Wang L, Dai T, Jin K, Zhang Z, Wang S, *et al.* Tumor-derived exosomes antagonize innate antiviral immunity. Nat Immunol 2018;19:233-45.

25. Xu R, Greening DW, Zhu HJ, Takahashi N, Simpson RJ. Extracellular vesicle isolation and characterization: toward clinical application. J Clin Invest 2016;126:1152-62.

26. Bishop P, Rocca D, Henley JM. Ubiquitin C-terminal hydrolase L1 (UCH-L1): structure, distribution and roles in brain function and dysfunction. Biochem J 2016;473:2453-62.

27. Liu Y, Fallon L, Lashuel HA, Liu Z, Lansbury PT, Jr. The UCH-L1 gene encodes two opposing enzymatic activities that affect α-synuclein degradation and Parkinson's disease susceptibility. Cell 2002;111:209-18.

28. Papa L, Brophy GM, Welch RD, Lewis LM, Braga CF, Tan CN, *et al.* Time Course and Diagnostic Accuracy of Glial and Neuronal Blood Biomarkers GFAP and UCH-L1 in a Large Cohort of Trauma Patients With and Without Mild Traumatic Brain Injury. JAMA Neurol 2016;73:551-60.

29. Melo SA, Luecke LB, Kahlert C, Fernandez AF, Gammon ST, Kaye J, *et al.* Glypican-1 identifies cancer exosomes and detects early pancreatic cancer. Nature 2015;523:177-82.

30. Mathieu M, Martin-Jaular L, Lavieu G, Théry C. Specificities of secretion and uptake of exosomes and other extracellular vesicles for cell-to-cell communication. Nat Cell Biol 2019;21:9-17.

31. Chakraborty S, Hosen MI, Ahmed M, Shekhar HU. Onco-Multi-OMICS Approach: A New Frontier in Cancer Research. Biomed Res Int 2018;2018:9836256.

4

32. Xiao Z, Zhang P, Ma L. The role of deubiquitinases in breast cancer. Cancer Metastasis Rev 2016;35:589-600.

33. Zhang L, Zhou F, Drabsch Y, Gao R, Snaar-Jagalska BE, Mickanin C*, et al.* USP4 is regulated by AKT phosphorylation and directly deubiquitylates TGF-β type I receptor. Nat Cell Biol 2012;14:717-26.

34. Yuan L, Lv Y, Li H, Gao H, Song S, Zhang Y*, et al.* Deubiquitylase OTUD3 regulates PTEN stability and suppresses tumorigenesis. Nat Cell Biol 2015;17:1169-81.

35. Lien HC, Wang CC, Lin CH, Lu YS, Huang CS, Hsiao LP*, et al.* Differential expression of ubiquitin carboxy-terminal hydrolase L1 in breast carcinoma and its biological significance. Hum Pathol 2013;44:1838-48.

36. Hurst-Kennedy J, Chin L-S, Li L. Ubiquitin C-terminal hydrolase L1 in tumorigenesis. Biochem Res Int 2012;2012:123706.

37. Yakymovych I, Yakymovych M, Heldin CH. Intracellular trafficking of transforming growth factor β receptors. Acta Biochim Biophys Sin 2018;50:3-11.

38. Goto Y, Zeng L, Yeom CJ, Zhu Y, Morinibu A, Shinomiya K*, et al.* UCHL1 provides diagnostic and antimetastatic strategies due to its deubiquitinating effect on HIF-1α. Nat Commun 2015;6:6153.

39. Liu Y, Lashuel HA, Choi S, Xing X, Case A, Ni J*, et al.* Discovery of inhibitors that elucidate the role of UCH-L1 activity in the H1299 lung cancer cell line. Chem Biol 2003;10:837-46.

40. Pfoh R, Lacdao IK, Saridakis V. Deubiquitinases and the new therapeutic opportunities offered to cancer. Endocr Relat Cancer 2015;22:T35-54.

41. McAndrews KM, Kalluri R. Mechanisms associated with biogenesis of exosomes in cancer. Mol Cancer 2019;18:52.

42. Ning K, Wang T, Sun X, Zhang P, Chen Y, Jin J*, et al.* UCH-L1-containing exosomes mediate chemotherapeutic resistance transfer in breast cancer. J Surg Oncol 2017;115:932-40.

Chapter 5

A Small-Molecule Activity-Based Probe for Monitoring UCHL1 Activity in Live Cells and Zebrafish Embryos

Paul P. Geurink,*[a1] Raymond Kooij,[a1] Aysegul Sapmaz,[a1] Sijia Liu,[a1] Bo-Tao Xin,[a] George M. C. Janssen,[b] Peter A. van Veelen,[b] Peter ten Dijke,[a] and Huib Ovaa*[a]

[a] Department of Cell and Chemical Biology, Leiden University Medical Center, Leiden, The Netherlands
[b] Center for Proteomics and Metabolomics, Leiden University Medical Center, Leiden, The Netherlands

Chapter 5

ABSTRACT

Many reagents have emerged to study the function of specific enzymes *in vitro*. On the other hand, target specific reagents are scarce or need improvement allowing investigations of the function of individual enzymes in a cellular context. We here report the development of a target-selective fluorescent small-molecule activity-based DUB probe that is active in live cells and whole animals. The probe labels active Ubiquitin Carboxy-terminal Hydrolase L1 (UCHL1), also known as neuron-specific protein PGP9.5 (PGP9.5) and parkinson disease 5 (PARK5), a DUB active in neurons that constitutes 1-2% of total brain protein. UCHL1 variants have been linked with the neurodegenerative disorders Parkinson's and Alzheimer's disease. In addition, high levels of UCHL1 also correlate often with cancer and especially metastasis. The function of UCHL1 or its role in cancer and neurodegenerative disease is poorly understood and few UCHL1 specific research tools exist. We show that the reagents reported here are specific for UCHL1 over all other DUBs detectable by competitive activity-based protein profiling and by mass spectrometry. Our probe, which contains a cyanimide reactive moiety, binds to the active-site cysteine residue of UCHL1 irreversibly in an activity-dependent manner. Its use is demonstrated by labelling of UCHL1 both *in vitro* and in cells. We furthermore show that this probe can report UCHL1 activity during the development of zebrafish embryos.

INTRODUCTION

The Ubiquitin system relies to a great extent on cysteine catalysis. Ubiquitin is a small protein that consists of 76 amino acids that can modify target proteins through lysine residues although it is also occasionally found to modify N-termini as well as cysteine and threonine residues (1-3). Addition of ubiquitin is catalyzed by E1 (2), E2 (~40) and E3 (>600) enzymes in an ATP-dependent conjugation reaction by specific combinations of E1, E2 and E3 enzymes and it is reversed by any of ~100 deubiquitylating enzymes (DUBs) in humans (4) (5). The enzyme Ubiquitin Carboxy-terminal Hydrolase L1 (UCHL1), also known as neuron-specific protein PGP9.5 (PGP9.5) and parkinson disease 5 (PARK5), is a small protease that is thought to remove ubiquitin from small substrates and it belongs to the small family of Ubiquitin C-terminal Hydrolases (UCHs) (6).

It is clear that UCHL1 can cleave ubiquitin and that mutation and reduced activity has been associated with neurodegenerative diseases, including Parkinson's and Alzheimer's disease (7-12). High UCHL1 levels also correlate with malignancy and metastasis in many cancers (13) (14) and high UCHL1 levels have also been attributed to cellular stress, although the molecular mechanism of all these processes is unclear.

We earlier observed extreme levels of UCHL1 activity in lysates from prostate and lung cancer cells using a ubiquitin-derived activity-based probe that targets all cysteine DUBs (15). We reasoned that a good cell-permeable activity-based probe that targets UCHL1 specifically amongst other cysteine DUBs would be a highly valuable tool to understand its function in malignant transformation and its role in the development of neurodegenerative diseases.

UCHL1, like many DUBs, is a cysteine protease, a class of enzymes considered extremely difficult to inhibit with small molecules as this class of enzymes is associated with unspecific reaction with cysteine alkylating agents and with redox-cycling artifacts in assays (16). In addition, DUBs intrinsically bind ubiquitin through a protein-protein interaction, which is by

definition difficult to interfere with using small molecules. Many DUBs, including UCHL1, are inactive without a substrate and substrate binding aligns the catalytic triad for cleavage (17). Nevertheless, recently significant successes have been booked in the development of reversible and irreversible selective small-molecule inhibitors of the DUB USP7 (18-23). We have recently reported the development of a selective covalent small-molecule inhibitor of the DUB ovarian tumor (OTU) protease OTUB2 using a covalent fragment approach and parallel X-ray crystallography (24). We reasoned that such covalent molecules are a good inroad for the further elaboration of specific activity-based probes (ABPs) also inspired by earlier work from the Tate lab that recently reported a small-molecule broadly acting DUB probe (25). We were pleased to find a good starting point in patent literature (26) that we used in our studies for the design of fluorescent ABPs. We here report the development of a fluorescent small-molecule ABP that can report UCHL1 activity in human cells and in zebrafish embryos.

RESULTS AND DISCUSSION

The development of a small-molecule-based DUB ABP starts with the identification of an appropriate DUB-selective small-molecule covalent binder. We reasoned that an ideal compound needed to meet two criteria: 1) it binds covalently to the active-site cysteine residue of a DUB and 2) it can easily be modified by chemical synthesis. Our attention was drawn to a collection of (*S*)-1-cyanopyrrolidine-3-carboxamide-based compounds reported to inhibit UCHL1 activity with submicromolar affinity (26). These compounds are equipped with a cyanimide moiety that is known to react with thiols to form an isothiourea covalent adduct (Figure 1A) and thought to react reversibly (27). Despite the expected reversible nature we decided to investigate this compound as a potential probe starting point.

Characterizing UCHL1 cyanimide inhibitors.

In order to gain insight into the mode of action and DUB selectivity of these inhibitors we synthesized and characterized one compound (compound **6RK73**, Figure 1B) that in our hands inhibits UCHL1 with an IC_{50} of 0.23 μM after 30 minutes of incubation in a biochemical activity assay using fluorogenic Ub-Rho-morpholine (28) substrate (for preparation see Supporting Information) in the presence of 2 mM cysteine. Beneficially, **6RK73** proved to be almost unreactive towards the closest DUB family members UCHL3 and UCHL5 (Figure 1C). Selectivity for UCHL1 was further confirmed by IC_{50} determination against a panel of other cysteine DUBs (including USP7, USP30 and USP16) and the non-DUB cysteine protease papain, showing over 50-fold difference in IC_{50} value (Figure 1C and Supporting Information Table S1).

We next performed a jump dilution experiment (29) in which 100× final assay concentration of UCHL1 was treated with 10 μM of **6RK73** followed by 100 times dilution into substrate-containing buffer and direct fluorescence read-out (Figure 1C, D). Only after 30 minutes a negligible increase in fluorescence signal could be detected which indicates that the inhibitor acts basically irreversible. The formation of a stable covalent complex between UCHL1 and a single **6RK73** molecule was confirmed in an experiment where UCHL1 was incubated with **6RK73** and the reaction followed by LC-MS analysis (see Supporting Information). Next, we investigated whether the compound would inhibit UCHL1 in live cells. HEK293T cells were treated with 5 μM **6RK73** or the commercially available active-site directed reversible

UCHL1 inhibitor LDN-57444 (30) for 24h, followed by cell lysis and treatment with the fluorescent broad-spectrum DUB probe Rhodamine-Ubiquitin-propargylamide (Rh-Ub-PA) to label all residual cysteine-DUB activity (31-32). The samples were denatured, resolved by SDS-PAGE and scanned for Rhodamine fluorescence (Figure 1E). Each band represents an active DUB that reacted with the probe and the ability of a compound to inhibit a DUB is reflected by disappearance of its corresponding band. Indeed, the band belonging to UCHL1 (33) disappears upon treatment with **6RK73**, whereas all other bands remain unchanged, indicating that **6RK73** selectively inhibits UCHL1 in the presence of other DUBs in cells. In comparison, UCHL1 is hardly inhibited by LDN-57444 in this experiment, despite their comparable IC_{50} values (0.88 µM for LDN-57444), which might be attributed to the fast-reversible nature of this inhibitor (30).
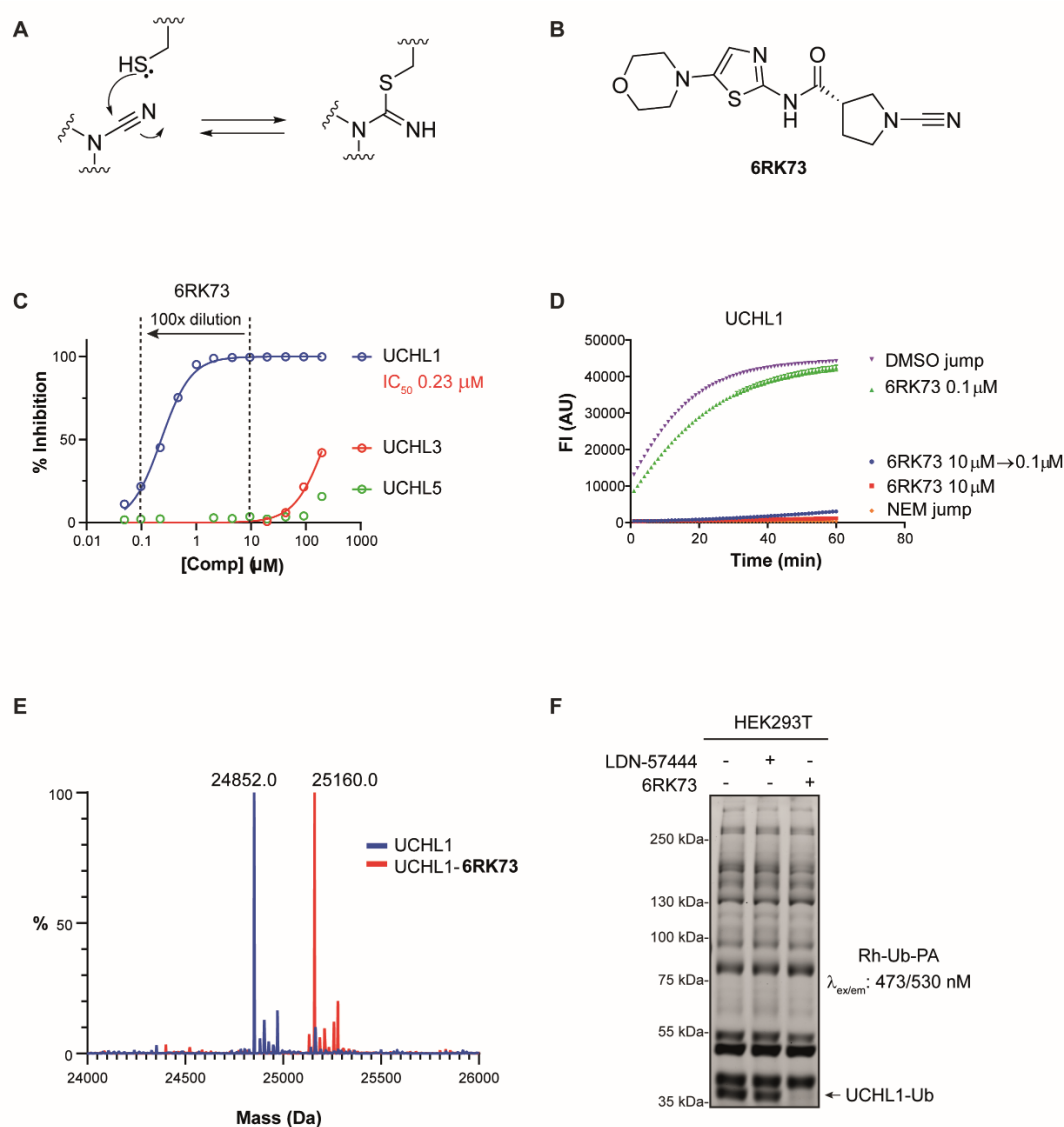
Figure 1. Biochemical characterization of UCHL1 inhibitor **6RK73**. A) Reaction of a thiol with a cyanimide results in the formation of an isothiourea adduct. B) Structure of UCHL1 inhibitor **6RK73**. C) IC_{50} determination of **6RK73** for UCHL1, UCHL3 and UCHL5. D) Progress curves for UCHL1 proteolytic activity after jump dilution (see also Figure C). DMSO and *N*-ethylmaleimide (NEM) are used as controls. E) Deconvoluted mass spectra of UCHL1 before (blue) and after (red) reaction with **6RK73**. F) Fluorescence labelling of remaining DUB activity in HEK293T cells upon treatment with UCHL1 inhibitors LDN-57444 and **6RK73**.

From inhibitor to probe.

Given the high inhibitory potency and UCHL1 selectivity both *in vitro* and in cells and the fact that it forms an irreversible covalent bond we envisioned that this type of cyanimide-containing molecules can serve as an ideal starting point for the construction of small-molecule selective DUB ABPs. This would require the instalment of a reporter group (e.g. fluorescent label) onto the molecule. Upon close inspection of **6RK73** however, we realized that this molecule does not provide an appropriate site for modification.

We therefore generated azide **8RK64** to which then several reporter groups were coupled using the copper(I)-catalyzed azide alkyne cycloaddition (CuAAC) or 'click reaction'. The compounds and their synthesis routes are shown in Scheme 1. Compound **2** was synthesized from 4-piperidinone (**1**) in four steps according to a reported procedure (26). The Fmoc-protected piperidine amine was liberated with DBU and coupled to 2-azidoacetic acid resulting in compound **3**.
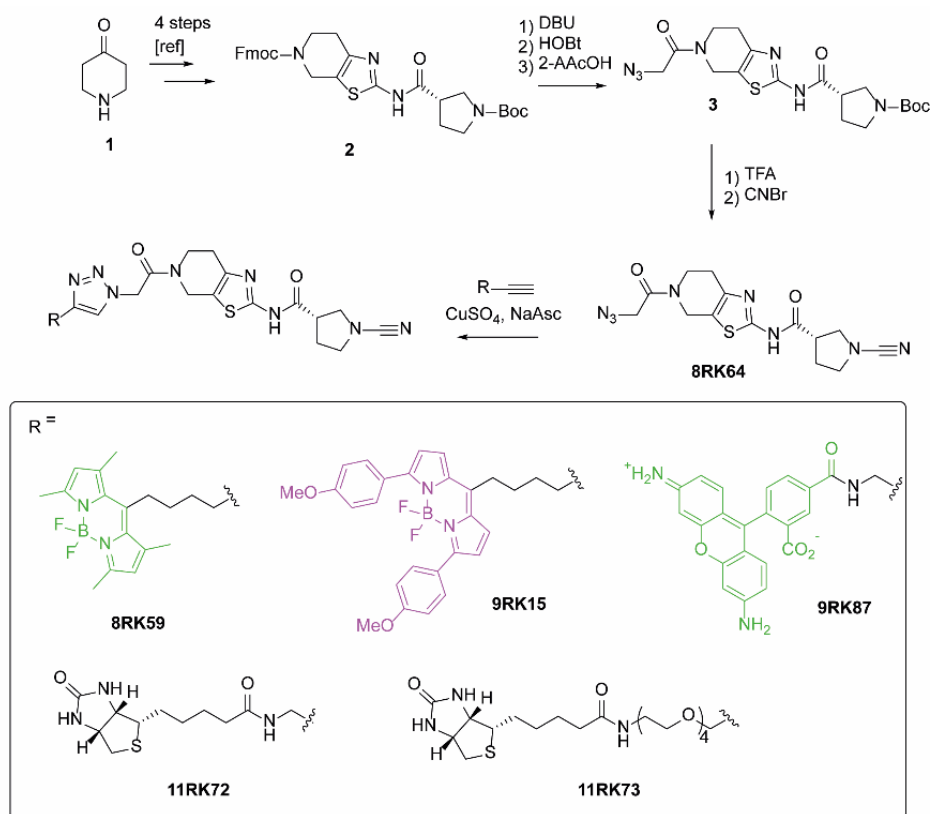
Scheme 1. Synthesis of azide-containing UCHL1 inhibitor 8RK64 and fluorescent and biotinylated probe derivatives thereof. [a] Synthetic steps described in literature (26).

Next, the Boc protecting group was removed from the pyrrolidine amine, followed by a reaction with cyanogen bromide to install the cyanimide moiety resulting in **8RK64**. Treatment of UCHL1 with this compound followed by IC_{50} determination and LC-MS analysis gave results comparable to those for **6RK73** (Figure 2A, B, Supporting Information), which indicates that **8RK64** also functions as a UCHL1 covalent inhibitor. With an IC_{50} value of 0.32 µM towards UCHL1 and 216 µM and >1 mM towards UCHL3 and UCHL5 respectively (Figure 2A, Supporting Information Table S1), this compound also retained its UCHL1 selectivity.

In addition, **8RK64**, like **6RK73**, also inhibits UCHL1 activity in cells as shown in a DUB profiling experiment in HEK293T cells using a Cy5-Ub-PA probe (Figure 2C). Notably, **8RK64** could potentially be used as '2-step ABP' by taking advantage of its azide moiety (34).
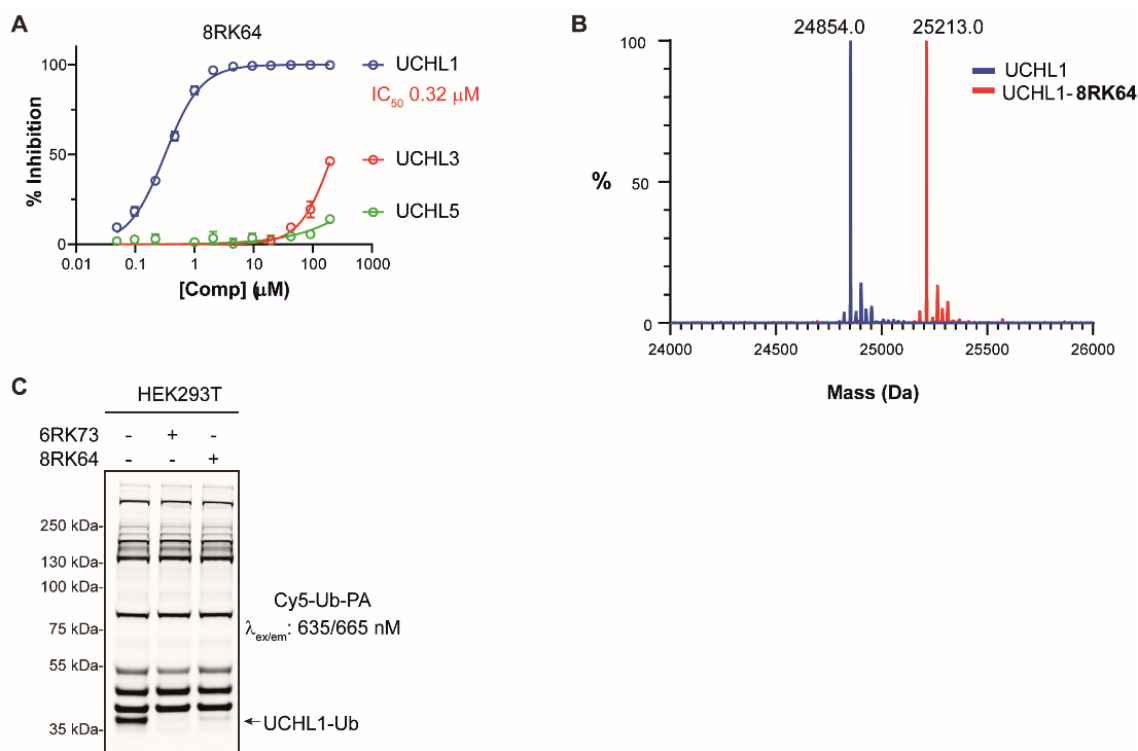
Figure 2. Biochemical characterization of **8RK64**. A) IC_{50} determination of **8RK64** for UCHL1, UCHL3 and UCHL5. B) Deconvoluted mass spectra of UCHL1 before (blue) and after (red) reaction with **8RK64**. C) Fluorescence labelling of remaining DUB activity in HEK293T cells upon treatment with UCHL1 inhibitors **8RK64** and **6RK73**.

Installation of a dye preserves inhibitory properties.

As it was unclear what the effect of coupling a bulky fluorescent group would have on the UCHL1 inhibition profiles and cell permeability we decided to test three commonly used fluorophores. BodipyFL-alkyne, BodipyTMR-alkyne (35) and Rhodamine110-alkyne (for preparation see Supporting Information) were coupled using copper(I)-mediated click chemistry to the azide of **8RK64**, resulting in compounds **8RK59**, **9RK15** and **9RK87** (Scheme 1). These 'one-step' ABPs can potentially be used for visualization of UCHL1 activity without the need for additional bio-orthogonal chemistry procedures. IC_{50} determination of these probes against UCHL1 revealed that the instalment of the dyes effected the inhibitory potency only marginally (Figure 3A and Supporting Information Table S1). Rhodamine110 probe **9RK87** is almost as potent as its azide precursor **8RK64** with IC_{50} values of 0.44 µM and 0.32 µM respectively. Instalment of BodipyTMR (**9RK15**) on the other hand, resulted in a 10-fold potency decrease, although the data points could not be fitted properly to a dose-response function. The less bulky BodipyFL-ABP **8RK59**, although not as potent as **8RK64**, showed a very acceptable inhibition of UCHL1 with an IC_{50} close to 1 µM. The ability of **8RK59** to form a covalent complex with UCHL1 was confirmed in an LC-MS experiment as described above (Supporting Information).

ABPs can visualize UCHL1 activity and the covalent linkage is thermally reversed.

We next set out to investigate whether the probes can be used to label and visualize UCHL1 activity after SDS-PAGE and fluorescence gel scanning similar to the Rh-Ub-PA probe. To our surprise for neither of the three small-molecule probes a clear band corresponding to probe-labelled UCHL1 could be detected after incubation with purified recombinant human UCHL1. We reasoned that the isothiourea bond between UCHL1 and probe, which is stable under the conditions used for inhibition and LC-MS experiments (*vide supra*), might be susceptible to the conditions used for protein denaturation, e.g. boiling in the presence of ~300 mM β-mercaptoethanol. Indeed, when the same samples were resolved by SDS-PAGE under non-denaturing conditions (no boiling and absence of β-mercaptoethanol) a clear band appeared that corresponds to probe-labelled UCHL1 for all three probes (Figure 3B). We also investigated if the ABP-UCHL1 bond would survive when β-mercaptoethanol is replaced by tris(2-carboxyethyl)phosphine) (TCEP), both of which are used to create a reducing environment. Figure 3B clearly shows that the ABP-UCHL1 bands remain intact in the presence of 50 mM TCEP and show a better resolved profile (less smearing) compared to the non-reducing samples. The Rh-Ub-PA control samples show that nearly all UCHL1 is labeled and that the formed bond for this probe is stable under denaturing conditions, which corroborates earlier findings (31). The bands corresponding to Rh-Ub-PA and **9RK87** bound to UCHL1 (both bearing the same dye and present in equal amounts) are of similar intensity, which indicates that the small-molecule probes bind UCHL1 efficiently and that all UCHL1 is active upon probe engagement.

ABPs bind to the active site cysteine residue of UCHL1 and visualize UCHL1 activity in various cell lines.

We next assessed the ability of the probes to bind and inhibit UCHL1 in a cell lysate by treating HEK293T cell extracts with 5 μM of the three fluorescent probes, as well as their azide precursor **8RK64** and inhibitor **6RK73** for 1 hour followed by labelling of all residual DUB activity with Cy5-Ub-PA. The Cy5-labelled Ub probe was used here to circumvent spectral interference with either of the other dyes used in the small-molecule probes. Fluorescent scanning of the gel after SDS-PAGE as well as Western blotting using anti-UCHL1 antibody clearly showed that Rhodamine probe **9RK87** inhibits UCHL1 activity similar to **8RK64** and **6RK73** (Figure 3C). Both Bodipy probes also potently inhibit UCHL1 in a cell lysate, although to a somewhat lesser extent, which could be expected on the basis of their IC_{50} values. All other bands are unchanged, which demonstrates that all compounds are able to bind UCHL1 selectively with respect to other DUBs in a cell lysate.

Encouraged by these results we set out to assess the ability of the probes to penetrate the cell membrane and to label active UCHL1 in cells. HEK293T cells were treated with 5 μM of the probes for 24 hours followed by cell lysis, SDS-PAGE (in the absence of β-mercaptoethanol and boiling) and fluorescence scanning at two wavelengths to detect all fluorescent dyes (Figure 3D). A clear band just above 25 kDa is observed for both Bodipy probes (**8RK59** and **9RK15**), which likely corresponds to ABP-labelled UCHL1 with an expected mass of ~25.5 kDa. In addition to this band a few extra bands are visible including one just below UCHL1 and one more pronounced band around 55 kDa. Interestingly, hardly any band can be seen for the so-far most potent probe **9RK87**. We attributed this effect to the difference in cell permeability between Bodipy and Rhodamine dyes, with the latter known to be less capable

of crossing the cell membrane (36). Indeed, upon further investigation using microscopy in ABP-treated HeLa and HEK293T cells we confirmed that Rhodamine probe **9RK87** is unable to enter these cells, whereas both Bodipy ABPs clearly are (Supporting Information Figure S1). For this reason and because the BodipyFL-ABP proved to be a better inhibitor compared to its BodipyTMR analogue we decided to continue with **8RK59** as the preferred probe for all further experiments.
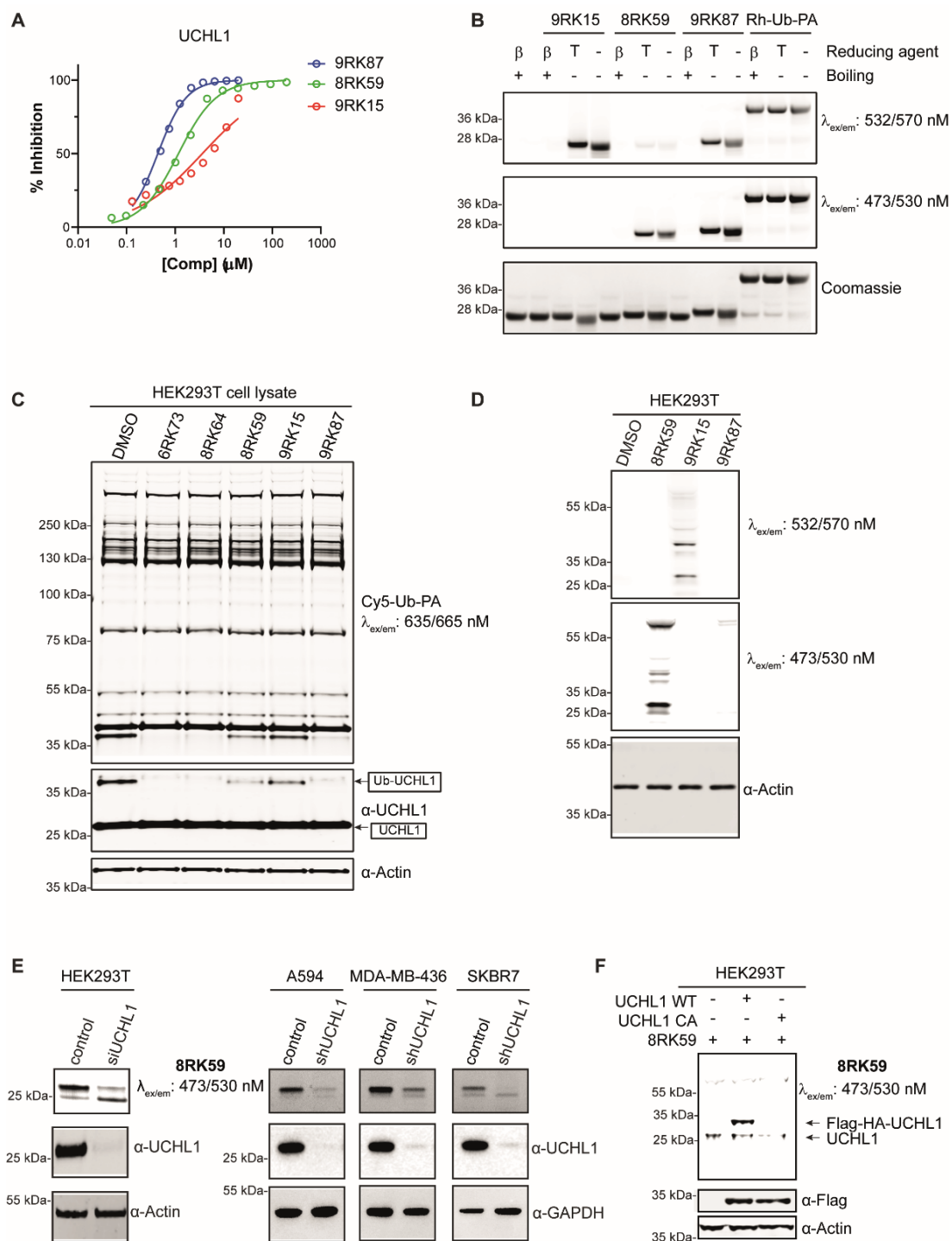
Figure 3. Characterization of the fluorescent UCHL1 probes *in vitro* and in cells. A) IC$_{50}$ determination of **8RK59**, **9RK15** and **9RK87** for UCHL1. B) Labelling of purified recombinant human UCHL1 by the three probes and Rh-Ub-PA. β: β-mercaptoethanol; T: TCEP. C) Fluorescence

labelling by Cy5-Ub-PA of remaining DUB activity in HEK293T cell lysate upon treatment with UCHL1 inhibitors and probes. D) Fluorescence scans showing the labelling pattern in HEK293T cells of the three probes. E) Fluorescence labelling of UCHL1 activity in HEK293T, A549, MDA-MB-436 and SKBR7 cells with **8RK59**. F) **8RK59** labels overexpressed Flag-HA-UCHL1 wt but not the C90A active site mutant in HEK293T cells.

The ability of **8RK59** to label UCHL1 activity in different cell lines was further explored in HEK293T cells and in three cancer cell lines known to express high levels of endogenous UCHL1: non-small cell lung cancer (NSCLC) A549 cells, triple negative breast cancer (TNBC) MDA-MB-436 cells and SKBR7 cells (37). Cells transfected with UCHL1 shRNA knock-down (shUCHL1) or siUCHL1 as well as empty vector control or scrambled oligo (siControl) were treated with 5 µM of each probe for 24 hours, followed by cell lysis, SDS-PAGE (without boiling and β-mercaptoethanol) and fluorescence scanning (Figure 3E). A clear band appears in the fluorescence scan at the expected height (~25.5 kDa) in all four cell lines and this band is significantly decreased in the UCHL1 knock-down samples, indicating that this band indeed corresponds to ABP-labelled UCHL1.

To confirm that **8RK59** binds the active site cysteine residue in UCHL1 we overexpressed Flag-HA-tagged UCHL1 and its C90A catalytic inactive mutant in HEK293T cells and incubated these cells with 5 µM **8RK59** for 24 hours. Fluorescence scanning and anti-FLAG Western blotting shows that **8RK59** only binds to wild-type UCHL1 but not to catalytically inactive UCHL1, indicating that the probe binding site is the active site cysteine (Figure 3F).

Determination of DUB selectivity and potential off-targets of the ABP.

As mentioned before, besides the band corresponding to ABP-labelled UCHL1 a few other bands appeared on gel (Figure 3D) but based on the DUB profiling results (Figure 3C) these band can most likely not be attributed to other DUBs. In order to gain more insight into potential off-targets we performed pull-down experiments coupled to mass spectrometry to identify the proteins binding to our probe. We started with a '2-step ABP' approach in which HEK293T cells were incubated with azide-containing compound **8RK64** or DMSO control, followed by a post-lysis click reaction with biotin-alkyne (38) and subsequent pull-down with streptavidin-coated beads (Supporting Information Figure S2A, B). Samples were run (1 cm) on a SDS-PAGE gel, lanes were cut into two pieces and the proteins were subjected to trypsin digestion and analyzed by LC-MSMS. As expected, the most enriched protein identified from this experiment was UCHL1 (Supporting Information Figure S2C). Only one additional protein was also highly enriched, a protein deglycase named DJ-1 (PARK7) with a molecular weight of 20 kDa, which most likely corresponds to the band just below UCHL1 in Figure 3D. This enzyme also harbors an active site cysteine residue which could potentially bind to our probe. Indeed, incubation of UCHL1 and PARK7 knock-down cells with **8RK59**, followed by anti-UCHL1 and anti-PARK7 Western blotting, revealed that PARK7 also reacts with **8RK59** and that the gel band just below UCHL1 corresponds to PARK7 (Supporting Information Figure S2D).

In addition to UCHL1 and PARK7, a few other bands can be seen on gel, yet we only identified these two enzymes in the 2-step ABP approach. We therefore performed a 1-step pull-down experiment where we used two biotinylated versions of **8RK64**: compound **11RK72** where biotin is directly linked to the inhibitor and compound **11RK73** with a PEG spacer in between. Both compounds show high inhibitory potential towards UCHL1 (Figure

4A) and form a covalent bond with UCHL1 (Supporting Information). HEK293T cell lysate was incubated with both biotin-ABPs, followed by pull-down with streptavidin-coated beads and subjected to full proteome LC-MSMS analysis (Figure 4B, Supporting Information Figure S2E). Efficient UCHL1 pull-down was confirmed for both biotinylated probes but not the DMSO and biotin-alkyne-treated control samples by Western blotting using anti-UCHL1 antibody (Figure 4C). From the LC-MSMS data, the relative protein abundances were calculated in the pull-down samples and compared to control samples. The list of identified proteins was ranked for total abundance to identify the highest enriched proteins (Supporting Information). Inspection of the list of all enzymes related to Ub (Ub-like proteins, DUBs, E1, E2 and E3 ligases) further substantiates the specificity of the probes for UCHL1 within the Ub system as shown in Figure 4D. Only a few of these enzymes were identified in the pull-down experiment with at least 150-fold lower abundance compared to UCHL1. The first other DUB on the list is UCHL3, the closest UCHL1 family member, and one of the most abundant DUBs in cells, which could explain this result.

The abundances of the top-10 highest ranked proteins are shown in Figure 4E. In line with the results obtained with the 2-step approach, the highest ranked proteins are UCHL1 and PARK7. PARK 7 shows a slightly higher abundance here, which contradicts our previous results from the in-cell labeling and 2-step pull-down experiments and might be attributed to the use of a different (biotinylated) version of the ABP or a peptide ionization difference during LC-MSMS measurements. The next highest ranked group of proteins, albeit at much lower abundance levels, includes two amidases NIT1 and NIT2, both harboring an active-site cysteine residue, the isochorismatase domain-containing protein 2 (ISOC2) and glutamine amidotransferase-like class-1 domain-containing protein 3B (GATD3B). Overall, the shorter (**11RK72**) and longer (**11RK73**) biotin probes give similar results, so the distance between probe and biotin does not seem to influence the binding nor the pull-down efficiency.

Upon comparison of the pull-down data (Figure 4) with the fluorescent probe labeling (Figure 3) we were unable to assign all bands to proteins. The majority of most abundant proteins in the pull-down experiment have a molecular weight between 20 and 35 kDa. Especially the pronounced band around 55 kDa in Figure 3D remains elusive. In a final attempt to assign this band we resolved the pull-down protein sample from the 1-step labeling experiment by SDS-PAGE. All proteins were visualized by silver staining after which the bands were excised and analyzed by LC-MSMS (Supporting Information Figure S2F). Again, UCHL1 and PARK7 were clearly the main proteins identified from the bands at ~25 kDa. The proteins corresponding to the other bands were less clear but the main candidates were GAPDH at ~40 kDa and Elongation factor 1α, tubulin or glutathione reductase (GSR) at ~60 kDa. Whether or not these proteins actually bind to the probe or that these results are due to their high expression levels, remains elusive. Based on the result that we identified UCHL1 as the major probe target in three individual experiments and that we found PARK7 as the only major off-target, we reasoned that **8RK59** could well be used for in-cell and *in vivo* labelling of UCHL1 activity.

Probing UCHL1 activity in cells with 8RK59.

To assess the application of **8RK59** in live cells, we used inverted fluorescent microscopy to image the **8RK59** signal in MDA-MB-436 and A549 cells after a 16-hour treatment with **8RK59**. Results showed that **8RK59** could penetrate and label the cells (Figure 5A).
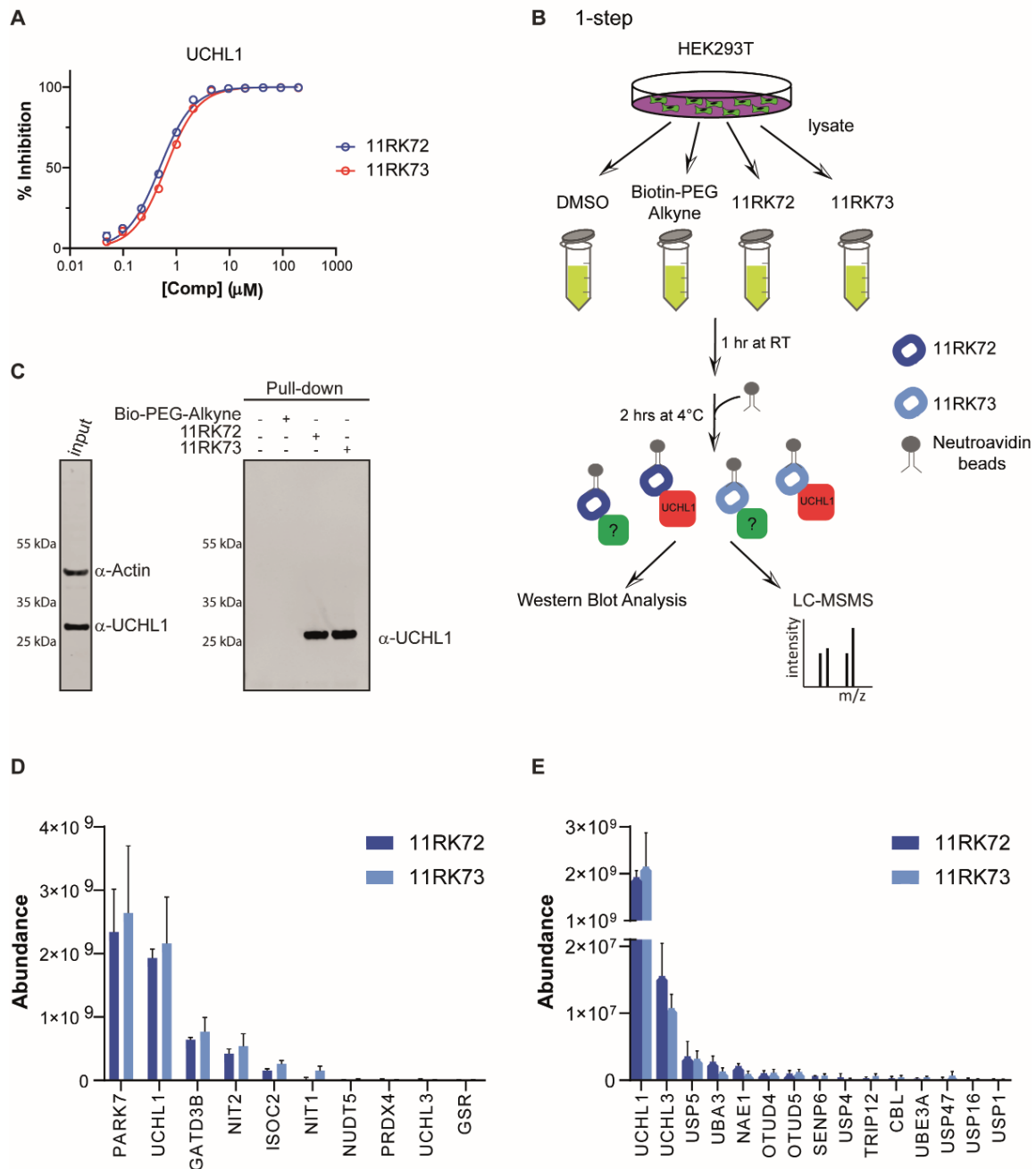
Figure 4. Proteomics experiments with biotinylated ABP analogs to identify ABP targets. A) IC_{50} determination of **11RK72** and **11RK73** for UCHL1. B) Schematic representation of pull-down experiment to identify ABP binding proteins. C) Confirmation of UCHL1 pull-down with biotinylated ABP analogs by Western Blot Analysis. Immunoblotting was performed using UCHL1 and Actin antibodies. Actin was used as a loading control and incubated together with UCHL1 antibody in the input sample. D) Abundances of all enzymes related to the Ub(-like) system identified in the pull-down LC-MSMS experiment averaged over three replicates. E) Abundances of the top-10 highest ranked proteins from the pull-down LC-MSMS experiment averaged over three replicates.

Compared to the control group, the BodipyFL signal was significantly decreased in UCHL1 knock-down MDA-MB-436 cells and similar results were observed for A549 cells (Supporting Information Figure S3). After imaging, MDA-MB-436 cells were lysed and followed with SDS-PAGE, fluorescence gel scanning and immunoblotting. A decreased UCHL1 signal was detected in MDA-MB-436 UCHL1 knock-down cells by **8RK59** and by

antibody stain (Figure 5B).To further validate whether we can visualize UCHL1 specific activity inside cells, control and UCHL1 depleted A549 cells were pre-incubated with **8RK59** probe for 16 hours and stained with UCHL1 antibody (Figure 5C). We observed changes in the distribution of the probe inside the cells. In the control cells **8RK59** accumulated in both UCHL1-positive and negative subcellular compartments while in the UCHL1 knock-down cells the **8RK59** signal was largely decreased in the UCHL1-positive compartments, implying that UCHL1 binds to **8RK59** probe. In agreement with the gel–based labeling data shown in Figure 3 and the proteomics data shown in Figure 4 (and Supporting Information), we still observed some background subcellular localization of **8RK59** in UCHL1 knock-down cells, which may be the result of PARK7 staining. Taken all together, this result shows that the cellular distribution of **8RK59** probe changes upon depletion of UCHL1 and it can therefore be used to monitor UCHL1 activity in cells.
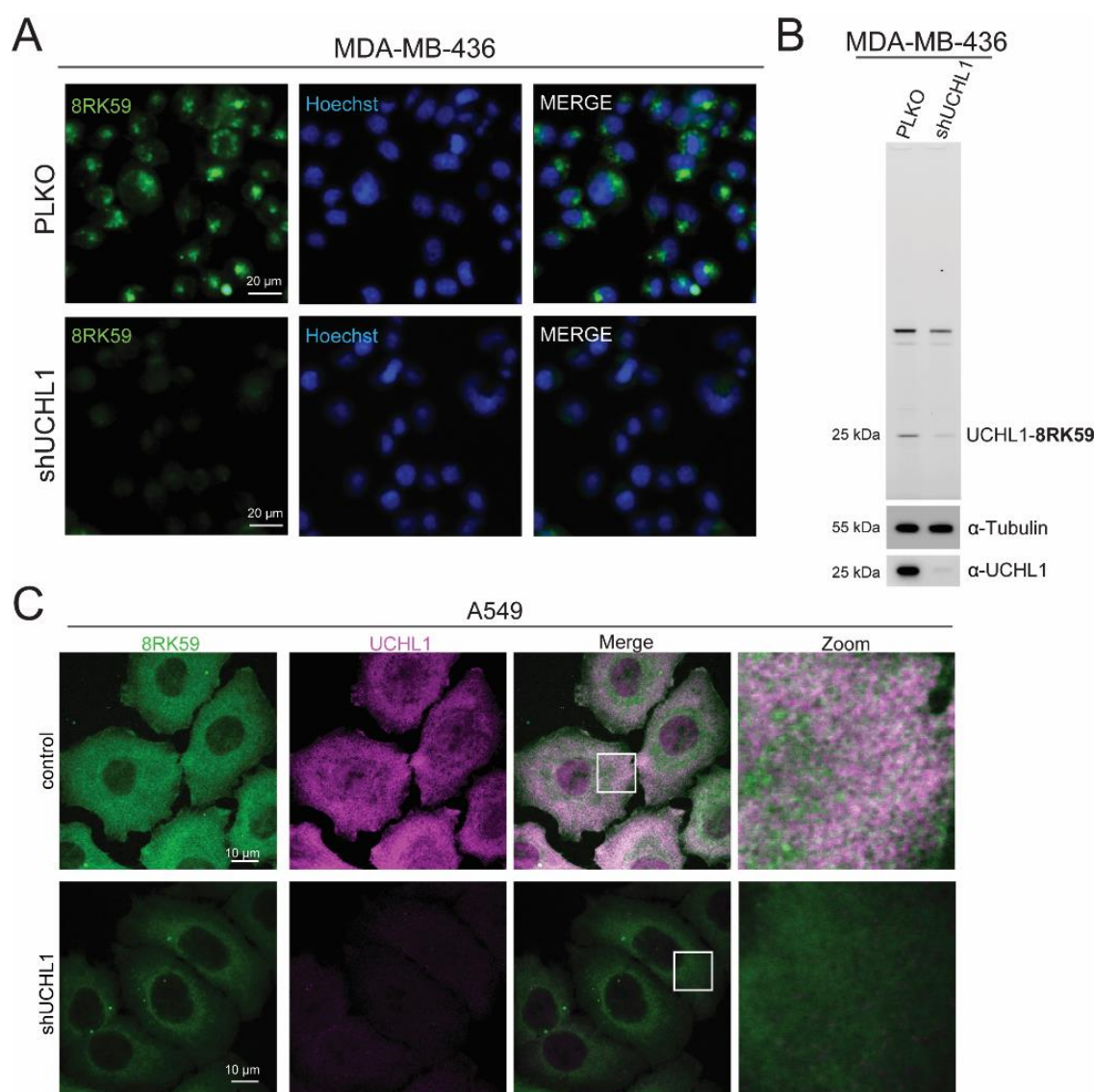
Figure 5. Probing UCHL1 activity in cells with **8RK59**. A) Live-cell fluorescence imaging of PLKO and shUCHL1 MDA-MB-436 cells treated with **8RK59**. B) Fluorescence labeling of endogenous UCHL1 in PLKO and shUCHL1 MDA-MB-436 cells treated with **8RK59** in SDS-PAGE gel. Immunoblotting was performed using UCHL1 antibody, and Tubulin was used as a loading control. C) Immunofluorescent staining of UCHL1 in **8RK59** pretreated PLKO and shUCHL1 A549 cells.

Probing UCHL1 activity in zebrafish embryos with 8RK59.

To investigate the application of **8RK59** in tracking UCHL1 activity in an *in vivo* model, we chose the zebrafish (*Danio rerio*) due to their high genetic homology to humans and the transparency of their embryos (39). Firstly, we treated zebrafish embryos with **8RK59** and recorded fluorescent images during the development of embryos from 1 to 7 days post fertilization (dpf). Results showed **8RK59** mainly labeled the nose, eye and brain of the zebrafish embryos (Figure 6A). Interestingly, all these organs are enriched in nerve cells and highly express *Uchl1* Mrna (40).
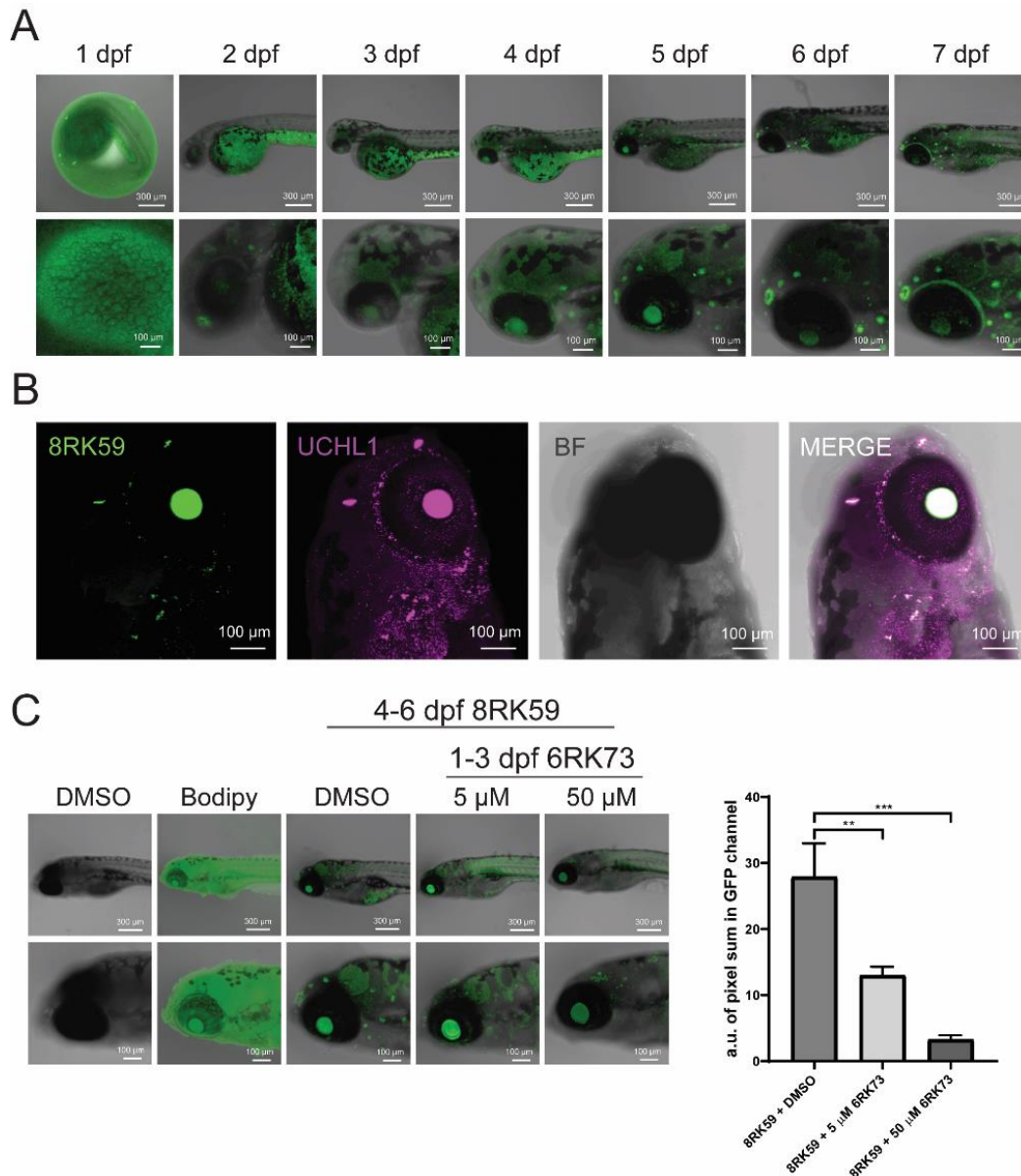
Figure 6. Probing UCHL1 activity in zebrafish embryos with **8RK59**. A) Tracking the localization of active UCHL1 with **8RK59** during the development of zebrafish embryos from 1 to 7 dpf. B) Immunofluorescent staining of UCHL1 in 6 dpf zebrafish embryo pretreated with **8RK59**. C) Monitoring UCHL1 activity changes in 6 dpf zebrafish embryos with **8RK59** pretreated with UCHL1 inhibitor **6RK73**. Representative images from five groups with zoom in of the brain area are shown in the left panel. The quantification of **8RK59** signal in three **6RK73** treatment groups are shown in the right panel. DMSO and BodipyFL dye were used as controls. **, P < 0.01, ***, P < 0.001, two-way ANOVA.

To validate that the labelling of **8RK59** in zebrafish embryos is specific to UCHL1 protein, we fixed the **8RK59** labelled embryos and performed IF staining with UCHL1 antibody. Results demonstrated both the **8RK59** and UCHL1 antibody label similar organs of zebrafish embryos (Figure 6B). To assess whether **8RK59** could detect the UCHL1 activity changes in zebrafish embryos, we pretreated the zebrafish embryos with UCHL1 activity inhibitor **6RK73** from 1 to 3 dpf, and then labelled the embryos with **8RK59** from 4 to 6 dpf. We found that increasing concentrations of **6RK73**-pretreated zebrafish embryos resulted in significantly lower **8RK59** signal labelling (Figure 6C). In addition, the lysate of **6RK73**-pretreated zebrafish embryos showed decreased UCHL1 signal in fluorescence scans of a corresponding SDS-PAGE gel (Supporting Information Figure S4). These *in vivo* experiments indicate that **8RK59** can visualize and track UCHL1 activity during the development of zebrafish embryos.

CONCLUSIONS

One of the key challenges within DUB research is the creation of activity-based probes that target a single DUB type and at the same time are able to cross the cell membrane, in order to study these enzymes inside living cells or even living organisms (41). It has recently been shown by us and others that Ub-based tools (such as ABPs) can be made sub-type specific by engineering the amino acid sequence in Ub (32) (42) (43), however these ABPs are not cell-permeable. ABPs based on small-molecule inhibitors on the other hand are often cell-permeable and can be tuned chemically to become selective (44) (45), although such ABPs for DUBs have been lacking so far. We here provide evidence for the first fluorescent small-molecule target specific DUB ABP (**8RK59**) that hits UCHL1 activity *in vitro*, in cells and *in vivo*. We based our design on a cyanimide-containing inhibitor and show, in contrast to what has been reported in literature (27), that cyanimides can act as (near to) irreversible binders. Whether the irreversible bond formation results from the chemical nature of the cyanimide used here or from its binding mode within the UCHL1 active site and whether this property can be extended to other DUBs, remains to be investigated. Instalment of a fluorescent group onto a small-molecule inhibitor can have a detrimental effect on its inhibitory properties. Our data show that the installation of a Rhodamine fluorophore hardly, and a BodipyFL fluorophore only marginally effected the inhibitory potency towards UCHL1, whereas our Ub-ABP experiments confirmed the preservation of their selectivity for UCHL1 among other cysteine DUBs. From these two probes Rhodamine-tagged **9RK87** showed better *in vitro* characteristics, e.g. lower IC_{50} value and more potent in cell lysate, but unfortunately proved to be unable to cross the cell membrane. As such, this probe could be preferred for *in vitro* experiments and might be optimized for in-cell use by chemically improving the cell-penetrating properties of Rhodamine (28).

Small-molecule inhibitors or probes almost inevitably result in unspecific interactors and this is not different for our compounds. We have considerably invested in the identification of potential off-targets of our probes by means of a proteomics approach. The data generated in this effort are not only useful for our own study but also provide valuable information for others working on this type of cyanimide-containing compounds. The proteomics data is in line with the Ub-probe experiments, confirming that these compounds are UCHL1 specific within the Ub system and to enzymes of the closely related Ub-like systems (e.g. Nedd8, SUMO, etc.). We indeed found a few potential off-targets, the main one being the protein and

nucleotide deglycase PARK7. These cyanimide compounds may therefore provide a good starting point for small-molecule probes targeting PARK7, which, in spite of its important enzymatic function in protein and DNA repair in virtually any cell, have not been developed yet. Based on our data we expect that the potency and selectivity of the probe can be further improved by means of chemical alterations of the inhibitor. A better knowledge on the structural determinants of the interactions between probe and UCHL1 will be of great value for this, unfortunately despite several crystallization attempts we were unable to obtain appropriately diffracting crystals. During preparation of our manuscript Flaherty and co-workers (46) reported on a related (*S*)-1-cyanopyrrolidine-2-carboxamide-based UCHL1 inhibitor and they applied NMR and molecular modeling to gain insight in the interactions between inhibitor and UCHL1, which could provide useful information to further optimize our probes. In addition, they modified their inhibitor with an alkyne moiety, which, unlike our molecules, resulted in a decrease in potency towards UCHL1 and selectivity with respect to UCHL3. This 2-step probe was then used to identify off-targets in KMS11 cells but remarkably none of their identified proteins show overlap with our list.

In conclusion, we have developed a fluorescent small-molecule activity-based probe that labels UCHL1 activity *in vitro*, in cells and *in vivo*. It is the first example of a '1-step' DUB-selective, cell-permeable ABP and therefore serves as a unique addition to the 'Ub toolbox', concomitantly addressing two of the outstanding challenges within this field. Our results show that the probe works in several different cell lines and we therefore foresee a potential wide application of the probe in studying UCHL1 activity related to neurodegenerative disorders and cancer. In Chapter 4, we showed that **6RK73** decreases UCHL1 activity and thereby inhibits TGFβ/SMAD2 and SMAD3 signaling and breast cancer migration and extravasation (47). We are convinced that the here reported strategy of small-molecule cyanimide-based probes can be expanded to other cysteine proteases and specifically DUBs. With the rising importance of the Ub system as source of practical drug targets we believe that these ABP tools will fill an unmet need allowing us to study active DUBs in their native environment in live cells or animals and as such aid in the development of future therapeutics that target diseases associated with ubiquitination.

METHODS

IC$_{50}$ determination. The *in vitro* enzyme inhibition assays were performed in "non-binding surface flat bottom low flange" black 384-well plates (Corning) at room temperature in a buffer containing 50 mM Tris·HCl, 100 mM NaCl, pH 7.6, 2.0 mM cysteine, 1 mg/mL 3-[(3-cholamidopropyl) dimethylammonio] propanesulfonic acid (CHAPS) and 0.5 mg/mL γ-globulins from bovine blood (BGG) in triplicate. Each well had a final volume of 20.4 µL. All dispensing steps involving buffered solutions were performed on a Biotek MultiFlowFX dispenser. The compounds were dissolved in DMSO as 10 mM, 1 mM and 0.1 mM stock solutions and appropriate volumes were transferred from these stocks to the empty plate using a Labcyte Echo550 acoustic dispenser and accompanying dose-response software to obtain a 12 point serial dilution (3 replicates) of 0.05 to 200 µM. A DMSO back-fill was performed to obtain equal volumes of DMSO (400 µL) in each well. 10 mM *N*-ethylmaleimide (NEM) was used a positive control (100% inhibition) and DMSO as negative control (0% inhibition). 10 µL buffer was added and the plate was vigorously shaken for 20 sec. Next, 5 µL of a 4× final concentration enzymes stock was added followed by incubation

_____

for 30 min. 5 µL of the substrate (Ub-Rho-morpholine (final concentration 400 nM) or Cbz-PheArg-AMC (final concentration 10 µM) in the case of Papain) and the increase in fluorescence intensity over time was recorded using a BMG Labtech CLARIOstar or PHERAstar plate reader (excitation 487 nm, emission 535 nm). The initial enzyme velocities were calculated from the slopes, normalized to the positive and negative controls and plotted against the inhibitor concentrations (in M) using the built-in equation "[inhibitor] vs. response – Variable slope (four parameters), least squares fit" with constraints "Bottom = 0" and "Top = 100" in GraphPad Prism 7 software to obtain the IC_{50} values.

Jump dilution assay. All assays were performed in triplicate. The assay was performed in a buffer containing 50 mM Tris·HCl, 100 mM NaCl, pH 7.6, 2.0 mM cysteine, 1 mg/mL 3-[(3-cholamidopropyl) dimethylammonio] propanesulfonic acid (CHAPS) and 0.5 mg/mL γ-globulins from bovine blood (BGG). The final concentrations used were: 3 nM UCHL1, 400 nM Ub-Rho-morpholine, 10 µM or 0.1 µM or a jump dilution of 10 µM to 0.1 µM inhibitor. Samples of 20 µL containing 300 nM UCHL1 and 20 µM inhibitor (2% DMSO), 2% DMSO or 20 mM *N*-ethylmaleimide (NEM) were incubated for 30 min. at room temperature. 5 µL of each sample was then diluted into a 500 µL solution containing 400 nM Ub-Rho-morpholine. After a brief mixing 20 µL of each of these solutions was quickly transferred to a "non-binding surface flat bottom low flange" black 384-well plate (Corning) and the increase in fluorescence over time was recorded using a BMG Labtech CLARIOstar plate reader (excitation 487 nm, emission 535 nm). As a control, samples were taken along in which 40 µL of a 20 µM and 0.2 µM inhibitor solution in buffer (2% DMSO) were added to 20 µL of a 12 nM UCHL1 solution. After 30 min. incubation 20 µL of a 1.6 µM Ub-Rho-morpholine solution was added after which 20 µL of each solution was transferred to the same 384 well plate mentioned above and the increase in fluorescent intensity was measured concomitantly. Fluorescent intensities were plotted against time using GraphPad Prism 7.

Covalent complex formation mass spectrometry analysis. Samples of 1.4 µM UCHL1 in 70 µL buffer containing 50 mM Tris·HCl, 100 mM NaCl, pH 7.6, 2.0 mM cysteine and 1 mg/mL 3-[(3-cholamidopropyl) dimethylammonio] propanesulfonic acid (CHAPS) were prepared. These samples were treated with 1 µL DMSO or 1 µL of a 10 mM inhibitor/probe stock solution in DMSO (140 µM final concentration) and incubated for 30 min. at room temperature. Samples were then 3× diluted with water and analyzed by mass spectrometry by injecting 1 µL on a Waters XEVO-G2 XS Q-TOF mass spectrometer equipped with an electrospray ion source in positive mode (capillary voltage 1.2 kV, desolvation gas flow 900 L/hour, T = 60 ºC) with a resolution R = 26,000. Samples were run using 2 mobile phases: A = 0.1% formic acid in water and B = 0.1% formic acid in CH_3CN on a Waters Acquity UPLC Protein BEH C4 column, 300 Å, 1.7 µm (2.1 × 50 mm); flow rate = 0.5 mL/min, runtime = 14.00 min, column T = 60 °C, mass detection 200-2500 Da. Gradient: 2 – 100% B. Data processing was performed using Waters MassLynx Mass Spectrometry Software 4.1 and ion peaks were deconvoluted using the built-in MaxEnt1 function.

Probe labeling of purified recombinant UCHL1. The assay was performed in a buffer containing 50 mM Tris·HCl, 100 mM NaCl, pH 7.6, 2.0 mM cysteine and 1 mg/mL 3-[(3-cholamidopropyl) dimethylammonio] propanesulfonic acid (CHAPS). A stock solution containing 8 µM UCHL1 and stock solutions containing 20 µM **8RK59**, **9RK15**, **9RK87** and Rho-Ub-PA in buffer were prepared. 50 µL of the UCHL1 stock solution was mixed with 50

µL of all probe solutions followed by incubation for 60 min. at 37 °C. Three aliquots of 10 µL of each sample were taken and treated with 1) 5 µL loading buffer with β-mercaptoethanol, followed by 5 min. heating at 95 °C; 2) 5 µL loading buffer with 50 mM TCEP; 3) 5 µL loading buffer. Samples were resolved by SDS-PAGE using a 4-12% Bis-Tris gel (Invitrogen, NuPAGE) with MES SDS running buffer (Novex, NuPAGE) for 45 min. at 190V. Gels were scanned for fluorescence on a GE Typhoon FLA 9500 using a green ($\lambda_{ex/em}$ 473/530 nm) and red ($\lambda_{ex/em}$ 532/570 nm) channel followed by staining with InstantBlue Coomassie protein stain (Expedeon) after which the gel was scanned on a GE Amersham Imager 600.

Cell lines and cell culture. HEK293T, HeLa, A549 and MDA-MB-436 cells were originally obtained from American Type Culture Collection (ATCC) and SKBR7 cells were obtained from Dr. J. Martens (Erasmus University Medical Center, Rotterdam, The Netherlands). Cells were cultured in Dulbecco's modified Eagles's medium (DMEM) supplemented with 10% fetal bovine serum (FBS) and 100 U/mL penicillin-streptomycin (15140122; Gibco). Stable shUCHL1 A549 and shUCHL1 MDA-MB-436 cell lines were generated by lentiviral infection and the cell lines were continuously cultured under puromycin selection. Four UCHL1 shRNAs were identified and tested, the most effective shRNA (TRCN0000007273; Sigma) for lentiviral infection were used for experiments. All cell lines were regularly tested for absence of mycoplasma and were authenticated.

Transfection. For shRNA expression, lentiviruses were produced by transfecting shRNA-targeting plasmids together with helper plasmids pCMV–VSVG, pMDLg–RRE (gag–pol), and pRSV–REV into HEK293T cells. Cell supernatants were collected 48 hours after transfection and were used to infect cells. To obtain stable shUCHL1 A549 and shUCHL1 MDA-MB-436 UCHL1 knock-down cell lines, cells were infected at low confluence (40%) for 12 hours with lentiviruses in the presence of 5 ng/mL Polybrene (Sigma). Cells were subjected to 1 µg/mL puromycin selection 48 hours after infection. Four UCHL1 shRNAs were identified and tested, the most effective UCHL1 shRNA (TRCN0000007273; Sigma) for lentiviral infection was used for the experiments.

For siRNA transfection, siRNAs targeting UCHL1 (Set of 4: siGENOME; MQ-004309-00-0002 2 nmol) and PARK7 (Set of 4: siGENOME; MQ-005984-00-0002 2 nmol) were obtained from Dharmacon. Knock-down of UCHL1 and PARK7 in HEK293T cells was performed as follows: for 6-well plate format 200 µL siRNA (500 nM stock) were incubated with 4 µL Dharmafectin reagent 1 (Dharmacon) diluted in 200 µL medium without supplements by shaking for 20 min. at room temperature. The transfection mix was added to cells and cultured at 37 °C and 5 % CO_2. 48 hours after transfection **8RK59** was added to the cells and incubated for 24 hours. Cells were harvested and analysed as described under the section "DUB activity profiling and competition with Ub-PA DUB probes".

For the expression of UCHL1 in HEK293T cells, Flag-HA-UCHL1 construct was obtained from Addgene (22563). Catalytically inactive mutant (C90A) UCHL1 was generated using site-directed mutagenesis. Wild-type and C90A mutant UCHL1 were transfected into HEK293T cells using PEI transfection reagent. 24 hours after transfection **8RK59** was added to the cells and incubated for 24 hours. Cells were harvested and analysed as described under the section "DUB activity profiling and competition with Ub-PA DUB probes".

5

Chapter 5

Immunoblotting. Cells were lysed in HR lysis buffer (50 mM Tris, 5 mM MgCl$_2$, 250 mM sucrose and 2 mM DTT, pH 7.4) with protease inhibitor cocktail for 10 min. on ice. The lysates were sonicated using 10 cycles of 30 sec. pulse on, 30 sec. pulse off. The lysates were centrifuged at maximun speed for 20 min. at 4 °C, thereafter protein concentrations were measured using the DC protein assay (500-0111; Bio-Rad) and equal amounts of proteins were used for each condition that was analyzed by immunoblotting with following antibodies: UCHL1 (ab27053; Abcam), Tubulin (2148; Cell Signaling), GAPDH (MAB374; Millipore), Actin (A5441; Sigma-Aldrich,).

Immunofluorescence staining. Cells were fixed for 20 min. in 4% paraformaldehyde and then permeabilized in 0.1% Triton-X for 10 min. Non-specific binding was blocked with blocking buffer (1% BSA in 0.1% PBS-Tween) for 30 min. The primary antibody UCHL1 (ab27053; Abcam) was diluted in blocking buffer and added to the cell for 1 hour. After 3 times washing with PBS, the secondary antibody donkey anti rabbit IgG Alexa Fluorescence 555 (Invitrogen #A31572) was added and incubated for 30 min. After 3 times washing with PBS, samples were mounted with VECTASHIELD antifade mounting medium with DAPI (H-1200; Vector Laboratories). Fluorescence images were acquired with TCS SP8 confocal microscope (Leica).

Zebrafish embryos were fixed with 4% paraformaldehyde 2 hours at room temperature. Samples were dehydrated with 33%, 66%, 100% methanol in PBS, followed by a rehydration step. Thereafter, the embryos were successively treated with 10 µg/mL proteinase K for 60 min. at 37 °C, permeabilized with 0.25% Triton in PBS for 30 min. on ice, and blocked with 10% FBS in PBS for 1 hour at room temperature. Embryos were incubated with primary antibody (ab27053; Abcam) for at least 12 hours at 4 °C. After washing with 0.1% Triton in PBS for 3 times 10 min., the samples were incubated with fluorescein-conjugated secondary antibody donkey anti rabbit IgG Alexa Fluorescence 555 (Invitrogen #A31572) for 2 hours at room temperature. After washing with PBS (0.1% Triton), samples were analyzed using a confocal microscope SP5 STED (Leica, Rijswijk, Netherlands).

DUB activity profiling and competition with Ub-PA DUB probes. HEK293T cells were treated with 5 µM final concentration of the indicated compounds for 24 hours. Cells were lysed in HR lysis buffer supplemented with protease inhibitor cocktail (11836145001; Roche). Samples were kept on ice and lysed by sonication (10 cycles of 30 seconds on and 30 seconds off). 25 µg protein extract was labelled with either 1 µM Rh-Ub-PA probe or 0.5 µM Cy5-Ub-PA probe for 30 min. at 37 °C. For the cell lysate incubation, HEK293T cells were lysate as described above. HEK293T cell lysates were preincubated with 5 µM final concentration of compounds for 1 hour, followed by incubation with 0.5 µM Cy5-Ub-PA probe for 30 min. at 37 °C. Labelling reactions were terminated with sample buffer and heating to 100 °C for 10 min. Samples were size-separated in SDS-PAGE gels. In-gel fluorescence signals were scanned employing the Typhoon FLA 9500 Molecular Imager (GE Healthcare). Images were analyzed using ImageJ software.

Probe labelling of endogenous UCHL1 in living cell. Cell lines were transfected with shRNAs, siRNAs or UCHL1 constructs as described above. 5 µM final concentration of probes were added to the cell a day before harvesting. Cells were harvested in HR buffer as described above. NuPAGE LDS sample buffer containing 50 mM TCEP was added to cell lysates. Samples were resolved by SDS-PAGE using a 4-12% Bis-Tris gel (Invitrogen,

NuPAGE) with MES SDS running buffer (Novex, NuPAGE) for 45 min. at 190V. Gels were scanned for fluorescence on a GE Typhoon FLA 9500 using a green ($\lambda_{ex/em}$ 473/530 nm) and red ($\lambda_{ex/em}$ 532/570 nm) channel followed by transferring proteins to nitrocellulose membrane (Amersham) and western blot analysis.

Proteomics. For 1-step approach, 4×10^6 HEK293T cells were seeded into 10 cm dishes for each treatment. 48 hours later, HEK293T cells were harvested in lysis buffer containing 50 mM HEPES pH 7.3, 150 mM NaCl and 1% NP-40 and 1× protease inhibitor cocktail and incubated for 30 min. on ice. Cell lysates were centrifuged at maximum speed for 20 min. The lysates were incubated with 5 µM final concentration of Biotin-PEG$_4$-alkyne, **11RK72** or **11RK73** or same volume of DMSO for 1 hour at room temperature. 30 µL of neutravidin beads slurry (50%) were added to each sample. The samples were then incubated for 2 hours at 4 °C. Beads were washed six times in wash buffer containing 50 mM HEPES pH 7.3, 150 mM NaCl and 1% NP-40. After completely removing the washing buffer, NuPAGE LDS sample buffer (containing 7.5% β-mercaptoethanol) was added to the beads followed by 15 min. incubation at 95 °C.

For 2-step approach, 4×10^6 HEK293T cells were seeded into 10 cm dishes for each treatment. 24 hours later, 5 µM final concentration of 8RK64 or same volume of DMSO was added to the cells. After 24 hours incubation, HEK293T cells were harvested in lysis buffer containing 50 mM HEPES pH 7.3, 150 mM NaCl and 1% NP-40 and 1× protease inhibitor cocktail and incubated for 30 min. on ice. Cell lysates were centrifuged at maximum speed for 20 min. 1× volume of click cocktail (100 mM CuSO4.5H2O, 1M sodium ascorbate, 100 mM TBTA (Tris[(1-benzyl-1H-1,2,3-triazol-4-yl)methyl]amine) ligand, 0.1 M HEPES pH 7.3 and 5 µM biotin-alkyne) were added to 2× volume of cell lysates and incubated for 45 min. 30 µL of neutravidin beads slurry (50%) were added to each sample. The samples were then incubated for 2 hours at 4 °C. Beads were washed six times in wash buffer containing 50 mM HEPES pH 7.3, 150 mM NaCl and 1% NP-40. After completely removing the washing buffer, SDS sample buffer (containing 7.5% β-mercaptoethanol) was added to the beads followed by 15 min. incubation at 95 °C. For MS analysis proteins were run for 1-2 cm on a 4-12% PAGE (NuPAGE Bis-Tris Precast Gel, Life Technologies) and stained with silver (SilverQuest Silver Stain, Life Technologies). The lane was cut into two equal parts, and gel slices subjected to reduction with dithiothreitol, alkylation with iodoacetamide and in-gel trypsin digestion using a Proteineer DP digestion robot (Bruker).

Tryptic peptides were extracted from the gel slices, lyophilized, dissolved in 95/3/0.1 v/v/v water/acetonitril/formic acid and subsequently analyzed by on-line C18 nanoHPLC MS/MS with a system consisting of an Easy nLC 1000 gradient HPLC system (Thermo, Bremen, Germany), and a LUMOS mass spectrometer (Thermo). Fractions were injected onto a homemade precolumn (100 µm × 15 mm; Reprosil-Pur C18-AQ 3 µm, Dr. Maisch, Ammerbuch, Germany) and eluted via a homemade analytical nano-HPLC column (15 cm × 50 µm; Reprosil-Pur C18-AQ 3 µm). The gradient was run from 0% to 50% solvent B (20/80/0.1 water/acetonitrile/formic acid v/v/v) in 20 min. The nano-HPLC column was drawn to a tip of ~5 µm and acted as the electrospray needle of the MS source. The LUMOS mass spectrometer was operated in data-dependent MS/MS (top-10 mode) with collision energy at 32 V and recording of the MS2 spectrum in the orbitrap. In the master scan (MS1) the resolution was 120,000, the scan range 400-1500, at an AGC target of 400,000

@maximum fill time of 50 ms. Dynamic exclusion after n=1 with exclusion duration of 10 s. Charge states 2-5 were included. For MS2 precursors were isolated with the quadrupole with an isolation width of 1.2 Da. HCD collision energy was set to 32V. First mass was set to 110 Da. The MS2 scan resolution was 30,000 with an AGC target of 50,000 @maximum fill time of 60 ms.

In a post-analysis process, raw data were first converted to peak lists using Proteome Discoverer version 2.2.0.388 (Thermo Electron), and then submitted to the Uniprot Homo sapiens database (67911 entries), using Mascot v. 2.2.04 (www.matrixscience.com) for protein identification. Mascot searches were with 10 ppm and 0.02 Da deviation for precursor and fragment mass, respectively, and trypsin as enzyme. Up to two missed cleavages were allowed, and methionine oxidation was set as a variable modification; carbamidomethyl on Cys was set as a fixed modification. Protein abundance calculation and statistical analysis was performed using Proteome Discoverer software.

Zebrafish experiments. Transgenic zebrafish lines Tg (kdrl: mTurquois) were raised, staged and maintained according to standard procedures in compliance with the local Institutional Committee for Animal Welfare of the Leiden University. Zebrafish embryos were treated with 5 μM **8RK59** or gradient **6RK73** concentration in the egg water. Fluorescent image acquisition was performed with a Leica SP5 STED confocal microscope (Leica, Rijswijk, Netherlands). The quantification of **8RK59** signal was analyzed by Leica microscope software platform LAS X. 30 zebrafish were treated in each group and 3 representative images were taken and analyzed. Statistical analysis was performed using Graphpad Prism 8 software. Numerical data from triplicates are presented as the mean ± SD. Two-way analysis of variance (ANOVA) has been used to analyze multiple subjects.

SUPPORTING INFORMATION
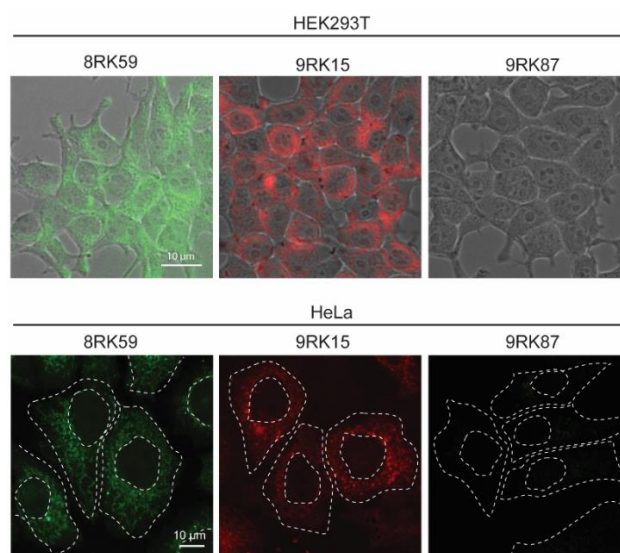
Figure S1. Cell permeability of 8RK59, 9RK15, and 9RK87 probes. HEK293T (top panel) and HeLa (bottom panel) cells were incubated with 5 μM final concentration of indicated probes for 24 hours at 37 °C. HEK293T cells were visualized using EVOS® FL Cell Imaging System. Nikon Plan Fluor 40×/0.75, infinity/0.17 objective was used. HeLa cells were fixed by 3.7% formaldehyde and then mounted using ProLong Gold antifade mounting medium with DAPI. Nuclei and cell boundaries are shown in dashed white lines. HeLa cells were imaged using Leica SP8 microscopes. HCX PL 63× 1.32 oil objectives and HyD detectors were used in confocal images.
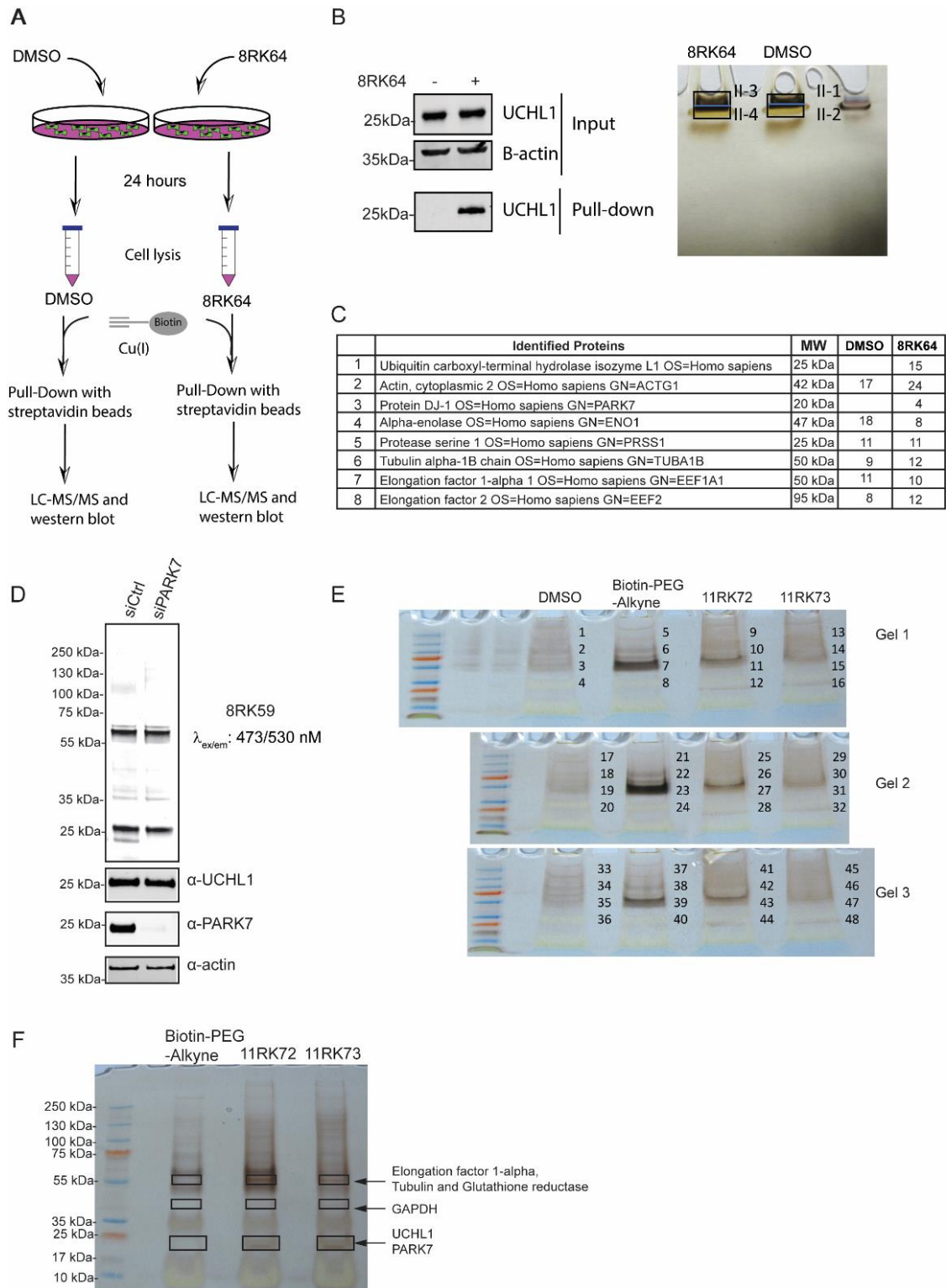
Figure S2. Pull-down and proteomics analysis either via a 1-step approach with biotin tagged-probes or via a 2-step labeling approach with click-chemistry. A) Schematic representation of 2-step labeling and pull-down approach. B) Western blot (left panel) and silver staining (right panel) of the samples obtained from 2-step labeling approach. Neutravidin beads from DMSO or 8RK64 treated samples were boiled in NuPAGE LDS sample buffer at 95 °C for 15 min. Proteins were run on 4-12% SDS-PAGE (1 cm for right panel) and either immunoblotted against PARK7, UCHL1 and Actin or stained using SilverQuest Silver Stain. The numbers on the gel indicate slices cut from the gel. C) List of the top eight proteins identified from proteomics experiment using 2-step labeling and pull-down approach. D) Confirmation of PARK7 labeling with 8RK59 via Fluorescent labeling and western blot

analysis. Labeled proteins with 8RK59 were analyzed using in-gel fluorescence scanning followed by immunoblot against UCHL1. Actin is used as a loading control. E) Silver staining of three independent gels obtained from 1-step labeling approach. Related to Figure 4. Neutravidin beads from DMSO, Biotin-PEG4-Alkyne, 11RK72 or 11RK73 treated samples were boiled in NuPAGE LDS sample buffer at 95 °C for 15 min. Proteins were run for 2 cm on 4-12% SDS-PAGE and stained using SilverQuest Silver Stain. The numbers on the gels indicate slices cut from the gels. F) Silver staining of the samples obtained from 1-step labeling approach. Neutravidin beads from Biotin-PEG4-Alkyne, 11RK72 or 11RK73 treated samples were boiled in NuPAGE LDS sample buffer at 95 °C for 15 min. Proteins were run on 4-12% SDS-PAGE and stained using SilverQuest Silver Stain. Rectangles indicate the gel slices analyzed by LC-MS/MS.
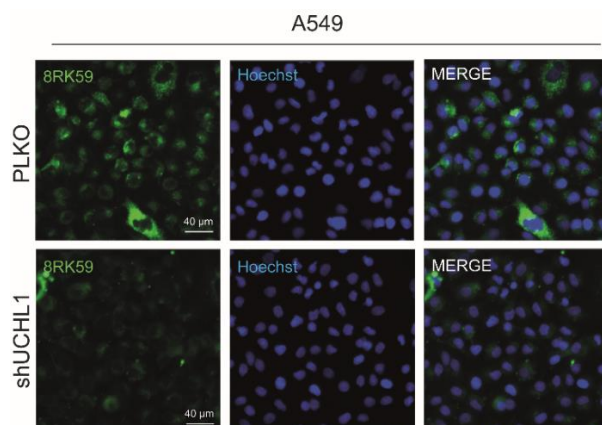
Figure S3. Probing UCHL1 activity in cells with 8RK59. A549 PLKO and shUCHL1 cells were incubated with 5 μM 8RK59 for 16 hours at 37 °C. 1 μg/mL Hoechst 33342 was used to stain the nuclei of the live cells for 30 min. at 37 °C. Images were acquired with Leica DMi8 Inverted Fluorescent Microscope. HC PL FLUOTAR L 40x/0.60 DRY was used.
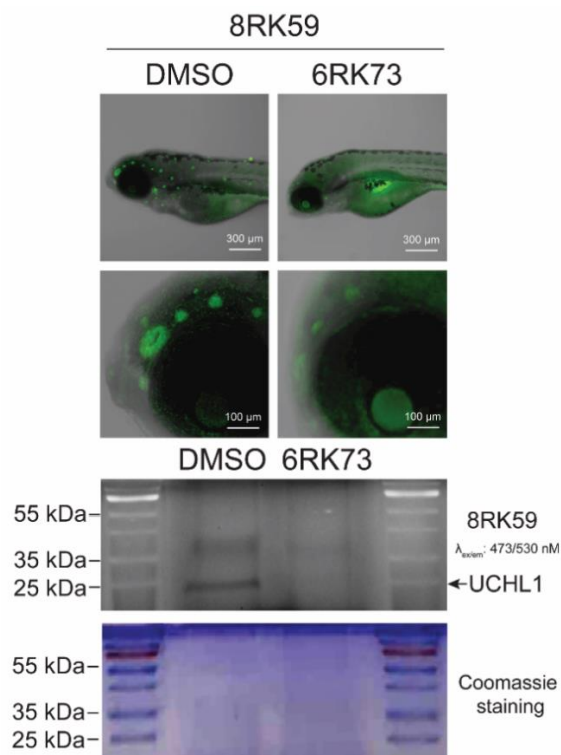
Figure S4. Fluorescence labeling of endogenous UCHL1 in zebrafish embryo and lysates with 8RK59. Images of 8RK59 signal in zebrafish embryos pre-treated with DMSO or 5 μM 6RK73 (top panel). Fluorescence scan of corresponding zebrafish lysate in SDS-PAGE gel (bottom panel). Coomassie staining serves as loading control.

Table S1: IC$_{50}$ values[a]

Compound	DUB (concentration)	IC$_{50}$ (μM)
6RK73	UCHL1 (1 nM)	0.23
6RK73	UCHL3 (0.01 nM)	235
6RK73	UCHL5 (1 nM)	>>100
6RK73	USP7 (1 nM)	68.8
6RK73	USP16 (2 nM)	>>100
6RK73	USP30 (10 nM)	9.8
6RK73	Papain (3 nM)	10.7
8RK64	UCHL1 (1 nM)	0.32
8RK64	UCHL3 (0.01 nM)	216
8RK64	UCHL5 (1 nM)	>>100
8RK59	UCHL1 (1 nM)	1.2
9RK15	UCHL1 (1 nM)	3.6
9RK87	UCHL1 (1 nM)	0.44
11RK72	UCHL1 (1 nM)	0.50
11RK73	UCHL1 (1 nM)	0.64

[a] After 30 min. of incubation of enzyme with inhibitor.

Author Contributions

Compound synthesis (RK PG BTX), manuscript writing (PG AS SL HO), enzyme inhibition assays (PG), cell culture and immunoblotting (AS SL), zebrafish experiments (SL), experiment design (PG RK AS SL), proteomics (AS GJ PvV), study supervision (PG HO PtD).

Ethics Statement

Zebrafish were raised, staged and maintained according to standard procedures in compliance with the local Institutional Committee for Animal Welfare of the Leiden University.

ACKNOWLEDGEMENTS

5

Chapter 5

REFERENCES

1. Komander D, Rape M. The ubiquitin code. Annu Rev Biochem 2012;81:203-29.
2. Cadwell K, Coscoy L. Ubiquitination on nonlysine residues by a viral E3 ubiquitin ligase. Science 2005;309(5731):127-30.
3. Pao KC, Wood NT, Knebel A, Rafie K, Stanley M, Mabbitt PD, *et al.* Activity-based E3 ligase profiling uncovers an E3 ligase with esterification activity. Nature 2018;556(7701):381-5.
4. Mevissen TET, Komander D. Mechanisms of Deubiquitinase Specificity and Regulation. Annu Rev Biochem 2017;86:159-192.
5. Behrends C, Harper JW. Constructing and decoding unconventional ubiquitin chains. Nat Struct Mol Biol 2011;18(5):520-8.
6. Wilkinson KD, Lee K, Deshpande S, Duerksenhughes P, Boss JM, Pohl J. The Neuron-specific protein PGP-9.5 is a ubiquitin carboxyl-terminal hydrolase. Science 1989;246(4930):670-3.
7. Leroy E, Boyer R, Auburger G, Leube B, Ulm G, Mezey E, *et al.* The ubiquitin pathway in Parkinson's disease. Nature 1998;395(6701):451-2.
8. Maraganore DM, Farrer MJ, Hardy JA, Lincoln SJ, McDonnell SK, Rocca WA. Case-control study of the ubiquitin carboxy-terminal hydrolase L1 gene in Parkinson's disease. Neurology 1999;53(8):1858-60.
9. Lunati A, Lesage S, Brice A. The genetic landscape of Parkinson's disease. Rev Neurol 2018;174(9):628-43.
10. Bilguvar K, Tyagi NK, Ozkara C, Tuysuz B, Bakircioglu M, Choi M, *et al.* Recessive loss of function of the neuronal ubiquitin hydrolase UCHL1 leads to early-onset progressive neurodegeneration. Proc Natl Acad Sci U S A 2013;110(9):3489-94.
11. Zhang M, Cai F, Zhang S, Zhang S, Song W. Overexpression of ubiquitin carboxyl-terminal hydrolase L1 (UCHL1) delays Alzheimer's progression in vivo. Sci Rep 2014;4:7298.
12. Bishop P, Rocca D, Henley JM. Ubiquitin C-terminal hydrolase L1 (UCH-L1): structure, distribution and roles in brain function and dysfunction. Biochem J 2016; 473(16):2453-62.
13. Hussain S, Foreman O, Perkins SL, Witzig TE, Miles RR, van Deursen J, *et al.* The de-ubiquitinase UCH-L1 is an oncogene that drives the development of lymphoma in vivo by deregulating PHLPP1 and Akt signaling. Leukemia 2010;24(9):1641-55.
14. Hurst-Kennedy J, Chin LS, Li L. Ubiquitin C-terminal hydrolase L1 in tumorigenesis. Biochem Res Int 2012;2012:123706.
15. de Jong A, Merkx R, Berlin I, Rodenko B, Wijdeven RH, El Atmioui D, *et al.* Ubiquitin-based probes prepared by total synthesis to profile the activity of deubiquitinating enzymes. Chembiochem 2012;13(15):2251-8.
16. Harrigan JA, Jacq X, Martin NM, Jackson SP. Deubiquitylating enzymes and drug discovery: emerging opportunities. Nat Rev Drug Discov 2018;17(1):57-78.
17. Das C, Hoang QQ, Kreinbring CA, Luchansky SJ, Meray RK, Ray SS, *et al.* Structural basis for conformational plasticity of the Parkinson's disease-associated ubiquitin hydrolase UCH-L1. Proc Natl Acad Sci U S A 2006;103(12):4675-80.
18. Gavory G, O'Dowd CR, Helm MD, Flasz J, Arkoudis E, Dossang A, *et al.* Discovery and characterization of highly potent and selective allosteric USP7 inhibitors. Nat Chem Biol 2018;14(2):118-25.
19. O'Dowd CR, Helm MD, Rountree JSS, Flasz JT, Arkoudis E, Miel H, *et al.* Identification and Structure-Guided Development of Pyrimidinone Based USP7 Inhibitors. ACS Med Chem Lett 2018;9(3):238-43.
20. Turnbull AP, Ioannidis S, Krajewski WW, Pinto-Fernandez A, Heride C, Martin ACL, *et al.* Molecular basis of USP7 inhibition by selective small-molecule inhibitors. Nature 2017;550(7677):481-6.
21. Lamberto I, Liu X, Seo HS, Schauer NJ, Iacob RE, Hu W, *et al.* Structure-Guided Development of a Potent and Selective Non-covalent Active-Site Inhibitor of USP7. Cell Chem Biol 2017;24(12):1490-1500.

22. Kategaya L, Di Lello P, Rouge L, Pastor R, Clark KR, Drummond J, *et al.* USP7 small-molecule inhibitors interfere with ubiquitin binding. Nature 2017;550(7677): 534-8.

23. Pozhidaeva A, Valles G, Wang F, Wu J, Sterner DE, Nguyen P, *et al.* USP7-Specific Inhibitors Target and Modify the Enzyme's Active Site via Distinct Chemical Mechanisms. Cell Chem Biol 2017;24(12):1501-1512.

24. Resnick E, Bradley A, Gan J, Douangamath A, Krojer T, Sethi R, *et al.* Rapid Covalent-Probe Discovery by Electrophile-Fragment Screening. J Am Chem Soc 2019;141(22):8951-68.

25. Ward JA, McLellan L, Stockley M, Gibson KR, Whitlock GA, Knights C, *et al.* Quantitative Chemical Proteomic Profiling of Ubiquitin Specific Proteases in Intact Cancer Cells. ACS Chem Biol 2016;11(12):3268-72.

26. Jones A, Kemp MI, Stockley ML, Gibson KR, Whitlock GA, Madin A. Novel compounds. 2016.

27. Falgueyret JP, Oballa RM, Okamoto O, Wesolowski G, Aubin Y, Rydzewski RM, *et al.* Novel, nonpeptidic cyanamides as potent and reversible inhibitors of human cathepsins K and L. J Med Chem 2001;44(1):94-104.

28. Lavis LD, Chao TY, Raines RT. Fluorogenic label for biomolecular imaging. ACS Chem Biol 2006;1(4):252-60.

29. Copeland RA, Basavapathruni A, Moyer M, Scott MP. Impact of enzyme concentration and residence time on apparent activity recovery in jump dilution analysis. Anal Biochem 2011;416(2):206-10.

30. Liu Y, Lashuel HA, Choi S, Xing X, Case A, Ni J, *et al.* Discovery of inhibitors that elucidate the role of UCH-L1 activity in the H1299 lung cancer cell line. Chem Biol 2003;10(9):837-46.

31. Ekkebus R, van Kasteren SI, Kulathu Y, Scholten A, Berlin I, Geurink PP, *et al.* On terminal alkynes that can react with active-site cysteine nucleophiles in proteases. J Am Chem Soc 2013;135(8):2867-70.

32. Gjonaj L, Sapmaz A, Gonzalez-Prieto R, Vertegaal ACO, Flierman D, Ovaa H. USP7: combining tools towards selectivity. Chem Commun 2019;55(35):5075-8.

33. Altun M, Kramer HB, Willems LI, McDermott JL, Leach CA, Goldenberg SJ, *et al.* Activity-Based Chemical Proteomics Accelerates Inhibitor Development for Deubiquitylating Enzymes. Chem Biol 2011;18(11):1401-12.

34. Cravatt BF, Wright AT, Kozarich JW. Activity-based protein profiling: from enzyme chemistry to proteomic chemistry. Annu Rev Biochem 2008;77:383-414.

35. Verdoes M, Hillaert U, Florea BI, Sae-Heng M, Risseeuw MDP, Filippov DV, *et al.* Acetylene functionalized BODIPY dyes and their application in the synthesis of activity based proteasome probes. Bioorg Med Chem Lett 2007;17(22):6169-71.

36. Butkevich AN, Mitronova GY, Sidenstein SC, Klocke JL, Kamin D, Meineke DNH, *et al.* Fluorescent Rhodamines and Fluorogenic Carbopyronines for Super-Resolution STED Microscopy in Living Cells. Angew Chem Int Ed Engl 2016;55(10):3290-4.

37. Thul PJ, Akesson L, Wiking M, Mahdessian D, Geladaki A, Ait Blal H, *et al.* A subcellular map of the human proteome. Science 2017;356(6340).

38. Meier JL, Mercer AC, Rivera H, Burkart MD. Synthesis and evaluation of bioorthogonal pantetheine analogues for in vivo protein modification. J Am Chem Soc 2006;128 (37):12174-84.

39. Ren J, Liu S, Cui C, Ten Dijke P. Invasive Behavior of Human Breast Cancer Cells in Embryonic Zebrafish. J Vis Exp. 2017;(122).

40. Son OL, Kim HT, Ji MH, Yoo KW, Rhee M, Kim CH. Cloning and expression analysis of a Parkinson's disease gene, UCH-L1, and its promoter in zebrafish. Biochem Biophys Res Commun 2003;312(3):601-7.

41. Hewings DS, Flygare JA, Bogyo M, Wertz IE. Activity-based probes for the ubiquitin conjugation-deconjugation machinery: new chemistries, new tools, and new insights. FEBS J 2017;284(10):1555-76.

42. Ernst A, Avvakumov G, Tong JF, Fan YH, Zhao YL, Alberts P, *et al.* A Strategy for Modulation of Enzymes in the Ubiquitin System. Science 2013;339(6119):590-5.

43. Gjonaj L, Sapmaz A, Flierman D, Janssen GJ, van Veelen PA, Ovaa H. Development of a DUB-selective fluorogenic substrate. Chem Sci 2019;10(44):10290-10296.

5

44. Sanman LE, Bogyo M. Activity-Based Profiling of Proteases. Annu Rev Biochem 2014;83:249-73.
45. Verdoes M, Verhelst SHL. Detection of protease activity in cells and animals. Biochim Biophys Acta 2016;1864(1):130-42.
46. Krabill AD, Chen H, Hussain S, Feng C, Abdullah A, Das C, *et al.* Biochemical and cellular characterization of a cyanopyrrolidine covalent Ubiquitin C-terminal hydrolase L1 inhibitor. Chembiochem 2020;21(5):712-722.
47. Liu S, González Prieto R, Zhang M, Geurink PP, Kooij R, Vasudevan Iyengar P, *et al.* Deubiquitinase activity profiling identifies UCHL1 as a candidate oncoprotein that promotes TGFβ-induced breast cancer metastasis. Clin Cancer Res 2020;26(6):1460-1473.

Chapter 6

Mutational activation of BRAF confers sensitivity to TGFβ inhibitors in human cancer cells

Lindsay C. Spender[1,9], G. John Ferguson[1,10], Sijia Liu[4], Chao Cui[4], Maria Romina Girotti[5], Gary Sibbet[1], Ellen B. Higgs[9], Morven K. Shuttleworth[9], Tom Hamilton[2], Paul Lorigan[6], Michael Weller[7], David F. Vincent[3], Owen J. Sansom[3], Margaret Frame[8], Peter ten Dijke[4], Richard Marais[5] and Gareth J. Inman[1,9]

[1] Growth Factor Signalling Laboratory, The Beatson Institute for Cancer Research, Bearsden, Glasgow, United Kingdom
[2] Biological Services, The Beatson Institute for Cancer Research, Bearsden, Glasgow, United Kingdom
[3] Colorectal Cancer and Wnt Signalling, The Beatson Institute for Cancer Research, Bearsden, Glasgow, United Kingdom
[4] Department of Molecular Cell Biology, Leiden University Medical Center, Netherlands
[5] Cancer Research UK Manchester Institute, The University of Manchester, Withington, Manchester, United Kingdom
[6] The University of Manchester, The Christie NHS Foundation Trust, Manchester, United Kingdom
[7] Department of Neurology, University Hospital Zurich, Frauenklinikstrasse, Zurich, Switzerland
[8] The Institute of Genetics and Molecular Medicine, University of Edinburgh, Western General Hospital, United Kingdom
[9] Division of Cancer Research, School of Medicine, University of Dundee, Dundee, United Kingdom
[10] Department of Respiratory, Inflammation and Autoimmunity Research, Cambridge, United Kingdom

Chapter 6

Abstract

Recent data implicate elevated transforming growth factor-β (TGFβ) signaling in BRAF inhibitor drug-resistance mechanisms, but the potential for targeting TGFβ signaling in cases of advanced melanoma has not been investigated. We show that mutant BRAFV600E confers an intrinsic dependence on TGFβ/TGFβ receptor 1 (TGFBR1) signaling for clonogenicity of murine melanocytes. Pharmacological inhibition of the TGFBR1 blocked the clonogenicity of human mutant BRAF melanoma cells through SMAD4-independent inhibition of mitosis, and also inhibited metastasis in xenografted zebrafish. When investigating the therapeutic potential of combining inhibitors of mutant BRAF and TGFBR1, we noted that unexpectedly, low-dose PLX-4720 (a vemurafenib analogue) promoted proliferation of drug-naïve melanoma cells. Pharmacological or pharmacogenetic inhibition of TGFBR1 blocked growth promotion and phosphorylation of SRC, which is frequently associated with vemurafenib resistance mechanisms. Importantly, vemurafenib-resistant patient derived cells retained sensitivity to TGFBR1 inhibition, suggesting that TGFBR1 could be targeted therapeutically to combat the development of vemurafenib drug-resistance.

Introduction

Malignant melanoma is the most aggressive form of skin cancer with around 55,500 deaths worldwide in 2012 (1). While primary localized melanoma may be cured by surgical removal alone, metastatic melanoma is associated with poor long-term prognosis. Somatic mutations that constitutively activate the RAS-RAF-mitogen activated protein kinase-extracellular signal-regulated kinase (RAS-RAF-MEK-ERK) signaling pathway are frequently detected in melanoma; mutations in BRAF and NRAS have been detected in approximately 50% and 20% of melanomas, respectively (2). The identification of genetic drivers of melanoma (2) has led to the development of small-molecule inhibitors (e.g. vemurafenib, dabrafenib) (BRAFi), which selectively target mutant BRAF. Their use in the clinic has significantly increased survival of metastatic melanoma patients (3-5). However, the development of drug resistance remains a significant problem with the vast majority of patients with advanced melanoma dying of drug-resistant disease.

Numerous mechanisms of resistance to BRAF inhibitors have been described, many involving reactivation of the MAPK pathway (reviewed in (6)). As a result, the combined use of BRAF inhibitors with MEK inhibitors (e.g. cobimetinib, trametinib) has been proposed as a way to overcome the development of resistance (7-9). While this approach significantly improves patient survival (resulting in a median expected survival of approximately 25 months for eligible patients), the efficacy of combinatorial therapies which target the same signaling pathway ultimately may be limited because of augmented BRAF inhibitor drug resistance mechanisms or secondary mutations (10, 11).

Additionally, secondary epigenetic events that do not necessarily affect MEK/ERK activity can occur to limit the tumor cells' dependence on the MAPK pathway, or restrict tumor immune surveillance. These resistance mechanisms include changes in the methylome affecting tumor cell apoptosis (12), increases in PI3K/AKT activity (13-15) and/or increases in receptor tyrosine kinase (RTK) signaling. For instance, loss of microphthalmia associated transcription factor (MITF) expression correlates with increased RTK expression and resistance (16). Vemurafenib-resistance induced increases in EGFR signaling have been

shown to activate an EGFR-SRCSTAT3 signaling cascade in melanoma, and targeting this pathway using inhibitors of SRC inhibits growth of vemurafenib-resistant xenografts (17, 18).

As well as cell autonomous effects, drug-induced stimulation of melanoma-associated fibroblasts stimulates matrix remodeling and, in this case, signals via integrins to increase SRC and FAK activity. This change in the microenvironment promotes melanoma cell survival and provides a "safe haven" to enable emergence of drug resistant tumor cells (19). Clearly, stromal remodeling and SRC activation have emerged as contributors to BRAF inhibitor resistance, and it is apparent that the therapy induced secretome is key in driving resistance. Increased transforming growth factor-β (TGFβ) secretion may be part of the therapy-induced secretome, and has been implicated in both in vitro derived drug resistance (20) and in vemurafenib-resistant patient material (21). Increased TGFβ signaling can result in an upregulation of EGFR and PDGFR (21), positioning TGFβ signaling upstream of well described vemurafenib-resistance associated RTK pathways. Despite this, the potential for TGFβ pathway inhibitors in combating BRAF kinase inhibitor resistance has not been studied to date.

TGFβ ligand binds to the constitutively active high affinity type 2 serine/threonine kinase receptor TGFBR2 which trans-phosphorylates and activates TGFBR1. As part of the canonical signaling pathway, TGFBR1 phosphorylates and activates the intracellular signaling transcription factors SMAD2 and SMAD3, and following binding to SMAD4, the SMAD complex accumulates in the nucleus where it regulates target gene transcription. Additionally, TGFβ can signal via numerous noncanonical pathways including RHO/ROCK, MAPK, and PI3-Kinase (reviewed in (22)). In normal melanocytes, TGFβ inhibits proliferation and DNA synthesis and induces melanocyte stem cell quiescence, however, melanoma cells are able to evade the tumor suppressive effects of TGFβ. TGFβ levels are elevated in the plasma of melanoma patients (regardless of their exposure to BRAF inhibitors), and increases in expression are associated with progressive disease (23). The mechanisms of growth arrest and their evasion by melanoma cells, however, have not been fully characterized and are likely to be multi-factorial (reviewed in (24)).

There is little evidence of mutation of TGFβ receptors in melanoma (25), so, it appears that with functional receptors and apparently intact SMAD function (26, 27), melanoma cells are able to evade growth suppressive effects of TGFβ while simultaneously utilizing pro-tumorigenic functions of TGFβ. TGFβ signaling promotes migration of BRAF-transformed melanocytes in *in vitro* organotypic skin cultures (28) and is involved in metastasis of mouse melanoma cells to the bone through expression of tissue-specific genes known to promote bone osteolysis (26, 29). In addition, melanoma cells engineered to over-express TGFβ exert paracrine effects on stromal fibroblasts whereby they secrete matrix components (including fibronectin, collagens, and tenascin) to promote melanoma tumor formation (30). These observations are reminiscent of the vemurafenib-induced activation of melanoma-associated fibroblasts providing a "safe haven" for melanoma tumor cells, however, no link has been formally established between vemurafenib-induced fibroblast activation and TGFβ signaling.

In this study, we now provide evidence that melanoma cells are "hard-wired" to depend on autocrine TGFβ signaling through TGFBR1 for tumor establishment and clonogenicity. We show that the fundamental addiction of melanoma cells to TGFβ is: induced by the presence of mutant BRAF; mediated by a SMAD4-independent pathway; and correlates with TGFβ

regulation of RHOA activity, thus providing support for the notion that non-canonical signaling pathways are key mediators of pro-tumorigenic TGFβ function in melanoma. Importantly, we also provide evidence that vemurafenib resistant patient-derived cells retain sensitivity to inhibitors of TGFBR1. TGFBR1 inhibitors block the enhanced proliferation of paradoxically activated PLX-4720 treated melanoma cells, and can be used to effectively inhibit metastatic melanoma in a zebrafish xenograft model.

Mutant BRAF confers TGFβ addiction

We demonstrated previously that autocrine signaling through TGFBR1, is required for transformation of rodent fibroblasts by oncogenic BRAF (31), but did not investigate this dependence in human models of activated RAS/RAF-driven cancer. Since mutational activation of BRAF is frequently observed in melanoma (2), we tested the susceptibility of immortalised mouse melanocytes stably transfected with either wild-type or mutant BRAF to inhibition by the TGFBR1 kinase inhibitor SB-431542. Unlike parental or wildtype BRAF transfected cells, melanocytes transfected with oncogenic V600E BRAF required TGFBR1 kinase activity for their proliferation since SB-431542 decreased cell numbers (Figure 1a). These data suggest that the presence of mutant BRAF in melanocytes confers a dependence (or addiction) on the TGFβ/TGFBR1 signaling pathway for cell proliferation. Similar results were observed in soft agar assays measuring anchorage independent growth (Figure 1b). We determined the amount of autocrine TGFβ produced by the transfected melanocytes, using a bioassay of NIH3T3 cells stably transfected with a CAGA12-luciferase reporter construct (Supplementary Figure 1a). The dependence on TGFBR1 activity for colony formation did not correlate simply with an increase in latent autocrine TGFβ production following transfection with mutant BRAF (no active TGFβ was detectable without medium acidification) (Supplementary Figure 1b). There was also no elevated signaling via the TGFβ receptor-regulated intracellular signaling transcription factor, SMAD2 in SB-431542 sensitive cells (Supplementary Figure 1c).

We tested whether human cancer cells with activating mutations in MAPK pathway components were also dependent on TGFBR1 for growth. A panel of human tumor cell lines carrying wild type RAS/BRAF or mutations in BRAF, HRAS, KRAS or NRAS (details of all cell lines are given in Supplementary Table 1) were tested for sensitivity to SB-431542 (Figure 1c). Inhibition of TGFBR1 resulted in a range of cellular responses in the wildtype, H-, K-, and N-RAS mutant groups, such that any dependence on TGFBR1 for colony formation could not be predicted in cells carrying these mutations. However, consistent with data obtained in mouse melanocytes (Figure 1b), colony formation in all seven human cell lines carrying mutant BRAF was significantly inhibited (Figure 1c). Again, sensitivity to the TGFBR1 inhibitor did not correlate with levels of autocrine TGFβ production (Supplementary Table S2). The effect of SB-431542 was dose-dependent in low density 2D-culture assay conditions established to assess more accurately clonogenic potential, reaching statistically significant inhibitory concentrations at 10μM (Figure 1d and 1e). Similar dose dependent effects were seen in anchorage-independent soft agar assays (Figure 1f). We attempted to select out TGFBR1 inhibitor-resistant cells following repeated rounds of treatment for over a month, but saw no evidence of outgrowth of refractory subpopulations or acquired resistance during this time frame (Figure 1g). Taken together these data suggest that

cells with mutational activation of BRAF, require TGFBR1 for efficient colony formation and that TGFβ would predictably function as a tumor promoter.
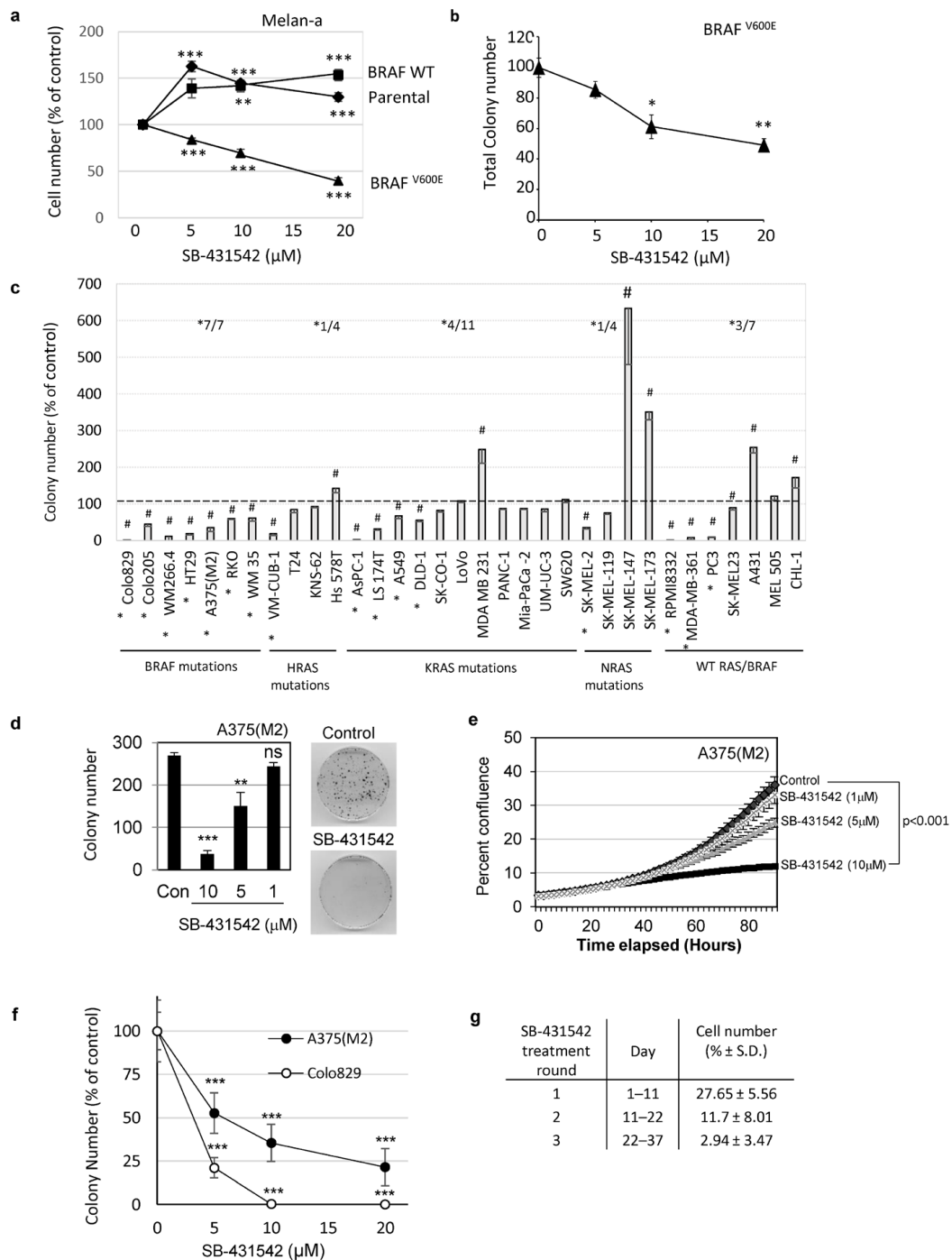
Figure 1: BRAFV600E confers sensitivity to TGFBR1 inhibition. a., b. Melan-a cells expressing the indicated BRAF construct were seeded on plastic **a.,** or in soft agar for cells able to form anchorage independent colonies (mutant BRAF only) **b.,** in the presence of concentrations of SB-431542 as shown. The mean (± SEM) cell number after 6 days **a.** or colony number after 3-4 weeks **b.**were counted and presented as a percentage of the vehicle control. Data was pooled from n = 3-5 independent experiments each performed in triplicate. **c.** Cell lines with activating mutations in BRAF, HRAS, KRAS or NRAS or with wildtype BRAF/RAS were seeded in soft agar in the presence of 10μM SB-431542. Data is presented as a mean (± SD) colony number as a percentage of the vehicle control. Colony counts that were significantly different from controls following treatment with 10μM

SB-431542 are indicated by (#) (TTEST, $p < 0.05$). SK-MEL-147 cells showed no colony formation in the presence of 0.2% DMSO and were assigned a value of 1 to allow analysis. The proportion of cell lines whose colony formation was inhibited by SB-431542 by more than 1/3 within each group is indicated on the histogram (*). **d.-g.** Mutant BRAFV600E human melanoma cell lines A375(M2) (**d-g**) and Colo829 **f.** were treated with either vehicle control or the indicated concentrations of SB-431542. Colony growth on plastic **d.** or in soft agar **f.** were counted after 14 days and 4 weeks, respectively. **e.** Live cell imaging using an IncuCyte Zoom was used to determine the growth kinetics of A375(M2) cells seeded at low cell density (100 cells/ well of 96-well plate) and treated with SB-431542. The mean percent confluence (± SEM) of 4 images per well ($n = 24$ from a representative experiment) is shown. Statistical analysis was carried out by pairwise comparison using the compareGrowthCurves function in statmod (R project). The adjusted p value ($p < 0.001$) is shown **g.** A375(M2) cells were serially passaged in the presence of 10μM SB-431542 to select resistant cells. Surviving cells after each round of treatment were reseeded at low cell density. Cell counts were determined at the end of each treatment round, and the results expressed as the mean (± SD) cell number from 6 wells as a percentage of the control (solvent control treated cells).

## Autocrine TGFβ is required for in vivo melanoma xenograft tumor formation

Melanoma cells engineered to over-express TGFβ1 have increased tumor forming ability (30). To discover whether endogenous autocrine TGFβ expression is required for tumor formation, we generated ligand knockdown clones of A375(M2) cells using stably transfected shRNA constructs targeting TGFβ1. Knockdown of TGFβ1 to levels below 20pg per 1x105 cells/hr (Figure 2a) was sufficient to decrease the ability of A375(M2) cells to form colonies in vitro (Figure 2b) and Supplementary Figure 2a). In xenograft assays, ligand knockdown reduced the percentage of mice with palpable tumors at all recorded time-points (Figure 2c), and significantly reduced tumor growth (Figure 2d). Immunohistochemical (IHC) staining of xenograft sections revealed increased expression of the cyclin-dependent kinase inhibitor CDKN1A (p21CIP1) in tumors generated by TGFβ knockdown cells (Figure 2e and 2f). Elevated CDKN1ACIP1 expression was also observed following SB-431542 treatment of A375(M2) cells (Supplementary Figure 2b).

So far, our data implicate autocrine TGFβ signaling through TGFBR1 as a critical factor in melanoma clonogenicity and tumor formation, however, it was important to rule out off-target effects of the inhibitor. We therefore assessed colony formation following transient transfection with two independent siRNAs targeting TGFBR1. TGFBR1 knockdown (Supplementary Figure 3a) reduced TGFBR1 protein expression and phosphorylation of SMAD2 in response to exogenous TGFβ (Figures 3a and 3b), and recapitulated the effect of chemical inhibition of the receptor. Colony formation and cell proliferation decreased following TGFBR1 knockdown (Figure 3c, 3d, and Supplementary Figure 3b and 3c), confirming that TGFBR1 is required for melanoma colony formation.

To discover whether the canonical SMAD pathway is required for either melanoma cell colony formation or for the inhibitory response to SB-431542, transient knockdown of the co-SMAD, SMAD4 was performed. Knockdown of SMAD4 (Figure 3e) had no significant effect on A375(M2) colony formation (Figure 3f) and significantly increased Colo829 cell proliferation (Figure 3g). These data suggest that SMAD4-dependent signaling is not necessary for colony outgrowth and may, in fact, repress colony growth in Colo829 cells. SMAD4 knockdown also did not block the inhibitory effect of SB-431542 (Figure 3h), indicating that the mechanism of inhibition is SMAD4 independent. In case the levels of

knockdown were not sufficient to accurately assess the contribution of SMAD4, we tested a mutant BRAF/SMAD4 null cell line (HT29). These cells were also sensitive to TGFBR1 inhibition (Supplementary Figure 4a and 4b) thus supporting our conclusion that functional SMAD4 is not necessary for inhibition of colony formation by SB-431542.
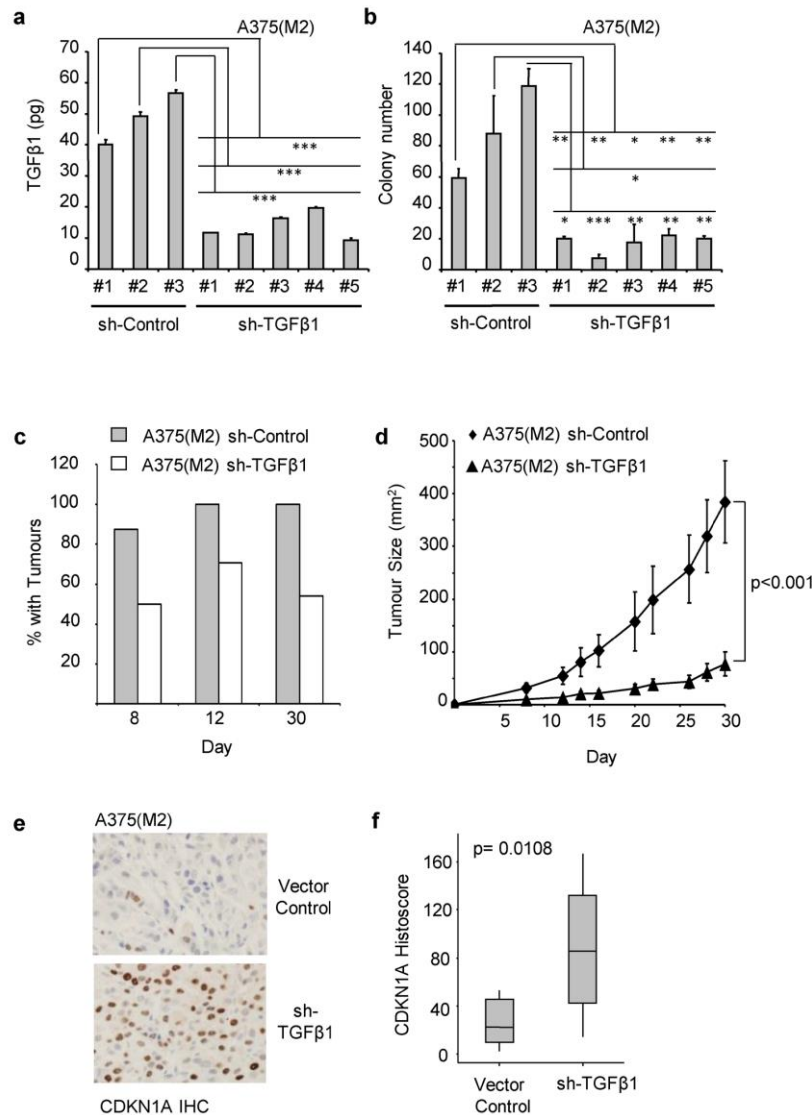
Figure 2: Colony and *in vivo* tumor formation require the autocrine production of TGFβ1. A375(M2) clones stably expressing a Control shRNA, or a TGFβ1 shRNA were analysed for TGFβ1 production **a.** and seeded into soft agar assays **b.**. **a.** TGFβ1 levels were analysed by ELISA and are expressed as the amount (pg) of TGFβ1 produced by 1x105 cells/hour. Data shown are the means ± SD ($n = 3$) . Colonies were counted and presented as the mean ± SD colony number ($n = 3$) **b.**. Statistical significance was measured using Students TTESTS (* = $p < 0.05$, ** = $p < 0.01$, *** = $p < 0.001$). (c-f) A375 (M2) clones, stably expressing either vector control or TGFβ1 shRNA were subcutaneously injected into the flanks of CD1 nude mice and tumors were allowed to develop. Palpable tumors were first detected after 8 days and were measured for a further 21 days. **c.** The number of mice (as a percentage of injected mice) that had palpable tumors on the indicated day (sh-Control, $n = 16$. sh-TGFβ1, $n = 24$). Statistical significance was measured using Students TTESTS (* = $p < 0.05$, ** = $p < 0.01$). **d.** Tumor volumes (mm2, mean ± SEM) were estimated on the indicated days post injection (sh-Control $n = 16$, sh-TGFβ1 $n = 24$). Statistical analysis was carried out using compare Growth Curves (Statmod). **e., f.** sh-control and sh-TGFβ1 tumor sections were stained for CDKN1A and counterstained with haematoxylin (sh-control, $n = 8$. sh-TGFβ1, $n = 9$). Representative images are shown in **e.** and the quantification of the resultant images by histoscore are shown in **f.**. The horizontal bar indicates the median histoscore, the grey boxes and vertical bars indicate 95% CI and range, respectively. P value following statistical analysis using Mann-Whitney U-test is shown.
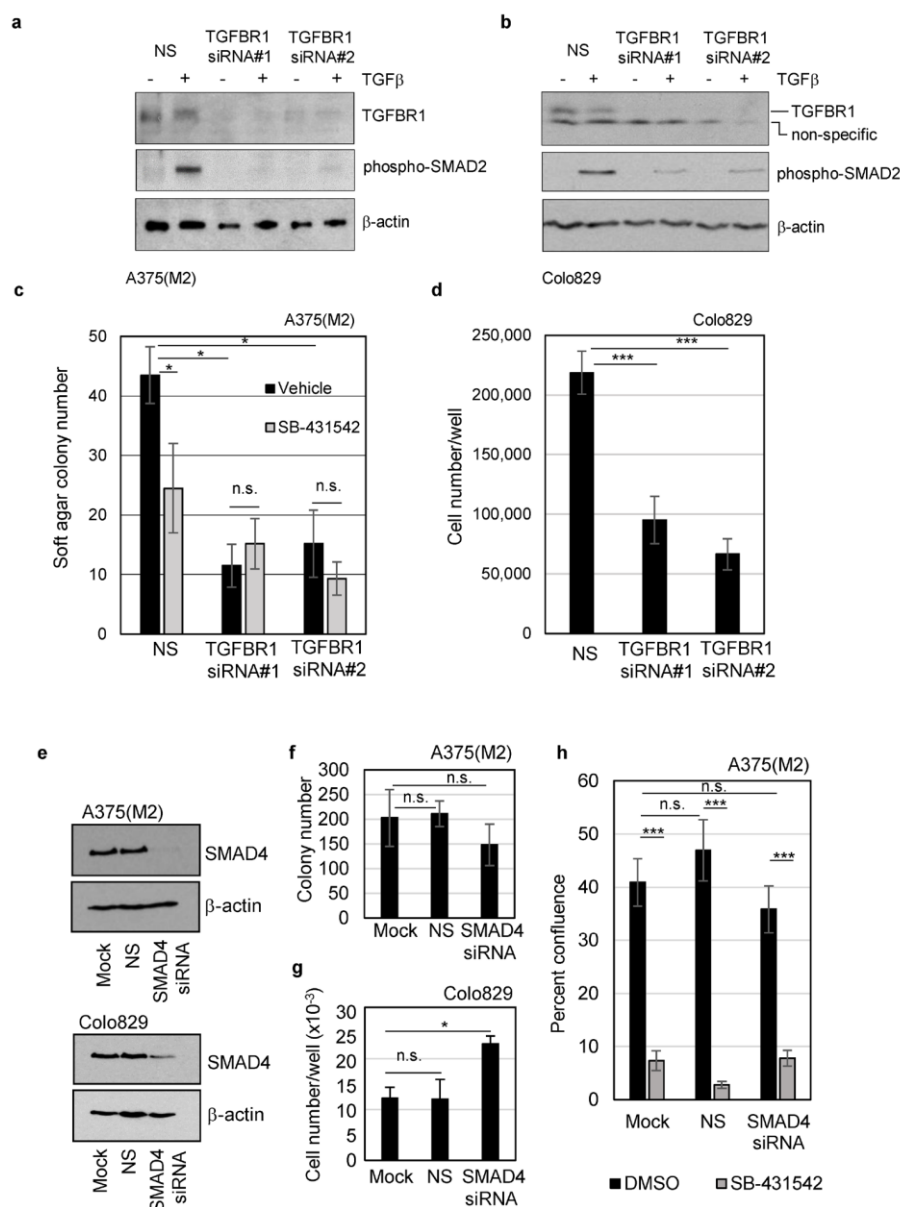
Figure 3: TGFBR1, but not SMAD4, is required for clonogenicity of mutant BRAFV600E melanoma cells. A375(M2) **a., c.** and Colo829 **b., d.** cells were transiently transfected with a non-silencing control siRNA (NS) or two independent siRNAs targeting *TGFBR1* (#1 and #2). **a., b.** Western blot analysis of lysates from untreated or TGFβ treated cells (2 hours) were included to confirm a reduction in TGFBR1 expression and decreased signaling *via* phospho-SMAD2 following TGFBR1 knockdown. **c.** A375(M2) knockdown cells were seeded into soft agar assays in the presence of either vehicle control (DMSO, 0.1%) or SB-431542 (10μM). Mean colony numbers (± SD) are given and significant [(*) $p < 0.05$] and non-significant (n.s.) changes in colony number determined by Student's TTEST are indicated. **d.** Colo829 cells transfected for 48 hours with non-silencing, or TGFBR1 siRNA in triplicate were seeded in 6-well plates. Cells were fed by 50% media replacement every 2 days and cell proliferation determined after 11 days. Mean (± SD) cell number is given and analysed for statistical significance by Student's TTEST compared to the non-silencing control. **e.** A375(M2) and Colo829 cells were transiently transfected with a non-silencing control siRNA (NS) or smartpool siRNA targeting SMAD4. Cell lysates were analysed by SDS-PAGE and western blotting for knockdown levels (f, g) Colony formation **f.** or cell proliferation **g.** was determined following SMAD4 knockdown in A375(M2) and Colo829 cells, respectively. Statistical analysis was performed using Students TTEST and n.s indicates non-significant and * indicates $p < 0.05$. **h.** A375(M2) cells were transiently transfected with smartpool siRNA targeting SMAD4, treated with either vehicle control (DMSO, 0.1%) or SB-431542 (10μM) and assayed by live cell imaging for drug sensitivity. Data shown are the means ± SEM percent confluence of 9 wells (4 fields/well) from a representative experiment. Statistical analysis was performed using Students TTEST and n.s indicates non-significant and *** indicates $p < 0.001$.

We next considered any non-canonical signaling pathways that might be affected by TGFβ signaling in melanoma cells. We previously reported that a noncanonical TGFβ/TGFBR1/RHOA signaling pathway is necessary for initiation and maintenance of rodent fibroblast BRAFV600E transformed cultures (31). Thus, in mutant BRAF human melanoma cells, it seemed plausible that this pathway could be involved in regulating melanoma cell clonogenicity. SB-431542 treatment reduced levels of active-GTP bound RHOA (Supplementary Figure 4c), while transfection of melanoma cells with the exoenzyme C3 transferase to inhibit RHOA (32) mimicked the effect SB-431542 (Supplementary Figure 4d).

In addition, overexpression of either constitutively active RHOA, or the constitutively active RHOA specific guanine nucleotide exchange factors Δ558LARG or onco-LBC (to activate endogenous RHOA) (33), blocked the effect of the TGFBR1 inhibitor on colony formation (Supplementary Figure 4e). These data are consistent with our previous findings in rodent fibroblasts.

To gain further insight into the cellular pathways involved in the inhibition of colony formation, we analysed cells by microscopy for division and apoptosis, using BRDU incorporation or fluorogenic apoptosis reagents respectively. Initial experiments revealed that SB-431542 treatment significantly reduced BRDU incorporation but induced little apoptosis (Supplementary Figure 5a and data not shown). We questioned whether an apparently modest reduction in BRDU incorporation was sufficient to account for the dramatic reduction in colony formation and cell proliferation.

To investigate in more detail, we generated A375(M2) cell lines stably transfected with an H2B-red fluorescent protein (RFP) fusion protein expression construct to enable kinetic single cell tracking using IncuCyte imaging. Imaging between days four and six of treatment (Supplementary Figure 5b) showed a reduction in their number, and a significant increase in the length of time cells remained in interphase (Supplementary Figure 5c). There were slight increases in the mean number of cells that failed to enter into mitosis or detached upon treatment, but these differences did not reach statistical significance (Supplementary Figure 5d and 5e). TGFBR1 inhibition, therefore, predominantly affects the proportion of cells in S-phase, and significantly affects the clonogenic potential of BRAF mutant cells through effects on the cell cycle.

BRAF inhibitor resistance

The addiction of mutant BRAF melanoma cells to signaling through TGFBR1 suggests a potential novel therapeutic approach for mutant BRAF-driven cancers. Ideally, not only would a novel treatment be effective as a single agent without evidence of refractory disease (Figure 1), but the novel therapeutic drug would act in combination with existing therapies to enhance their efficacy or prevent the development of resistance.

The current therapeutic modality for mutant BRAF metastatic melanoma is treatment with BRAF inhibitors vemurafenib or dabrafenib in combination with MEK inhibitors for suitable patients. However, the development of BRAF inhibitor-resistant disease through a variety of different mechanisms, including the paradoxical activation of the MAPK pathway, remains a significant clinical problem.
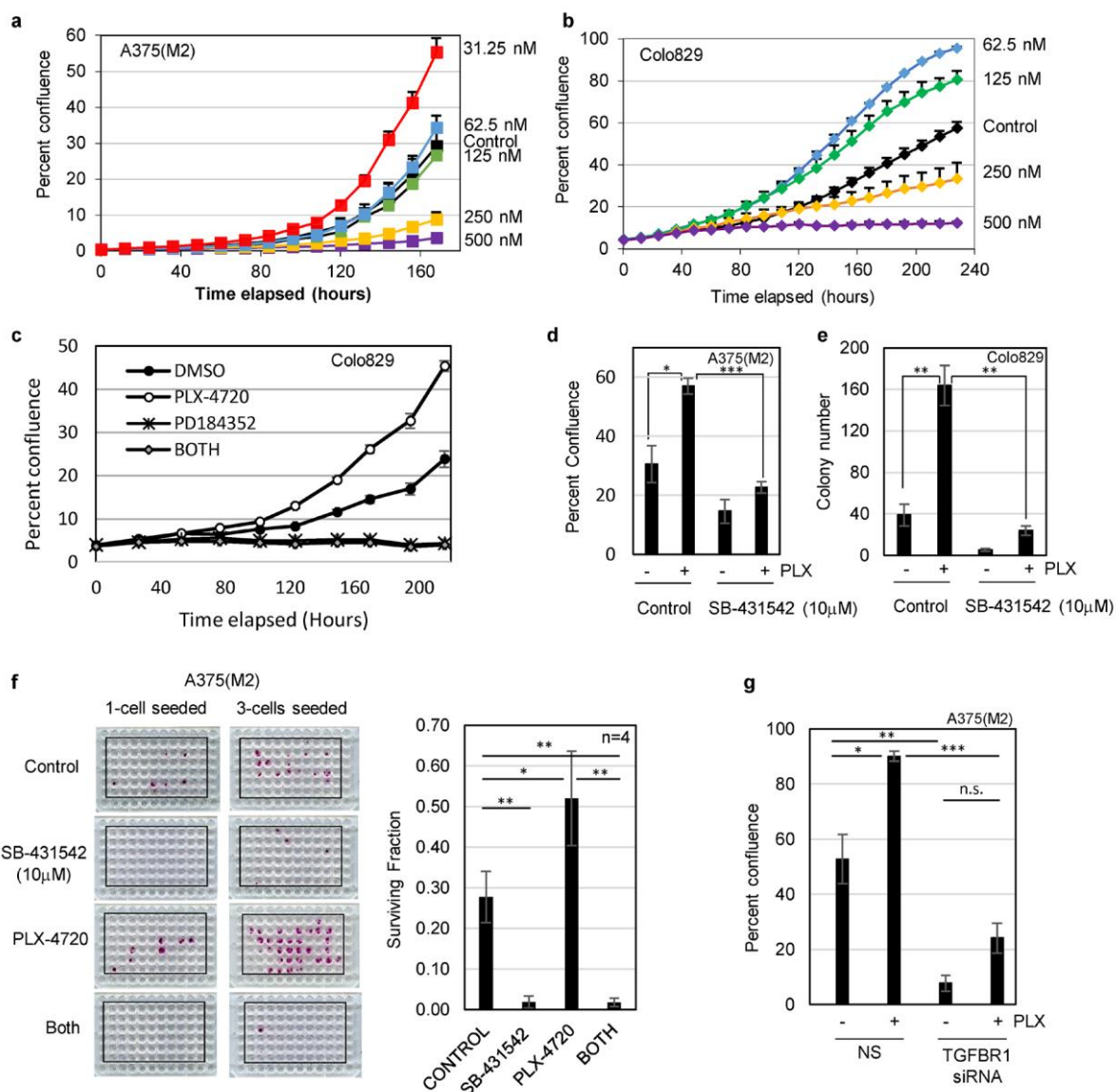
Figure 4: Low dose BRAF inhibitor (PLX-4720) enhances proliferation of drug naïve melanoma cells. a., **b.** Cell proliferation assays were carried out by live cell imaging (IncuCyte Zoom). Colo829 (1500 cells/well of 96-well pate) and A375(M2) cells (100 cells/well of 96-well plate) were seeded overnight and treated with PLX-4720 at the concentrations indicated. The mean percent confluence (± SEM) from 8 fields (Colo829) and 9 fields (A375M2) from a representative experiment is shown. **c.** Colo829 cells were treated with solvent control (DMSO, 0.1%), PLX-4720 (62.5nM), the MEK inhibitor PD184352 (2µM) or PLX-4720 + PD184352 (BOTH) and cell proliferation analysed by live cell imaging. The mean percent confluence (± SEM) from 24 fields across 6 wells in a representative experiment is shown. **d.** A375(M2) cells were assayed for cell proliferation for 8 days following treatment with inhibitors of both mutant BRAF (PLX-4720, 31.25 nM) and TGFBR1 (SB-431542, 10µM). Statistical analysis was performed using Students TTEST and $* = p < 0.05$ and $*** = p < 0.001$. **e.** Colo829 cells (40000/10cm dish) were seeded overnight prior to treatment with solvent control (DMSO, 0.1%), PLX-4720 (62.5nM), SB-431542 (10µM) or PLX-4720 + SB-431542. Cells were fed by 50% media replacement every 3 days and colonies were fixed, stained and counted at day 16. Statistical analysis was performed using Students TTEST and $* = p < 0.05$ and $** = p < 0.01$. **f.** Clonogenicity assays with A375(M2) cells seeded at 1 and 3 cells/well were carried out with vehicle control, SB-431542 (10µM), PLX- 4720 (31.25nM) or both drugs (BOTH) for 14 days. Representative plates stained with SRB are shown (left panel). The mean surviving fraction of colonies (± SD) (right panel) was determined (as described in the methods section) from plates seeded with both 1 and 3 cells/ well from independent replicate experiments ($n = 4$). Statistical analysis was performed using Students TTEST and $* = p < 0.05$ and $** = p < 0.01$. **g.** A375(M2) cells were assayed for cell proliferation following transfection with non-silencing (NS) siRNA or siRNA targeting TGFBR1 followed by treatment with PLX-4720 (31.25nM). Statistical analysis was performed using Students TTEST and $* = p < 0.05$, $** = p < 0.01$, $*** = p < 0.001$ and n.s = not significant.

Targeting TGFβ signaling to improve drug-resistant melanoma treatment

To assess the potential for a combination therapy targeting both BRAF and TGFBR1, we first tested the sensitivity of previously drug naïve A375(M2) and Colo829 to the mutant BRAF kinase inhibitor PLX-4720 in our clonogenic, low density assay conditions. As expected, at doses exceeding 250nM, growth of both cell lines was inhibited, however, at lower doses, we noted an unexpected significant increase in cell proliferation (Figures 4a, 4b and Supplementary Figure 6a). Suboptimal doses of PLX-4720 induced phosphorylation of ERK (Supplementary Figure 6b), and the enhanced proliferation of Colo829 (Figure 4c) and A375(M2) cells (data not shown) were abrogated by co-treatment with the MEK inhibitor PD184352 (Figure 4c).

These data are consistent with low dose PLX-4720 paradoxically activating the RAS-MAPK pathway. Since both cell lines carry BRAFV600E and are wild type for RAS, the most likely interpretation is that low dose PLX-4720 relieves an inhibitory autophosphorylation (34). Consistent with this hypothesis, low dose PLX-4720 did not promote the proliferation of three melanoma cell lines carrying wild type RAF/RAS (Supplementary Figure 7).

Importantly cotreatment of PLX-4720 treated mutant BRAF cells with SB-431542 (10μM) abolished the increase in cell growth caused by low dose PLX-4720 (Figure 4d and 4e). We quantified the effect on clonogenicity (35) and showed that not only did SB-431542 significantly reduce clonogenicity as a single agent, but that the significant increase in clonogenicity induced by PLX-4720 alone was reversed by SB-431542 (Figure 4f and Supplementary Figure 6c). This result was recapitulated by siRNA knockdown of TGFBR1 (Figure 4g).

To investigate further the potential for TGFBR1 inhibitors to prevent vemurafenib resistance, we tested both in vitro derived resistant lines (A375R), and patient derived vemurafenib-resistant recurrent tumor cells for sensitivity to SB-431542 (10μM). Patients #2 and #35 (stage IV) achieved a partial response having received vemurafenib for 3 months. Patient #5 (stage IV) had progressive disease and received vemurafenib for 2 months (Supplementary Table 1). The growth of vemurafenibnaïve A375 (Figure 5a) and patient tumor derived cells (Patient#1) (Figure 5b) (18) were both inhibited by SB-431542.

Importantly, in vitro derived PLX-4720 resistant A375R cells (cultured in the presence of 1μM PLX-4720) were growth inhibited by SB-431542 (Figure 5a). The patient-derived vemurafenib resistant cells had readily detectable levels of phosphorylated SMAD2 that were reduced on SB-431542 treatment, indicating that they all had active autocrine TGFβ signaling (Figure 5c).

In addition, all vemurafenib-resistant lines derived from patients were growth inhibited by SB-431542 in proliferation assays (Figure 5d) and in longer term colony formation assays (Figure 5e). Vemurafenib resistant cells therefore retain their sensitivity to inhibitors of the TGFβ signaling pathway.
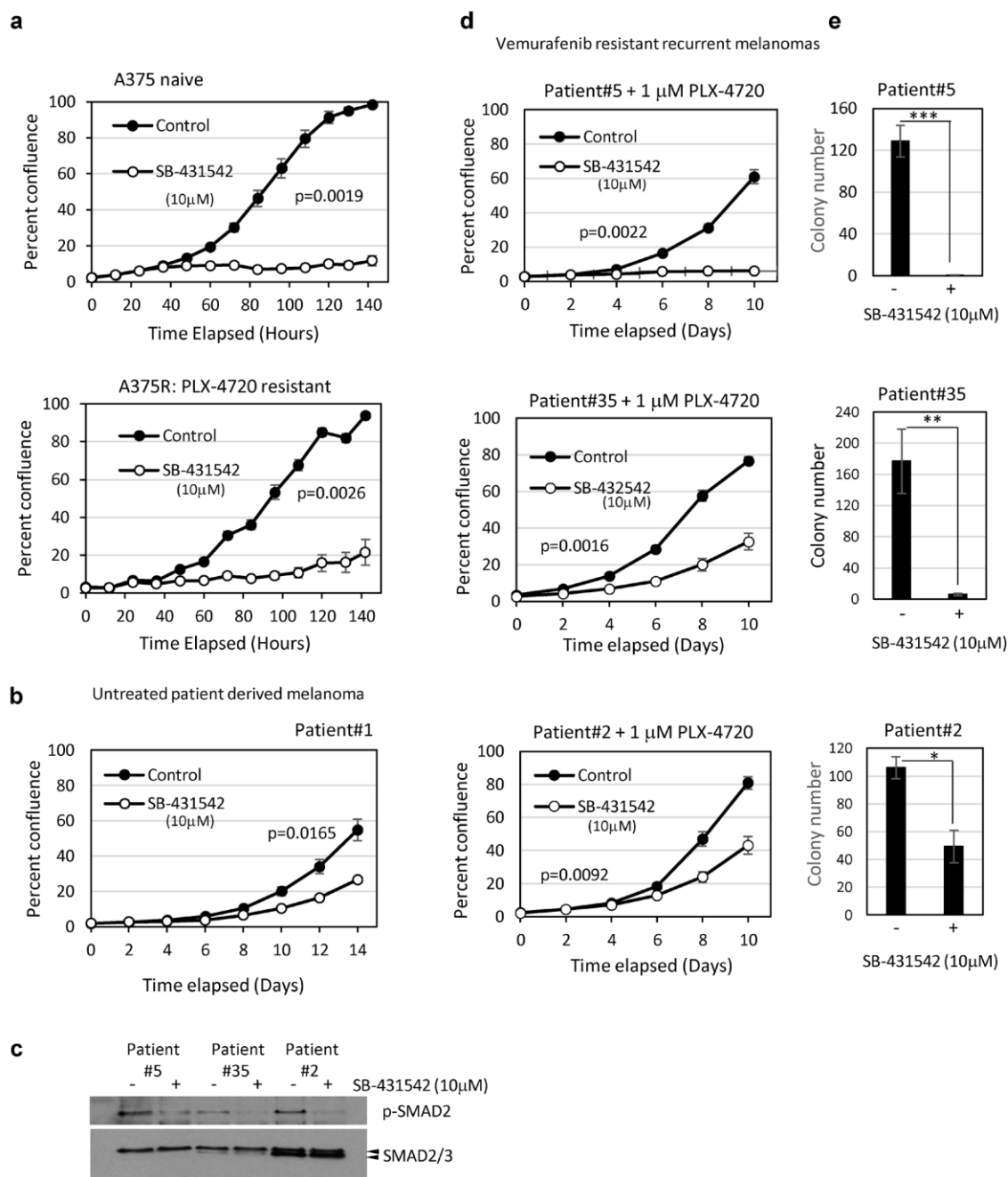
Figure 5: Patient-derived BRAF inhibitor resistant tumor cells are sensitive to TGFBR1 inhibition. a., b., d. Cells seeded at 500 - 800/well in 96-well plates were assayed for proliferation in the presence of solvent control (DMS0, 0.1%) or SB-431542 (10μM). A375 cells and the PLX-4720 resistant derivative A375R **a.**, patient-derived drug naïve **b.**, and vemurafenib resistant patient tumor derived cell lines **c.**, **d.** were tested. Vemurafenib resistant patient-derived recurrent tumor cells shown in **d.** were routinely cultured in the presence of 1μM PLX-4720. Data is presented as the mean percent confluence (± SEM) from 6 replicate wells, 4 fields/well from representative experiments. Statistical analysis was performed using compareGrowthCurves (Statmod). **c.** Lysates from vemurafenib resistant patient-derived recurrent tumor cells were assayed by western blot for constitutive TGFβ signaling and the response to TGFBR1 inhibition (4 hours, 10μM SB-431542). Phosphorylation of SMAD2 was used as a marker of TGFβ activity. **e.** Vemurafenib resistant recurrent melanoma patient cell lines were seeded in 10cm dishes at 1000 cells (Patient#35, $n = 4$), 16,000 cells (Patient 5, $n = 4$) and 1000 cells (Patient#2, $n = 3$) per dish and treated with solvent control or SB-431542 (10μM). Colonies were stained, counted and the mean colony number ± SD presented. Statistical analysis was carried out by Student TTEST, $* = p < 0.05$, $*** = p < 0.001$.

Several reports indicate that the development of resistance to BRAF kinase inhibitors may be associated with signaling through SRC-family kinases, and that resistance can be overcome by inhibition of SRC activity (17-19, 36). We therefore tested whether TGFβ signaling was associated with SRC phosphorylation in A375(M2) and Colo829 cells (Figure 6). We noted that phosphorylated-SRC levels increased during the five-day incubation period in cells initially plated at low density. SB-431542 (10μM) (Figure 6a) and TGFBR1 siRNA (Figure 6b) prevented any accumulation of phosphorylated SRC during the time course, and SB-431542 blocked an increase in phospho-SRC levels induced by low-dose PLX-4720 in A375(M2) cells (Figure 6a). An important implication of these data is that inhibition of TGFBR1 signaling may restrict signaling through a known mediator of vemurafenib resistance.
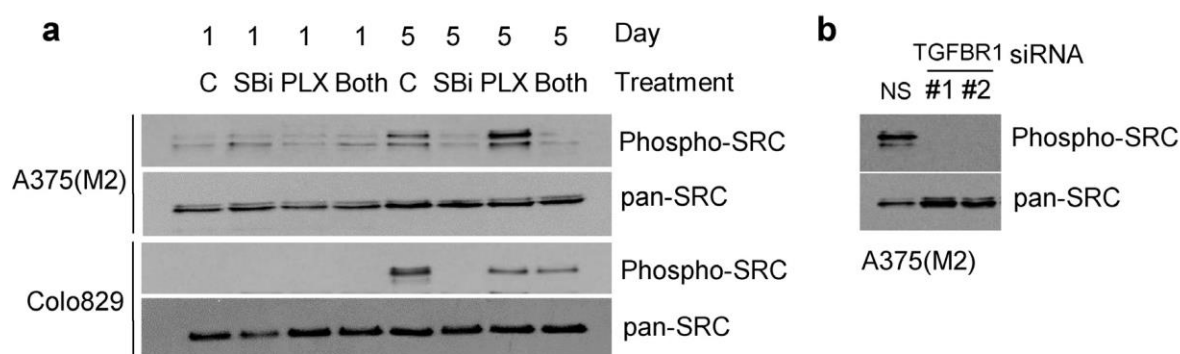

Figure 6: SB-431542 treatment and TGFBR1 knockdown inhibit phosphorylation of SRC. a. A375(M2) and Colo829 cells were seeded at low density in 10cm dishes in the presence of SB-431542 (SBi) (10μM) and/or PLX-4720 (62.5nM and 31.25nM for A375(M2) and Colo829 cells respectively). Samples treated with both SB-431542 and PLX-4720 are labelled (Both). At Day 1 and Day 5, cells were harvested and analysed by SDS-PAGE and western blotting using the antibodies indicated. **b.** A375(M2) cells were transfected with non-silencing siRNA or siRNAs (#1 and #2) targeting TGFBR1. Cells were seeded at low cell density and after five days harvested for SDS-PAGE analysis and western blotting for the proteins indicated.

Zebrafish embryo xenograft metastasis model

So far, our murine xenograft assays, and inhibition of clonogenic potential of melanoma cells in low cell density 3D and 2D culture systems, suggest that TGFBR1 inhibitors would be effective in preventing establishment of disease. To further examine whether TGFBR1 inhibitors could effectively treat established cell cultures, we seeded cells at low cell density and progressively delayed addition of drug throughout the lag phase of cell growth. SB-431542 was effective if administered during the lag phase, but delaying treatment until the cells start to exit the lag phase considerably reduced its efficacy (Supplementary Figure 8a). Similarly, seeding cells at higher cell numbers also reduced the efficacy of SB-431542 in both vemurafenib naïve and resistant cells (Supplementary Figure 8b). Given these observations, we posit that cell:cell contact and/or allowing the secretion of growth factors or matrix components has a protective effect against TGFBR1 inhibitors; the implication is that TGFBR1 inhibitors might not be useful as first line, single agents or as debulking therapeutic agents in established solid tumors. Nevertheless, the dependence of melanoma cells on TGFBR1 for clonogenicity suggests that TGFBR1 inhibitors could be effective in preventing spread or outgrowth of micrometastases. To test this hypothesis we used a zebrafish embryo metastasis model (37, 38) to visualise and quantify numbers of invasive melanoma cells. This

model has been used successfully to examine the effect of SB-431542 on breast cancer cell invasion [39]. We generated stable TGFBR1 knockdown A375(M2) cell lines using LMP-TGFBR1 shRNA plasmids, which had reduced TGFBR1 protein expression and reduced capacity to signal (Figure 7a) as well as reduced ability to form colonies on plastic (Figure 7b). The stable lines were labelled with the mCherry fluorophore, injected into the Duct of Cuvier (DoC) of zebrafish embryos and the numbers of invasive cells in the avascular tail fins were analysed. Representative con-focal images of metastatic spread into the tail fin are shown in Figure 7c. Control non-silencing (NS) A375(M2) cells were capable of metastatic spread into the fish fin (arrows indicate micrometastases). Using doses of 1μM SB-431542 (SBi), we observed a significant decrease in the ability of SB-431542 treated NS cells to invade. Stable TGFBR1 knockdown also reduced colonisation of zebrafish tissue (Figure 7d). Our data overall suggest that TGFBR1 inhibitors would reduce the metastatic burden in BRAF mutant melanoma by preventing invasion and/or outgrowth of metastatic colonies.
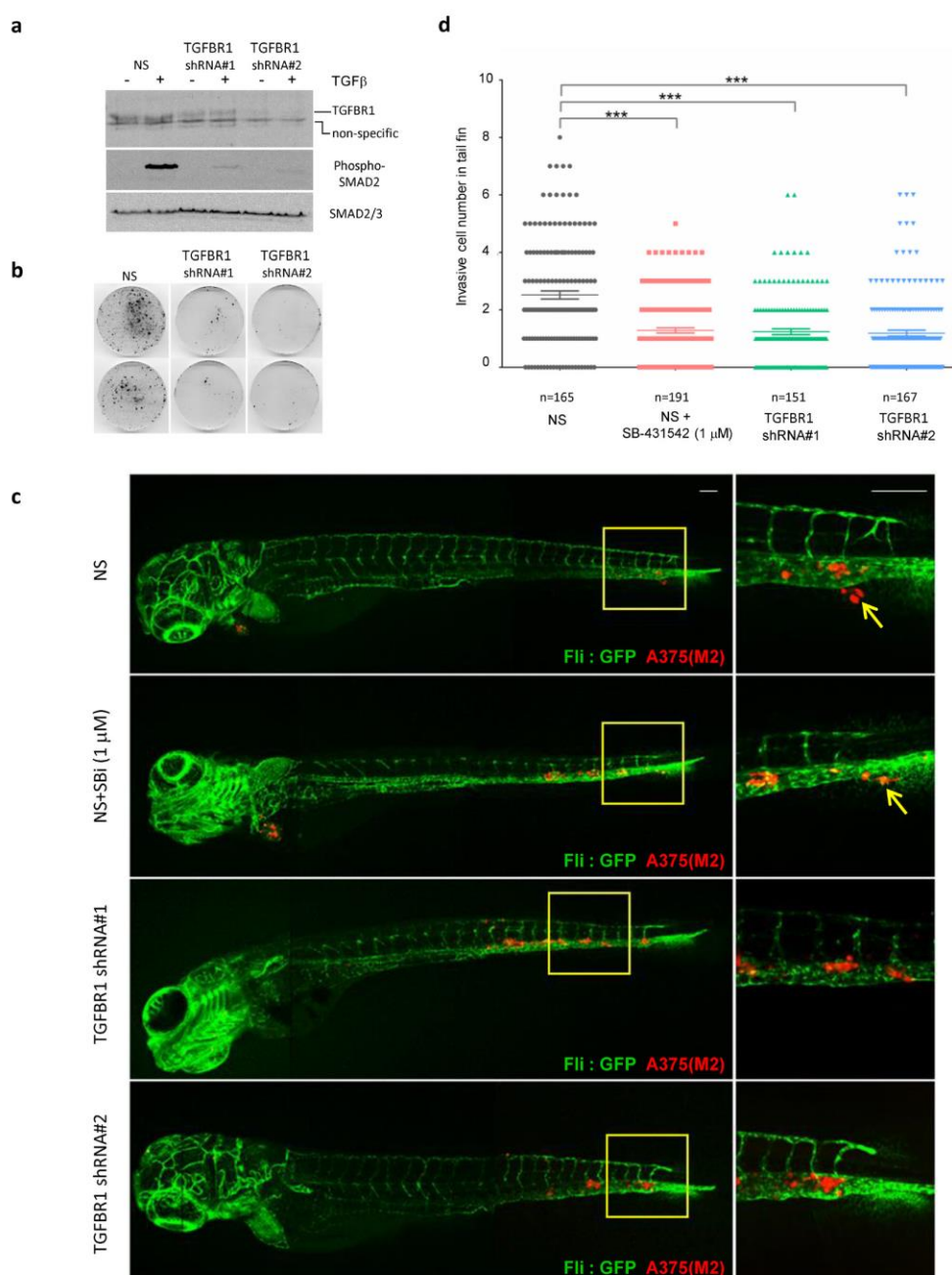
Figure 7: TGFBR1 is required for tumor cell metastasis in xenografted zebrafish. a., b. A375(M2) cells stably transfected with a non-silencing shRNA control plasmid or two independent shRNA vectors targeting TGFBR1 were assessed by western blotting for a reduction in TGFBR1 expression and signaling in response to exogenous TGFβ addition **a.** and colony formation **b.**. **c.** Cells described in **a.** were labelled with mCherry and implanted into the Duct of Cuvier of zebrafish at 2 days post-fertilization (dpf). SB-431542 (1μM) was added to the egg water of the non-silencing (NS) + SB-431542 group. Confocal images were taken at 4 days post implantation (dpi). Arrows indicate invasive tumor cells, scale bar: 100 μm. **d.** Invasive cell numbers in tail fin of each zebrafish in each group. Statistical analysis was performed using one-way analysis of variance (ANOVA) followed by the Tukey's method for multiple comparison *** $p < 0.001$. Data are combined from four independent experiments and the total number of embryos (n) in each group is indicated.

DISCUSSION

The outcome for patients with advanced melanoma has improved dramatically in recent years. The development of targeted therapy of the MAPK pathway, and advances in immunotherapy have resulted in improvements in median survival from 9 months to 25-31 months. However, long-term prognosis remains uncertain. For targeted therapy using BRAFi, drug resistance mechanisms identified to date are numerous, and there is no established effective second-line targeted therapy for patients progressing on combination BRAFi + MEKi. Often, drug-resistance mechanisms involve induction of either an autocrine, or a paracrine, drug-induced secretome which helps to promote expansion and dissemination of the drug-resistant cells (15) and/or protect potentially sensitive tumor cells from the inhibitory effects of the chemotherapeutic agent (15, 19, 21). Phosphorylated ERK and SRC are frequently elevated in resistant tumors (18) suggesting that paradoxical activation of the MAPK pathway and growth factor signaling are involved in resistance development. In this study we investigated the potential of targeting TGFβ1 as second-line therapy for advanced melanoma.

We found that autocrine TGFβ signaling through TGFBR1 is an intrinsic requirement for the clonogenic potential of mutant BRAF transformed cells, indicating that mutation of BRAF may be useful as a biomarker for TGFβ tumor promoting activity in melanoma. Although TGFβ levels are elevated post-vemurafenib treatment (20, 21), our data suggest that a TGFβ/TGFBR1-dependent state is an adaptation to the presence of mutant BRAF. Thus, with pro-tumorigenic autocrine TGFβ signaling pathways having already been established, elevated levels of signaling during therapy are perhaps more readily selected for than would otherwise be the case. How the initial switch from tumor suppressor to tumor promoter function of TGFβ in melanocytes is mediated by mutant BRAF remains to be determined.

Our in vitro assays were specifically designed to mimic conditions of cellular stress (i.e. low density 2D and anchorage independent colony formation assays) to more accurately assess the clonogenic potential of melanoma cells and their cancer stem-cell like properties. TGFBR1 inhibition was highly effective in inhibiting growth of both naïve and vemurafenib-resistant cells when administered during the lag phase of growth; less so when cell seeding numbers were increased. The implication of these data is that targeting TGFβ/TGFBR1 may not be an effective therapeutic strategy in established tumors. A secondary consideration is that TGFBR1 inhibition affected proliferation of the tumor cells without inducing apoptosis, and so may not result in significant tumor shrinkage. As a consequence, we predicted that inhibiting TGFβ/TGFBR1 signaling would more likely be effective in preventing tumor metastasis and outgrowth of micrometastasis, rather than reducing established tumor burden.

Indeed, our murine and zebrafish xenograft models show that targeting autocrine TGFβ secretion and TGFBR1 kinase activity inhibits xenograft tumor establishment in mice and prevents metastatic spread in zebrafish tissues. TGFBR1 inhibitors therefore may have potential as an adjuvant therapy in high risk, resected disease, or a maintenance therapy in patients responding to BRAF inhibitors. The inhibition of glioblastoma cancer initiating (stem) cells by TGFBR1 inhibitors (40, 41) is consistent with our data, and provides support for our conclusion that TGFBR1 activity is required for melanoma stem-cell like properties.

Given the vast number of context specific genes regulated by TGFβ, it is likely that a number of different downstream effectors will mediate the autocrine TGFβ-induced promotion of melanoma cell growth and drug-resistance. We showed that although melanoma cells rely on TGFBR1 kinase activity, they do not require SMAD4 for either colony formation, or for the response to TGFBR1 inhibition. Signaling via RHOA, however, rescued the effect of SB-431542 which is both consistent with our previous analysis of rodent fibroblast transformation (31), and with a role for TGFβ-activated non-canonical signaling pathways in this response. The establishment of an adaptive autocrine TGFβ/TGFBR1 signaling pathway through RHOA following BRAF mutation may be necessary to overcome CDKN1A expression and growth arrest induced as a response to oncogenic stress (31, 42). Consistent with this are our data showing CDKN1A induction by disrupting TGFβ signaling both in vitro and in vivo (Figure 2 and Supplementary Figure S2). Interestingly, inhibition of ROCK (using Y27632), a downstream target of RHOA signaling, also induces CDKN1A in melanoma (43), and ROCK1 has been identified as a potential candidate for combinatorial therapy with BRAF inhibitors. In these studies inhibition of ROCK1 sensitises melanoma cells to PLX-4720 (44). Our data now suggest that the involvement of ROCK1 in resistance mechanisms is potentially a result of TGFβ/TGFBR1/RHOA signaling. Although the SMAD-dependent induction of RHO GEFs has been described in other studies, (45, 46) how TGFBR1 directly activates RHOA in melanoma cells in a SMAD independent manner is unclear at present.

Several other TGFβ target genes have been implicated in melanoma biological responses. Melanoma cells exposed to the high levels of exogenous TGFβ present in bone, upregulate osteolytic genes (including IL-11, PTHrP, and CTGF) which may aid more effective colonisation of this metastatic niche. Blocking receptor function by over-expression of the natural inhibitor SMAD7 extended survival of mice xenografted with SMAD7 expressing melanoma cells. However, a causal role for the TGFβ-regulated osteolytic genes in bone metastasis was not directly demonstrated (26). Similarly, the balance between the TGFβ target gene GLI2 and the melanocyte specific isoform of MITF (M-MITF) appears important for invasion through matrigel in vitro, with high GLI-2/low M-MITF correlating with invasion. However, these expression profiles were independent of BRAF mutation status and did not correlate with either proliferation in vitro or with subcutaneous xenograft tumor establishment (47). We suspect that TGFβ target genes induced by exogenous TGFβ exposure may be quite different from those genes regulated by non-canonical signaling as a result of autocrine TGFβ 'addiction' established following BRAF mutation. Further work to identify which are the key TGFβ target genes involved in both promoting these stem-cell properties, and in driving drug-resistance, is underway and we expect that these studies will suggest novel, selective therapeutic targets.

Targeting TGFβ signaling to improve drug-resistant melanoma treatment

We show that drug-naïve melanoma cells are growth promoted by low-dose PLX-4720, likely by paradoxical activation of the MAPK pathway. This may have important implications clinically, since low doses of bioavailable BRAFi reaching some tumor tissue could actually potentiate tumor growth. Importantly, we show that both paradoxically activated, previously drug naïve cells, as well as vemurafenib resistant cells, retain sensitivity to TGFBR1 inhibitors. In addition, SB-431542 prevented phosphorylation of SRC which is frequently associated with vemurafenib resistance, suggesting that TGFBR1 inhibitors would prevent relapse with vemurafenib-resistant metastases. How SB-431542 regulates SRC activation is currently under investigation in our laboratory. It will be important to test the sensitivity of BRAFi/MEKi resistant cells derived from patients treated with combination therapy when established. Nevertheless, we predict that targeting an independent signaling pathway may have some advantages over combination therapies which target different components of the same signaling pathway. In addition, blocking the immunosuppressive effects of TGFβ could potentiate the efficacy of immune based therapeutics. Since dependence on TGFβ signaling appears to be universal in mutant BRAF melanoma cells, targeting TGFβ or downstream effectors may also provide useful therapeutic options for blocking metastatic outgrowth of vemurafenib refractory disease which occurs in approximately 20% of patients receiving treatment. There are currently a number of TGFβ pathway inhibitors progressing through Phase 1-3 clinical trials (48). The small molecule TGFBR1 inhibitor Galunisertib is being evaluated in cancer patients with unmet need. This inhibitor is deemed tolerable, with an acceptable margin of safety when administered using intermittent dosing regimens (49), demonstrating that TGFBR1 inhibitors are suitable for clinical use and may provide new opportunities for therapy of BRAF-inhibitor resistant cancer.

MATERIALS AND METHODS

Western blotting

Cell lysates were analysed by SDS-PAGE using the following antibodies: PO4-SMAD2 (Ser465/467) (rabbit polyclonal, #3101, Cell Signaling Technology [CST]), SMAD2 (mouse monoclonal, C16D3, CST), SMAD2/3 (mouse monoclonal, Clone 18, BD transduction Laboratories), SMAD4 (mouse monoclonal, B-8, Santa Cruz Biotechnology), TGFBR1 (rabbit polyclonal, V-22, Santa Cruz Biotechnology), CDKN1A (rabbit polyclonal, C19, Santa Cruz Biotechnology), RHOA (mouse monoclonal, 26C4, Santa Cruz Biotechnology), PO4-SRC (Tyr416) (rabbit monoclonal, D49G4, CST), SRC (rabbit monoclonal, 36D10, CST), PO4-p44/p42 MAPK (ERK1/2) (Thr202/Tyr404) (rabbit polyclonal, #9101, CST), p44/p42 MAPK (ERK1/2) (rabbit polyclonal, #9102, CST), β-actin (mouse monoclonal, AC-74, Sigma). Secondary HRP-conjugated antibodies (Dako) and enhanced chemiluminescence (GE Healthcare) was used to detect bound antibody.

Cell culture

Details of the cell lines and media supplements used are shown in Supplementary Table S1. All cells lines were tested regularly for mycoplasma contamination by the Institute's mycoplasma testing service. Patient derived cell lines were passaged for approximately 1 month. Where indicated the cells were transfected with Lipofectamine or Lipofectamine 2000 (Invitrogen) using the following plasmids; pRK5 C3-transferase and pEF-Flag LARG Δ558

(kind gifts of R. Grosse), pRK5-RhoA V14 (kindly supplied by Alan Hall), pSR-Flag onco LBC (kindly supplied by Mike Olson), or pSuper-TGFβ1. LMP scrambled non-silencing (NS) and LMP-TGFBR1 shRNA constructs were generated in house with the following hairpin sequences:

NS - 5' CGAGAAGGTATATTGCTGTTGACAGTGAGCGACT
CATAGCGATGTGAACTCAATAGTGAAGCCACAGA
TGTATTGAGTTCACATCGCTATGAGCTGCCTACTG CCTCGG -3';

TGFBR1#1 - 5'
TCGAGAAGGTATATTGCTGTTGACAGTGAGCGACTCATAGAGATTTGAAATCAATAGTGAAGCCA
CAGATGTATTGATTTCAAATCTCTATGAGCTGCCTACTGCCTCGG -3';

TGFBR1#2 - 5'
TCGAGAAGGTATATTGCTGTTGACAGTGAGCGACAGTGTAATAAAGTCAATTAATAGTGAAGCCA
CAGATGTATTAATTGACTTTATTACACTGCTGCCTACTGCCTCGG. -3'.

Cells were transfected with either Oligofectamine or HiPerFect (Qiagen) to introduce, at a final concentration of 20 - -50nM, the following siRNA; allstars negative control, TGFBR1 [HS_TGFBR1_6 (TGFBR1#1) and HS_TGFBR1_7 (TGFBR1#2) (Qiagen)] or SMAD4 (Dharmacon smartpool). Mock transfections (no siRNA) were included in each experiment. A375(M2) pSuper or pSuper-TGFβ1 stable cell lines were selected and maintained in 0.6mg/mL puromycin. A375(M2) histone H2B-RFP stable cell lines were selected and maintained in 800μg/mL G418, and LMP-scrambled or LMP-TGFBR1 shRNA derivatives were maintained in 800μg/mL G418 plus 1μg/mL puromycin. Where indicated the cells were treated with SB-431542 (Tocris) (50), PLX-4720 (Selleck Chemicals) or PD184352 (Cell Signaling) (prepared in DMSO).

Soft agar assay

Soft agar assays were carried out essentially as previously described (31). Briefly, six well plates were coated in 2mLs of media supplemented with 0.9% low melting point agar (Invitrogen). 2mL cells (1x104/mL) in media supplemented with 0.45% low melting point agar were overlaid with either SB-431542 or vehicle control. Wells were fed twice weekly for 2-4 weeks, and the number of colonies (> 80μm in diameter) in nine fields of view was scored using an Olympus CKX41 microscope, fitted with a 4X objective and an eyepiece graticule (250μm gradations). Statistical analyses were carried out by Students TTEST unless stated otherwise.

Proliferation assay

Cell proliferation kinetics were either monitored using an IncuCyte ZoomTM imaging system and software (percent confluence) (Essen Biosciences), or by trypsinisation and cell counts using a Casy cell-counter (model TT, Innovatis).

Colony formation and clonogenicity assays

Colony formation: Cells were seeded in 10cm dishes at an appropriate density to form approximately 250 discrete colonies after 2-3 weeks in culture. Colonies were fixed in methanol and stained with toluidine blue/borax solution for counting.

Clonogenicity: Cells were seeded overnight at 1 and 3 cells/well in 60 wells of a 96-well plate, prior to treatment. Wells were fed twice weekly, and wells examined by light

microscopy. After approximately two weeks, media was removed, colonies fixed in methanol and stained with 0.4% (w/v) sulforhodamineB (SRB)/1% acetic acid. Colonies > 50 cells in size were counted, and the plating efficiency and surviving fractions after drug treatment determined according to Franken et al [35].

TGFβ1 ELISA

The TGFβ1 assay has been described previously (31). Briefly, cells were cultured in media containing 0.1% FBS for 24 hours. Media was harvested and the cells trypsinized and counted. The media was acid treated to activate latent TGFβ, and TGFβ1 levels determined by ELISA using anti-TGFβ1 (MAB1835) (capture antibody) and biotinylated anti-TGFβ1 (BAF240) (detection antibody). Recombinant hTGFβ1 (Peprotech) was used as a standard. Results were expressed as TGFβ1 produced per 1x105 cells/hour.

Mouse xenografts

Nude mouse subcutaneous xenograft experiments were performed according to Home Office guidelines and were approved by the local research and ethics committee (BICRLREC). 1x106 cells were injected subcutaneously into the flank of CD1 nude mice (n = 8) (Charles Rivers). Palpable tumors were observed 8 days post-injection and tumor volumes were calculated using caliper measurement and the formula $V = (E2xA)/2$ where E =shortest and A = the longest diameter measurement.

Immunohistochemistry

Sections from formalin, paraffin embedded, pSuper (Control shRNA) or pSuper-TGFβ1 shRNA tumors were stained for CDKN1A (M19, Santa Cruz Biotechnology) using an Envision kit (Dako) according to the manufacturer's instructions. The sections were counter stained with Haemotoxylin and were scored for CDKN1A expression. One representative field of view (that contained a minimum of 350 cells) was scored (blind) for each tumor.

IncuCyte zoom and analysis

An IncuCyte Zoom live cell imaging microscope (Essen Biosciences) with 10x objective and data management software was used to monitor kinetic cell proliferation. The mean ± SEM percent confluence from four phase-contrast images/well, with a minimum of 3 replicate wells/treatment was determined according to software processing definitions as recommended by the manufacturer. Statistical analysis was carried out using Graphpad software and pairwise comparisons using the compareGrowthCurves function (statmod, R project, 10,000 permutations).

Embryo preparation and tumor cell implantation

Zebrafish and embryos were raised, staged and maintained according to standard procedures. The Institutional Committee for Animal Welfare of the Leiden University Medical Center (LUMC) approved this study. Tg(Fli1:GFP) zebrafish embryos were dechorionated at two days post-fertilisation (dpf). Single cell suspensions of melanoma cells were prepared in PBS and kept at 4°C before implantation. The cell suspension was loaded into borosilicate glass capillary needles (1 mm O.D. × 0.78 mm I.D.; Harvard Apparatus) and the injections were performed using a Pneumatic Picopump and a manipulator (World Precision Instruments, Stevenage, UK). Dechorionated embryos were anaesthetised with 0.003% 3-amino benzoic

acid ethyl ester [tricaine, (Sigma)] and mounted on 10 cm Petridishes coated with 1% agarose. Approximately 200 cells were injected at the duct of Cuvier (DoC). Implanted zebrafish embryos were maintained at 33°C. Zebrafish in the Non-Silencing (NS) + SB431542 group were treated with 1μM SB-431542 added to the eggwater. All implantations were repeated at least three times with at least 30 embryos per group.

Microscopy and analysis of zebrafish

Zebrafish embryos were fixed with 4% paraformaldehyde for two hours at room temperature. Embryos were imaged in PBS/0.1% Tween-20 (Merck, Amsterdam, Netherlands) using a Leica SP5 STED confocal microscope (Leica, Rijswijk, Netherlands). Confocal stacks were processed for maximum intensity projections with Image J. Images were adjusted for brightness and contrast, and overlays created using Adobe Photoshop CS6. Statistical analysis was performed using Prism 4 software (GraphPad, La Jolla, USA). Results are expressed as the mean ± SD. One-way analysis of variance (ANOVA) were performed followed by the Tukey's method for multiple comparison. $P < 0.05$ was considered to be statistically significant (*$0.01 < P < 0.05$; **$0.001< P < 0.01$; *** $P < 0.001$). In one experiment the results were scored blinded; all results were confirmed by an independent observer.

REFERENCES

1. Ferlay J, Soerjomataram I, Dikshit R, Eser S, Mathers C, Rebelo M, et al. Cancer incidence and mortality worldwide: sources, methods and major patterns in GLOBOCAN 2012. Int J Cancer. 2015;136:E359-86.
2. Davies H, Bignell GR, Cox C, Stephens P, Edkins S, Clegg S, et al. Mutations of the BRAF gene in human cancer. Nature. 2002; 417:949-54.
3. Sosman JA, Kim KB, Schuchter L, Gonzalez R, Pavlick AC, Weber JS, et al. Survival in BRAF V600-mutant advanced melanoma treated with vemurafenib. N Engl J Med 2012; 366:707-14.
4. Chapman PB, Hauschild A, Robert C, Haanen JB, Ascierto P, Larkin J, et al. Improved survival with vemurafenib in melanoma with BRAF V600E mutation. N Engl J Med 2011; 364:2507-16.
5. Flaherty KT, Puzanov I, Kim KB, Ribas A, McArthur GA, Sosman JA, et al. Inhibition of mutated, activated BRAF in metastatic melanoma. N Engl J Med 2010; 363:809-19.
6. Lito P, Rosen N and Solit DB. Tumor adaptation and resistance to RAF inhibitors. Nat Med. 2013; 19:1401-9.
7. Ribas A, Gonzalez R, Pavlick A, Hamid O, Gajewski TF, Daud A, et al. Combination of vemurafenib and cobimetinib in patients with advanced BRAF(V600)-mutated melanoma: a phase 1b study. Lancet Oncol. 2014; 15:954-65.
8. Long GV, Stroyakovskiy D, Gogas H, Levchenko E, de Braud F, Larkin J, et al. Combined BRAF and MEK inhibition versus BRAF inhibition alone in melanoma. N Engl J Med 2014; 371:1877-88.
9. Flaherty KT, Infante JR, Daud A, Gonzalez R, Kefford RF, Sosman J, et al. Combined BRAF and MEK inhibition in melanoma with BRAF V600 mutations. N Engl J Med 2012; 367:1694-703.
10. Moriceau G, Hugo W, Hong A, Shi H, Kong X, Yu CC, et al. Tunable-combinatorial mechanisms of acquired resistance limit the efficacy of BRAF/MEK cotargeting but result in melanoma drug addiction. Cancer Cell. 2015;27:240-56.
11. Wagle N, Van Allen EM, Treacy DJ, Frederick DT, Cooper ZA, Taylor-Weiner A, et al. MAP kinase pathway alterations in BRAF-mutant melanoma patients with acquired resistance to combined RAF/MEK inhibition. Cancer Discov. 2014; 4:61-8.
12. Hugo W, Shi H, Sun L, Piva M, Song C, Kong X, et al. Non-genomic and Immune Evolution of Melanoma Acquiring MAPKi Resistance. Cell. 2015; 162:1271-85.
13. Xing F, Persaud Y, Pratilas CA, Taylor BS, Janakiraman M, She QB, et al. Concurrent loss of the PTEN and RB1 tumor suppressors attenuates RAF dependence in melanomas harboring (V600E)BRAF. Oncogene. 2012; 31:446-57.
14. Turajlic S, Furney SJ, Stamp G, Rana S, Ricken G, Oduko Y, et al. Whole-genome sequencing reveals complex mechanisms of intrinsic resistance to BRAF inhibition. Ann Oncol. 2014; 25:959-67.
15. Obenauf AC, Zou Y, Ji AL, Vanharanta S, Shu W, Shi H, Kong X, Bosenberg MC, et al. Therapy-induced tumor secretomes promote resistance and tumor progression. Nature. 2015; 520:368-72.
16. Muller J, Krijgsman O, Tsoi J, Robert L, Hugo W, Song C, et al. Low MITF/AXL ratio predicts early resistance to multiple targeted drugs in melanoma. Nat Commun. 2014; 5:5712.
17. Girotti MR, Pedersen M, Sanchez-Laorden B, Viros A, Turajlic S, Niculescu-Duvaz D, et al. Inhibiting EGF receptor or SRC family kinase signaling overcomes BRAF inhibitor resistance in melanoma. Cancer Discov. 2013; 3:158-67.
18. Girotti MR, Lopes F, Preece N, Niculescu-Duvaz D, Zambon A, Davies L, et al. Paradox-breaking RAF inhibitors that also target SRC are effective in drug-resistant BRAF mutant melanoma. Cancer Cell. 2015; 27:85-96.
19. Hirata E, Girotti MR, Viros A, Hooper S, Spencer-Dene B, Matsuda M, et al. Intravital imaging reveals how BRAF inhibition generates drugtolerant microenvironments with high integrin β1/FAK signaling. Cancer Cell. 2015; 27:574-88.
20. Huang S, Holzel M, Knijnenburg T, Schlicker A, Roepman P, McDermott U, et al. MED12 controls the response to multiple cancer drugs through regulation of TGF-β receptor signaling. Cell. 2012; 151:937-50.

21. Sun C, Wang L, Huang S, Heynen GJ, Prahallad A, Robert C, et al. Reversible and adaptive resistance to BRAF(V600E) inhibition in melanoma. Nature. 2014; 508:118-22.

22. Derynck R and Zhang YE. Smad-dependent and Smad independent pathways in TGF-β family signalling. Nature. 2003; 425:577-84.

23. Reed JA, McNutt NS, Prieto VG and Albino AP. Expression of transforming growth factor-β 2 in malignant melanoma correlates with the depth of tumor invasion. Implications for tumor progression. Am J Pathol.1994; 145:97-104.

24. Lasfar A and Cohen-Solal KA. Resistance to transforming growth factor β-mediated tumor suppression in melanoma: are multiple mechanisms in place? Carcinogenesis. 2010; 31:1710-17.

25. Javelaud D, Alexaki VI and Mauviel A. Transforming growth factor-β in cutaneous melanoma. Pigment Cell Melanoma Res. 2008; 21:123-32.

26. Javelaud D, Mohammad KS, McKenna CR, Fournier P, Luciani F, Niewolna M, et al. Stable overexpression of Smad7 in human melanoma cells impairs bone metastasis. Cancer Res. 2007; 67:2317-24.

27. Javelaud D, van Kempen L, Alexaki VI, Le Scolan E, Luo K and Mauviel A. Efficient TGF-β/SMAD signaling in human melanoma cells associated with high c-SKI/SnoN expression. Mol Cancer. 2011; 10:2.

28. Lo RS and Witte ON. Transforming growth factor-β activation promotes genetic context-dependent invasion of immortalized melanocytes. Cancer Res. 2008; 68:4248-57.

29. Mohammad KS, Javelaud D, Fournier PG, Niewolna M, McKenna CR, Peng XH, et al. TGF-β-RI kinase inhibitor SD-208 reduces the development and progression of melanoma bone metastases. Cancer Res. 2011; 71:175-84.

30. Berking C, Takemoto R, Schaider H, Showe L, Satyamoorthy K, Robbins P et al. Transforming growth factor-β1 increases survival of human melanoma through stroma remodeling. Cancer Res. 2001; 61:8306-16.

31. Fleming YM, Ferguson GJ, Spender LC, Larsson J, Karlsson S, Ozanne BW, et al. TGFβ-mediated activation of RhoA signalling is required for efficient (V12)HaRas and (V600E)BRAF transformation. Oncogene. 2009; 28:983-93.

32. Morii N, Teru-uchi T, Tominaga T, Kumagai N, Kozaki S, Ushikubi F et al. A rho gene product in human blood platelets. II. Effects of the ADP-ribosylation by botulinum C3 ADP-ribosyltransferase on platelet aggregation. J Biol Chem 1992; 267:20921-6.

33. Zheng Y, Olson MF, Hall A, Cerione RA and Toksoz D. Direct involvement of the small GTP-binding protein Rho in lbc oncogene function. J Biol Chem. 1995; 270:9031-4.

34. Holderfield M, Merritt H, Chan J, Wallroth M, Tandeske L, Zhai H, et al. RAF inhibitors activate the MAPK pathway by relieving inhibitory autophosphorylation. Cancer Cell. 2013; 23:594-602.

35. Franken NA, Rodermond HM, Stap J, Haveman J and van Bree C. Clonogenic assay of cells in vitro. Nat Protoc. 2006; 1:2315-9.

36. Vergani E, Vallacchi V, Frigerio S, Deho P, Mondellini P, Perego P, et al. Identification of MET and SRC activation in melanoma cell lines showing primary resistance to PLX4032. Neoplasia. 2011; 13:1132-42.

37. Teng Y, Xie X, Walker S, White DT, Mumm JS and Cowell JK. Evaluating human cancer cell metastasis in zebrafish. BMC Cancer. 2013; 13:453.

38. Konantz M, Balci TB, Hartwig UF, Dellaire G, Andre MC, Berman JN et al. Zebrafish xenografts as a tool for in vivo studies on human cancer. Ann N Y Acad Sci. 2012; 1266:124-37.

39. Drabsch Y, He S, Zhang L, Snaar-Jagalska BE and ten Dijke P. Transforming growth factor-β signaling controls human breast cancer metastasis in a zebrafish xenograft model. Breast Cancer Res. 2013; 15:R106.

40. Anido J, Saez-Borderias A, Gonzalez-Junca A, Rodon L, Folch G, Carmona MA, et al. TGF-β Receptor Inhibitors Target the CD44(high)/Id1(high) Glioma-Initiating Cell Population in Human Glioblastoma. Cancer Cell. 2010; 18:655-68.

41. Penuelas S, Anido J, Prieto-Sanchez RM, Folch G, Barba I, Cuartas I, et al. TGF-β increases gliomainitiating cell self-renewal through the induction of LIF in human glioblastoma. Cancer Cell. 2009; 15:315-27.

42. Olson MF, Paterson HF and Marshall CJ. Signals from Ras and Rho GTPases interact to regulate expression of p21Waf1/Cip1. Nature. 1998; 394:295-99.

43. Cantelli G, Orgaz JL, Rodriguez-Hernandez I, Karagiannis P, Maiques O, Matias-Guiu X, et al. TGF-β-Induced Transcription Sustains Amoeboid Melanoma Migration and Dissemination. Curr Biol 2015; 25:2899-914.

44. Smit MA, Maddalo G, Greig K, Raaijmakers LM, Possik PA, van Breukelen B, et al. ROCK1 is a potential combinatorial drug target for BRAF mutant melanoma. Mol Syst Biol. 2014;10:772.

45. Tsapara A, Luthert P, Greenwood J, Hill CS, Matter K and Balda MS. The RhoA activator GEF-H1/Lfc is a transforming growth factor-β target gene and effector that regulates alpha-smooth muscle actin expression and cell migration. Mol Biol Cell 2010; 21:860-70.

46. Lee J, Moon HJ, Lee JM and Joo CK. Smad3 regulates Rho signaling via NET1 in the transforming growth factorβ-induced epithelial-mesenchymal transition of human retinal pigment epithelial cells. J Biol Chem 2010; 285:26618-27.

47. Javelaud D, Alexaki VI, Pierrat MJ, Hoek KS, Dennler S, Van Kempen L, et al. GLI2 and M-MITF transcription factors control exclusive gene expression programs and inversely regulate invasion in human melanoma cells. Pigment Cell Melanoma Res. 2011; 24:932-43.

48. Akhurst RJ and Hata A. Targeting the TGFβ signaling pathway in disease. Nat Rev Drug Discov. 2012; 11:790-811.

49. Herbertz S, Sawyer JS, Stauber AJ, Gueorguieva I, Driscoll KE, Estrem ST, et al. Clinical development of galunisertib (LY2157299 monohydrate), a small molecule inhibitor of transforming growth factor-β signaling pathway. Drug Des Devel Ther. 2015; 9:4479-99.

50. Inman GJ, Nicolas FJ, Callahan JF, Harling JD, Gaster LM, Reith AD, et al. SB-431542 is a potent and specific inhibitor of transforming growth factor-β superfamily type I activin receptor-like kinase (ALK) receptors ALK4, ALK5, and ALK7. Mol Pharmacol 2002; 62:65-74.

6

Chapter 7

General discussion

Chapter 7

___

Cancer is the second leading cause of death. Globally, approximately 1 in 6 deaths are due to cancer (1). Patients with metastatic cancer are normally treated with systemic therapies, including chemotherapy, targeted therapy, hormonal therapy, and more recently immunotherapy (1). In breast cancer, HER2-positive patients can be treated with *trastuzumab* (*Herceptin*), a monoclonal antibody targeting the HER2 protein (2). Breast cancer patients who are carriers of germline BRCA mutations can be treated with poly(ADP-ribose) polymerase (PARP) inhibitors (3). However, for most TNBC patients, who have the most aggressive breast cancer phenotype and the worst poor prognosis, there is no clinically meaningful targeted therapy available. Thus, there is an urgent need to identify new therapeutic targets and develop novel treatment regimens (4). In this thesis, we focused on uncovering novel signaling mechanisms that promote TNBC metastasis and identifying new druggable targets for the treatment of TNBC patients. For metastatic melanoma, patients with the V600E BRAF mutation can benefit from BRAF inhibitors. However, approximately 40% of patients will develop resistance during chemotherapy, and melanoma recurs (5). Hence, in this thesis, I investigated the possibility of overcoming the drug resistance of metastatic melanoma by targeting TGFβ signaling with a small molecule TGFβ type I receptor kinase inhibitor.

Uncovering the DUB activity landscape in breast cancer

In the late stage of breast cancer, TGFβ-induced cytostatic effects are blunted, and instead, TGFβ promotes cancer progression by stimulating epithelial to mesenchymal transition (EMT), invasion and metastasis of cancer cells (6). The reversible ubiquitination of TGFβ signaling components is emerging as a key process regulating the intensity, duration and specificity of TGFβ intracellular signaling pathways. Deubiquitinating enzymes (DUBs) that are overly active (or amplified or mutated in cancer) in aggressive cancers and promote TGFβ-induced pro-oncogenic effects are considered potential targets for specific inhibitor development. In **Chapter 2**, we provide an overview of the DUBs that regulate TGFβ/BMP signaling and discuss the potential of several DUB inhibitors for cancer treatment. Breast cancer is a very heterogeneous disease, and it has been divided into multiple subclasses based upon histopathological characteristics and molecular/cellular features. To further classify breast cancer and develop prognostic and predictive biomarkers, large-scale conventional genomic, proteomic and metabolomic profiling studies have been performed (7). However, no large-scale DUB activity profiling has thus far been performed on breast cancer cell lines and clinical samples. Thus, in **Chapter 4**, we describe experiments in which we established two DUB activity profiling platforms to uncover the landscape of global DUBs in 52 human breast cancer cell lines and 52 patient tumor tissues. In our study, both profiling methods identified UCHL1 as a potential target in TNBC and aggressive tumors. These two DUB activity profiling methods can also be applied in the future study of other cancers or diseases.

Establishing animal xenograft models for studying cancer metastasis

To better understand the molecular mechanisms that underlie cancer metastasis *in vivo* and identify and validate new therapeutic targets, we need rapid, robust and clinically relevant animal models. We established an efficient, reliable and low-cost model in which human fluorescently labeled cancer cells are injected into early zebrafish embryos. In **Chapter 3**, a detailed protocol is provided on how to construct these zebrafish xenograft model

experiments by injecting human breast cancer cells into the perivitelline space or duct of Cuvier (Doc) to analyze the intravasation or extravasation of cancer cells at 6 days after injection. We took advantage of the transparency of transgenic (*fli:EGFP*) zebrafish embryos (8), which have enhanced green fluorescent protein-labeled vasculature, to quickly assess the invasive behavior of the injected mCherry fluorescently labeled cancer cells in the zebrafish embryos. Moreover, the pharmacological inhibition of druggable targets can be easily performed by adding small-molecule compounds to the water containing zebrafish eggs. We applied this model in experiments in **Chapter 4** to test UCHL1's function in TNBC metastasis by overexpressing/knocking down the gene encoding the UCHL1 protein or inhibiting UCHL1 activity with the specific covalent inhibitor 6RK73. In addition, we also describe experiments using this model to investigate the potential for genetic and pharmacological targeting of the TGFβ type I receptor in vemurafenib-resistant melanoma in **Chapter 6**. In addition to the zebrafish models, rodent xenograft cancer models were employed, as detailed in **Chapter 4**, to further validate and consolidate the metastatic ability of UCHL1 by intracardially injecting TNBC cells with misexpression of UCHL1 into female BALB/c athymic nude mice. Both the zebrafish and mouse xenograft TNBC models showed that high UCHL1 activity correlated with pronounced metastatic traits.

Unraveling the mechanism by which UCHL1 promotes TNBC metastasis

During breast cancer metastasis, EMT plays an important role by mediating breast cancer cell invasion. During EMT, the cobble stone-appearing and highly polarized epithelial cancer cell phenotype switches to a highly motile mesenchymal cell phenotype with a fibroblastic-like appearance. In **Chapter 4**, we first investigated the effect of UCHL1 knockdown in TNBC cells on several mesenchymal markers and found that UCHL1 depletion decreased mesenchymal markers at both the RNA and protein levels. Since TGFβ signaling is a key driver of the EMT process, we next examined the correlation between UCHL1 expression and TGFβ/SMAD signaling. We observed that UCHL1 can promote the levels of carboxy-tail phosphorylated and activated SMAD2/SMAD3 by protecting TβRI and SMAD2 from ubiquitination and subsequent degradation (Figure 1). The interaction of UCHL1 and TβRI occurred in early endosomes and was triggered by TGFβ ligand stimulation. Importantly, the promoting function of UCHL1 in metastasis could be blocked by a selective TβRI chemical inhibitor in TNBC cells. Although our results indicated a key role for UCHL1 in stimulating breast cancer metastasis by regulating TGFβ signaling, we do not exclude the possibility that UCHL1 may also promote metastasis by targeting other signaling pathways. Previous studies have shown that UCHL1 can also regulate AKT signaling (9) and hypoxia-inducible factor (HIF)1α signaling (10).

Discovery of potential blood-based biomarkers for metastatic TNBC

As UCHL1 is abundantly present in all neurons (accounting for 1-2% of total brain protein) (11), UCHL1 has been developed as a blood-based biomarker for the clinical diagnosis of traumatic brain injury (12). To investigate the possibility of using UCHL1 as a potential biomarker for the clinical diagnosis of metastatic TNBC, we tested UCHL1 levels by ELISA and observed that TNBC patient sera contained higher UCHL1 levels than sera from normal individuals (**Chapter 4**). Furthermore, we found that UCHL1 was highly enriched in the exosome fraction of ER- patient sera and TNBC cell conditioned media (Figure 1). Moreover,

7

exosomes isolated from TNBC cells were found to promote TGFβ/SMAD signaling and promote the migration and extravasation of recipient TNBC cells. Recently, two groups also detected UCHL1 in exosomes. One group found higher UCHL1 protein levels in patient serum exosomes than in serum exosomes from normal individuals, which could be correlated with chemotherapy resistance in breast cancer (13). Another group detected higher levels of UCHL1 mRNA in exosome preparations from serum samples from patients with early-stage high-grade neuroendocrine lung cancer than in exosomes derived from patients with early-stage non-small-cell lung cancer and healthy donors (14). Taken together, these studies suggest that extracellular vesicle-derived UCHL1 levels play an important role and that UCHL1 may act in cancer cells in both autonomous and paracrine manners to stimulate tumorigenesis.
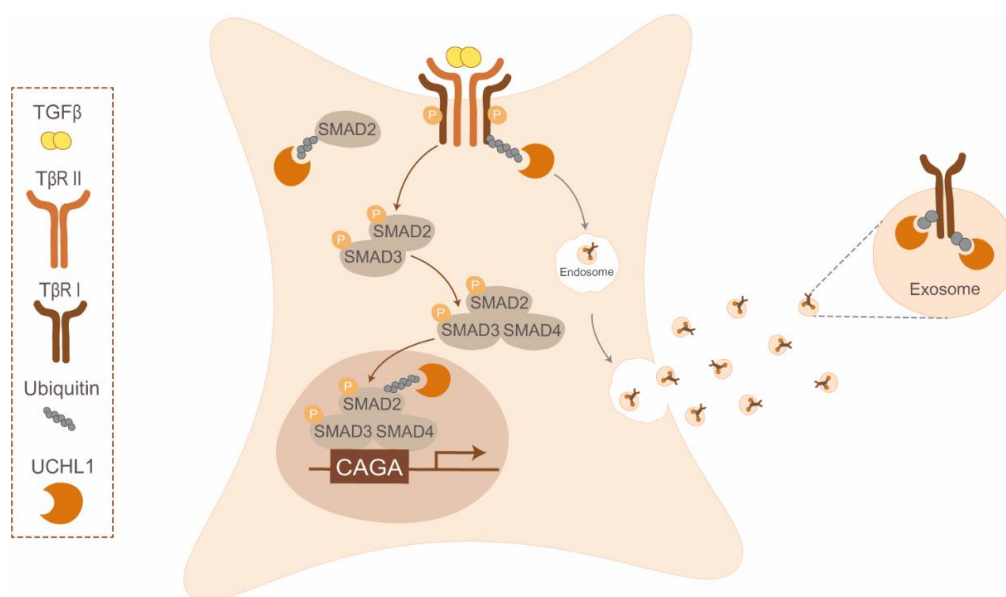

Figure 1. A working model for the role of UCHL1 in TGFβ signaling. UCHL1 promotes the phosphorylation of SMAD2 by protecting TβRI and SMAD2 from ubiquitination in TNBC cells. The interaction between UCHL1 and TβRI occurs in the early endosome. The interaction between UCHL1 and SMAD2 shifts from the cytoplasm to the nucleus after TGFβ treatment. UCHL1 can also be detected in TNBC cell exosomes.

Investigating a potential drug for targeting UCHL1 activity in TNBC

The ability of UCHL1 to promote TGFβ/SMAD signaling critically depends on its catalytic DUB activity. Mutation of the UCHL1 protein from WT to C90A (DUB activity-inactivating mutation) abolishes its stimulatory effect on TGFβ receptor signaling, migration and invasion in TNBC cells. We therefore attempted to find a specific inhibitor of UCHL1 activity. This inhibitor was identified in a patent application of Mission Therapeutics (15). This led to the chemical synthesis and characterization of highly selective and potent UCHL1 inhibitors, including 6RK73 (**Chapter 4**). The 6RK73 compound covalently binds to UCHL1 and blocks its activity both *in vitro* and *in vivo*. When we tested 6RK73 in TNBC cells and patient samples, it showed specific inhibition of UCHL1 among all the DUBs in the breast cancer cell and patient tissue lysates. Mechanistically, 6RK73 strongly inhibited pSMAD2, which functions in TGFβ signaling, by inducing the degradation of TβRI/SMAD2 in TNBC cells (Figure 2). Importantly, 6RK73 strongly inhibited TNBC cell migration and extravasation in

the scratch assay and zebrafish xenograft model. Thus, 6RK73 (or its analogues) has the potential to become a new drug for TNBC treatment. In addition, UCHL1 has been reported as a novel functional marker for liver fibroblasts and a therapeutic target in chronic liver disease (16). This study highlighted the opportunity for applying UCHL1 activity inhibitors in chronic liver disease treatment. However, many of the reported DUB inhibitors have off-target effects, which inhibits their clinical development (17). For 6RK73, we have not yet found such off-target effects, but future studies may reveal them. Another challenge is that DUBs are promiscuous and have multiple substrates. This may also lead to unwanted side effects of specific DUB inhibitors. A specific inhibitor that targets the DUB–substrate interaction may provide more accurate DUB-target interference (18). Therefore, in the future, we can target the UCHL1-TβRI interaction to more specifically interfere with the ability of UCHL1 to promote TGFβ receptor signaling.

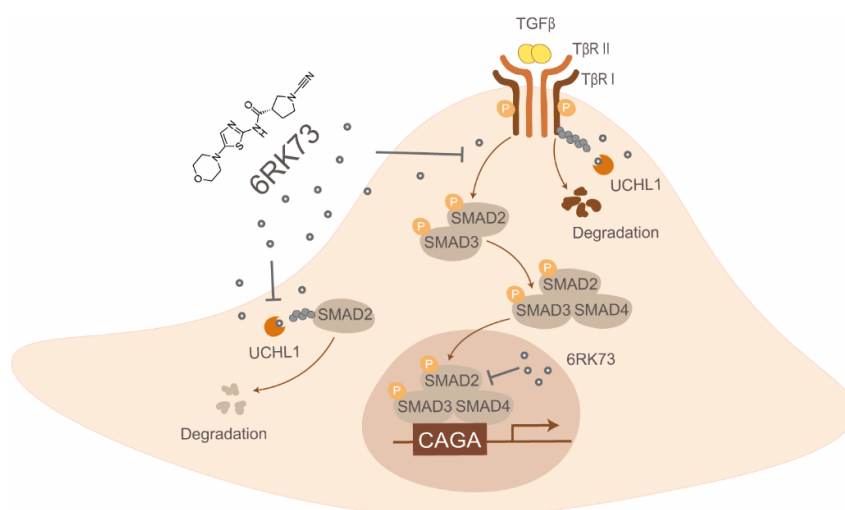Figure 2. The role of 6RK73 in TGFβ signaling. 6RK73 blocks UCHL1 activity covalently and inhibits the phosphorylation of SMAD2 by decreasing the levels of TβRI and SMAD2 in TNBC cells.

Development of an activity-based probe for monitoring UCHL1 activity *in vivo*

To further study UCHL1 activity *in vivo*, we attempted to make a UCHL1 activity-based probe. However, we were faced with many challenges. More than 100 DUBs have been identified, which can be grouped into different subfamilies. Within each subfamily, there is extensive sequence/structural similarity in the catalytic domains, making the design of selective inhibitors difficult. Additionally, creating inhibitors with the ability to penetrate the cell membrane and retain DUB inhibitor activity upon modification with fluorescent groups is difficult (19). In **Chapter 5**, we provided evidence for the first potential small-molecule UCHL1 activity-based probe (8RK59) that can specifically label an active version of UCHL1 *in vitro*. Moreover, this probe can efficiently pass through the cell membrane and monitor UCHL1 activity in (living) cells and in zebrafish embryos. In the follow-up study, we found that this probe could be used for tracking UCHL1 activity in TNBC cells during the metastatic process in a zebrafish xenograft model (Figure 3). Although 8RK59 only targets UCHL1 among all the DUBs, we also identified a non-DUB target, Parkinson's disease protein 7 (PARK7), using an unbiased mass spectrometry-based approach. UCHL1 is also called PARK5; both UCHL1 and PARK7 have been functionally linked to Parkinson's

disease (20). In addition, profiling Parkin-binding partners identified UCHL1 and PARK7 in the same protein-protein interaction network using tandem affinity purification (21), which indicated that these two proteins may interact with each other. However, further studies are needed to clarify the underlying correlation between UCHL1 (PARK5) and PARK7 and to further improve the selectivity of the UCHL1 activity probe.
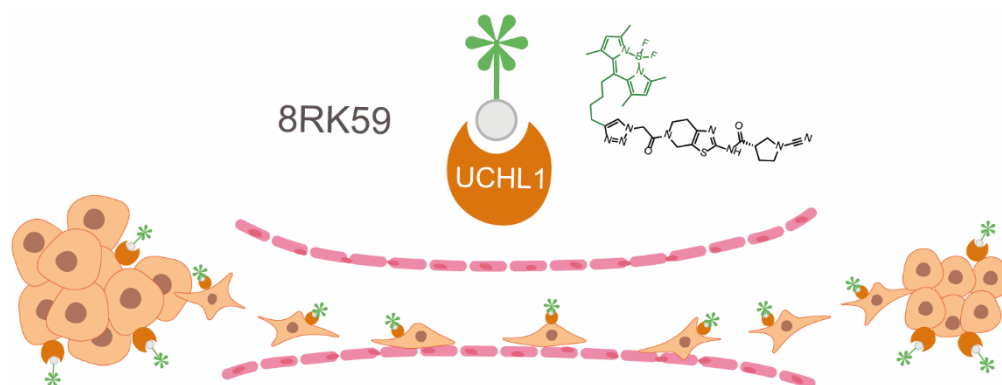

Figure 3. The application of 8RK59 in tracking UCHL1 activity during TNBC metastasis.

Targeting TGFβ signaling to improve drug-resistant melanoma treatment

Drug resistance is a major reason for the high mortality rate in late-stage melanoma. Recent studies have revealed elevated TGFβ signaling in BRAF inhibitor-resistant melanoma (22). However, the potential for targeting TGFβ signaling in cases of advanced melanoma has not been investigated. In **Chapter 6**, we provided evidence that the TβRI inhibitor SB-431542 blocked the proliferation and SMAD2 phosphorylation of vemurafenib-resistant patient-derived cells. Importantly, pharmacological and genetic inhibition of TβRI effectively blocked the clonogenicity of human BRAF-mutant melanoma cells and inhibited extravasation of melanoma in a zebrafish xenograft model. Although targeting of TGFβ signaling has been considered a potential therapy in several metastatic cancers, first-generation inhibitors targeting TβRI have failed because of overt cardiac toxicity (23). Hence, when applying TβRI inhibitors in clinical treatment, unwanted side effects need to be taken into consideration, and applying treatment with an intermittent dosing regimen may overcome cardiac toxicity (24-26).

Conclusion

Overall, this thesis uncovered the DUB activity landscape in breast cancer and identified UCHL1 as a potential tumor-promoting protein that facilitates TGFβ-induced TNBC metastasis. The UCHL1 activity inhibitor 6RK73 strongly mitigated TNBC invasion and metastasis. Moreover, the development of the UCHL1 activity-based probe 8RK59 has opened a new window for monitoring UCHL1 *in vivo*. Significantly, TNBC patient sera contain high UCHL1 levels, suggesting that UCHL1 may be a candidate blood-based biomarker. It will be interesting in future studies to test the value of measuring UCHL1 expression and/or activity in detecting disease early, selecting patients and/or monitoring therapy response. This thesis suggests the potential therapeutic value of targeting TGFβ signaling in the (pre)clinical setting for drug-resistant melanoma.

References:

1. Ferlay J, Colombet M, Bray F. Global Cancer Observatory. International Agency for Research on Cancer. 2018.
2. Bange J, Zwick E, Ullrich A. Molecular targets for breast cancer therapy and prevention. Nat Med 2001;7(5):548-52.
3. Geenen JJJ, Linn SC, Beijnen JH, Schellens JHM. PARP Inhibitors in the Treatment of Triple-Negative Breast Cancer. Clin Pharmacokinet 2018;57(4):427-37.
4. Bianchini G, Balko JM, Mayer IA, Sanders ME, Gianni L. Triple-negative breast cancer: challenges and opportunities of a heterogeneous disease. Nat Rev Clin Oncol 2016;13(11):674-90.
5. Pasquali S, Hadjinicolaou AV, Chiarion Sileni V, Rossi CR, Mocellin S. Systemic treatments for metastatic cutaneous melanoma. Cochrane Database Syst Rev 2018;2(2):CD011123.
6. Massague J. TGFβ in Cancer. Cell 2008;134(2):215-30.
7. Chakraborty S, Hosen MI, Ahmed M, Shekhar HU. Onco-Multi-OMICS Approach: A New Frontier in Cancer Research. Biomed Res Int 2018; 9836256.
8. Lawson ND, Weinstein BM. In vivo imaging of embryonic vascular development using transgenic zebrafish. Dev Biol 2002;248(2):307-18
9. Hurst-Kennedy J, Chin L-S, Li L. Ubiquitin C-terminal hydrolase L1 in tumorigenesis. Biochem Res Int 2012; 123706.
10. Goto Y, Zeng L, Yeom CJ, Zhu Y, Morinibu A, Shinomiya K, et al. UCHL1 provides diagnostic and antimetastatic strategies due to its deubiquitinating effect on HIF-1alpha. Nat Commun 2015;6:6153.
11. Doran JF, Jackson P, Kynoch PA, Thompson RJ. Isolation of PGP 9.5, a new human neurone-specific protein detected by high-resolution two-dimensional electrophoresis. J Neurochem 1983;40(6):1542-7.
12. Papa L, Brophy GM, Welch RD, Lewis LM, Braga CF, Tan CN, et al. Time Course and Diagnostic Accuracy of Glial and Neuronal Blood Biomarkers GFAP and UCH-L1 in a Large Cohort of Trauma Patients With and Without Mild Traumatic Brain Injury. JAMA Neurol 2016;73(5):551-60.
13. Ning K, Wang T, Sun X, Zhang P, Chen Y, Jin J, et al. UCH-L1-containing exosomes mediate chemotherapeutic resistance transfer in breast cancer. J Surg Oncol 2017;115(8):932-40.
14. Shimada Y, Kudo Y, Maehara S, Matsubayashi J, Otaki Y, Kajiwara N, et al. Ubiquitin C-terminal hydrolase-L1 has prognostic relevance and is a therapeutic target for high-grade neuroendocrine lung cancers. Cancer Science 2020;111(2):610-20.
15. Jones A, Kemp M, Stockley M, Gibson K, Whitlock G, Madin AJW. Novel Compounds. 2016.
16. Wilson CL, Murphy LB, Leslie J, Kendrick S, French J, Fox CR, et al. Ubiquitin C-terminal hydrolase 1: A novel functional marker for liver myofibroblasts and a therapeutic target in chronic liver disease. J Hepatol 2015;63(6):1421-8.
17. Harrigan JA, Jacq X, Martin NM, Jackson SP. Deubiquitylating enzymes and drug discovery: emerging opportunities. Nat Rev Drug Discov 2018;17(1):57-78.
18. Crunkhorn S. Inhibiting protein–protein interactions. Nat Rev Drug Discov 2016;15(4):234.
19. Hewings DS, Flygare JA, Bogyo M, Wertz IE. Activity-based probes for the ubiquitin conjugation-deconjugation machinery: new chemistries, new tools, and new insights. FEBS J 2017;284(10):1555-76.
20. Greenamyre JT, Hastings TG. Biomedicine. Parkinson's-divergent causes, convergent mechanisms. Science 2004;304(5674):1120-2.
21. Zanon A, Rakovic A, Blankenburg H, Doncheva NT, Schwienbacher C, Serafin A, et al. Profiling of Parkin-binding partners using tandem affinity purification. PLoS One 2013;8(11):e78648.
22. Menon DR, Wels C, Bonyadi Rad E, Joshi S, Knausz H, Lade-Keller J, et al. TGF-β1 and TNF-alpha differentially regulate Twist1 mediated resistance towards BRAF/MEK inhibition in melanoma. Pigment Cell Melanoma Res 2013;26(6):912-6.

7

23.   Anderton MJ, Mellor HR, Bell A, Sadler C, Pass M, Powell S, et al. Induction of heart valve lesions by small-molecule ALK5 inhibitors. Toxicol Pathol 2011;39(6):916-24.
24.   Kovacs RJ, Maldonado G, Azaro A, Fernandez MS, Romero FL, Sepulveda-Sanchez JM, et al. Cardiac Safety of TGF-β Receptor I Kinase Inhibitor LY2157299 Monohydrate in Cancer Patients in a First-in-Human Dose Study. Cardiovasc Toxicol 2015;15(4):309-23.
25.   Colak S, Ten Dijke P. Targeting TGF-β Signaling in Cancer. Trends Cancer 2017;3(1):56-71.
26.   Huynh LK, Hipolito CJ, Ten Dijke P. A Perspective on the Development of TGF-β Inhibitors for Cancer Treatment. Biomolecules 2019;9(11).

Appendix

English Summary
Nederlandse Samenvatting
Abbreviations
List of Publications
Curriculum Vitae
Acknowledgements

English Summary

In cancer cells, aberrant TGFβ signaling can lead to loss of growth inhibition and increase in epithelial to mesenchymal transition (EMT), migration and metastasis. Targeting TGFβ is currently being explored as a potential therapy against certain invasive and metastatic cancer types. However, current drugs tested in clinical trials inhibit all TGFβ (good and bad) responses and suffer from unwanted side effects. The ubiquitin system is emerging as an important post-translational regulatory mechanism for the TGFβ pathway. Targeting of E3 ubiquitin ligases and deubiquitinating enzymes that are highly active in aggressive cancer and promote tumor promoting functions of TGFβ might offer new therapeutic opportunities. In **Chapter 2**, we summarized the role of DUBs that contribute to the regulation of TGFβ signaling in cancer, and discussed the DUB inhibitors in preclinical trials for cancer treatment.

Metastasis is the underlying cause of death for majority of cancer patients. Numerous rodent models are available for investigating cancer metastasis, but to enable a quick assessment of the potential effect of (epi)genetic changes or pharmacological compounds we need more efficient, reliable, low-cost *in vivo* models. In **Chapter 3**, we describe the possibility of using zebrafish xenograft models to study the metastasis progression of breast cancer cells.

Among all the breast cancer cases, TNBC remains the most challenging subtype to treat. To discovery new targets, in **Chapter 4**, we profiled global DUB activities in breast cancer cell lines and tumor samples, and identified UCHL1 as a candidate oncoprotein. Mechanistically, we found that UCHL1 facilitates TGFβ signaling-induced metastasis by protecting TβRI and SMAD2 from ubiquitination. We further found a UCHL1 covalent activity inhibitor 6RK73 that specifically inhibited UCHL1 activity and blocked metastasis in TNBC. Significantly, we observed that TNBC patient sera contained high UCHL1 levels, which may represent a potential blood-based biomarker for diagnosis of metastatic TNBC.

In order to better study the activity of UCHL1 *in vivo*, we developed a cell permeable fluorescent activity-based probe for UCHL1 in **Chapter 5**. This probe 8RK59 binds to the active-site cysteine residue of UCHL1 in an activity-dependent manner and irreversibly. Its application was demonstrated by labelling UCHL1 activity *in vitro* and in cells. Furthermore, we applied the probe in monitoring UCHL1 activity in zebrafish embryos during development. This small molecule probe may have potential other targets, such as PARK7. Additional studies are needed to increase the selectivity of the probe.

For metastatic melanoma, the median survival of BRAF(V600E) patients has improved by treatment with BRAF inhibitors, but drug resistance remains a problem for a significant fraction (about 40%) of melanoma patients. Recent studies showed that TGFβ signaling is increased in BRAF inhibitor resistance melanoma. In **Chapter 6**, we investigated the potential for targeting TGFβ signaling in the treatment of drug resistance melanoma. We found that pharmacologic or genetic inhibition of TβRI blocked BRAF mutant melanoma cells metastasis in xenograft zebrafish model.

In summary, this thesis focused on the understanding the underlying mechanisms driving TNBC metastatic progression. We established DUB activity profiling methods and identified UCHL1 as a candidate oncoprotein that promotes TGFβ-induced breast cancer metastasis. Importantly, we found UCHL1 activity inhibitor as a potential drug for TNBC therapy and

A

developed UCHL1 activity-based probe. For vemurafenib-resistance melanoma, we provided insights that targeting TGFβ signaling may help to overcome drug resistant phenotype.

I hope that all the fundamental and translational studies in my PhD thesis may contribute to increased survival and improved quality of life for cancer patients.

Nederlandse Samenvatting

Ontregeling van "transforming growth factor-β" (TGFβ)-signalering in kankercellen kan leiden tot verlies van groeiremming en een toename in zogenaamde epitheliale naar mesenchymale overgang (EMT), celmigratie en metastase. Remming van TGFβ signalering wordt momenteel onderzocht in de kliniek als een potentiële therapie tegen invasieve en metastatische kankertypen. Echter, de huidige TGFβ remmers blokkeren alle effecten, goed en slecht, van TGFβ en vertonen schadelijke bijeffecten. Het ubiquitine systeem is een belangrijk post-translationeel regulatiemechanisme voor de TGFβ-route en biedt als zodanig aangrijpingsmogelijkheden voor de ontwikkeling van nieuwe anti-TGFβ therapieën. In plaats van het TGFβ ligand of de TGFβ receptor direct te remmen, kunnen de componenten van het ubiquitine systeem worden geremd die specifiek de expressie of activiteit van TGFβ signaleringscomponenten stimuleren in agressieve tumoren. H**oofdstuk 2** geeft een samenvatting van de rol die deubiquitinerings enzymen (DUBs) spelen in TGFβ-signalering bij kanker en worden DUB-remmers besproken waarvan de effecten nu worden geanalyseerd in preklinische kanker studies.

Uitzaaiingen (metastasen) zijn de onderliggende doodsoorzaak voor de meerderheid van kankerpatiënten. Er zijn talloze knaagdiermodellen beschikbaar voor het onderzoeken van metastase van kanker, maar om snel toegang te krijgen tot het potentiële effect van (epi) genetische veranderingen of farmacologische verbindingen zijn er efficiënte, betrouwbare en goedkope *in vivo* kankermodellen nodig. In **hoofdstuk 3** wordt weergegeven hoe zebravis xenograft-modellen kunnen worden gebruikt om dit te bewerkstelligen. Er wordt in detail beschreven hoe de kwaadaardige uitzaaiing van menselijke borstkankercellen kan worden bestudeerd in zebravis embryo's.

Van alle gevallen van borstkanker blijft triple negatieve borstkanker ((TNBC) de meest uitdagende borstkankersubtype om te behandelen. Om nieuwe therapeutische doelen te ontdekken, worden in **hoofdstuk 4** de globale DUB-activiteiten in borstkankercellijnen en tumormonsters geanalyseerd. Hierin is UCHL1 geïdentificeerd als kandidaat-onco-eiwit. Er is gevonden dat UCHL1 de TGFβ-geïnduceerde metastase mogelijk maakt door de TGFβ receptor en intracellulaire SMAD2 effector te beschermen tegen ubiquitinering en afbraak. Er is verder gevonden dat een UCHL1-covalente activiteitsremmer 6RK73 heel specifiek de UCHL1-activiteit remde en metastase van TNBC blokkeerde. Tevens is er vastgesteld dat de sera van TNBC-patiënten hoge UCHL1-niveaus bevatten. UCHL1 is daarmee een potentiële op bloed gebaseerde biomarker voor de diagnose van metastasering van TNBC.

Om de activiteit van UCHL1 *in vivo* te bestuderen, is er in **hoofdstuk 5** een celpermeabele fluorescente activiteits-gebaseerde probe voor UCHL1 ontwikkeld. Deze probe 8RK59 bindt zich op een activiteitsafhankelijke manier en onomkeerbaar aan de cysteïne in de actieve site van het UCHL1 enzym. De toepasbaarheid van de probe werd gedemonstreerd door UCHL1-activiteit *in vitro* en in levende cellen te labelen. Verder hebben we de activiteitsprobe toegepast bij het volgen van de UCHL1-activiteit tijdens de ontwikkeling van zebravis embryo's. Deze probe kan echter potentiële andere doelen hebben, zoals PARK7. Aanvullende studies zijn daarom nodig om de selectiviteit van de probe te verhogen.

A

Appendix

Voor het gemetastaseerd melanoom is de mediane overleving van BRAF (V600E) patiënten verbeterd door toepassing van BRAF-remmers, maar resistentie tegen geneesmiddelen blijft een probleem voor ongeveer 40% van melanoompatiënten. Recente studies hebben

aangetoond dat TGFβ-signalering is verhoogd in melanoom dat resistent is tegen BRAF-remmers. In **hoofdstuk 6** is het effect onderzocht van het remmen TGFβ-signalering in resistente melanoom cellen. Er is gevonden dat farmacologische of genetische remming van TβRI in BRAF-mutante melanoomcellen de invasie blokkeerde in het xenograft zebravismodel.

Samenvattend, één van de belangrijke doelen van dit onderzoek was het verkrijgen van nieuwe inzichten in de onderliggende mechanismen van TNBC metastasering. Er zijn methoden ontwikkeld om DUB-activiteiten te profileren in bostkanker cellijnen en klinisch materiaal. UCHL1 is geïdentificeerd als een kandidaat-onco-eiwit dat de TGFβ-geïnduceerde metastase van borstkanker bevordert. Belangrijk is dat de UCHL1-activiteitsremmer als een potentieel medicijn voor TNBC-therapie is gevonden en een op UCHL1-activiteit gebaseerde probe is ontwikkeld. Voor vemurafenib-resistente huidkankers hebben we aangetoond dat het remmen van TGFβ-signalering kan helpen om de resistentie tegen het geneesmiddel te overwinnen.

Hopelijk zullen de fundamentele en translationele studies beschreven in dit proefschrift uiteindelijk bijdragen aan een verhoogde overleving en verbeterde kwaliteit van leven voor kankerpatiënten.

Abbreviations

ABP	Activity-based probe
AKT	Protein kinase B
AMSH	Associated molecule with SH3 domain proteases
ATCC	American Type Culture Collection
ATXN3	Ataxin-3
BGG	Globulins from bovine blood
BLI	Bioluminescent imaging
BMP	Bone morphogenetic protein
BRCC36	BRCA1/BRCA2-containing complex subunit 36
CHIP	Carboxy terminus of Hsc70-interacting protein
CHT	Caudal hematopoietic tissue
CSN5	COP9 signalosome subunit 5
CuAAC	Copper(I)-catalyzed azide alkyne cycloaddition
DoC	Duct of Cuvier
dpf	Days post-fertilization
dpi	Days post-injection
DUB	Deubiquitinase
E1	Ubiquitin-activating enzyme
E2	Ubiquitin-conjugating enzyme
E3	Ubiquitin ligase enzyme
Ecto	Ectodermin
ELISA	Enzyme-linked immunosorbent assay
EMT	Epithelial-to-mesenchymal transition
ER	Estrogen receptor
FBS	Fetal bovine serum
GATD3B	Glutamine amidotransferase-like class-1 domain-containing protein 3B
GSR	Glutathione reductase
HECT	Homologous to the E6AP carboxyl terminus
HER2	Human epidermal growth factor receptor 2
HIF1α	Hypoxia-inducible factor 1 α
HNSCC	Head and neck squamous cell carcinoma
hpf	Hours post-fertilization
hpi	Hours post-injection
IB	Immunoblotting
IC$_{50}$	Half-maximum inhibitory concentration
IF	Immunofluorescence
IGF-I	Insulin-like growth factor 1
IKK	IκB kinase
IP	Immunoprecipitation
ISOC2	Isochorismatase domain-containing protein 2
JAB1	Jun activating binding protein
JAMMs	JAB1/ MPN/MOV34 proteases
JNK	C-Jun NH2-terminal kinase
JOSD1	Josephin domain containing 1

Appendix

LC/MS	Liquid chromatography-tandem mass spectrometry
LFQ	Label-free quantification
LPS	Lipopolysaccharide
MAPKs	Mitogen-activated protein kinases
MITF	Microphthalmia associated transcription factor
MJDs	Machado-Joseph disease proteases
MPN	Mpr1-Pad1-N-terminal
MPND	MPN domain-containing protein
MYSM1	Myb-like with SWIRM and MPN domains 1
NEM	N-ethylmaleimide
NSCLC	Non-small cell lung cancer
NTA	Nanoparticle tracking analysis
OUT	Ovarian tumor protease
PARK5	Parkinson disease 5
PARK7	Parkinson disease 7
PFA	Paraformaldehyde
PGP9.5	Neuron-specific protein PGP9.5
PI	Proteasome inhibitor
PI3K	Phosphoinositde 3 kinase
PLA	Proximity ligation assay
POH1	Proteasome-associated PAD1 homolog1
PR	Progesterone receptor
PSMD14	Proteasome 26S Subunit Non-ATPase 14
Rh-Ub-PA	Rhodamine-Ubiquitin-propargylamide
RING	Really interesting new gene
RPMI	Roswell Park Memorial Institute
RTK	Receptor tyrosine kinase
Smad	Sma and Mad related proteins
Smurf	Smad ubiquitin regulatory factor
TAK1	Transforming growth factor-β-activated kinase 1
TAMRA	5-carboxytetramethylrhodamine
TCEP	Tris(2-carboxyethyl)phosphine
TEM	Transmission electron microscopy
TGFBR	TGFβ receptor
TGFβ	Transforming growth factor-β
TNBC	Triple-negative breast cancer
TNFα	Tumor necrosis factor-α
TRAFs	Tumor necrosis factor receptor-associated factors
Tregs	T cells
Ub	Ubiquitin
UBA	Ubiquitin-associated domain
UCHL1	Ubiquitin Carboxy-terminal Hydrolase L1
UIM	Ubiquitin-interacting motif
USP	Ubiquitin specific protease
VME	Vinyl methyl ester

List of Publications

Deubiquitinase activity profiling identifies UCHL1 as a candidate oncoprotein that promotes TGFβ-induced breast cancer metastasis.
Liu S, González-Prieto R, Zhang M, Geurink PP, Kooij R, Iyengar PV, van Dinther M, Bos E, Zhang X, Le Dévédec SE, van de Water B, Koning RI, Zhu HJ, Mesker WE, Vertegaal ACO, Ovaa H, Zhang L, Martens JWM, Ten Dijke P.
Clin Cancer Res. 2020 Mar 15;26(6):1460-1473.

Invasive Behavior of Human Breast Cancer Cells in Embryonic Zebrafish.
Ren J*, **Liu S***, Cui C, Ten Dijke P.
J Vis Exp. 2017 Apr 25;(122).

Mutational activation of BRAF confers sensitivity to transforming growth factor β inhibitors in human cancer cells.
Spender LC, Ferguson GJ, **Liu S**, Cui C, Girotti MR, Sibbet G, Higgs EB, Shuttleworth MK, Hamilton T, Lorigan P, Weller M, Vincent DF, Sansom OJ, Frame M, ten Dijke P, Marais R, Inman GJ.
Oncotarget. 2016 Dec 13;7(50):81995-82012.

Regulation of the TGF-β pathway by deubiquitinases in cancer.
Liu S, de Boeck M, van Dam H, Ten Dijke P.
Int J Biochem Cell Biol. 2016 Jul;76:135-45.

Electroneutralized Amphiphilic Triblock Copolymer with a Peptide Dendron for Efficient Muscular Gene Delivery.
Pu L, Geng Y, **Liu S**, Chen J, Luo K, Wang G, Gu Z.
ACS Appl Mater Interfaces. 2014 Sep 10;6(17):15344-51.

Pluronic L64-mediated stable HIF-1α expression in muscle for therapeutic angiogenesis in mouse ischemic limb.
Song H, **Liu S**, Li C, Geng Y, Wang G, Gu Z.
Int J Nanomedicine. 2014 Jul 21;9:3439-52.

Safe and efficient local gene delivery into skeletal muscle via a combination of Pluronic L64 and modified electrotransfer.
Liu S, Ma L, Tan R, Lu Q, Geng Y, Wang G, Gu Z.
Gene Ther. 2014 Jun;21(6):558-65.

* Equal contribution

A

Appendix

Curriculum Vitae

Sijia Liu was born on the 14th of July 1988 in Chengde, China. From 10th September 2007, she started her bachelor study in biotechnology at Southwest University for Nationality, Chengdu, China. During her bachelor internship, she joined the lab of Prof. Yongli Wen and worked on bioinformatic analysis of alternative spliceosome for melatonin synthetase gene HOIMT. She obtained her bachelor degree on the 16th of June 2011. From 1st September 2011, Sijia started her master study in chemical biology at Sichuan University, Chengdu, China. During her master internship, she investigated high-efficient and safe muscular gene delivery of HIF-1α for therapeutic angiogenesis with the supervision of Prof. Gang Wang in the lab of National Engineering Research Center for Biomaterials. She obtained her master degree on the 19th of June 2014. From 4th September 2014, Sijia started her PhD study in cell biology at Leiden University Medical Center, Leiden, The Netherlands. During her PhD, she studied TGFβ signaling in cancer progression with the supervision of Prof. Peter ten Dijke. She focused on understanding of the underlying mechanisms driving metastatic progression of triple-negative breast cancer (TNBC) and identified UCHL1 as a candidate oncoprotein that promotes TGFβ-induced breast cancer metastasis. From 1st September 2018 till now, Sijia continued her research in ten Dijke's lab with the support from Cancer Genomics Center Netherlands. Her work focused on investigating UCHL1 activity inhibitor as a potential drug for TNBC therapy and developed cell permeable fluorescent activity-based probe for UCHL1.

Acknowledgements

It's time to express my sincere appreciation to all the people who raise me up during my PhD study, without your encouragement and support this book will not exist!

First of all, I would like to express my deepest gratitude to my promotor Prof. Peter ten Dijke. Thank you for guiding me into the field of TGFβ signaling with your profound knowledge, open-mind enlightenment and field-leading foresight. You are not only a mentor for my scientific work but also a model for my future career. Next, I want to express my heartfelt gratitude to my co-promotor Dr. Paul P. Geurink. Thank you for opening a window for me to see the landscape of chemical biology. I also want to express my special appreciation to Prof. Alfred Vertegaal, Dr. Román González-Prieto, Prof. John Martens, Prof. Long Zhang, Mengdi Zhang, Prof. Bob van de water, Dr. Sylvia Le Dévédec. Xiaobing Zhang, Prof. Wilma Mesker, Kiki Vangangelt, Prof. Huib Ovaa and Raymond Kooij. Without your great support I can't finish such multi-disciplinary crossed project.

It's my pleasure to become a member of the big TGFβ group. I am very grateful to our TGFβ families. Thanks Maarten, Midory, Sharon and Gerard for great technical assistance and excellent lab organization. Thanks David and Hans for professional guidance during my PhD study. Thanks Prasanna, Chao, Catalina, Laila and Mauri for introducing me into the field of ubiquitin, zebrafish, autophagy, mice and cross-linking. Thanks our palladian think tank: Marten, Amaya, Gonzalo, Chloé, Mar, Selcuk, Xiaofei, Juan, Yongsheng, Abhishek and Yifan for generously sharing valuable experience and knowledge. Special thanks our PhD commando: Jiang, Yihao, Jie, Miriam, Chuannan, Jing, Jin, Dieuwke, Wan and Yang for fighting side by side and supporting shoulder by shoulder tenaciously. Also thanks Ana and Aliaa for together with me exploring new techniques and digging out new projects.

Many thanks also go to our CCB department. Thanks Julia for your great help on my graduation application and countless arrangements of documents and meetings. Thanks our strong microscope team: Annelies, Willem, Lennard, Erik and Roman for your powerful help on generating all the beautiful images and lively videos. Thanks our CCB sweet colleagues and great scientists: Martijn, Steve, Gelilla, Ben, Jacques, Marie-José, Manuel, Harald, Stephan, AG, Karoly, Anke, Babu, Ruud, Baoxu, Aysegul, Katharina, Botao, Xiaoyu, Jin, Qian, Yuqing, Jin and Yufeng for precious feedback on my presentation and memorable moments at CCB borrel.

Last but not the least, I want to thank my families and friends for their endless love and care to encourage me face with all the challenge and pass through every struggling moment.

Life is a long long journey, PhD is not an end but a new start. Thank you all for being in my life, I will bring all the wonderful memories to seek for the next adventure!

A